A BROADBAND MAGNETOTELLURIC INVESTIGATION IN SOUTHEAST SCOTLAND

PETER OJO SULE

DOCTOR OF PHILOSOPHY

UNIVERSITY OF EDINBURGH

1985

DECLARATION

I hereby declare that the work presented in this thesis is my own, unless otherwise stated in the text and that the thesis has been composed by myself.

P. O. Sule

ABSTRACT

Magnetotelluric (AMT/MT) soundings were made in 1982-84 at 22 sites in SE Scotland in the range 0.01-1000 Hz. These are the first AMT measurements in this region. Eight sites lie on a profile almost normal to the Southern Uplands Fault (SUF), while the rest lie in a 2D array near Duns, where Habberjam resistivity methods (HAB) have previously been used. VLF/R measurements were also made at 10 of the sites.

Classical tensorial data analysis techniques have been used. Comparison of averaging techniques indicates it is preferable to average impedance lognormally. A qualitative approach for processing noisy data has been devised, thus enabling useful results to be obtained.

1D inversions of apparent resistivity and phase data using the Bostick transform and a Monte-Carlo algorithm have yielded very similar models, but the Bostick transform is computationally more efficient. It is preferable to model invariant apparent resistivity and phase data (ϱ_{eff}, φ_{eff}).

AMT/MT and HAB are compared in detail. They give comparable 1D models. However, AMT/MT is more cost- and exploration-effective with a much greater depth and lateral resolution.

The Duns sites have been projected onto the SUF profile to give a single traverse. 2D modelling based on the finite difference method of Brewitt-Taylor and Weaver (1976) has yielded a geoelectrical model in good agreement with previous results in South Scotland and elsewhere. It

provides a much better resolution of the subsurface structures owing to close station spacing, broadband data and improved data quality.

The main conclusions from the geoelectrical model are:

(a) It shows a significant lateral variation in the conductivity structure. A series of conductive sedimentary basin-like structures is in evidence within the uppermost 2 km.

(b) It exhibits more near-surface complexity in the Midland Valley than in the Southern Uplands in good agreement with geology.

(c) The existence of a low resistivity layer in the lower crust and upper mantle, indicated by earlier studies, is confirmed. The hitherto poorly resolved upper boundary of the conductor is delineated. The conductor extends into the upper crust and the lateral depth variation to it is clearly shown.

(d) The conductor rises near the surface (<4 km) in the neighbourhood of SAW and BUG and the axis of an elongated magnetic variation anomaly and it dips to the north and south of these sites. This conducting zone is suggested as being associated with ancient subduction and hence linked with the Iapetus suture. This provides a hitherto unknown near-surface conductive zone coincident with the geomagnetic anomaly.

(e) A localized lateral variation in the depth to the crustal/mantle conductor exists in the Duns area in the neighbourhood of KET; this may be coincident with a fault zone.

(f) The most probable cause of the upper mantle conductor is partial melting. The upper/lower crustal conductor is probably due mainly to electrolytic conduction in the rock pores and fissures and presence of hydrated minerals.

(g) It is proposed that a partly serpentinized basaltic composition satisfies the geophysical evidence indicating the presence of rock of high conductivity, moderate magnetisation and low density. This overcomes the shortcomings of the granite composition proposed from previous gravity studies.

(h) 1D modelling clearly shows that a very thin and very conductive upper/lower crustal layer is precluded by AMT/MT data.

(i) The final 2D model is very similar to the 2D section derived from a collation of individual site 1D models of ϱ_{eff} and φ_{eff}, demonstrating that the latter give correct averages for both 1D and 2D structures in this case.

ACKNOWLEDGEMENTS

I would like to express my thanks to Dr. V. R. S. Hutton who suggested the magnetotelluric project and also acted as my main supervisor; her hospitality is gratefully acknowledged. My special thanks to Dr. B. A. Hobbs who was my second supervisor. I also thank Mr. G. J. K. Dawes for help in various aspects of the project, particularly computing advice. My thanks to Professor K. M. Creer, the Head of Geophysics Department and the entire departmental staff for useful discussions and help during the course of my study.

My thanks are extended to fellow postgraduate students in the induction group, particularly Mr. E. R. G. Hill with whom I shared an office, for help with my fieldwork and useful discussions. I am grateful to those geophysics undergraduate students and Mr. A. Jackson who have provided help with the fieldwork. The fieldwork assistance rendered by Mr. D. K. Milling of York University, while learning to use the Edinburgh magnetotelluric system, is greatly appreciated. The suggestion of Dr. C. R. Brewitt-Taylor which enabled the use of a large grid size for the 2D modelling programme is highly appreciated. The author has benefited from discussions with Professor D. I. Gough of University of Alberta and Dr. E. Lagios of Athens University.

I thank Dr. Habberjam and his colleagues at Leeds University for providing information about their deep resistivity sounding in the Duns area. I also thank all the landowners and farmers on whose land the magnetotelluric measurements have been made. My thanks to all others who have in any way helped in the completion of this study.

The Study Fellowship award by Ahmadu Bello University, Zaria (Nigeria) and the Nigerian Federal Government Scholarship, without which I could not have undertaken the study at Edinburgh University, are greatly appreciated.

LIST OF CONTENTS

LIST OF FIGURES

LIST OF TABLES

CHAPTER 1

INTRODUCTION

In this chapter, a brief historical background of the magnetotelluric method is given and followed by a discussion of the project outline and objectives. The magnetotelluric source field as well as the tectonic history, geology and geophysics of the project area are also reviewed.

1.1 General remarks

As a result of time varying electromagnetic (EM) fields impinging on the earth's surface from external sources (ionosphere and magnetosphere), electric currents (telluric currents) are induced in the earth. This phenomenon is called EM induction. These induced currents, which depend on conductivity (global, local or both), give rise to associated magnetic fields measurable on the earth's surface. The relation between the surface magnetic and electric fields can be defined in several ways, each providing a parameter which can be termed an earth response function. The earth's response is diagnostic of the electrical conductivity of the subsurface. From a knowledge of the electrical conductivity, information about other physical properties of the subsurface can be deduced;

from lateral conductivity variations, composition and structural information may be determined. These factors are of immense importance in our understanding of the past and present plate movements.

It is now well established that the magnetotelluric (MT) technique is one of the most effective of the EM induction methods. From an evaluation of the various techniques for detecting possible conductivity changes within the resistive deep crust and upper mantle, Vozoff (1980) has stated that in an exposed shield area, MT measurements alone can detect a change, but that the resolution improves by adding a few d.c. resistivity measurements with large electrode spacing.

With the MT technique, the variation of conductivity with depth is determined from the ratio at the earth's surface of the orthogonal horizontal magnetic and electric field components of the natural time variations of the earth's magnetic field of increasing period.

The recognition of the close relationship between the geomagnetic time variations and the telluric currents flowing in the ground stemmed from the early work of Tikhonov (1950), Kato and Kikuchi (1950) and Rikitake (1950,1951). However, the MT method of prospecting only started developing rapidly after the classic paper of Cagniard (1953) in which the basic concepts of the method were treated. Berdichevsky (1960) extended Cagniard's formulae to an n-layer case. Price (1962,1963) considered the theory for non-uniform and finite source field. This introduced an additional term dependent on the source

dimensions, period and the earth resistivity. This term is generally negligible for periods less than 1000 s (Porstendorfer, 1975). Srivastava (1965) investigated the influence of the earth's curvature on MT soundings. This is also negligible for periods less than one day (Porstendorfer, 1975). Gamble et al. (1979a,b) introduced the remote reference method to MT whereby impedance tensor elements that are unbiased by random noise may be obtained. The same group has also investigated the severity of the bias errors from correlated noises as the separation of the MT site and the remote reference is reduced to less than 1 km (Goubau et al., 1984).

Strangway et al. (1973) published the first detailed report on audiofrequency magnetotellurics (AMT). The AMT/MT technique has been used in several applications including permafrost studies, crustal/mantle soundings, regional tectonic studies, mapping of resistivities in shales, stratigraphic mapping, geothermal and mineral explorations and the evaluation of sedimentary basins in oil prospecting. Since the detection of time-dependent changes in crustal electrical resistivity over 25 years ago at the Aburatsubo Crustal Movement Observatory in Japan (see a review by Rikitake, 1976), it has been realised that resistivity may be useful as a sensitive indicator of stress changes in the ground. The time-dependent precursory effects of the MT impedances and geomagnetic transfer functions are now being increasingly monitored and used in earthquake predictions (see a review by Niblett and Honkura, 1980).

The MT technique is ideally suited to reconnaissance work. It is the most widely used EM sounding technique in the U.S.S.R. particularly in oil prospecting (Alperovitch et al., 1982; Spies, 1983). It is often used with success in areas unfavourable to the seismic method; for example as a result of shielding by thick basaltic and andesitic layers. Moreover, near vertical boundaries are poorly imaged by seismic techniques, but vertical conductivity boundaries are usually well resolved by MT. It is now increasingly being combined with other techniques in an integrated geophysical approach to investigate the subsurface structure. Berkman et al. (1984) have reported the successful use of the combination of MT and seismic techniques in defining the structure of the South Clay basin, Utah. They have indicated that the use of MT with seismics can produce a structural map at a small fraction of the cost of a similar coverage using seismics alone, while Young and Lucas (1984) have shown that the combined techniques can provide critical information for prospect evaluations in regions hampered by surface volcanics.

1.2 Project outline and objectives

The AMT/MT technique was used in the project. Natural time variations of the magnetic and electric components of the earth's field (3 magnetic and 2 electric components) were recorded in the frequency range 0.01 to 1000 Hz at 22 sites in SE Scotland using close station spacings. Figure 1.1 shows a map of SE Scotland with the site locations.

FIGURE 1.1

AMT/MT site locations in Southeast Scotland with National Grid reference (km):- D.G.F. and S.U.F. are the Dunbar-Gifford and Southern Uplands Faults respectively.

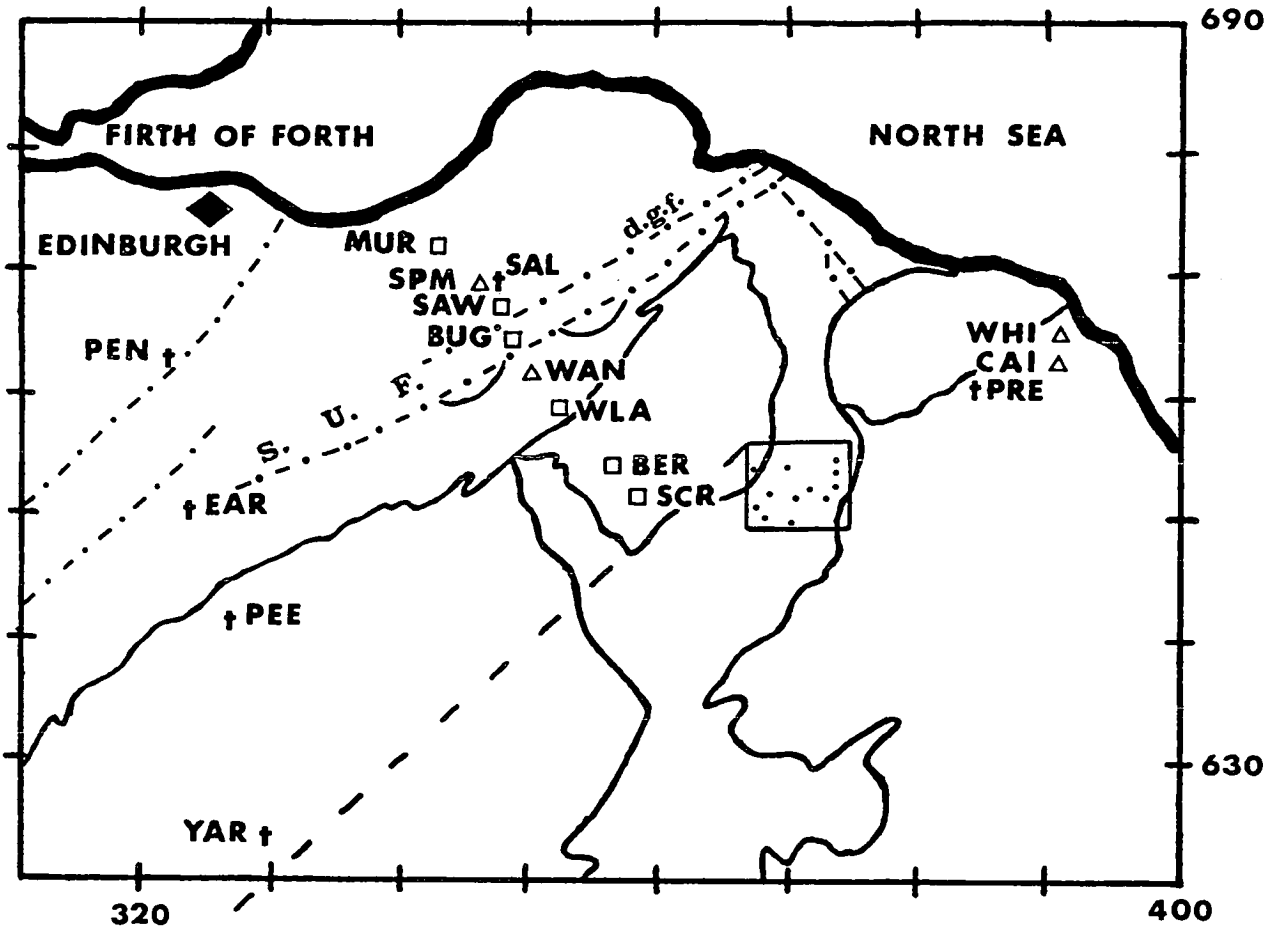

DUNS AREA

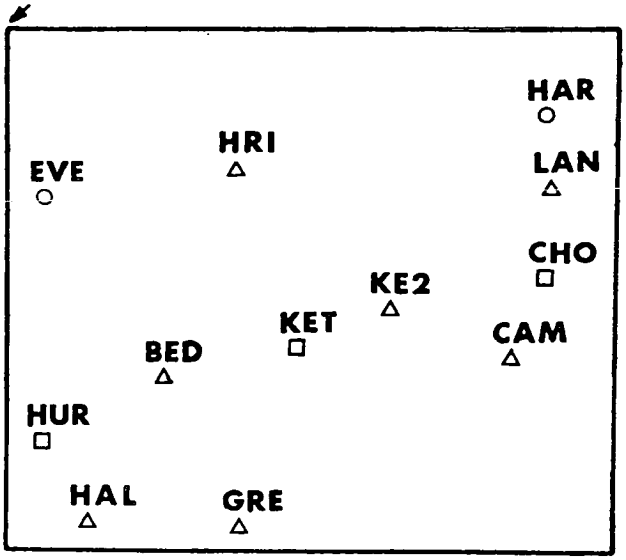

SITES	DATA BANDS
□	1 – 4
△	1 – 3
○	1 – 2
t	others

------ faults

Eight sites lie on a profile ($N40^0W$ geographic) approximately perpendicular to the Southern Uplands Fault (SUF) and these constitute the SUF profile; 12 sites lie in a two-dimensional (2D) array near Duns and constitute the Duns study, while a further 2 sites are located near Coldingham to the NE of Duns area. Also shown in the figure are some of the MT and GDS sites of Jones (1977) and Ingham (1981) which are referred to in chapter 8 dealing with the interpretation of the AMT/MT data. The SUF profile is almost parallel to the Southern Uplands/Midland Valley section (YAR to PEN) of the traverse of Ingham (1981). The data recordings were split into four overlapping bands (see Table 1.1). At some of the sites VLF/R measurements were made in addition to the AMT/MT measurements.

The main objectives of this project were three fold , viz,

(a) comparison of techniques;

(b) investigation of the upper and lower crustal conductivity structure of SE Scotland complementing earlier longer period MT and GDS studies of the deeper structure; the earlier studies were narrow band limited ($\approx$ 20-1000 s) and at widely spaced locations ($>$ 10 km station spacing) and hence their resolution of the upper crustal structure was poor and

(c) comparison of the resulting conductivity model with the recent models proposed by other workers and the evaluation of the contribution the conductivity model makes to our further understanding of the Iapetus suture

TABLE 1.1

Summary of AMT/MT data bands

Bands	1	2	3	4
Frequency range (Hz)	36 - 780	3 - 40	0.125 - 4	0.01 - 0.25
Sampling rate (Hz)	2048	128	16	1
Source field	Worldwide thunderstorms		Pc1, 2; Pi1, Pp	Pc2 - 4; Pc1, Pi1, 2
Induction coils	CM16	CM16	CM11E	CM11E
Electrode	Steel	Steel	Copper sulphate	Copper sulphate
Recording equipment	SPAM	SPAM	SPAM	Geologger
Digital data storage	Cartridges	Cartridges	Cartridges	Cassettes
Infield results	Cagniard apparent resistivities and phases, coherences, skew and number of estimates			None

SPAM = short period automatic magnetotelluric system (mark 1)

region and of the tectonics of SE Scotland.

To accomplish the first objective, AMT/MT measurements were made in 1982 and 1983 in a 2D array of sites in the Duns area, where the resistivity group of Leeds University under Dr. Habberjam had carried out measurements using Habberjam's square and dipole-dipole array techniques (Tsokas, 1980). The latter techniques will be referred to as HAB for short. HAB and AMT/MT results are compared in chapter 6 and an evaluation of the two techniques from the exploration viewpoint is given in section 6.3.

To accomplish the second objective, AMT/MT as well as VLF/R measurements were made in 1983 and 1984 along a profile across the SUF (see Fig. 1.1). The accomplishment of the third objective involved 1D and 2D modelling of the AMT/MT data and the interpretation of the resulting conductivity model.

1.3 Source field

The AMT/MT method makes use of the energy provided by the time variations of the earth's magnetic field, which induce eddy (telluric) currents in the earth. Their energy spans the period range from less than 1 millisecond to several years. The very short period variations do not normally penetrate into the earth appreciably (see Fig. 2.1) and hence are only useful in shallow electrical soundings.

A typical average amplitude spectrum of these magnetic variations (Fig. 1.2a) shows a minimum at about 1 Hz. Thus, the spectrum can be visualised as consisting of two types

FIGURE 1.2A

Typical amplitude spectrum of magnetic variations in the ELF range (after Keller and Frischknecht, 1966).

FIGURE 1.2B

Geomagnetic pulsation spectrum in the lower frequencies (after Campbell, 1966).

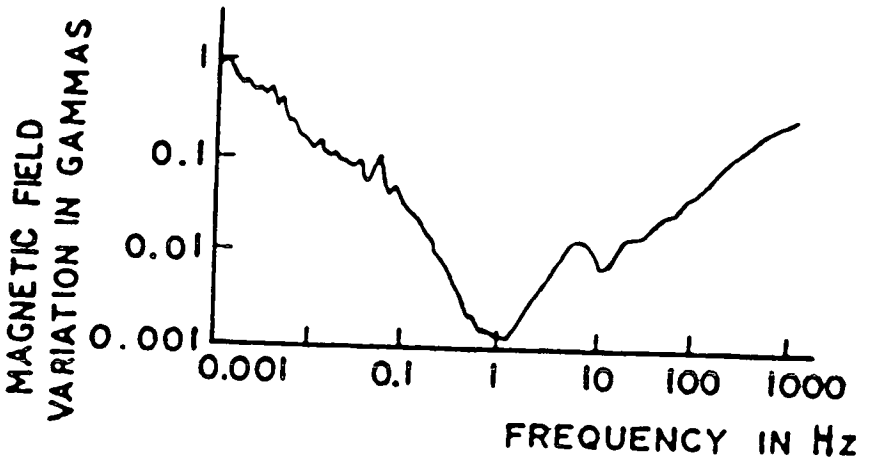
MAGNETIC FIELD
VARIATION IN GAMMAS
1
0.1
0.01
0.001
0.001
0.1
1
10
100
1000
FREQUENCY IN Hz

(a)

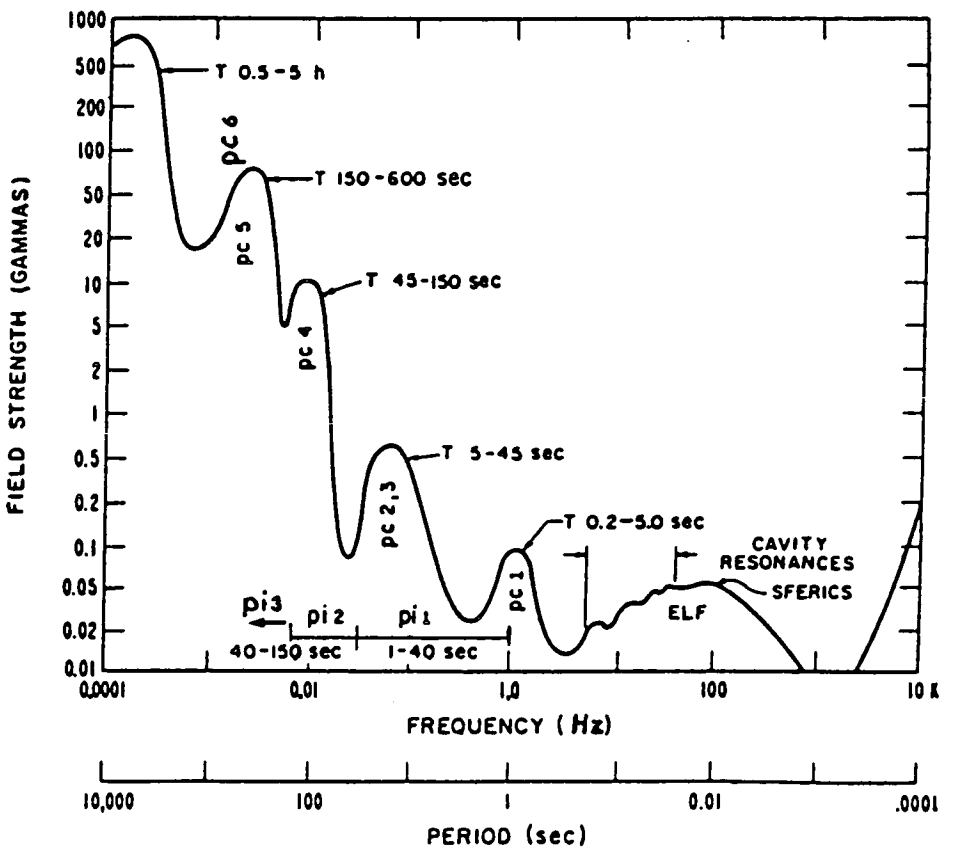
FIELD STRENGTH (GAMMAS)
1000
500
200
100
50
20
10
5
2
1
0.5
0.2
0.1
0.05
0.02
0.01
T 0.5-5 h
pc 6
T 150-600 sec
pc 5
T 45-150 sec
pc 4
T 5-45 sec
pc 2,3
T 0.2-5.0 sec
pc 1
CAVITY
RESONANCES
SFERICS
ELF
pi3
pi 2
pi 1
40-150 sec
1-40 sec
0.0001
0.01
1.0
100
10 k
FREQUENCY (Hz)
10,000
100
1
0.01
.0001
PERIOD (sec)

(b)

of activities, one above and the other below 1 Hz. Each of these is described below. A very general picture of the natural EM field variation in the lower frequencies is depicted in Fig. 1.2b.

(a) The source field above 1Hz

MT fields of frequencies above 1 Hz are generally produced by lightning strokes, whose signal is known as sferics. Worldwide thunderstorm activity is the primary source of these MT fields. The three main storm centres are located in Brazil, Central Africa and Malaysia, each of which has regionally at least 100 storm days per year and locally within them 200 storm days per year. These storm centres are geographically uniformly distributed with the result that on the average there is a storm in the making at any given time (Patra and Mallick, 1980). Frequent thunderstorm activity associated with the movement of cold fronts is also observed in the temperate zones.

It has been observed that the peaks of sferics activity occur in the early afternoon, local time. In most lightning strokes, a leader stroke travels from the cloud to the ground and this is followed by a return stroke. Very few lightning strokes are confined between clouds.

The sferics propagate round the world in the waveguide formed between the earth and the ionosphere. There is continuous reflection of energy between the lowermost layer of the ionosphere and the earth. Thus, the width of the waveguide is 60 km in the daytime and 90 km at night, the respective heights of the D- and E-layers of the ionosphere.

Although the source of sferics contains a very wide frequency spectrum, it has been found that as the pulse propagates round the world, certain frequencies are lost while some are enhanced. The enhanced ones are often called preferred frequencies and those at which energy peaks have readily been observed (8, 14, 20, 25 Hz) are called Schumann resonances. A strong absorption in the waveguide at about 2 kHz was first reported by Chapman and Mathews (1953). Strangway et al. (1973) have also reported this absorption and observed that it is stronger in the morning than in the evening. Although the sferics levels are dependent on the distance from the source, in general, the levels are higher in the lower latitudes, higher in the afternoon than in the morning and higher during the summer than winter (Patra and Mallick, 1980).

Wind vibration of the coils and ground vibrations can generate very low frequency spurious signals in the magnetic field, while similar signals are generated in the electric field by ground discharge currents from direct lightning strokes. Both spurious signals are often uncorrelated. Other sources of EM fields of frequency above 1 Hz are man-made power distribution systems; the energy from these sources is normally very limited.

(b) The source field below 1 Hz

This type of source field is produced by micropulsations (geomagnetic pulsations) which are quasi-periodic temporal variations in the earth's magnetic field. They result from the complex interactions between the earth's permanent magnetic field and the solar wind originating from the sun.

The amplitudes of micropulsations range from a small fraction of a nanotesla, nT (=1 gamma, γ) to a few hundred nT in the auroral zones/polar regions. This is an indication that the physical processes involved in their generation may differ greatly from one type to another. A detailed review of experimental and theoretical micropulsation studies has been presented by Orr (1973).

Micropulsation activity consists of regular pulsations Pc (pulsation continuous), irregular pulsations Pi (pulsation irregular) and "pearls" pulsations Pp. Their periods range from 0.2 to 1000 s as shown in Table 1.2 together with their predominant times of occurrence (after Jacobs et al., 1964 and Rokityansky, 1982).

TABLE 1.2

Classification of geomagnetic micropulsations

Type	Period range (s)	Dominant occurrence time
Pc 1	0.2 - 5	M and D
Pc 2	5 - 10	M to D
Pc 3	10 - 45	M to D
Pc 4	45 - 150	M to D
Pc 5	150 - 600	M to D and D to E
Pc 6	above 600	D and N
Pi 1	1 - 40	N, M, D
Pi 2	40 - 150	N, D
Pi 3	above 150	N, D
Pp	0.3 - 3	M and E

where M, D, E, N denote respectively morning, daytime, evening and night. The different occurrence times relating to different subtypes of Pi are separated by commas.

Micropulsations are assumed to be the direct result of the motion of charged particles above the base of the ionosphere. Thus, the current idea about micropulsations is that they arise from magnetohydrodynamic (MHD) waves which propagate in the earth's magnetosphere. On reaching the lower limits of the ionosphere, MHD waves are observed on the earth's surface as pulsations of the magnetic field and earth currents (Jacobs, 1970). The properties of these pulsations have been extensively studied by Jacobs et al. (1964), Troitskaya (1967), Campbell (1967), Jacobs (1970), Hessler et al. (1972), Baransky et al. (1981), Bosinger et al. (1981) and Kangas (1982) among others. However, the exact theories of the origin of geomagnetic pulsations are not yet fully understood and hence, pulsation research is an active area.

Several factors have been shown to affect micropulsation activity at any station, e.g., the time of day, the state of the local ionosphere, the level of geomagnetic activity which is controlled by the particles and EM radiation emitted by the sun, the time in the solar cycle and seasonal effects. The well established important effects of the ionosphere on micropulsations are a 90^0 rotation of the wave in the horizontal plane as it passes through the ionosphere to the ground (Inoue, 1973) and the attenuation and smoothing of the wave field between the ionosphere and the ground; more pronounced for short wavelengths.

Vero (1981) has shown that pulsation amplitudes correlate with solar wind velocities with the exception of

some months around December in solar maximum years, when they are significantly lower than those calculated from the corresponding solar wind velocities; this decrease can be caused by either a cutoff of the magnetospheric shell resonances or by local ionospheric damping. He has also shown that pulsation amplitudes depend slightly on geomagnetic activity and have a semi-annual activity change with maxima around the equinoxes.

The regular pulsations are the most prominent on any record of the variations of the electric or magnetic field components. Pc1 are narrow-band pulsations observed during quiet magnetospheric conditions and may last for about an hour. They are elliptically polarised and have amplitudes in the range 0.01 to 0.1 γ. They are considered to arise from magnetospheric ion cyclotron waves and propagate in wave packets along field lines between conjugate points. On account of dispersion, the wave packets will spread with the low frequency components travelling faster than the high frequency ones and hence result in the observed rising tone of the signal on the earth's surface (Troitskaya, 1967). Baransky et al. (1981) and Kangas (1982) have pointed out that (i) the source of the short period (< 1 s) Pc1 pulsations occurs well within the plasmapause, while that of the longer period Pc1 is near the plasmapause; (ii) the frequency of Pc1 exhibits a diurnal variation with the maximum frequency occurring during the local dawn hours (04 to 05 LT) and on the average rising prior to this and decreasing after; (iii) this diurnal variation is associated with the displacement of

the Pc1 source region, i.e., the source is displaced to higher L-values in the course of the local morning hours and (iv) this source displacement does not coincide with the diurnal movement of the plasmapause.

Pc2 - 4 pulsations are predominantly dayside phenomena, while Pc5 have occurrence peaks in the morning and evening hours (Jacobs and Sinno, 1960a,b). Pc6 are predominantly nightside phenomena (Rokityansky, 1982).

The period of Pc2 - 4 decreases with increasing disturbance so that Pc2 are associated with strongly disturbed magnetic conditions. Their amplitudes are higher at auroral and subauroral latitudes, but vary typically from 0.5 γ for Pc2 to 5 γ for Pc4. Pc5 are predominantly high latitude events with a sharp maximum near the auroral zone. The amplitude of Pc5 is commonly 100 γ, but occasionally much larger. Pc5 also show period variation with latitude and a reversal of the horizontal sense of polarisation across the latitude of resonance. The latitude of maximum amplitude increases with increasing period and the phase of the wave changes most rapidly across the latitude of resonance (Green, 1981). It has been suggested that the interaction of the solar wind with the magnetopause gives rise to Pc5 (Jacobs, 1970). Two forms of Pc6 have been recognised with their excitation occurring in the daytime and night hours. It is believed that these are respectively generated at the magnetopause and in the interior of the magnetosphere (Kaufman and Keller, 1981).

Irregular pulsations usually occur as damped trains of waves which often follow each other in irregular sequence.

They are associated with disturbed conditions in the magnetosphere and their existence is a part of the microstructure of substorms. Pi1 often appear as riders on the long period Pi2 pulsations. Pi2 have been observed to predominate in the night-time with maximum occurrence around local midnight, but some have been detected in the daytime (Volker, 1968). Pi2 pulsations are believed to originate from Alfven waves in the magnetospheric cavity in the region where the neutral sheet begins (Raspopov, 1968).

"Pearl" pulsations, Pp, appear to correlate with auroral displays and are commonly amplitude modulated with a modulation period of about 20-30 s (Patra and Mallick, 1980). They occur at sunrise and sunset indicating their probable association with a transient condition near the night-day boundary in the ionosphere.

1.4 Tectonic history, geology and geophysics of SE Scotland

Even though the project area is in SE Scotland, a discussion of the tectonic history, geology and geophysics of the area will invariably encompass the whole of South Scotland, which extends from the Grampian Highlands in the north to the Scottish Borders in the south. It consists of three regions, viz form north to south, the Grampian Highlands, the Midland Valley and the Southern Uplands. The Highland Boundary Fault separates the first two regions, while the Southern Uplands Fault separates the last two regions. Figure 1.1 shows the section of South

Scotland referred to here as SE Scotland.

1.4.1 Tectonic history

Moseley (1977) has given a detailed review of some of the many plate tectonic models (Figs. 1.3A-I) which have been advanced to explain the geology of the termination of the British Caledonides and hence only a brief discussion of the tectonic history is presented here. The notion that a proto-Atlantic ocean (the Iapetus) existed in the Lower Palaeozoic time, with the north of Scotland being part of the American plate and the Scottish Borders and England part of the European plate, was first put forward by Wilson (1966) from consideration of faunal, tectonic and stratigraphic evidence. Although it is now firmly accepted that South Scotland marks the point of closure of the Iapetus in the Upper Palaeozoic time, the processes leading to the closure is still uncertain and hence there is keen interest in studies related to the tectonic history of South Scotland.

Kennedy (1958) and George (1960) have suggested that Precambrian basement underlies the Midland Valley and probably the region further south. Dewey (1969,1971) and Dewey and Pankhurst (1970) have suggested that subduction took place both in the northwest near the SUF and in the southeast under the Solway-Northumberland basin (Fig. 1.3A). Fitton and Hughes (1970) and Church and Gayer (1973) have endorsed this subduction theory with their conclusions differing only in detail (Figs. 1.3B,C). Garson and Plant

FIGURE 1.3

Summaries of some of the hypotheses which have been advanced to explain the closing of the proto-Atlantic ocean or Iapetus:-

A to I (from Moseley, 1977), HB indicates the Highland Borders;

J (after Phillips et al., 1976).

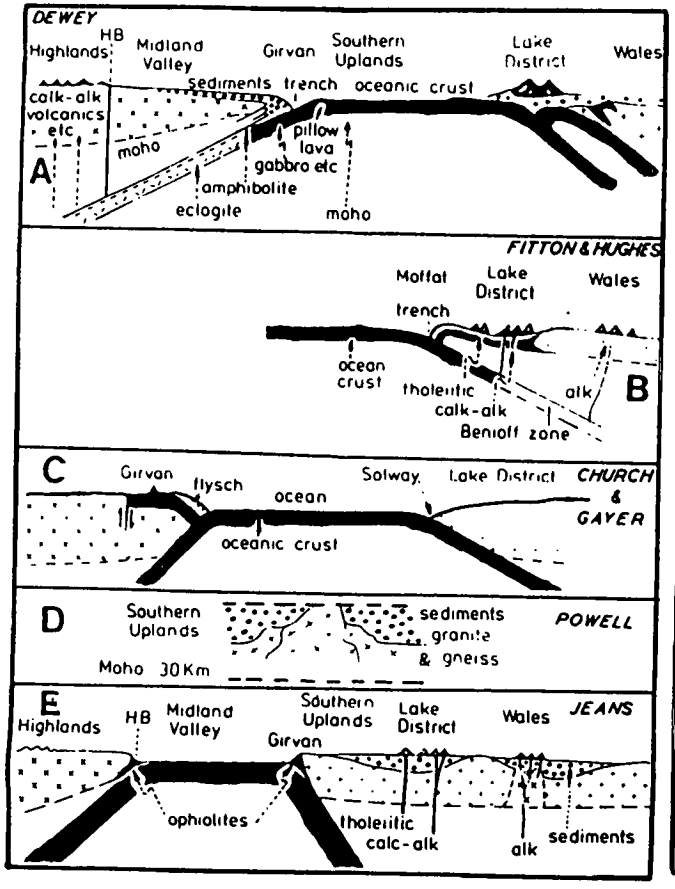
DEWEY
HB
Highlands
Midland Valley
Girvan
Southern Uplands
Lake District
Wales
sediments
trench
oceanic crust
calk-alk volcanics etc
moho
pillow lava
gabbro etc
A
amphibolite
eclogite
moho
FITTON & HUGHES
Moffat
Lake District
Wales
trench
ocean crust
tholeiitic
calk-alk
alk
B
Benioff zone
C
Girvan
flysch
ocean
Solway
Lake District
CHURCH & GAYER
oceanic crust
D
Southern Uplands
sediments
granite & gneiss
POWELL
Moho 30Km
E
Highlands
HB
Midland Valley
Southern Uplands
Girvan
Lake District
Wales
JEANS
ophiolites
tholeiitic calc-alk
alk
sediments

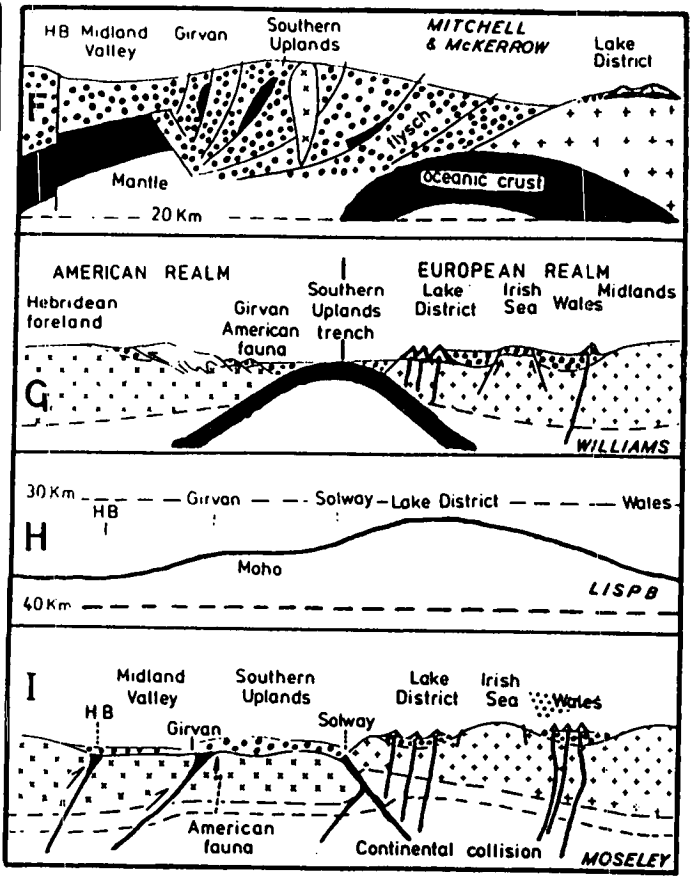
HB
Midland Valley
Girvan
Southern Uplands
MITCHELL & McKERROW
Lake District
F
flysch
Mantle
oceanic crust
20Km
AMERICAN REALM
EUROPEAN REALM
Hebridean foreland
Girvan American fauna
Southern Uplands trench
Lake District
Irish Sea
Wales
Midlands
G
WILLIAMS
30Km
Girvan
Solway
Lake District
Wales
HB
H
Moho
LISPB
40Km
I
Midland Valley
Southern Uplands
Lake District
Irish Sea
Wales
HB
Girvan
Solway
American fauna
Continental collision
MOSELEY

J

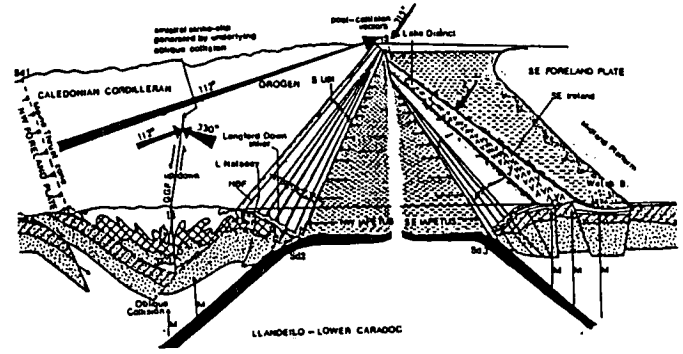
CALEDONIAN CORDILLERAN
OROGEN
SE FORELAND PLATE
LLANDEILO – LOWER CARADOC

(1973) have postulated the existence of a northward Benioff zone between the Midland Valley and Southern Uplands in their explanation of the calc-alkalic volcanicity in the Midland Valley in the Lower Devonian times. The models of Jeans (1973, see Fig. 1.3E) and Gunn (1973) also indicate an oceanic crust under the Midland Valley. Thus, the Midland Valley and possibly the Southern Uplands have been portrayed in all the above models as underlain by an oceanic crust.

The seismic refraction result of Agger and Carpenter (1964) in the vicinity of Eskdalemuir points to continental crust in the area. Powell (1971) has indicated with evidence from gravity, magnetic, resistivity and seismic results that continental crust underlies the Southern Uplands (Fig. 1.3D). From the analysis of the seismic refraction data from the Lithospheric Seismic Profile of Britain (LISPB), Bamford et al. (1976,1977,1978) have indicated the existence of continental crust, possibly Lewisian basement under the Midland Valley and that the same basement may lie under the Southern Uplands. They have determined the Moho to lie between 30 and 40 km depth (Fig. 1.3H). All these geophysical studies among others, support the speculation of Kennedy (1958) and George (1960) that continental crust is present under the Midland Valley, while contravening that of Dewey, Gunn and others that remnant oceanic crust exists there.

Mitchell and McKerrow (1975) have drawn an analogy between the tectonic evolution of the Caledonides in Britain in the Ordovician times and that of the Burma

orogeny of Tertiary age. They have compared the Scottish Grampian Highlands, the Midland Valley and Southern Uplands with the eastern Highlands, the central Lowlands and the Indoburman ranges of Burma respectively. Their model of the Scottish Caledonides encompasses two subduction zones dipping northwestwards, one on the northern margin of the Midland Valley and the other, which occurred later, on the south of the Southern Uplands (Fig. 1.3F). The Southern Uplands and the Midland Valley are underlain by oceanic crust in this model and the 30 km depth to the Moho (Powell, 1971) is explained either by tectonically thickened turbidites or by the under-riding of the region by the Lake District from the south when the final continental collision occurred. Figures 1.3G and I show respectively models proposed by Williams (1969,1976) and Moseley (1977).

Phillips et al. (1976) have proposed a comprehensive model (Fig. 1.3J) for the British Caledonides consisting of two Benioff zones, i.e., one each under the Southern Uplands and Northern England, which are at an angle of 14^0-18^0. Hence, the collision between the Southern Uplands and Northern England is considered to have occurred at a triple junction which has migrated progressively southwestwards. The latter can account for the progressively later volcanic activity to the southwest. Phillips et al. (1976) have argued that the final closure of the Iapetus occurred at the end of the Silurian and have placed the position of the final closure (Iapetus suture) in the present Solway Firth. This seems to be the currently accepted view. Leggett et al. (1979) have used this suture position in their crustal

evolution model to account for the geological processes in Southern Scotland, including stratigraphic differences and the occurrence of reverse strike faults.

From the above discussions, it is clear that the tectonic setting of South Scotland is very complex and its tectonic history is by no means certain. It is possible that there is now no relic of the oceanic crust to identify the final position of the Iapetus suture (Moseley, 1977).

1.4.2 Brief geology

SE Scotland is divided into two distinct parts by the SUF. North of the SUF is the Midland Valley and south of it is the Southern Uplands. A detailed description of each of these is contained in the respective handbook of the British Regional Geology series by MacGregor and MacGregor (1948) and Greig (1971) and what is presented here is an extract from these sources. The geological map of SE Scotland is shown in Fig. 1.4.

The Midland Valley is a broad undulating lowland tract occupied mainly by Devonian and Carboniferous sedimentary formations, with the latter occupying much the greater part. Since it is bounded by two faults, it is an ancient rift valley (graben). Broadly speaking, the Carboniferous rocks are arranged in a wide compound syncline underlain and flanked by strata of Old Red Sandstone age and the axes of folding are generally NE-SW (MacGregor and MacGregor, 1948). In both formations there are locally great thicknesses of contemporaneous igneous rocks (lavas

FIGURE 1.4

Geological map of SE Scotland; the two rectangles indicate the regions where the AMT/MT measurements of the present study have been made.

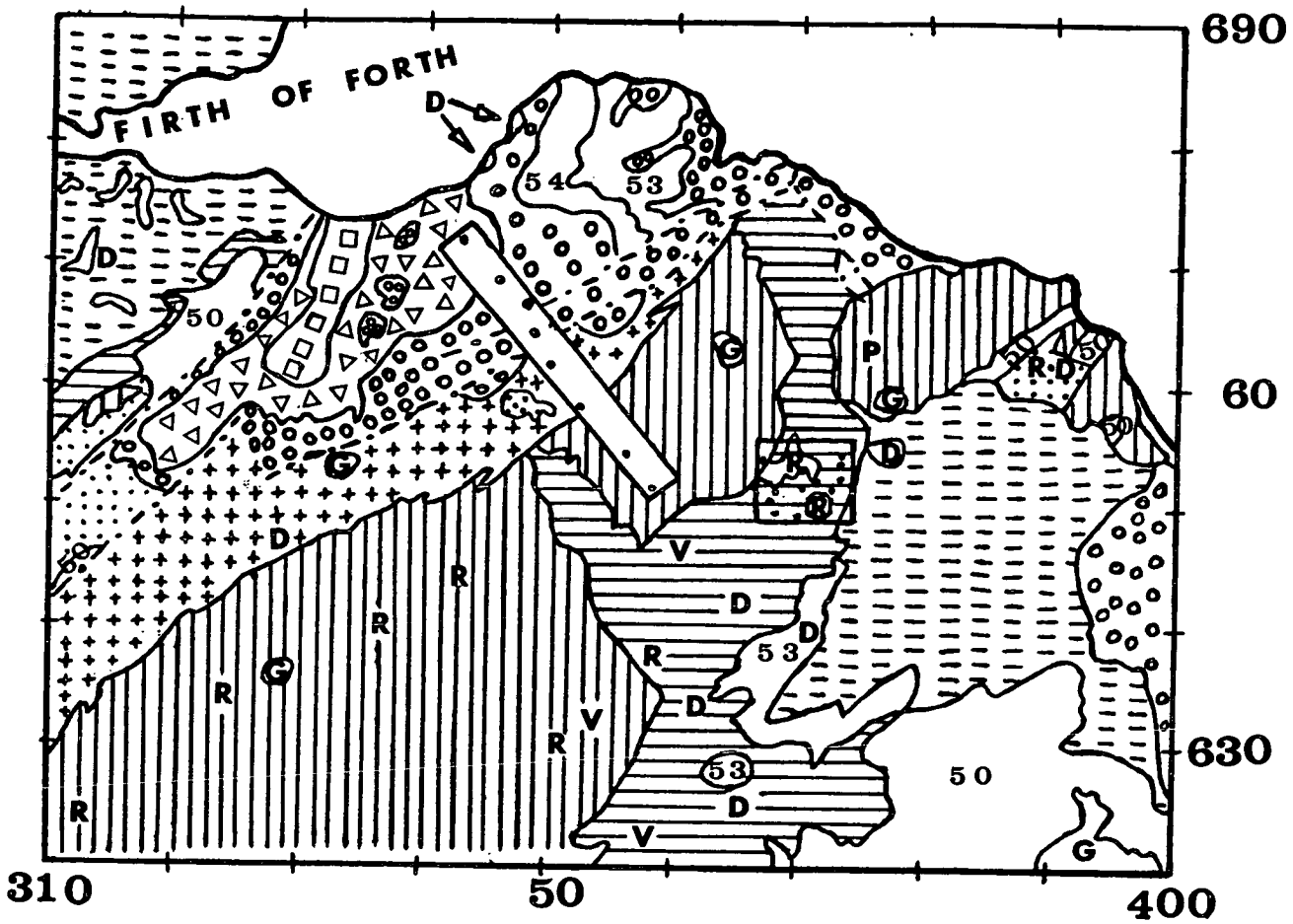
FIRTH OF FORTH
690
60
630
310
50
400
0
30 Km
Fault
coal measures
millstone grit series
Limestone series
Calciferous sandstone series
Carboniferous
Upper old red sandstone
Lower old red sandstone
Devonian
Llandovery and Birkhill shale
Silurian
Ashgill and Caradoc
Ordovician
54 Tracyte and rhyolite
53 Basalt and spilite
Extrusiv
50 Andesitic and basaltic lavas and tuffs, undifferentiated
V Agglomerate in neck
R Rhyolite, tracyte and felsite
P Porphyrite and lamprophyre
D Dolerite, basalt and Camptonite
G Granite, syenite and granophyre
Intrusiv

and tuffs) and many intrusions (vents, plugs, sills and dykes). The mainly olivine-basalt lavas indicate intense volcanic activity in Carboniferous times and the numerous basic intrusive sills represent subterranean injection of molten magma that accompanied surface eruptions (MacGregor and MacGregor, 1948). Rocks of Ordovician age cover a considerable area on the southwest margin of the Midland Valley and there are a number of Silurian inliers along the southern margin. The Midland Valley is traversed by numerous faults of varying magnitudes.

The Southern Uplands is a broad zone of dissected high land occupied mainly by Lower Palaeozoic sedimentary rocks of the Ordovician and Silurian systems (Greig, 1971). The Silurian rocks are highly folded and their outcrop is modified in several places by the presence of Ordovician inliers. In contrast to the younger formations, the beds are strongly folded with the trend of the structures between NE and ENE. These rocks are mainly greywackes, consisting of sandstone, siltstones and shales. They were deposited on the floor of an elongate marine trough, which was at the time evolving in response to the deep-seated stresses of the Caledonian earth movements and to the weight of the sediments themselves (Greig, 1971).

The broad structural pattern in the Southern Uplands is believed to be due to horizontal compression in a north-northwesterly to south-southeasterly direction, giving rise to folding along east-northeasterly axes and the development of strike faults. This compression is a

late expression of the Caledonian orogeny, which has been responsible in several Lower Palaeozoic phases for the development of the geosyncline in which the sediments of the Southern Uplands have been deposited.

Before the deposition of the Old Red Sandstone, the older rocks underwent severe earth-movements and were subjected to great erosion with the result that part of the area became a basin of deposition, the floor of which was occupied by one or more lakes (Greig, 1971). The deposits comprise two distinct subdivisions - the Lower Old Red Sandstone and the Upper Old Red Sandstone. The earliest sediments, consisting of sandstones and conglomerates, were laid down on the upturned edges of the older rocks. The conglomerates were deposited as torrential gravels. Great thicknesses of lava were poured out of volcanoes situated along the flanks of the high ground bordering the depressed area, with some of the lavas flowing into lakes where they were later covered by sediments.

The marked unconformity at the base of the Upper Old Red Sandstone is indicative of further upheaval and very extensive denudation of the area. During the subsidence which followed, sediments consisting mainly of conglomerates, sandstones and marls were spread over the Lower Palaeozoic rocks far beyond the boundary of the early basin. As a result of pre-Upper Old Red Sandstone denudation, the Lower Old Red Sandstone occupies relatively small areas of Southern Uplands and the extent of the denudation is exemplified by the disconnected nature of the

remnants of the earlier formation.

The extensive outcrops of lavas and the abundance of volcanic necks and various forms of intrusions in the south and east of the Southern Uplands (i.e., Duns area around Greenlaw and south) provide ample evidence of widespread volcanic activity in those areas in the Carboniferous times (Greig, 1971). Olivine-basalt is the most common volcanic rock.

1.4.3 Previous geophysical studies

This will be reviewed briefly under three main categories: electrical, gravity and seismic studies and hence not in chronological order across these categories.

Apart from the first MT measurements made at Eskdalemuir by Jain (1964) and Jain and Wilson (1967) who indicated the presence of a lower crustal conductor, the early induction studies in South Scotland used the geomagnetic deep sounding (GDS) technique. Osemeikhian and Everett (1968) reported an attenuation of the vertical magnetic field component in their GDS measurements at Eskdalemuir. This was termed the Eskdalemuir magnetic variation anomaly. Edwards et al. (1971) confirmed the presence of an anomalous region centred on Eskdalemuir from their magnetometer array study of the British Isles south of the SUF. They ascribed this anomaly to electric currents induced in the North Sea leaking through the lower crustal conductor indicated by Jain and Wilson (1967) under the Southern Uplands into the Irish Sea. From a

reinterpretation of the data of Edwards et al. using the hypothetical event technique of Bailey et al. (1974), Bailey and Edwards (1976) suggested that the lower crustal conductor could be the remains of the Iapetus oceanic crust.

From short period (10-600 s) micropulsation studies at Eskdalemuir and Earlyburn, Green (1975) suggested a resistivity contrast across the SUF with the Southern Uplands as the more resistive region.

A magnetometer array survey of the whole of Scotland which was undertaken by Hutton et al. (1977) also delineated the Eskdalemuir anomaly. The report by Jones and Hutton (1979a,b) of the 1D models of the extensive long period MT measurements in South Scotland made by Jones (1977) indicated a lower crustal conductor under the Midland Valley and the Southern Uplands with the depth to it in these two regions being about 12 and 24 km respectively. Ingham (1981) made long period MT measurements on a linear traverse across South Scotland. A 2D model resulting from the latter reported by Ingham and Hutton (1982a,b) indicated the presence of a lower crustal conductor under the Midland Valley and Southern Uplands at varying depths along the traverse in general agreement with Jones and Hutton (1979a,b). The AMT/MT profile in SE Scotland reported in this thesis is approximately parallel to Ingham's traverse but to the NE of it and hence, a detailed reference is made to his 2D model in chapter 8.

The resistivity group of Leeds University carried out a deep resistivity sounding in the Duns area of the Southern Uplands in 1980 using the square and dipole-dipole array techniques of Habberjam. The results of the interpretation of the Duns data by Tsokas (1980) and Roxis (1984) indicated a series of moderately conducting layers in the uppermost 1.2 km overlying a resistive half-space.

A gravity survey in the western part of the Midland Valley, SW part of the Grampian Highlands and Southern Uplands indicated that the regional Bouger gravity anomaly was characterised by a westwards gravity rise and by a gravity high over the Midland Valley, with the latter decreasing towards the Grampian Highlands and the Southern Uplands (McLean and Qureshi, 1966). They interpreted the latter gravity feature as indicating a crustal thickening under the Grampian Highlands and the Southern Uplands compared with the Midland Valley.

From a gravity survey in the Midlothian coalfield, covering the southern part of the Midlothian syncline and extending into the Penicuik syncline, Hipkin (1977a,b) suggested a Lower Devonian age for the Leadburn Fault (part of the SUF west of Earlyburn).

An extensive gravity survey was undertaken by Lagios (1979) in SE Scotland. From the interpretation of the resulting Bouger gravity anomaly as well as aeromagnetic modelling, Lagios (1979,1984) and Lagios and Hipkin (1979,1982) have concluded that a massive granite batholith underlies the greater part of the eastern Southern Uplands.

Blaxland et al. (1979) determined the lead isotopic composition of feldspar separates from granite samples from different parts of Scotland and found those from the Southern Uplands to be more radiogenic than the rest. They have concluded that the rocks to the north of the SUF contain a significant component of Lewisian crust, while those from the south are younger with a composition close to either the underlying mantle or a mixture of the latter and the overlying sediment.

Using the Eskdalemuir seismological array, Jacob (1969) reported a distinct refraction horizon at 12 km under the Southern Uplands and that the seismic velocity increased from 5.54 km/s near the surface to 5.94 km/s at about 12 km depth followed by a sudden jump to 6.44 km/s at this depth. Also using the Eskdalemuir array and stations from the Firth of Forth, Christie (1978) reported an upper crustal layer with a compressional wave velocity of 5.7 km/s overlying a 6.4 km/s layer. These results indicate a nomal continental crust, about 30 km thick. From seismic studies at several sites in the Midland Valley, Hall (1970,1971,1974) reported a compressional wave velocity of 3.65-4.30 km/s for the near surface Lower Palaeozoic rocks.

The 1974 LISPB deep seismic refraction profile was carried out on a N-S traverse across Britain. From an analysis of the South Scotland section of this profile, Bamford et al. (1978) have shown that the nature of the Moho discontinuity changes from a sharp transition under the northern part of the Midland Valley to a gradual change under the Southern Uplands. They have also stated

that there is possibly a major horizontal discontinuity in the pre-Caledonian basement between the Midland Valley and the Southern Uplands in the neighbourhood of the SUF and that the lower crustal layer appears to shallow beneath the Southern Uplands. Hall et al. (1983) have reappraised old data (LISPB and others) and have presented evidence to indicate the presence in the Southern Uplands of Scotland of crystalline rocks of continental affinity at shallow depth (1-5 km) in at least two zones approximately parallel to the Caledonoid strike. This is in contrast with the implied discontinuity in the pre-Caledonian basement by Bamford et al. (1978) based on the lack of crystalline rocks.

The results of some of the above studies will be discussed further in chapter 8 in conjunction with the results of the AMT/MT project reported in this thesis.

CHAPTER 2

REVIEW OF THE MT THEORETICAL FORMALISM

The theoretical foundation of the AMT/MT technique is reviewed. The theory relevant to induction in one-dimensional, two-dimensional and three-dimensional structures is discussed. This is followed by a discussion of the response functions of the earth and direct transformation of AMT/MT data.

2.1 Basic MT theory

Using Maxwell's equations and the constitutive relations (S.I. units), it can be shown that the equation representing the propagation of the electric field vector $\underline{E}$ in a homogeneous and isotropic medium is of the form

$$\nabla^2\underline{E} = \mu\sigma\partial\underline{E}/\partial t + \mu\varepsilon\partial^2\underline{E}/\partial t^2 \qquad (2.1)$$

where σ, μ, ε are respectively the conductivity, permeability and permittivity of the medium. The equation for the propagation of the magnetic field vector $\underline{H}$ is obtained by replacing $\underline{E}$ by $\underline{H}$ in equation (2.1).

Assuming a time dependence of the form $\exp(i\omega t)$, where ω is the angular frequency of the source field and $i=\sqrt{(-1)}$, equation (2.1) becomes

$$\nabla^2\underline{E} = \omega^2\mu\varepsilon(i\sigma/\omega\varepsilon - 1)\underline{E} \qquad (2.2)$$

In AMT/MT induction studies in the earth, $\sigma/\omega\varepsilon >> 1$ for most frequencies of interest. This implies that displacement currents are negligible compared with conduction currents. Thus, equation (2.2) reduces to

$$\nabla^2\underline{E} = i\omega\mu\sigma\underline{E} \qquad (2.3)$$

The induction problem can thus be considered as that of diffusion of the incident field into the earth (Price, 1962).

2.1.1 One-dimensional (1D) MT theory

In the 1D case, conductivity is assumed to vary only with depth. A right-handed Cartesian coordinate system x, y, z with the +z-axis vertically downwards from the earth's surface is assumed.

(a) Uniform half-space

The earth is treated as a conducting half-space with a plane surface. A general theory of EM induction in such a conductor has developed from the classic paper of Price (1950).

The simplifying assumptions usually made about the source field (Cagniard, 1953) are that it is homogeneous, infinite in dimension and effectively at infinity so that plane EM waves impinge on the earth's surface. Under these conditions, there are no horizontal variations of the EM field, i.e., $\partial/\partial x = \partial/\partial y = 0$. Hence, $H_z = 0 = E_z$ and for the x component, equation (2.3) reduces to

$$d^2E_x/dz^2 = K^2E_x \qquad (2.4)$$

where $K^2 = i\omega\mu\sigma$. From Maxwell's equations

$$H_y = (i/\omega\mu)dE_x/dz \qquad (2.5)$$

Since the fields originate from a source above the earth, all the field quantities must remain finite at $z = \infty$. Hence, the solution of equation (2.4) is of the form

$$E_x = Qe^{-Kz} \qquad (2.6)$$

where Q is a constant.

The ratio of E_x to H_y is termed the impedance Z, i.e.,

$$Z = E_x/H_y = i\omega\mu/K$$

$$= \sqrt{(i\omega\mu/\sigma)} \qquad (2.7)$$

From Schelkunoff (1943), the intrinsic impedance of the medium is given by $(E_x/H_y)|_{z=0}$ and has the same expression as equation (2.7).

From equation (2.7), it can be seen that in a homogeneous and isotropic half-space, the magnetic field lags behind the electric field by $\pi/4$ radians.

The true resistivity of the half-space is

$$\rho = 1/\sigma = (1/\omega\mu)|Z|^2$$

$$= (\tau/2\pi\mu)|Z|^2 \qquad (2.8)$$

In practical EM units, Cagniard (1953) obtained

$$\rho = 0.2\tau|E_x/H_y|^2 \qquad (2.9)$$

where

ϱ = resistivity in ohm-metre;

E_x = variation in the horizontal electric field in mV/km;

H_y = variation in the orthogonal horizontal magnetic field in gamma ($=10^{-9}$ tesla = 1 nT) and

τ = period in seconds.

When the earth resistivity is non-uniform, the right hand sides of equations (2.8) and (2.9) provide apparent resistivities, ϱ_a, which are time dependent.

The depth of sounding is related to period through the depth of penetration or skin depth d which is defined as the depth at which the fields are attenuated to 1/e of their surface values. In other words, d(in metres) = 1/real(K); i.e.,

$$d = \sqrt{(2/\mu\omega\sigma)} \qquad (2.10a)$$

Figure 2.1 illustrates the depth of penetration d for different earth resistivities and EM source field frequencies. Equation (2.10a) is strictly valid for a homogeneous medium. In an inhomogeneous medium, the fields do not have a simple exponential decay and Sims and Bostick (1969) have defined a generalised skin depth d(ω) as

$$\text{Re}\ \{\int_0^{d(\omega)} \sqrt{\ [i\omega\mu\sigma(z)]dz}\ \} = 1 \qquad (2.10b)$$

Another parameter which is sometimes used is called the wavelength λ defined as

FIGURE 2.1

Depth of penetration (skin depth) of EM waves as a function of earth resistivity (10 to 1000 ohm-m) and frequency for the different data bands (after Dawes, 1981).

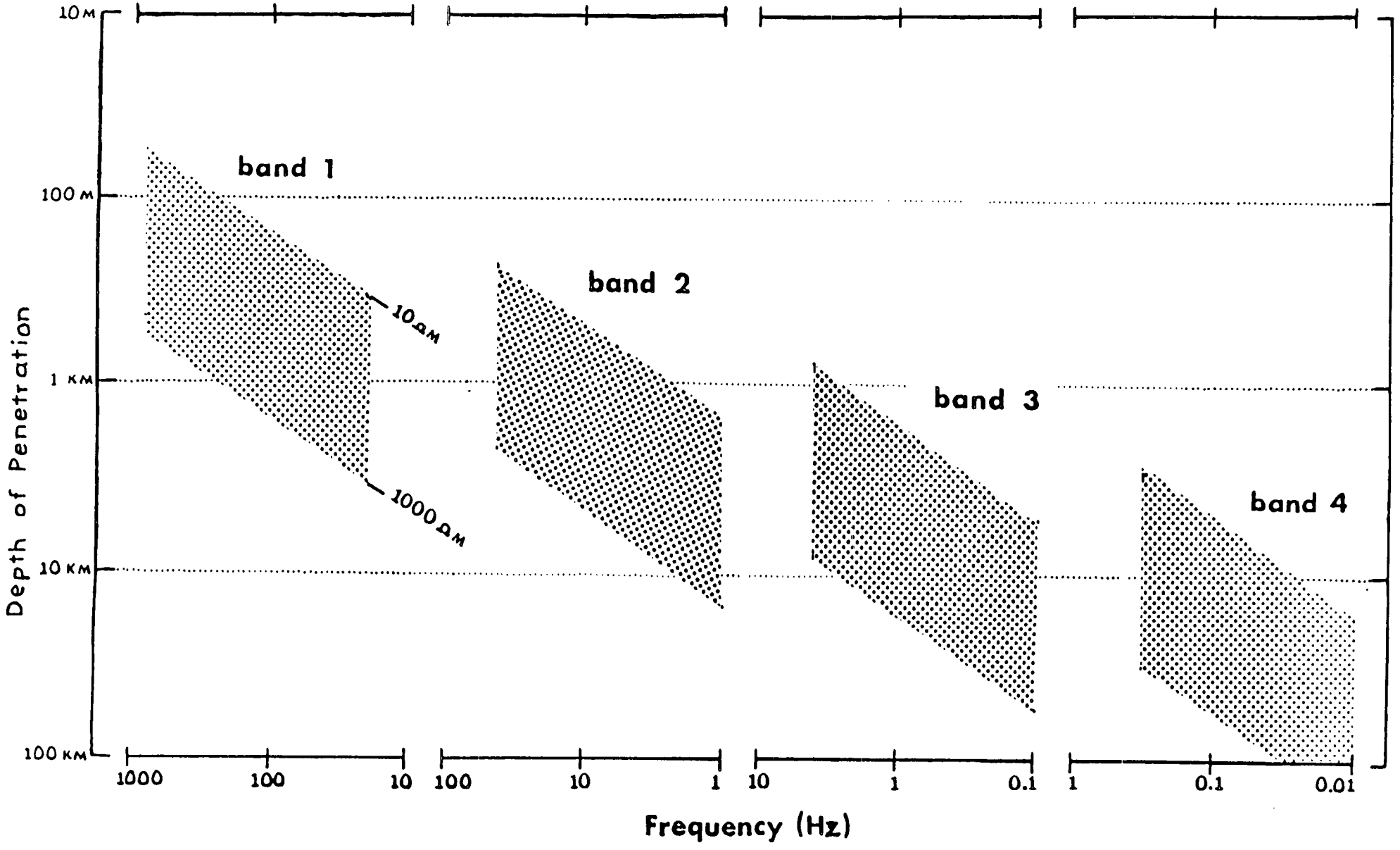
10 M
100 M
1 KM
10 KM
100 KM
Depth of Penetration
band 1
band 2
band 3
band 4
10 Ω M
1000 Ω M
1000
100
10
100
10
1
10
1
0.1
1
0.1
0.01
Frequency (Hz)

$$\lambda = 2\pi d \qquad (2.10c)$$

This parameter is not a characteristic of a propagating field since in MT we are dealing with a pure diffussion process.

The theory discussed so far is strictly valid if Cagniard's assumptions hold. From an investigation of the effect of non-plane wave sources on MT theory, Wait (1954) has pointed out some limitations of Cagniard's plane wave analysis and has shown that corrections for second and higher order spatial derivatives of the source fields must be applied in cases where the tangential electric and magnetic fields vary appreciably in a horizontal distance comparable with the skin depth in the ground. Price (1962) has shown that the limitations mentioned by Wait (1954) become more stringent when the dimensions and distribution of the source fields are considered. He has indicated the modifications which occur when the source field dimensions are taken into account and hence introduced a source field parameter into MT theory. He has given the range estimate of this parameter to be from 1.6×10^{-7} m^{-1} (global fields) to 1.6×10^{-5} m^{-1} (local fields). Madden and Nelson (1964), Srivastava (1965b), Caner (1969) and others have shown from their MT data interpretations with and without source field effects that Cagniard's wave assumption is valid in the vast majority of geological situations for MT periods less than 1000 seconds. Quon et al. (1979) have reviewed in detail the source effect studies.

Since the longest period used in this project is 100 seconds and the sounding depths are less than 100 km and in addition South Scotland is not near a highly localised current system like the auroral or equatorial electrojets, source field effects have been deemed to be insignificant and are hence neglected.

(b) An n-layered half-space

In this case, layer n is assumed to be semi-infinite; h_1, h_2, ..., h_{n-1} denote the thicknesses of layer 1, 2, ..., (n-1) respectively; z_1, z_2, ..., z_{n-1} denote the depths to layer 2, 3, ..., n and $z_0=0$ is the earth's surface.

Equation (2.4) holds within each layer. It is however not valid at the boundaries between the layers because the second derivatives of the electric and magnetic field components with respect to z are discontinuous.

From Jones (1964), the solution of equation (2.4) in layer L, say, is of the form

$$E_{x,L} = A_L\exp\{K_L(z-z_{L-1})\} + B_L\exp\{-K_L(z-z_{L-1})\} \qquad (2.11)$$

From equation (2.5), the magnetic field component is given by

$$H_{y,L} = (iK_L/\omega\mu)[A_L\exp\{K_L(z-z_{L-1})\} - B_L\exp\{-K_L(z-z_{L-1})\}] \qquad (2.12)$$

with $K_L^2 = i\omega\mu\sigma_L$

where σ_L is the conductivity of layer L. For layer n, $A_n=0$

and B_n can be chosen arbitrarily. The continuity of the tangential components of the electric and magnetic fields at each of the layer boundaries leads to recursion relations for the coefficients A_i and B_i [i=1 to (n-1)].

The impedance at depth z in layer L is

$$Z_L(z) = E_{x,L}/H_{y,L}$$

$$= \frac{\omega\mu}{iK_L} \frac{1 + (B_L/A_L)\exp\{-2K_L(z-z_{L-1})\}}{1 - (B_L/A_L)\exp\{-2K_L(z-z_{L-1})\}}$$

$$= (\omega\mu/iK_L)\coth\{K_L(z-z_{L-1}) - (1/2)\ln(B_L/A_L)\} \quad (2.13)$$

since $B_L/A_L \equiv \exp\{\ln(B_L/A_L)\}$. Hence, at depth z_{L-1} in layer L

$$Z_L(z_{L-1}) = (\omega\mu/iK_L)\coth\{\quad\quad -(1/2)\ln(B_L/A_L)\} \quad (2.14a)$$

Using equation (2.13) the impedance at depth z_L in layer L is

$$Z_L(z_L) = (\omega\mu/iK_L)\coth\{K_L(z_L - z_{L-1}) - (1/2)\ln(B_L/A_L)\} \quad (2.14b)$$

Substituting $(1/2)\ln\{B_L/A_L\}$ from equation (2.14b) into equation (2.14a) leads to the general expression for the impedance within any of the layers 1 to (n-1), i.e.,

$$Z_L(z_{L-1}) = (\omega\mu/iK_L)\coth\{K_L(z_L - z_{L-1}) + \coth^{-1}[(iK_L/\omega\mu)Z_L(z_L)]\} \quad (2.15)$$

But $Z_1(0)$ is the impedance measurable at the surface of the n-layered half-space. Similarly, $Z_1(z_1)$ is the impedance at the base of layer 1, etc. Thus, from equation (2.15)

$$Z_1(0) = (\omega\mu/iK_1)\coth\{K_1h_1+\coth^{-1}[(iK_1/\omega\mu)Z_1(z_1)]\}$$

$$Z_2(z_1) = (\omega\mu/iK_2)\coth\{K_2h_2+\coth^{-1}[(iK_2/\omega\mu)Z_2(z_2)]\} \qquad (2.16)$$

$$Z_3(z_2) = (\omega\mu/iK_3)\coth\{K_3h_3+\coth^{-1}[(iK_3/\omega\mu)Z_3(z_3)]\}$$

$$Z_n(z_{n-1}) = \omega\mu/(iK_n)$$

Across each layer interface, the continuity of the tangential components of the electric and magnetic fields implies the continuity of the impedance [e.g. $Z_n(z_{n-1}) = Z_{n-1}(z_{n-1})$]. Making use of the latter leads to the following expression for the impedance $Z_1(0)$ at the surface of an n-layered half-space;

$$Z_1(0) = (\omega\mu/iK_1)\coth\{K_1h_1+\coth^{-1}[(K_1/K_2)\coth\{K_2h_2 +$$
$$\coth^{-1}\{(K_2/K_3)\coth[K_3h_3+.....+\coth^{-1}(\{K_{n-2}/K_{n-1}\}$$
$$\coth\{K_{n-1}h_{n-1}+\coth^{-1}(K_{n-1}/K_n)\}).....]\})]\} \qquad (2.17)$$

A Monte-Carlo algorithm which uses equation (2.17) has been implemented in the 1D modelling of the AMT/MT data recorded in this study. The associated computer programme, with minor modifications by the author, has been derived by Dawes (1980) from that initially written by Jones (1977).

An alternative approach to solving the 1D problem is based on substituting $\underline{E} = (E_x,0,0)$, $\underline{H} = (0,H_y,0)$ and $Z(\omega,z) = E_x/H_y$ in Maxwell's equations neglecting displacement currents. This approach leads to the Riccati equation for

impedance of the form

$$\partial Z(\omega,z)/\partial z = -i\omega\mu + \sigma(z)Z^2(\omega,z) \qquad (2.18)$$

Knowing $\sigma(z)$ and the boundary condition at infinity, equation (2.18) can be integrated either analytically or numerically.

Using equation (2.18), Eckhardt (1963,1968) has developed a graphical approach. Transforming equation (2.18) to a first-order differential equation for the logarithm of the impedance and plotting the characteristic solution paths of the impedance, Eckhardt (1968) has produced a chart for graphical integration of multi-layered models. This chart can be used in the graphical evaluation of the impedances of a layered earth model at different frequencies.

2.1.2 Two-dimensional (2D) MT theory

In this case, conductivity σ is a function of depth (z) as well as one other coordinate, y say. Thus, the 2D structure extends infinitely in the x-direction which may be the geological strike direction. Unlike the 1D case, analytical solutions of 2D structures are very cumbersome and sometimes impossible owing to coupling between the field components.

The two equations for the $\underline{E}$ (same as equation 2.3) and $\underline{H}$ variations are

$$\nabla^2\underline{E} = i\omega\mu\sigma\underline{E} \qquad (2.19a)$$

and

$$\sigma\nabla^2\underline{H} = i\omega\mu\sigma^2\underline{H} - \nabla\sigma \wedge (\nabla \wedge \underline{H}) \qquad (2.19b)$$

Assuming an invariance with x, a general 2D field satisfying equations (2.19a,b) can be separated into two distinct modes, viz, E- and H- polarisations with $\underline{E}$ and $\underline{H}$ fields polarised parallel and perpendicular to the strike direction respectively. The concept of E- and H-polarisation is very relevant in 2D structures. The impedances due to these polarisations are not only different from each other (O'Brien and Morrison, 1967), but also depend on the observation sites. Thus, for the E-polarisation case

$$\underline{E} = E\underline{x} \; ; \quad \underline{H} = (i/\omega\mu)(\underline{y}\partial E/\partial z - \underline{z}\partial E/\partial y) \qquad (2.20a)$$

with $\partial H_z/\partial y - \partial H_y/\partial z = \sigma E_x$

and for the H-polarisation case

$$\underline{H} = H\underline{x} \; ; \quad \underline{E} = (1/\sigma)(\underline{y}\partial H/\partial z - \underline{z}\partial H/\partial y) \qquad (2.20b)$$

with $\partial E_z/\partial y - \partial E_y/\partial z = -i\omega\mu H_x$

where $\underline{x}$, $\underline{y}$ and $\underline{z}$ are unit vectors along the coordinate axes.

Equations (2.19a,b) are amenable to analytical solutions only for specialised cases such as those discussed by e.g. D'Erceville and Kunetz, 1962; Rankin, 1962 and Weaver, 1963 and hence there has been recourse to a numerical approach subjected to the following boundary conditions :

(i) at any boundary, both $\underline{E}$ and $\underline{H}$ parallel to it and the normal component of $\underline{H}$ are continuous across it;

(ii) the electric current density perpendicular to any boundary is continuous across it and is zero across z=0; the latter implies that E_z=0 inside the conductor at z=0;

(iii) at infinite depth in the earth, both $\underline{E}$ and $\underline{H}$ are zero;

(iv) the boundaries $z = \infty$ and $y = \pm\infty$ are assumed far enough from any lateral discontinuity so that the fields can be considered uniform there;

(v) at the earth's surface and everywhere above it, $\underline{H}$ is a constant for the H-polarisation case; there is no similar simplification in the E-polarisation case.

Several authors have used different techniques to compute numerical solutions to 2D induction problems. Reviews and papers on these techniques include among others Jones (1973), Ward et al. (1973), Hobbs (1975) and Praus (1975). The transmission line analogy method has been described by Swift (1967) and Madden and Swift (1969), the finite element method by Coggon (1971) and Reddy and Rankin (1972, 1973) and the finite difference method by Jones and Price (1970), Jones and Pascoe (1971), Pascoe and Jones (1972), Williamson et al. (1974) and Brewitt-Taylor and Weaver (1976).

In the transmission line analogy method, the conducting space and surroundings are represented by a mesh of grid points. The electric fields in Maxwell's equations are represented by currents in the branches of the mesh, while the magnetic fields are represented by voltages at the

nodes. Assuming the mesh to be composed of electrically homogeneous unit cells, Kirchoff's law of current continuity is applied at each node. The resulting equations are solved by matrix inversion to obtain the voltage at each node.

In the finite element method, the region of interest is divided into a mesh of finite elements and the energy in the EM field within each element is considered. The variational principle which states that EM field is formed such that its integral energy is a minimum, leads to a set of equations with respect to the unknown EM field values in the elements. These equations are solved numerically to obtain the EM fields.

In the finite difference method, Maxwell's differential equations and the boundary conditions are formulated in the form of finite differences for a mesh of grid points and numerical integration is carried out over the domain to determine the EM fields.

In these numerical methods continuous functions are represented by discrete values at points within a mesh of finite dimensions. Some functional relation (often linear) is assumed for the fields between the grid points and hence, the accuracy of the calculated field components depends on the grid size. The denser the grids, the higher is the accuracy of the calculations.

The finite difference method, as developed by Jones and Price (1970) and computer programmed by Jones and Pascoe (1971), was used extensively in the early 70s. A disadvantage of this method is the specification of sharply separated conductivity regions. This leads to difficulties

in fitting E and H field values across these sharp conductivity boundaries. To overcome these difficulties, Brewitt-Taylor and Weaver (1976) (improved boundary conditions for the E-polarisation case by Weaver and Brewitt-Taylor, 1978) have produced a modified finite difference method based on the assumption that the earth's conductivity is a smoothly-varying function of position. The computer programme for this method written by Brewitt-Taylor and Johns (1980) has been used in the 2D modelling undertaken in this study.

2.1.3 Three-dimensional (3D) MT theory

In some geophysical problems, the conductivity σ is a function of all the coordinates x, y, z. In these cases, analytical solutions of Maxwell's equations are intractable and hence either numerical solutions (e.g. Jones and Pascoe, 1972; Lines and Jones, 1973a,b; Raiche, 1974; Weidelt, 1975; Jones and Vozoff, 1978; Pridmore et al., 1981) or laboratory analogue models (e.g. Rankin et al., 1965; Dosso, 1966, 1973; Dosso et al., 1980; Nienaber et al., 1981) are used. Analogue model experiments are performed with a laboratory model which is a miniature copy of the real earth structure and the source field. Hence, both the laboratory and earth structure are electrodynamically similar.

Dawson and Weaver (1979) have approached 3D induction problems by considering an anomalous thin sheet above a

uniformly conducting half-space earth. Applying this method to the problem of an island off an irregularly shaped coastline, they have shown that in addition to horizontal current channelling around the island, electric currents also flow vertically between the ocean and the lower crust beneath the land.

There are very few 2D inversion programmes (e.g. Jupp and Vozoff, 1977). The existing 3D forward modelling programmes are few, expensive and not entirely reliable for use over a wide frequency range (Vozoff, 1980).

As indicated by Grant and West (1965), with the exception of water ($\varepsilon \approx 80\varepsilon_0$), for most minerals $\varepsilon \approx 9\varepsilon_0$ and also apart from ferromagnetic minerals, $\mu \approx \mu_0$, where ε_0, μ_0 are respectively permittivity and permeability of free space. Hence, $\varepsilon=\varepsilon_0$ and $\mu=\mu_0$ are assumed in all the previous equations and hereafter.

2.2 Response functions of the earth

Response functions (R, say) are conventionally expressed as $R(\omega) = \pm(i\omega)^{-1}Z$ (Schmucker, 1970; Weidelt, 1972). The upper sign is for $\exp(-i\omega t)$ time dependence and the lower one is for $\exp(i\omega t)$ time dependence. In the wider sense, an earth response function is any function which is determined from the earth's surface EM data and provides some insight to the subsurface conductivity distribution (Rokityansky, 1982).

2.2.1 Impedance tensor

The measured electric ($\underline{E}$) and magnetic ($\underline{H}$) field variations are related by the impedance tensor Z, i.e.,

$$\underline{E} = Z\underline{H} \tag{2.21}$$

where $\underline{E} = (E_x, E_y)$, $\underline{H} = (H_x, H_y)$ and

$$Z = \begin{bmatrix} Z_{xx} & Z_{xy} \\ Z_{yx} & Z_{yy} \end{bmatrix}$$

Z contains the relevant information about the subsurface resistivity distribution.

In 1D structures, $Z_{xx} = Z_{yy} = 0$, $Z_{xy} = -Z_{yx}$ and the tensor components are invariant with respect to coordinate axes rotation. For a 2D structure, Z_{xx}, Z_{yy} are non-zero ($Z_{xx} = -Z_{yy}$ and $Z_{xy} \neq -Z_{yx}$) in general and Z changes as the coordinate axes are rotated. Thus, inhomogeneities cause the measured impedances to be dependent on measuring orientation. For a clockwise rotation angle θ, the rotated impedances Z'_{ij} are given in terms of the measured impedances by

$$\begin{bmatrix} Z'_{xx} \\ Z'_{xy} \\ Z'_{yx} \\ Z'_{yy} \end{bmatrix} = \begin{bmatrix} C^2 & CS & CS & S^2 \\ -CS & C^2 & -S^2 & CS \\ -CS & -S^2 & C^2 & CS \\ S^2 & -CS & -CS & C^2 \end{bmatrix} \begin{bmatrix} Z_{xx} \\ Z_{xy} \\ Z_{yx} \\ Z_{yy} \end{bmatrix} \tag{2.22}$$

where C is $\cos\theta$ and S is $\sin\theta$.

The three invariants are

$$I_1 = Z_{xx}Z_{yy} - Z_{xy}Z_{yx} = Z^2_{eff} \tag{2.23a}$$

$$I_2 = Z_{xx} + Z_{yy} \quad \text{and} \tag{2.23b}$$

$$I_3 = Z_{xy} - Z_{yx} = 2Z_{av} \tag{2.23c}$$

I_1 is the determinant of the impedance tensor. Z_{eff} and Z_{av} are respectively called effective and mean impedances.

2.2.2 Strike and principal directions

The direction in which the conductivity of a 2D structure does not vary is termed the strike direction (principal conductivity axis). The angle between the principal conductivity axis and the x-axis is called the angle of strike. The axes parallel and perpendicular to the strike direction are the principal (preferred) directions. With reference to the latter axes, the impedance tensor is given by

$$\mathbf{Z} = \begin{bmatrix} 0 & Z_1 \\ Z_2 & 0 \end{bmatrix} \tag{2.24}$$

where Z_1, Z_2 are the impedances parallel and perpendicular to the strike direction respectively.

The angle of strike θ_0 is obtained from the measured impedances by maximising some suitable functions of Z_{xy} and Z_{yx} under rotation of axes. Two main functions in use are $|Z'_{xy}|$ (Everett and Hyndman, 1967a) and $|Z'_{xy}|^2+|Z'_{yx}|^2$ (Swift, 1967). The latter analytical maximisation on using equation (2.22) gives

$$\theta_0 = \frac{1}{4}\arctan\frac{(Z_{xx}-Z_{yy})(Z_{xy}+Z_{yx})^* + (Z_{xx}-Z_{yy})^*(Z_{xy}+Z_{yx})}{|Z_{xx}-Z_{yy}|^2 - |Z_{xy}+Z_{yx}|^2} \qquad (2.25)$$

where * denotes the complex conjugate.

For the above angle, Z'_{xx} and Z'_{yy} are zero for a 2D structure. However, owing to the ever present noise in the measured data, Z_{xx} and Z_{yy} never reduce to zero on rotation of axes, but only become very small compared with Z_{xy} and Z_{yx} (1D and 2D cases). In a 3D structure, Z_{xx} and Z_{yy} may still be quite appreciable after axes rotation, but Jones and Vozoff (1978) have indicated that equation (2.25) can still be used to obtain the gross 2D angle of strike of the 3D structure.

2.2.3 Apparent resistivity and phase

Apparent resistivity is calculated from the impedance estimates, e.g., Z_{ij} (i, j = x, y) as

$$\varrho_{aij} = (\omega\mu_0)^{-1}|Z_{ij}|^2 \qquad \text{in S.I. units}$$

$$= 0.2\tau|Z_{ij}|^2 \qquad \text{in practical MT units} \qquad (2.26a)$$

where $\omega = 2\pi/\tau$ is the angular frequency.

The phase is defined as the argument of the impedance tensor, i.e.,

$$\varphi_{ij} = \arg(Z_{ij}) = \arctan\{\mathrm{Im}(E_i/H_j)\}/[\mathrm{Re}(E_i/H_j)] \qquad (2.26b)$$

In 1D cases, a scalar treatment (i.e. $Z_{ij} = E_i/H_j$) will suffice. In more complex cases, tensor analysis is carried out and the complex surface impedance tensor is rotated to the preferred directions. The apparent resistivities and phases in these directions are termed the major and minor apparent resistivities (ϱ_{max} and ϱ_{min}) and phases given by

$$\varrho_{aij} = (\omega\mu_0)^{-1} |Z^R_{ij}|^2 \qquad (2.26c)$$

$$\varphi_{ij} = \arg(Z^R_{ij}) \qquad (2.26d)$$

where Z^R_{ij} are the components of the impedance tensor in the principal directions.

The ratio of ϱ_{max} to ϱ_{min} gives a measure of the anisotropy at the observation site. In a 2D case, the anisotropy increases as the conductivity discontinuity in the structure is approached. This ratio can thus be used as a dimensionality indicator.

The apparent resistivities corresponding to Z_1 and Z_2 in equation (2.24) are termed $\varrho_{\parallel}$ and $\varrho_{\perp}$ respectively. A discontinuous behaviour of $\varrho_{\perp}$ is always observed at a boundary since the induced current must be continuous across the boundary. From a consideration of several models e.g. fault, sloping shelf and step, Jones (1970) and Jones and Price (1971) have demonstrated that $\varrho_{\perp}$ is very sensitive to the shape of the boundary.

2.2.4 Source field polarisation

Polarisation characteristics can be used to check the nature of the source field; this is particularly essential in magnetometer array studies (Gough et al., 1974) and in MT studies involving synchronous recordings at different sites. Diagrams relating to source polarisation have been produced by Lilley (1976) and a discussion of the effects of polarisation has been given by Lienert (1980). Polarisation characteristics of geomagnetic pulsations provide information about the source, the mode of propagation and the effect of the ionosphere on the pulsations. They can also reveal the existence of anomalous conductivity zones. When the polarisation characteristics are studied at different locations, the spatial dependence of these characteristics can be revealed. A study of this spatial dependence has been made by Kunaratnam (1981).

Time variations in the polarisation of the source magnetic fields H_x and H_y can be represented by a polarisation ellipse (Bennett and Lilley, 1972) which shows the path described with time by the total horizontal magnetic field. The path described by the electric field can be similarly represented by an electric polarisation ellipse. The polarisation ellipses for the electric and magnetic fields are mutually perpendicular for plane waves in a horizontally layered medium (Kaufman and Keller, 1981). The polarisation angles θ^H, θ^E are the inclinations of the major (maximum) axes of the magnetic and electric polarisation ellipses respectively. The polarisation angles,

sometimes called tilt angles, are given by

$$\tan 2\theta^H = \frac{2H_x H_y \cos\Delta\varphi^H}{H_y^2 - H_x^2} \qquad (2.27a)$$

$$\tan 2\theta^E = \frac{2E_x E_y \cos\Delta\varphi^E}{E_y^2 - E_x^2} \qquad (2.27b)$$

where $\Delta\varphi^H = \varphi_x^H - \varphi_y^H$ and $\Delta\varphi^E = \varphi_x^E - \varphi_y^E$ are the phase differences; φ_x^H is the phase of H_x, etc.

In the present study, the above equations were used in the analysis of the recorded data to calculate the magnetic and electric polarisation angles, which enabled the rejection of highly polarised sub-frequency bands.

The ratio of the minor to the major axis of the polarisation ellipse is termed the ellipticity. For the magnetic polarisation ellipse, the ellipticity is given by (Smith and Ward, 1974)

$$e = \frac{H_x H_y \sin\Delta\varphi^H}{H_1^2} \qquad (2.28)$$

where $H_1 = |H_x \exp(i\Delta\varphi^H)\sin\theta^H + H_y\cos\theta^H|$

In VLF prospecting, the tilt angle and the ellipticity of the magnetic polarisation ellipse are generally determined. Paterson and Ronka (1971) have shown that the tangent of the tilt angle and the ellipticity are good approximations to (i) the ratio of the real component of the vertical secondary to the horizontal primary field and (ii) the ratio

of the quadrature component of the vertical secondary field to the horizontal primary field respectively.

2.2.5 Dimensionality indicators

Apart from the ratio of ϱ_{max} to ϱ_{min} referred to in section 2.2.3 above, other parameters used in determining the dimensionality of the earth structure under investigation are skew and tipper.

(a) Skew

Skew is defined as the ratio of the magnitude of the second invariant (equation 2.23b) to that of the third invariant (equation 2.23c), i.e.,

$$S = \frac{|Z_{xx} + Z_{yy}|}{|Z_{xy} - Z_{yx}|} \qquad (2.29)$$

Skew is a measure of the EM coupling between the measured electric and magnetic field variations in the same direction. There is no coupling for the case of a 1D structure and when measurements are made parallel and perpendicular to the strike of a 2D structure, but there is always coupling over a 3D structure except at a point of radial symmetry. Thus, for 1D and 2D structures, S should be zero. This is rarely the case in practice as a result of the ever present noise in the data. In a 2D case where the resistivity contrast across the structure is low, i.e., $|Z_{xy}-Z_{yx}| \approx 0$, S is large. For 3D structures S is generally

large.

(b) Tipper

Everett and Hyndman (1967b); Madden and Swift (1969) have defined the tipper coefficients (the single station vertical magnetic field transfer functions) A and B by expressing the vertical magnetic component H_z as a linear combination of the horizontal magnetic components (H_x, H_y), i.e.,

$$H_z = AH_x + BH_y \tag{2.30a}$$

These complex coefficients can be visualised as operating on the horizontal magnetic field and tipping part of it into the vertical. The magnitude of the tipper is given by

$$T = \sqrt{(A^2 + B^2)} \tag{2.30b}$$

The expressions for calculating the tipper coefficients are

$$A = \frac{\langle H_z H_x^* \rangle \langle H_y H_y^* \rangle - \langle H_z H_y^* \rangle \langle H_y H_x^* \rangle}{\langle H_x H_x^* \rangle \langle H_y H_y^* \rangle - \langle H_x H_y^* \rangle \langle H_y H_x^* \rangle} \tag{2.31a}$$

$$B = \frac{\langle H_z H_y^* \rangle \langle H_x H_x^* \rangle - \langle H_z H_x^* \rangle \langle H_x H_y^* \rangle}{\langle H_y H_y^* \rangle \langle H_x H_x^* \rangle - \langle H_y H_x^* \rangle \langle H_x H_y^* \rangle} \tag{2.31b}$$

where * denotes the complex conjugate. For a 2D structure with strike in the x-direction, A=0. Tipper can thus be used to identify the presence of 2D effects in the analysed data. Information from the vertical magnetic field transfer functions is helpful in determining the structural strike

direction (Vozoff, 1972) and is discussed further in section 2.2.6.

Jupp and Vozoff (1976) have shown that the angle which maximises the coherence between the horizontal and the vertical magnetic fields is given by

$$\varphi = T^{-2}[(Re^2A + Re^2B)\arctan(ReB/ReA) + (Im^2A + Im^2B)\arctan(ImB/ImA)] \quad (2.32)$$

The phase difference between H_z and H_φ gives the bearing of some structures.

They have also shown that the tipper skew γ is given by

$$\gamma = 2T^{-2}[ReA\ ImB - ImA\ ReB] \quad (2.33)$$

For 2D structures γ is zero. All the three quantities T, φ and γ are independent of axis rotation and provide some information about the subsurface structure.

The reliability of the calculated H_z (H_z^c) is estimated from the coherence between it and the measured H_z (H_z^m), i.e.,

$$coh[H_z^m, H_z^c] = \frac{A^*\langle H_z^m H_x^*\rangle + B^*\langle H_z^m H_y^*\rangle}{\{\langle H_z^m H_z^{m*}\rangle^{1/2}[AA^*\langle H_x H_x^*\rangle + BB^*\langle H_y H_y^*\rangle + 2Re\,(AB^*\langle H_x H_y^*\rangle)]^{1/2}\}} \quad (2.34)$$

with * denoting the complex conjugate.

2.2.6 Induction arrows

The vertical magnetic component (H_z) in conjunction with the horizontal magnetic components (H_x, H_y) can be used to obtain information about the subsurface electrical conductivity structure (Schmucker, 1964,1970; Everett and Hyndman, 1967b). At a single station, the linear relationship between the three magnetic components (equation 2.30a above) is usually of the form

$$H_z = AH_x + BH_y + \delta H_z \qquad (2.35)$$

where δH_z is the residual part of H_z which does not correlate with the horizontal field. Equation (2.35) is valid on the assumption that

(i) the normal vertical component of the inducing field (primary) is negligible compared with the measured variation H_z (secondary);

(ii) the anomalous horizontal fields are negligible compared with the inducing horizontal fields;

(iii) the inducing vertical field does not correlate with the inducing horizontal fields.

Banks (1973) has discussed the validity of the above assumptions and has concluded that they are adequate for induction studies in mid-latitudes. The possible biasing effects of the source field configuration on the transfer functions A and B have been discussed by Beamish (1979).

Equation (2.35) defines a preferred plane in which the magnetic variations tend to occur (Parkinson, 1959,1962).

The horizontal projection of a unit vector perpendicular to this plane is termed the Parkinson vector and it points towards anomalous current concentrations in the earth. The real ($\underline{R}$) and imaginary ($\underline{I}$) induction vectors are defined by

$$|\underline{R}| = (A_r^2 + B_r^2)^{1/2} \; ; \quad \theta_r = \arctan B_r/A_r \qquad (2.36a)$$

$$|\underline{I}| = (A_i^2 + B_i^2)^{1/2} \; ; \quad \theta_i = \arctan B_i/A_i \qquad (2.36b)$$

where A_r, A_i, B_r, B_i are the real and imaginary parts of the tipper coefficients A and B. $\underline{R}$ is the Wiese vector - it is in the direction of the horizontal component that correlates with the downward field. When the direction of $\underline{R}$ is reversed, it is equivalent to the Parkinson vector. The magnitude of $\underline{R}$ is proportional to the intensity of the anomalous current concentration. The expression relating the magnitude of the Wiese vector to that of the Parkinson vector is contained in a review on induction vectors by Gregori and Lanzerotti (1980). For a large and deep conductive body, the real vector is generally larger than the imaginary vector. The imaginary vector tends to be large in the presence of near-surface conductors. Both vectors are parallel or antiparallel on a 2D structure and when the angle between them approaches 90 degrees, the anomalous field is of 3D character at the observation point (Rokityansky, 1982). A map of induction arrows often indicates quite clearly the direction of the gradient of conductivity (Parkinson, 1983). Thus, the induction vectors provide qualitative information on the possible locations of

subsurface conductivity anomalies and their intensities.

In the present study, the measured vertical magnetic field variation was of very poor quality owing to instrumental problems and cultural noise. Hence, induction vectors and tipper were not used in the data interpretation.

2.3 Impedance calculation and coherence

Considering the i^{th} spectral estimates of the complex amplitudes of the magnetic and electric field variations at a given frequency, then from equation (2.21)

$$E_x^i = Z_{xx} H_x^i + Z_{xy} H_y^i \qquad (2.37a)$$

$$E_y^i = Z_{yx} H_x^i + Z_{yy} H_y^i \qquad (2.37b)$$

To solve these equations for the tensor elements of Z requires at least two independent estimates of each of the magnetic and electric components. Cantwell (1960) and Bostick and Smith (1962) have described procedures of obtaining the tensor elements using two independent data sets. A procedure for optimising the estimates of the tensor elements from a large number of independent record sets has been discussed by Sims and Bostick (1969) and Sims et al. (1971). A review of the above methods of estimating tensor elements as well as estimates using cross-correlation analysis of single record sets has been given by Hermance (1973).

From the various mean-square estimates, six distinct equations for each of the tensor elements emerge (Sims and Bostick, 1969 and Sims et al., 1971). In each case two of the expressions are relatively unstable for the 1D case when the incident fields are unpolarised. The four expressions which are quite stable in the absence of highly polarised incident fields are of the form

$$Z_{ij} = \frac{\langle E_i P^* \rangle \langle H_k Q^* \rangle - \langle E_i Q^* \rangle \langle H_k P^* \rangle}{\langle H_j P^* \rangle \langle H_k Q^* \rangle - \langle H_j Q^* \rangle \langle H_k P^* \rangle} \qquad (2.38)$$

where i, j = x, y with k=x when j=y and k=y when j=x. The asterisks denote the complex conjugates and the brackets denote averages over N individual spectral estimates, e.g.,

$$\langle H_j P^* \rangle = (1/N) \sum_{m=1}^{N} H_j^m P^{m*} \qquad (2.39)$$

P and Q are the two assumed noise free components out of E_x, E_y, H_x, H_y so that the resulting impedance expressions minimise noise on the remaining two components. Usually, P and Q are chosen to be H_x and H_y and this results in impedance estimates which are biased downwards by random noise on H_x and H_y (E-noise minimisation). On the other hand, choosing E_x and E_y, the resulting impedance estimates are biased upwards by random noise on E_x and E_y (H-noise minimisation). In remote reference method (Gamble et al., 1979a), P and Q are chosen as H_x and H_y recorded at a reference(second) site, sufficiently distant so that local noise contributions are independent.

Substituting the calculated impedance estimates into equations (2.37a,b), the predicted E_{xp} and E_{yp} values of the electric fields can be obtained. The predictabilities (Swift, 1967) of these fields are defined as the coherences between the measured and predicted fields (predicted coherences), e.g.,

$$\mathrm{coh}(E_x,E_{xp}) = \frac{|\langle E_x E_{xp}^{*}\rangle|}{[\langle E_x E_x^{*}\rangle\langle E_{xp} E_{xp}^{*}\rangle]^{1/2}} \qquad (2.40)$$

where * denotes the complex conjugate.

2.4 Direct transformation of AMT/MT data

In the 1D case, there are a number of schemes for transforming each apparent resistivity (ϱ_a) and phase (φ) values (as a function of period, τ) to a continuously varying real resistivity-depth profile on a 1 to 1 basis. The three schemes discussed here are the Molochnov (1968), Schmucker (1970) and Bostick (1976) transforms. Although these schemes are approximate, they provide a simple convenient means of solving the inverse problem (Rokityansky, 1982). Goldberg and Rotstein (1982) have demonstrated the advantages of the Bostick transform in the presentation of MT field data.

In the Molochnov transform, the depth D and the real resistivity $\varrho(D)$ at this depth are given by

$$D = [\varrho_a/(\mu_0\omega)]^{1/2} \qquad (2.41)$$

$$\varrho(D) = \varrho_a[1+\sqrt{(\tau/\varrho_a)}\partial\sqrt{\varrho_a}/\partial\sqrt{\tau}]^2 \qquad (2.42)$$

From Rokityansky (1982), the minimum phase criterion requires

$$\varphi = (\pi/4)[1 - d\ \log\varrho_a / d\ \log\tau] \qquad (2.43)$$

Equations (2.42) and (2.43) lead to

$$\varrho(D) = \varrho_a[2 - 4\varphi/\pi]^2 \qquad (2.44)$$

Equations (2.41) and (2.44) express Molochnov transform in a suitable form for easy comparisons with the other two transforms. The expressions for all the transforms are shown in table 2.1 below

Dekker (1983) has compared the three transforms by applying them to a suite of 1D models and concluded similar performance by the transforms in the case of accurate data, but found the Bostick transform to be the most accurate with respect to phase errors (for large phase angles) and the other two better for low phase angles.

In the current study, the Bostick transform has been used in the direct inversion of the data in addition to the layered 1D modelling of the data.

TABLE 2.1

Equations (S.I. units) for different transform schemes

SCHEME	DEPTH	RESISTIVITY
Molochnov	$D = [\varrho_a/\mu_0\omega]^{1/2}$	$\varrho(D) = \varrho_a[2-4\varphi/\pi]^2$
Schmucker	$D = [\varrho_a/\mu_0\omega]^{1/2}\sin\varphi$	$\varrho(D) = 2\varrho_a\cos^2\varphi$
Bostick	$D = [\varrho_a/\mu_0\omega]^{1/2}$	$\varrho(D) = \varrho_a[(\pi/2\varphi)-1]$

where ϱ_a and φ in radians are functions of frequency and ω is the angular frequency.

CHAPTER 3

INSTRUMENTATION AND SURVEY LOGISTICS

A brief description of the instrumentation used in this project and of the survey logistics is given in this chapter. For the AMT data recording, the Short Period Automatic Magnetotelluric system (Mk. 1) has been used. This is a battery operated, digital, 5 component data acquisition system which automatically selects and records data, analyses the data and plots the results in real-time. A N.E.R.C. geologger has been used to record the MT data. This records all the field variations and does not have any infield data analysis capability. A cross electrode configuration, aligned along the N-S and E-W geomagnetic axes, has been used in the AMT data recordings (with steel electrodes for bands 1 and 2 and $CuSO_4$ electrodes for band 3) and an L-shaped electrode configuration (with $CuSO_4$ electrodes) for the MT data recordings.

3.1 Electrodes

Petiau and Dupis (1980) have shown that for all electrodes, the electrode noise decreases with increasing frequency and above 10 Hz there is no significant difference between the noise levels of the various electrodes since other instrument noise, amplifier noise in

particular, is predominant. In addition to the above is the operational simplicity (ease of placement and recovery) of steel electrodes. Hence, steel electrodes were used throughout for the recording of data bands 1 and 2. Each steel electrode was 60 cm in length and 3 cm in diameter. It was tapered at one end with a 4 mm diameter hole near the other end for the insertion of a banana plug.

Petiau and Dupis have also shown that for noise below 10 Hz and for the stabilisation time, unpolarizable electrodes are clearly superior to polarizable ones. Hence, $CuSO_4$ electrodes were used for the recordings of data bands 3 and 4. Each of these electrodes consisted of a copper pipe inside a porous pot containing $CuSO_4$ gel (Fig. 3.1).

In preparing the gel, the author experimented with gelatin and agar and found the preparation of the $CuSO_4$ - gelatin gel to be more time consuming. A high temperature was required to melt the gelatin before adding the $CuSO_4$ crystals and quite a lengthy time for the product to set. No noticeable difference was observed between the performance of these two types of $CuSO_4$ gel. Hence, $CuSO_4$-agar gel was prepared and used.

The author also found that a proportion by volume of water, $CuSO_4$ and agar to produce a gel which would not deteriorate appreciably within at least eight weeks of fieldwork usage was 3 : 2 : 2 respectively.

In order to facilitate the checking of the state of the gel, the plastic lid was held onto the pot by means of insulating tape instead of a permanent seal. To ensure

FIGURE 3.1

Unpolarisable copper-copper sulphate electrode.

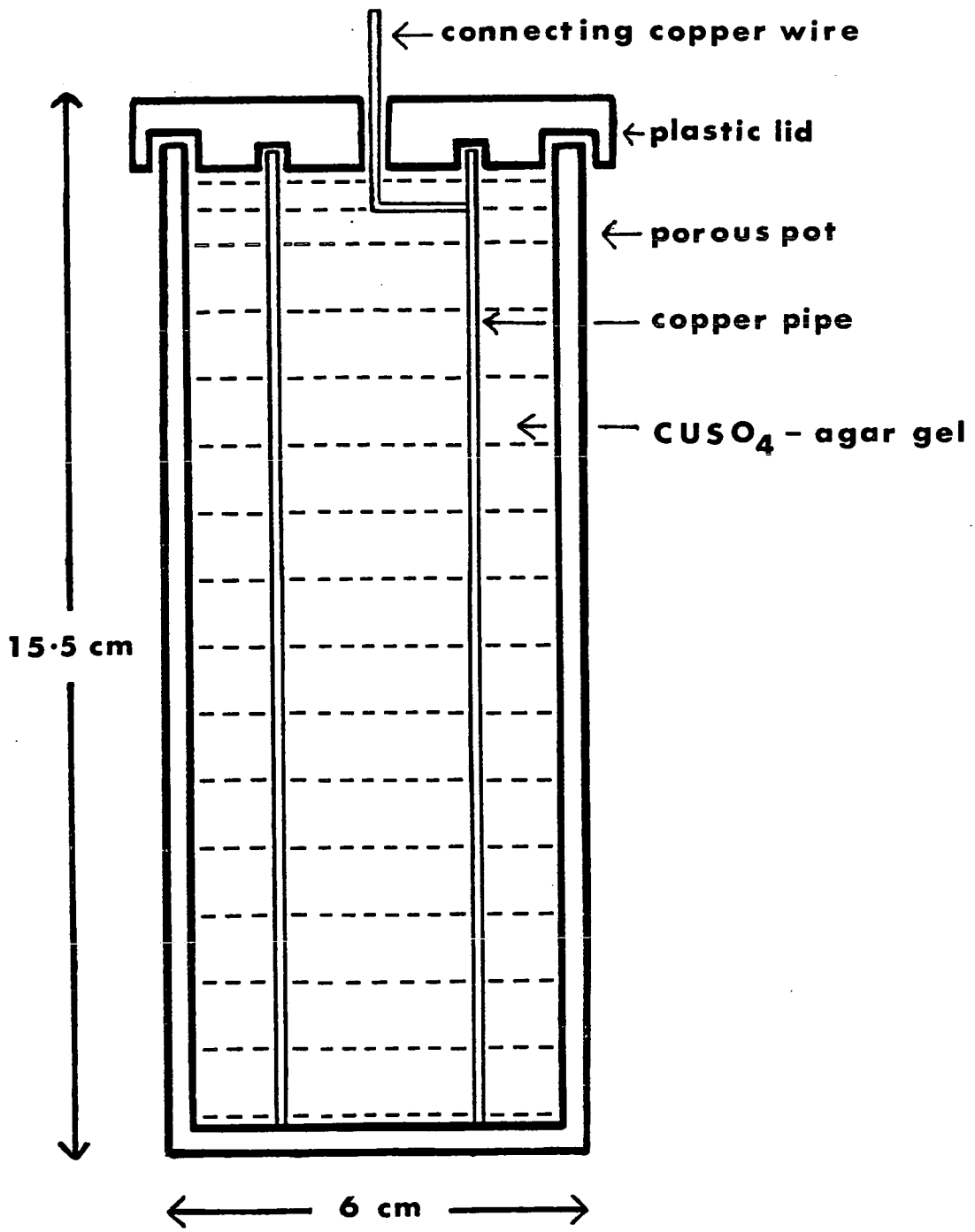
connecting copper wire
plastic lid
porous pot
copper pipe
$CUSO_4$ - agar gel
15·5 cm
6 cm

easy recovery from the ground at the end of the data recording, strong nylon twine was wound tightly round each pot with the knotted end above the ground. The latter was used to pull the electrode out of the ground without damaging it. The author also found that by storing the $CuSO_4$ electrodes inside a container of water, they could in fact last for more than six months without the need to prepare new ones - the same electrodes were used for the 1983 and 1984 fieldwork.

3.2 Magnetic field sensors

Two sets of E.C.A. induction coils were used. One set, consisting of three CM16 coils, was used for data bands 1 and 2 and a second set, consisting of three CM11E coils, was used for data bands 3 and 4. Each coil sensitivity was 50 mV/γ. The usable frequency range (flat amplitude response) of the CM16 coil was 3 to 800 Hz, while that of the CM11E coil was 0.012 to 100 Hz.

Each coil, enclosed in a waterproof casing, had a feedback system with the secondary winding operating in antiphase with respect to the primary. Both the primary and secondary windings were on a high permeability core. The electromotive force generated by the primary in response to magnetic field variations was amplified and the feedback voltage was used to drive the secondary whose field annulled that acting on the primary. The output from the sensor was this feedback voltage. There was provision for the feedback winding to be driven from an external

voltage source to test the functioning of the circuitry (1 mV/mV).

3.3 AMT recording equipment

The AMT system comprised the magnetic and telluric sensors, the power source and the recording equipment as shown in Fig. 3.2. At each field site, all the equipment except the sensors and the sensor distribution box was set up inside a Landrover. The necessary power requirement for the system was provided by two heavy-duty 12V and two small 12V lead-acid batteries.

The equipment used to digitally record the frequency bands 1 to 3 data on cartridge tapes was the Short Period Automatic Magnetotelluric system (SPAM - Mk. 1). This was built in the Edinburgh Geophysics Department by Dawes (1981) based on a similar design by Schnegg and Fischer (1979). It had five identical channels, each with a switchable 50 and 150 Hz notch filter to eliminate noise from power transmission lines.

SPAM (Mk. 1) consisted of six principal parts, viz, (i) a computer, a programmable amplifier/filter bank and a power regulator; (ii) an alphanumeric hand held terminal (V.D.U.); (iii) a dual (256 kilobytes) cartridge (TU58) deck; (iv) a miniature electrosensitive printer; (v) a power distribution box and (vi) a sensor distribution box.

It used a powerful microcomputer (LSI 11/2 with a 64 kilobyte Ram) which read programmes from one of the two cartridge tapes on the deck and wrote data on to the

FIGURE 3.2

Block diagram of the AMT system.

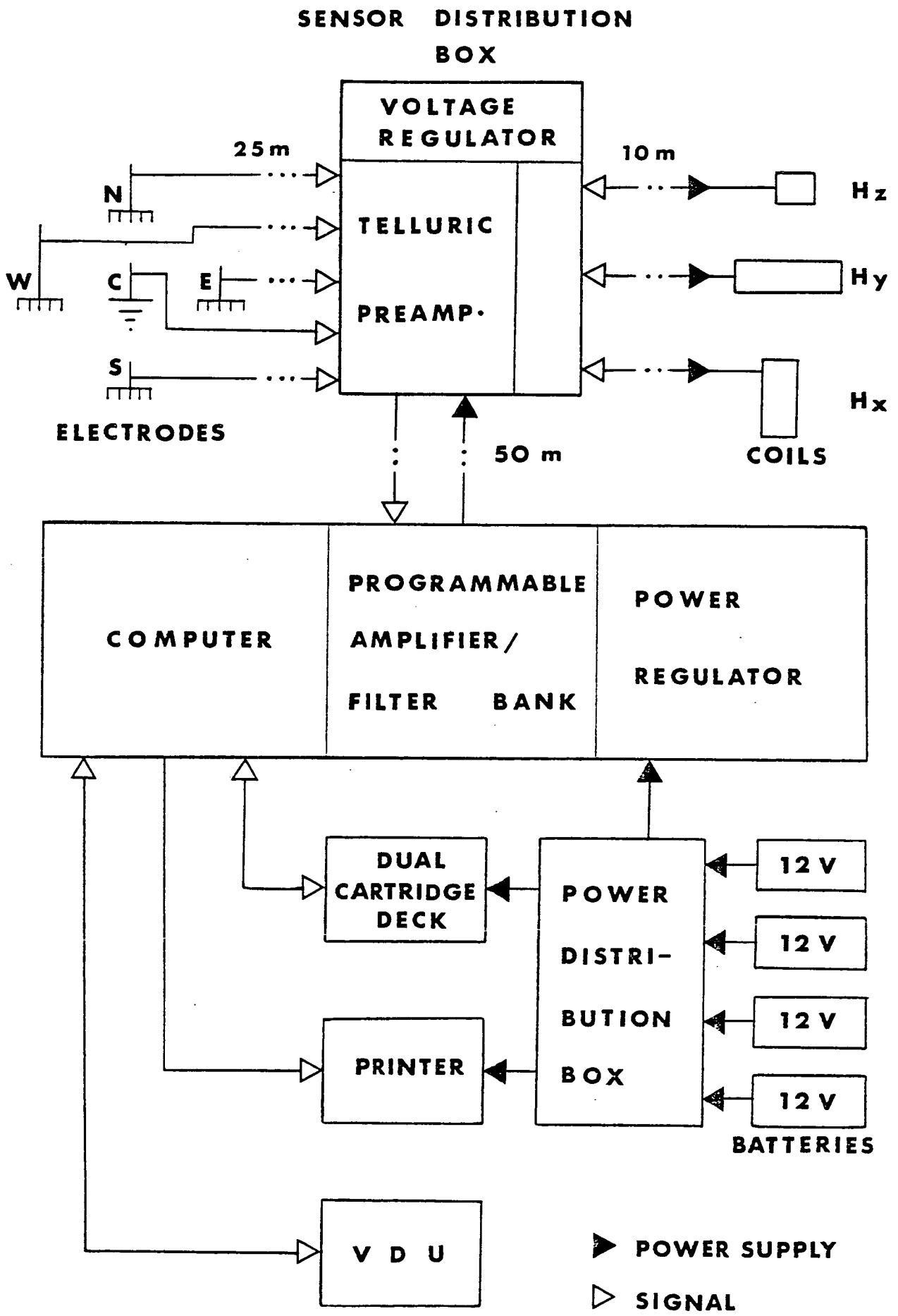
SENSOR DISTRIBUTION BOX
VOLTAGE REGULATOR
25 m
10 m
N
W
C
E
S
TELLURIC PREAMP.
Hz
Hy
Hx
ELECTRODES
50 m
COILS
COMPUTER
PROGRAMMABLE AMPLIFIER/ FILTER BANK
POWER REGULATOR
DUAL CARTRIDGE DECK
POWER DISTRI-BUTION BOX
12 V
12 V
12 V
12 V
BATTERIES
PRINTER
V D U
POWER SUPPLY
SIGNAL

second one. Only one data band could be written on each tape. The printer was used for the graph plots and character readouts. The sensor distribution box contained the telluric preamplifiers and voltage regulators which maintained a stable power supply to the preamplifiers and the coil amplifiers. Two 50 m cables connected the distribution box to the power regulator and computer-programmable amplifier/filter bank. One of these cables carried the power supply and the other carried the sensor signals.

SPAM automatically selected and recorded digitally AMT data satisfying preset criteria. It also analysed the data in real-time, plotted the apparent resistivities in the measuring directions and listed these apparent resistivities, their phases, coherences, skews and the number of estimates. These results were also stored on tape. The visual observation of these infield results provided an invaluable assessment of the success of the sounding before leaving any field site.

It had a hardware and a software data band selector. It applied automatic gain for the individual field components, with manual override, for optimal signal recording. It accepted or rejected an event automatically in both the time and frequency domains and also with manual override. The time domain criteria applied were: (a) the signal should not be less than a specified minimum level and (b) there should be no spike or saturation; if an event was rejected, there was no frequency domain analysis. The event was written as a file on to tape

simultaneously as the frequency domain analysis was proceeding. Each frequency band was divided into sub-frequency bands. The frequency domain criterion was that the number of these sub-frequency bands exhibiting predicted coherences greater than or equal to a preset minimum should not be less than a specified value. The event was rejected if the criterion was not satisfied and this filed event was overwritten by another event the next time around. There were sets of parameters which could be altered to cope with varying situations in the field. Figure 3.3 shows a simplified infield flowchart. LCDs gave continuous display of gain numbers, event number and average percentage errors and LEDs gave hardware and software status. There were switches for controlling the printer listing of each of the following: time domain analysis summary, frequency domain analysis summary; and results from all the recorded events (listed and/or plotted).

The length of time required to record each data band depended on the level of the natural signal as well as on the level of the artificial noise prevailing at a field site. On the average the times required to record on tape about 80 events of bands 1, 2 and 3 data were respectively 35 to 65 minutes, 45 to 85 minutes and 3 to 5 hours.

3.4 MT recording equipment

The MT (band 4) system comprised a battery pack, a geologger, 5 channel amplifier/filter bank, sensor

FIGURE 3.3

Simplified infield flowchart of the Short Period Automatic Magnetotelluric (SPAM, Mk.1) system.

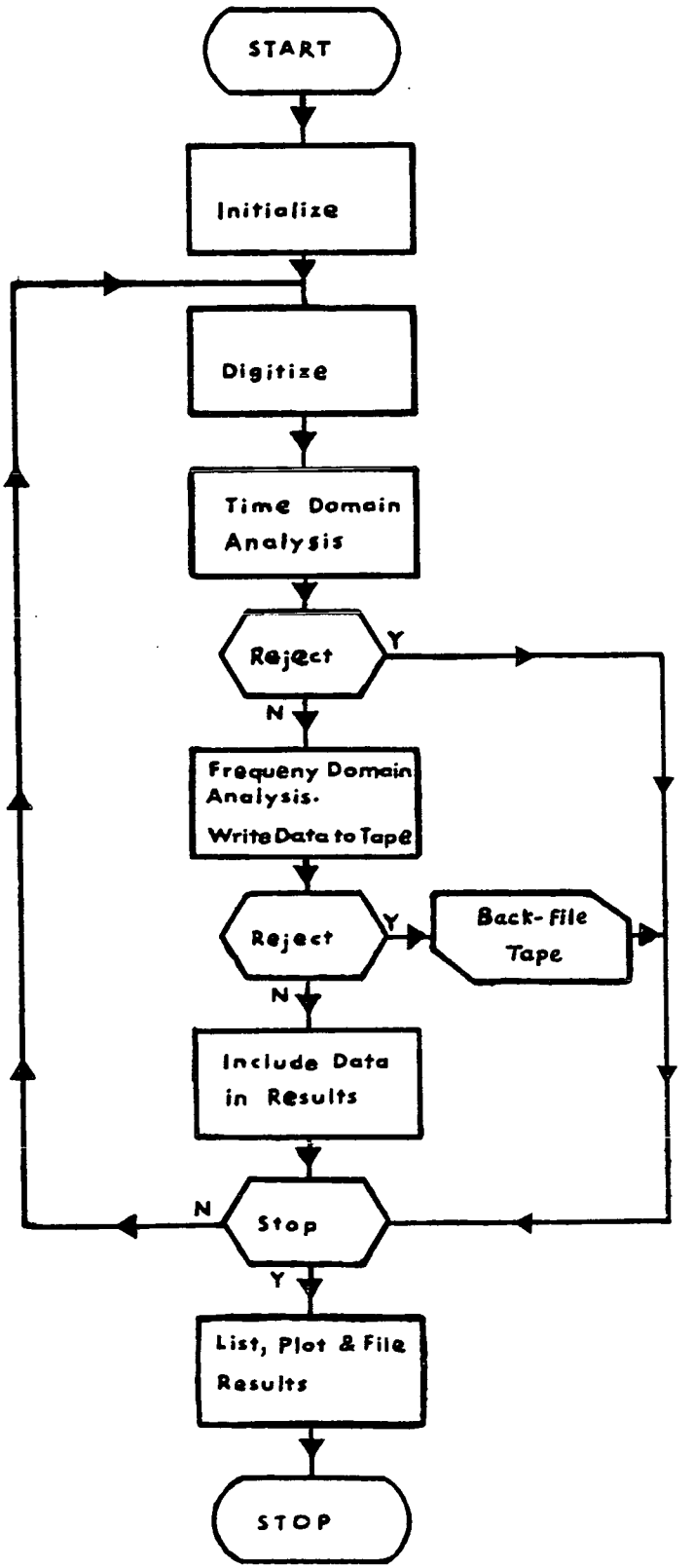
START
Initialize
Digitize
Time Domain Analysis
Reject
Y
N
Frequeny Domain Analysis.
Write Data to Tape
Reject
Y
Back-File Tape
N
Include Data in Results
N
Stop
Y
List, Plot & File Results
STOP

distribution box and the magnetic and telluric sensors. Figure 3.4 shows the block diagram of the usual set-up of the system at a field site. With the exception of the sensors, everything was kept in an aluminium box during the field operations. The necessary power requirement was provided by the battery pack containing sealed rechargeable lead-acid batteries. These usually lasted for 30 hours of continuous recording before needing to be recharged.

The data were digitally recorded on cassette tapes using a N.E.R.C. geologger. A detailed description of the geologger including its electronic circuitry and operating instructions are contained in a technical handbook written by Valiant (1976). Although the geologger originally had 16 channels and 7 selectable sampling rates, it was wired in this project so that it recorded on 5 channels at a fixed sampling rate of 1 Hz and a digitising step of 5 mV. The range of each channel was ±10 V. Each full cassette tape contained 6 hours of data. The geologger wrote 64 words per block of tape with a 12 bit gap between blocks. The tape format was a 16 bit binary word (12 bit data and 4 bit channel identification) preceded by a 2 bit gap. The gain control for the individual field components was manual.

3.5 Equipment calibration

The sophisticated facilities needed to calibrate the induction coils were unavailable in the Edinburgh Geophysics laboratory, but two years before the commencement of this

FIGURE 3.4

Block diagram of the MT system.

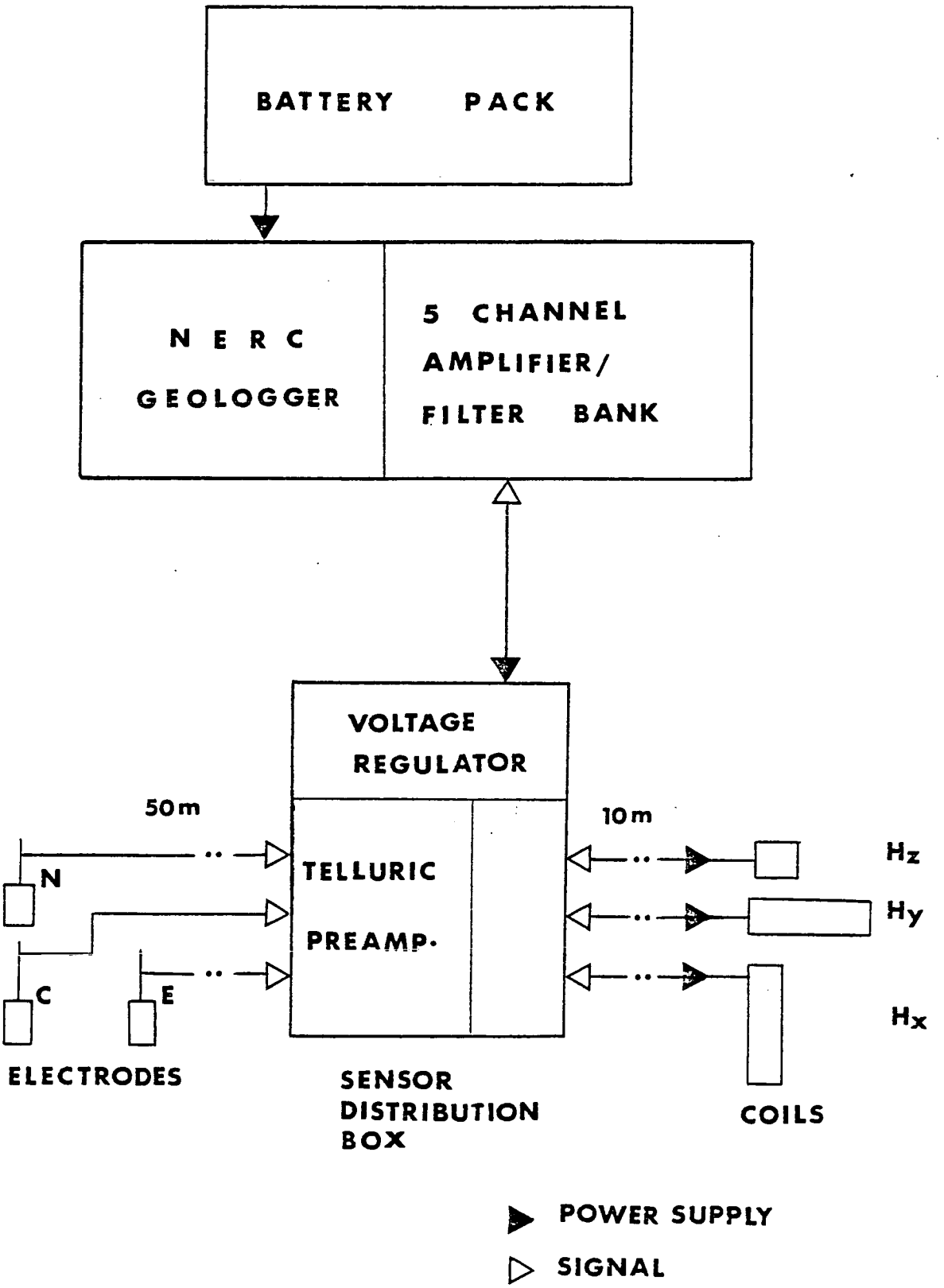
BATTERY PACK
N E R C
GEOLOGGER
5 CHANNEL
AMPLIFIER/
FILTER BANK
VOLTAGE
REGULATOR
50m
10m
TELLURIC
PREAMP.
N
C
E
Hz
Hy
Hx
ELECTRODES
SENSOR
DISTRIBUTION
BOX
COILS
POWER SUPPLY
SIGNAL

project in 1982, they were taken to Garchy Observatory, France for a complete re-calibration. These calibration data were used in the present study. Thus, with the exception of the sensors the calibration of the AMT and MT systems were carried out by the author in Edinburgh using a frequency response analyser (SE2450) from the N.E.R.C. equipment pool. Each system was set up as for field operation, but with the signal input provided by the internal generator in the frequency analyser and the individual response functions (amplitude and phase) were obtained. Figure 3.5A shows the SPAM programmable amplifier-filter response curves for the five identical channels. The overlap between the bands can be clearly seen. Figure 3.5B shows the telluric preamplifier and coil calibration curves for the AMT/MT systems from which the instrument correction parameters used in the data analysis stage were derived.

3.6 Survey logistics

The equipment was transported from one site to another during this project in a Landrover. Hence, it was essential that the sites for which permission had previously been obtained from the landowners were easily accessible by road. It was also essential that a flat area (about 50 m by 50 m) be available at each site to enable the telluric lines to be laid out. The project area was on the whole flat moorland for grazing and farming and hence the above was readily achieved. To minimize the contamination of the

FIGURE 3.5A

The SPAM programmable amplifier-filter response curves for the five identical channels; the numbers near the curves indicate the data bands.

FIGURE 3.5B

The telluric preamplifier and coil calibration curves (amplitude and phase) for the AMT and MT (band 4) systems.

A

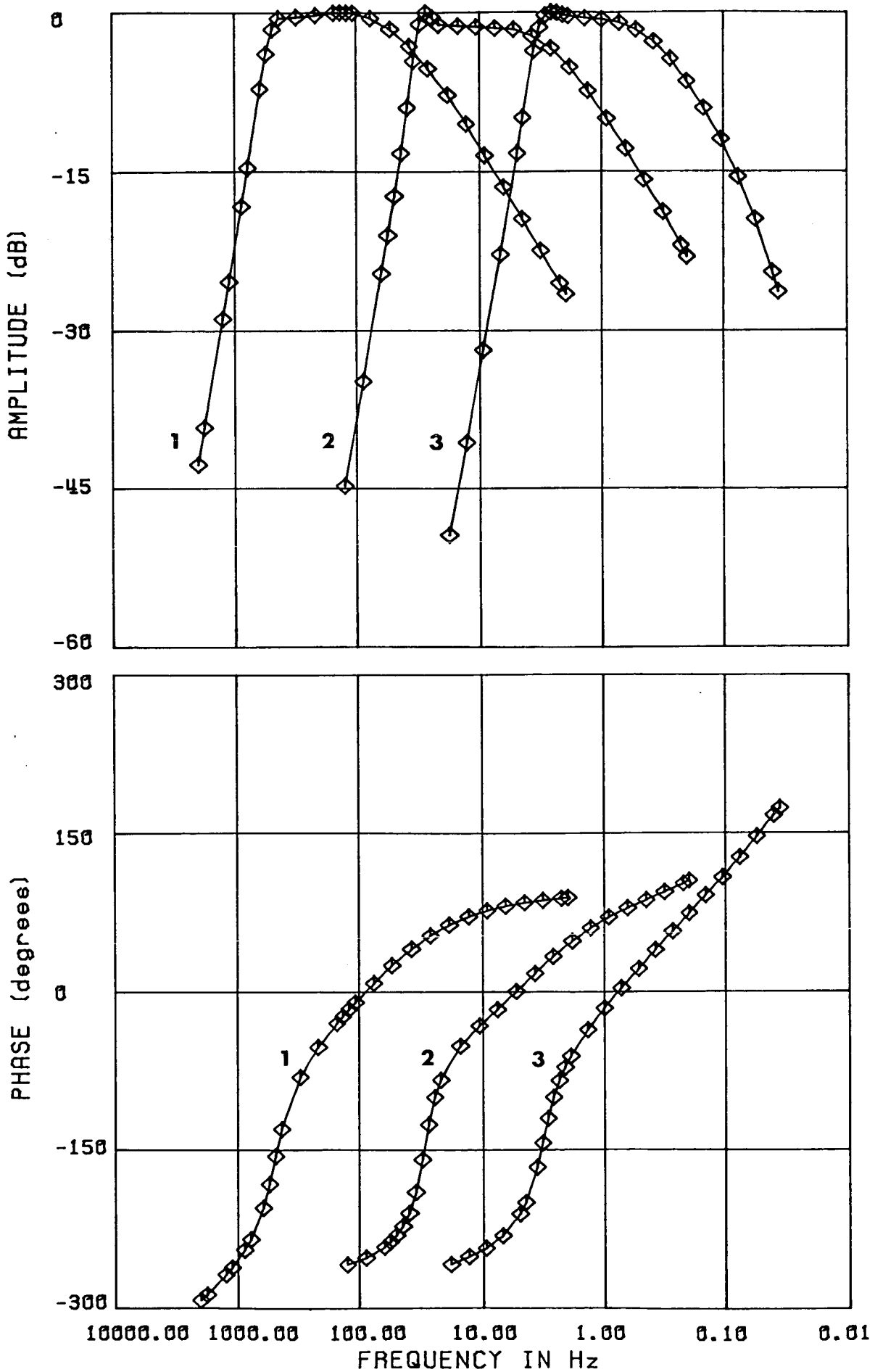
0
-15
-30
-45
-60
AMPLITUDE (dB)
1
2
3
300
150
0
-150
-300
PHASE (degrees)
1
2
3
10000.00
1000.00
100.00
10.00
1.00
0.10
0.01
FREQUENCY IN Hz

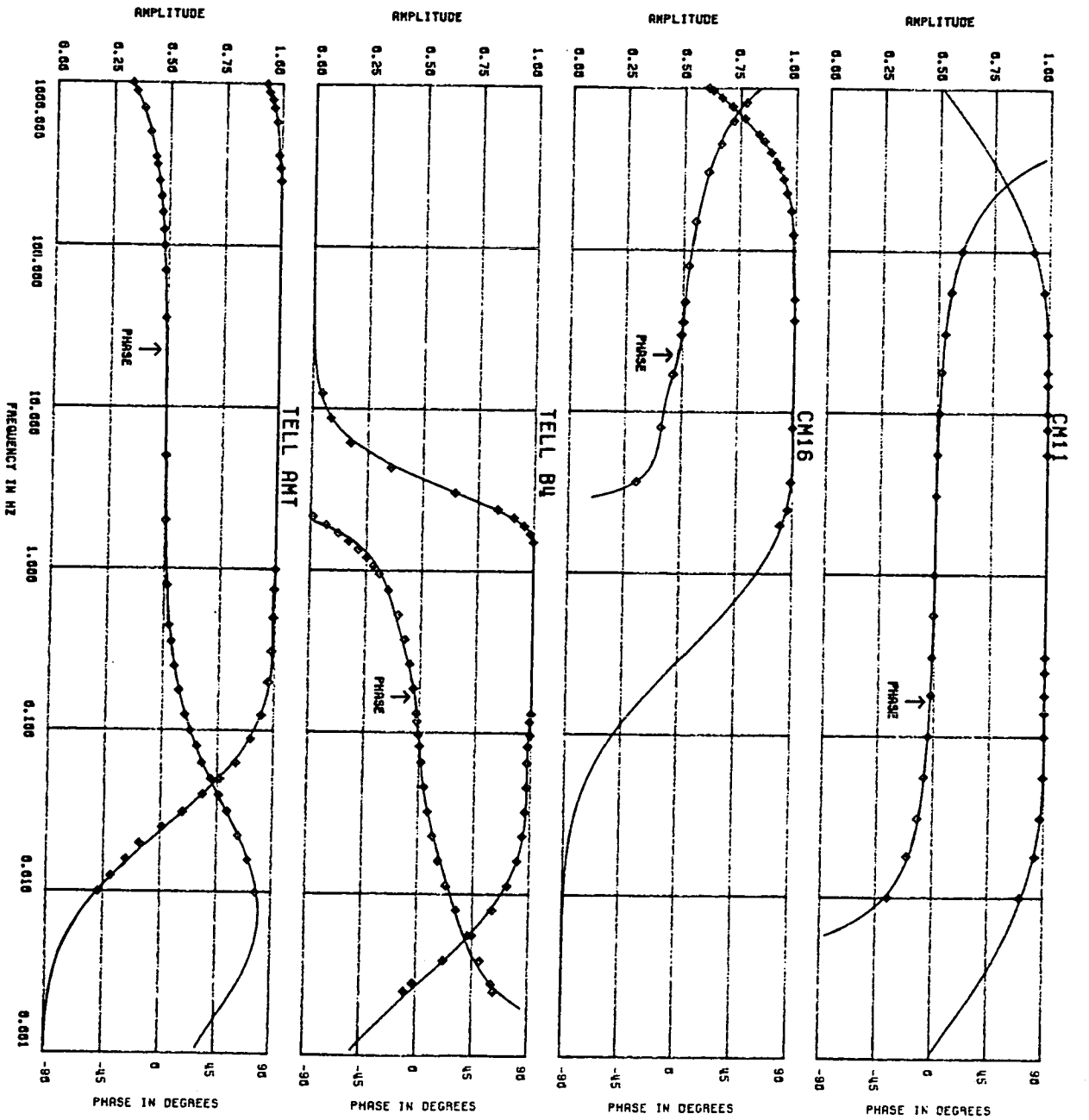
AMPLITUDE
0.00
0.25
0.50
0.75
1.00
PHASE
TELL AMT
TELL BH
CM16
CM11
FREQUENCY IN HZ
1000.000
100.000
10.000
1.000
0.100
0.010
0.001
PHASE IN DEGREES
-90
-45
0
45
90

natural signals by cultural noise, each site was as far as possible from moving and stationary magnetic objects, power transmission lines and streams. The magnetic sensors were located distant from tall trees to minimise vibrations during windy conditions. Thus, the ideal AMT/MT sites should be in fairly remote areas. Cultural noise contamination was not a significant problem at the Duns sites, but as shown in chapter 4, it was a serious problem at some of the profile sites because of the inevitable nearness to industrial works.

For the AMT data recording, a cross electrode configuration with steel electrodes (bands 1 and 2) was used at each site. At the centre of the configuration a steel electrode was driven into the ground leaving a few centimetres exposed. This was the equipment earth electrode connected by a short cable to the sensor distribution box which was insulated from the ground and placed nearby. The magnetic N-S and E-W directions were then established. Along these directions and 25 m on either side of the earth electrode, the remaining four steel electrodes were similarly driven into the ground. For data band 3, as indicated in section 3.1, $CuSO_4$ electrodes were used instead of the steel ones. Each electrode was connected by a cable to the distribution box. Thus, the E-W and N-S telluric lengths were each 50 m. The horizontal coils, fitted with spiked aluminium collars at the ends, were then aligned parallel to the telluric lines and levelled using a spirit level. They were protected from the adverse effects of the sun, rain and

wind by plastic shields. The vertical coil with its base buried to a depth of at least 50 cm was then levelled. The coils were each connected to the distribution box by a 10 m cable. The box was then connected by two 50 m cables to the SPAM in the Landrover (Fig. 3.2).

For the MT data recording an L-shaped electrode configuration with 50 m arms was used. The $CuSO_4$ electrodes were each buried in a hole 50 to 60 cm deep dug by means of an auger. The corner electrode, close to the sensor distribution box, was the earth electrode. The other two electrodes were the N- and E- electrodes. The coils were installed as described above. The electrodes and the coils were connected by cables to the distribution box and the geologger kept inside an aluminium box (Fig. 3.4).

The author usually went to each site with one other person to help set up the equipment and retrieve it at the end of the recording. On the average it took about one hour to set up the AMT system and a little longer for the band 4 set-up. It is however possible for one person to set up and operate the equipment.

3.7 VLF/R measurements

The VLF/R technique uses the signal in the frequency range 15 to 25 kHz from powerful military radio transmitter stations located at several places around the globe. At considerable distances from the transmitter stations, the primary field can be assumed as a uniform plane wave.

In this project, VLF/R measurements were made at 7 of the profile sites and 3 Duns sites. The Geonics (EM16 VLF-EM) equipment was used. It gave apparent resistivity and phase readings directly. The transmitter station at Rugby in England operating at a frequency of 16 kHz was used. Hence, the purpose of the VLF/R measurements was to provide resistivity information about the topmost few metres of the subsurface at a field site. The survey procedure was very simple and fast. It consisted of aligning the equipment with its fixed 10 m electrode line in the direction of the transmitter station and making two adjustments before reading off the apparent resistivity and phase values from the dials. The time for setting up and taking readings at a spot was usually less than 5 minutes. More than 10 spot readings were usually taken along N-S traverses within 100 m by 100 m array encompassing an AMT/MT field site.

CHAPTER 4

DATA ACQUISITION AND PROCESSING

A brief discussion of how the data used in the project have been acquired, transcribed and processed is now presented. Classical tensorial analysis techniques have been used. In order to elucidate the possible effects of data averaging on the earth's response functions, a comparison of different averaging techniques is given. In view of the ever present noise in measured data, a qualitative approach for extracting some useful results from noisy data is presented. Further development of this approach will no doubt extend the application of the AMT/MT technique to very culturally noisy areas.

4.1 Data acquisition

The AMT/MT data recording was carried out in 1982 and 1983 at 12 sites in the Duns area. As noted in section 1.2, these sites constituted the Duns study. The site locations are indicated in Fig. 1.1. Five of these sites (EVE, HUR, HAL, BED and KET) were within the square array used by the Leeds University resistivity group in their deep resistivity measurements. A comparison of the AMT/MT results with the latter is given in chapter 6. With the exception of HAR, all the Duns sites were mainly on flat

grass moorland. HAR was on the flat top of a hill. Data recording was also carried out at CAI and WHI to the northeast of Duns area. These sites were also on flat grass moorland.

During the 1982 fieldwork season, there was considerable recording time lost owing to equipment failure. One major problem was with the geologger and the cassettes; the geologger either did not write on to the cassette or what was written could not be read without numerous errors. The geologger was also affected by dampness which caused it to saturate. Hence, several attempts to record band 4 data failed. There was also problem with SPAM; it was often affected by dampness with the result that the desired small natural variations were swamped by large square waves. Thus, bands 1 to 3 could only be recorded on damp-free days. Some of these problems persisted in the early part of the 1983 fieldwork season. However, the dampness problem was eliminated after all the geologger circuit boards were dipped in varnish and allowed to dry, while the SPAM boards were only sprayed with varnish owing to the printed edge contacts of the boards. The problem with the geologger and the cassettes disappeared when new tapes were used.

In the latter part of the 1983 fieldwork season, AMT/MT measurements were started along a profile to the northwest of the Duns study. This profile was approximately normal to the SUF (Fig. 1.1). The measurements were continued in 1984. Data recordings were made at a total of 8 sites along this profile. In

addition to the AMT/MT measurements, VLF/R measurements were made at 7 of the profile sites and 3 Duns sites. The national grid references of all the sites and the number of times each data band was recorded are listed in Table 4.1. For each of data bands 1 to 3, one recording implies a cartridge tape containing usually 50 or more events. An event consists of 512 samples of each recorded component of the magnetic and electric field variations. For data band 4, a recording implies 3 or 4 cassette tapes, each usually containing 6 hours of continuous data. For the purpose of the 2D modelling discussed in chapter 7, all the Duns sites have been projected on to the SUF profile and Table 4.1 lists the sites in order starting from the northwest.

4.2 Data processing

4.2.1 Data transcription

As indicated in chapter 3 all the data were digitally recorded. It was also indicated that data bands 1 to 3 were recorded on cartridge tapes and data band 4 on cassette tapes. In order to present the results of all the recorded data bands using the main frame Edinburgh computer, it was essential to transcribe the data to a suitable format. Figure 4.1 shows the various stages involved in the data transcription. The data transfer at a field site is shown in (a) where the infield system is either the AMT or MT recording equipment and Q denotes

TABLE 4.1

Site specifications

SITES		GRID REF.		DATA BANDS			
Name	Code	Eastings	Northings	1	2	3	4
				(number of recordings)			
Muirpark	MUR	3426	6721	1	2	2	1
Spilmersford Mains	SPM	3452	6691	2	3	1	
Saltoun (West)	SAW	3472	6673	4	3	2	2
Bughtknowe	BUG	3477	6647	4	3	1	1
Wanside	WAN	3498	6619	2	4	2	
Windy Law	WLA	3524	6583	1	1	1	1
Bermuda	BER	3559	6536	4	4	1	1
Scoured Rig	SCR	3584	6516	2	3	1	1
Evelaw	EVE	3669	6531	1	1		
Hallywell Rig	HRI	3696	6539	2	1	1	
Hurdlaw	HUR	3667	6507	3	3	2	1
Bedshiel	BED	3684	6515	1	2	1	
Hallyburton	HAL	3672	6493	3	3	1	
Kettelshiel	KET	3704	6516	2	2	1	1
Hardens Hill	HAR	3737	6545	1	1		
Kettelshiel(2)	KE2	3709	6518	1	1	1	
Langtonlees	LAN	3736	6531	2	2	1	
Choicelee	CHO	3736	6517	4	3	2	1
Greenlaw	GRE	3702	6488	3	2	1	
Camp Moor	CAM	3729	6511	1	1	1	
Cairncross	CAI	3905	6628	1	1	1	
Whitecross	WHI	3908	6645	1	1	1	

FIGURE 4.1

Block diagram of the data transcription stages (after Dawes, 1981). Q denotes cartridge or cassette tape for the AMT and MT data respectively.

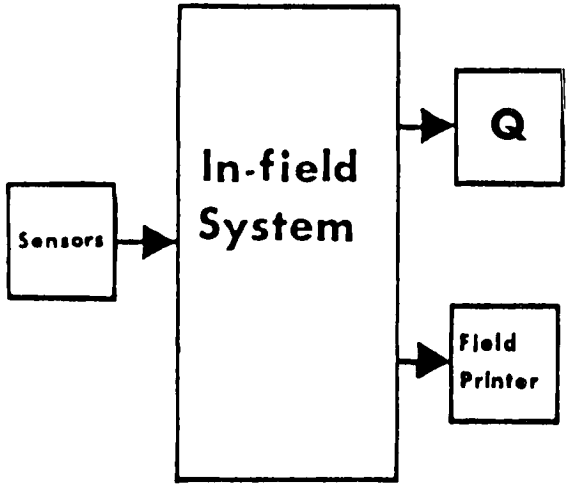
Sensors
In-field System
Q
Field Printer

[a]

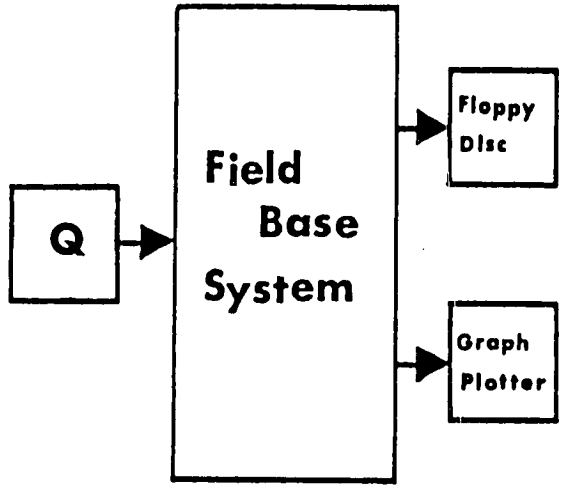
Q
Field Base System
Floppy Disc
Graph Plotter

[b]

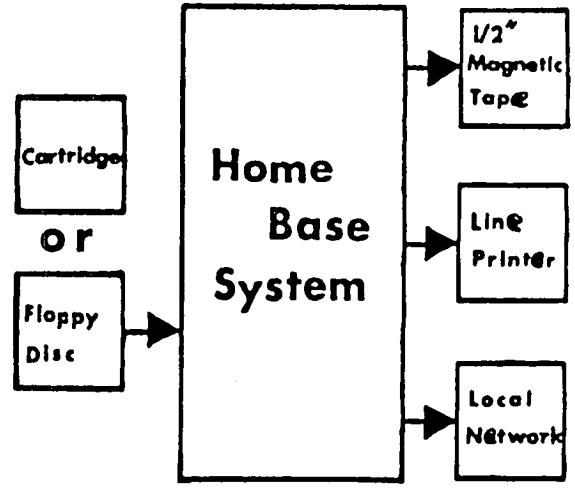
Cartridge
or
Floppy Disc
Home Base System
1/2" Magnetic Tape
Line Printer
Local Network

[c]

cartridge or cassette tape respectively. The field printer is only applicable to the AMT data. At a field base, the data from different sites can be read and written on to floppy discs. The latter is illustrated in (b) where the field base system denotes a DEC MINC-11 minicomputer. The graph plotter is used for plotting the infield AMT results (apparent resistivity, phase, etc.) or band 4 recorded time series. The field base data transfer can alternatively be done at the home base, i.e., Edinburgh Geophysics Department. The next stage of the data transfer is shown in (c), where the data are transcribed to 1/2" magnetic tape which can be read on the main frame computer. The line printer is used for visual display. The home base system is the same MINC-11 referred to above. Alternatively, it is possible to omit the magnetic tape and transfer data directly from floppy disc to the local network, i.e., the main frame computer. For data bands 1 to 3, the transcription stage (b) can be omitted so that the data are transferred directly from cartridge to magnetic tape (Fig. 4.1c).

The necessary computer programmes for data transcription were developed by G. Dawes in the Geophysics Department.

4.2.2 Selection of events

As pointed out in sections 3.3 and 3.4, SPAM automatically selected events satisfying preset criteria, while the geologger recorded all the field variations.

Hence, the event selection described here is applicable only to the geologger data band 4. This event selection is very similar to that for the long period MT described by Mbipom (1980); the only important difference is the use of the MINC terminal in the present study instead of the Tektronix 4014 terminal as in Mbipom's study.

Each recorded cassette tape was read and copied on to a floppy disc (Fig. 4.1b). The positions of any reading errors were noted. With the configuration in Fig. 4.1b reduced to Q and the MINC, Q was then replaced by the floppy disc containing the copied data and the programme 'Select' (Dawes, 1980) was then run. Each 20 minutes data segment not containing any reading error position was read and plotted on the MINC terminal. This was inspected and any data length of 15 to 17 minutes (most often 17 minutes) which

(a) showed high level of magnetic and telluric activity, i.e, high amplitude variations to ensure a good power level in the signal;

(b) contained several frequencies of variation;

(c) did not show any extraneous noise contamination and

(d) did not show any significant polarisation

was selected as a suitable event and filed on the floppy disc. About 10 such events were usually obtained from a full cassette tape.

All the selected events were then transcribed to the local network as shown in Fig. 4.1c. On the local network a formatting programme was then run at the end of which the band 4 data were in exactly the same format as the

AMT data bands 1 to 3 . Hence, all the data bands could be analysed using the same programme. Information relating to the data band, telluric lengths, coil sensitivity, recording gains, etc. are contained in a header block at the beginning of each event.

In Figs. 4.2A,B, a typical example of an event in each data band is shown. The electric field variations are in mV/km and the magnetic field variations in gamma ($=10^{-9}$ T). The band code identification is explained in the figure caption.

4.2.3 Event analysis

The main frame data analysis was done on the Edinburgh Multi Access System (EMAS) twin ICL 2972 and 2980. A review of the data analysis techniques used in EM induction work has been given by Hermance (1973). In the present study, the data were analysed using classical tensorial analysis techniques. The computer programmes used were originally written by Rooney (1976) and compiled into efficient packages by Dawes (1980). Thus, only a few modifications were made by the author.

As noted in section 4.2.2 above, after running the formatting programme on the selected data band 4 events, they constituted a cartridge for the purpose of the analysis programme. Originally, the analysis programme accepted all events from only one cartridge per band, but was modified by the author to accept one or more cartridges per data band. With this modification, repeat

FIGURE 4.2

Examples of the recorded natural variations in the electric and magnetic field components

(A) data band 1 at the top and band 2 at the bottom;

(B) data band 3 at the top and band 4 at the bottom.

The first digit of the first 5-digit identification code at the bottom of each group of plots indicates the last digit of the year of data recording, the next two digits together indicate the site number, the next digit shows the data band and the fifth digit, which is a letter, serves to distinguish repeat recordings of the same band; the second identification code shows the event number.

A

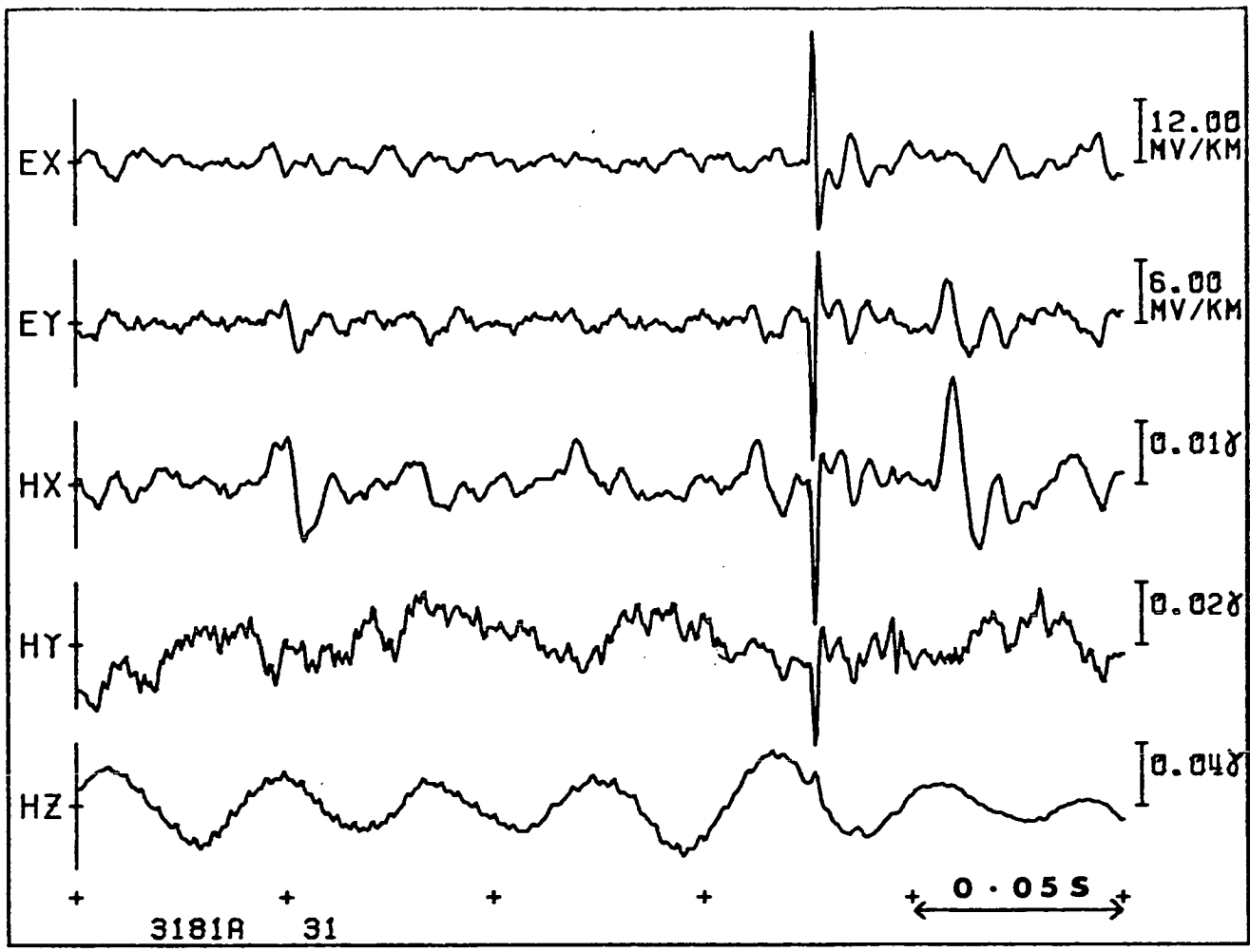
EX
EY
HX
HY
HZ
12.00 MV/KM
6.00 MV/KM
0.01γ
0.02γ
0.04γ
0·05S
3181A 31

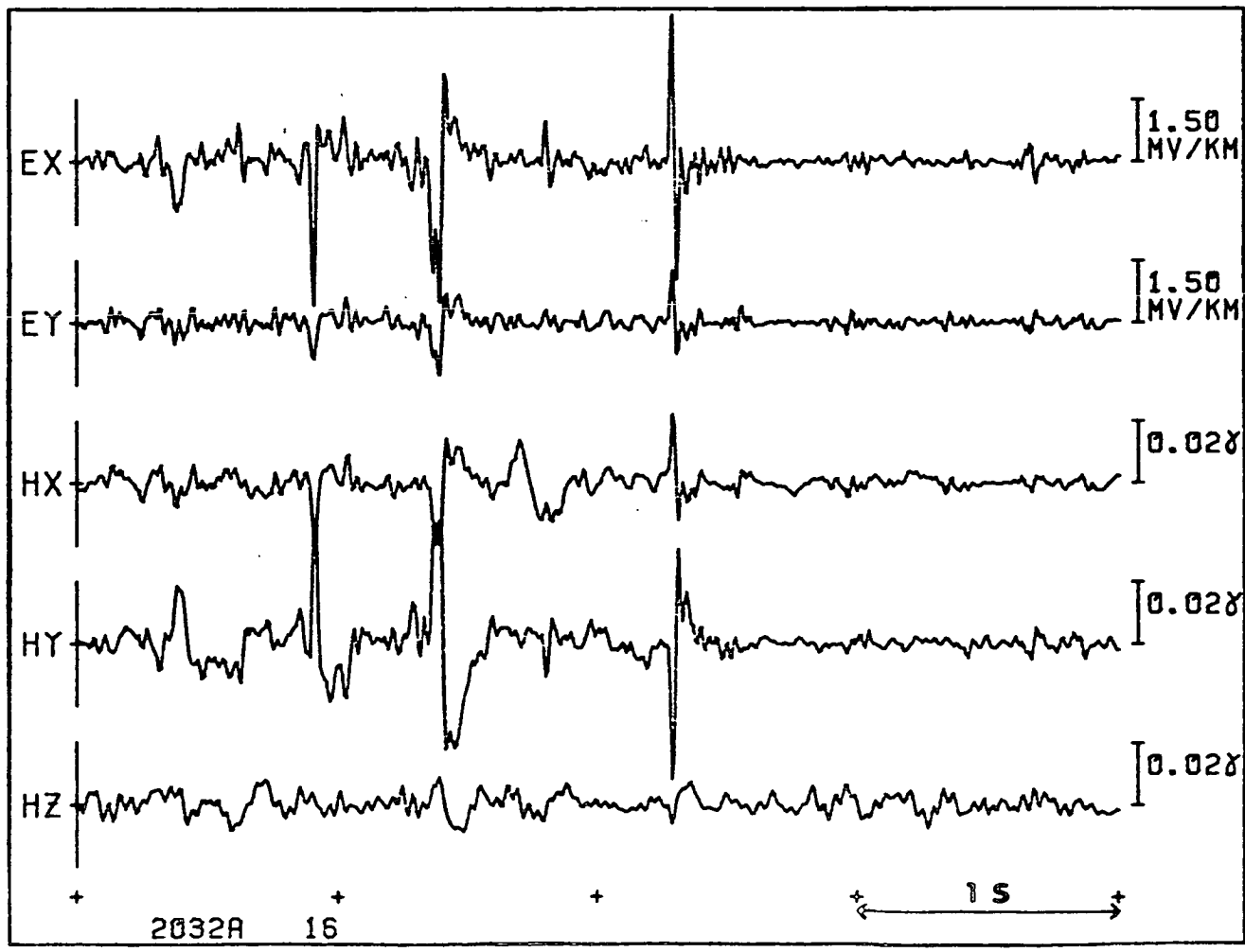
EX
EY
HX
HY
HZ
1.50 MV/KM
1.50 MV/KM
0.02γ
0.02γ
0.02γ
1S
2032A 16

B

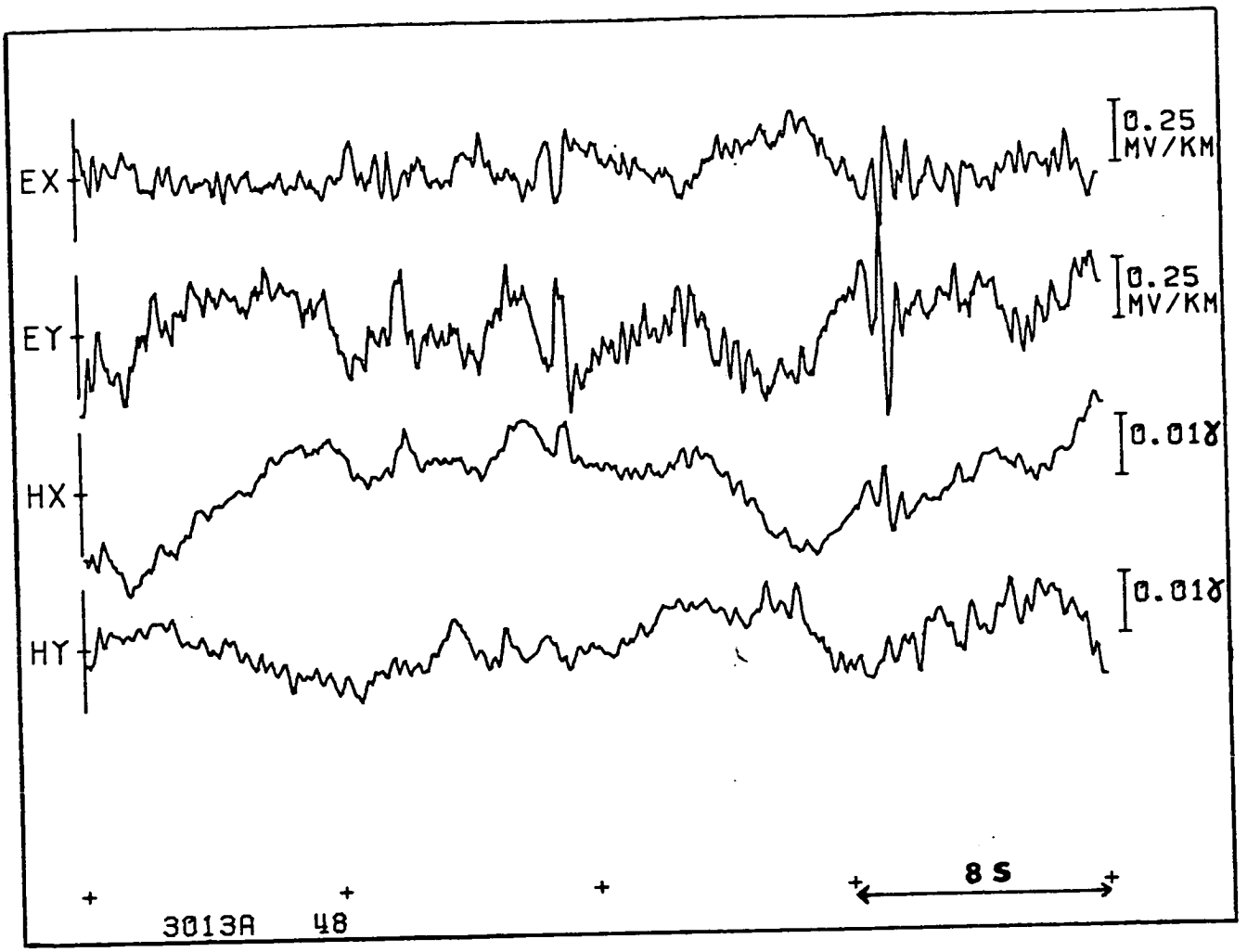
EX
EY
HX
HY
0.25 MV/KM
0.25 MV/KM
0.01γ
0.01γ
8 S
3013A 48

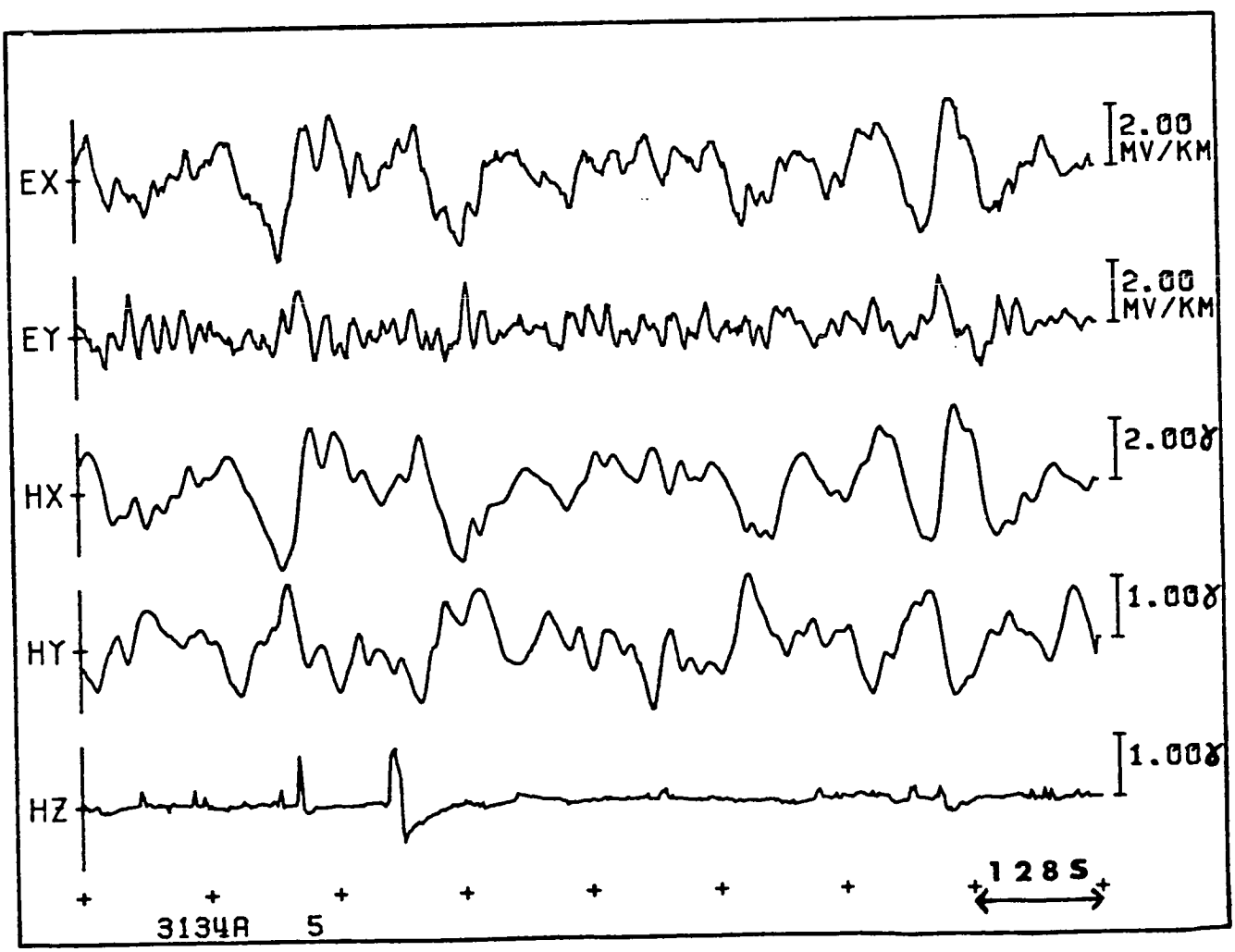
EX
EY
HX
HY
HZ
2.00 MV/KM
2.00 MV/KM
2.00γ
1.00γ
1.00γ
128 S
3134A 5

measurements of the same data band could be analysed either individually or collectively. The importance of this is highlighted in section 4.3 later.

The analysis of each field component of the individual event time series was done in the frequency domain. The following principal steps were carried out. (1) The time series was scaled using the recording gains. (2) The data were reduced to zero mean and zero trend (Bendat and Piersol, 1971) by using a least squares straight line fit - these two steps were used respectively to avoid discontinuities which would give rise to side lobes leading to leakage and to avoid spectra amplitude contamination by the non-periodic part. (3) The first and last 10% of the data set were tapered using a cosine bell window (Harris, 1978). (4) The data set was padded if necessary with zeros to make the total number of data points an exact power of 2 to satisfy the requirement of the Fast Fourier Transform (FFT) algorithm of Cooley and Tukey (1965). (5) FFT was performed using the above algorithm. (6) Frequencies containing 50 Hz and odd harmonics were removed along with their aliased frequencies. (7) Spectral smoothing was done by averaging over adjacent frequencies (Bendat and Piersol, 1971), followed by instrument response corrections. (8) Auto- and cross-spectral estimates .were then calculated and from these the impedance tensor elements were computed using equation (2.38) with P and Q chosen as H_x and H_y respectively. Further computations included the determination of apparent resistivities and phases in the measuring directions (Cagniard resistivities

and phases), polarisation, predicted H_z, E_x and E_y coherences, tipper coefficients and induction vectors using equations (2.26a,b), (2.27), (2.31) and (2.36) respectively. If desired, individual events could be plotted and/or listed.

4.2.4 Comparison of different averaging techniques

Averaging is an inherent part of experimental science since every measurement is usually made more than once and experimental MT is no exception. However, in most published MT work, there is hardly any mention of how the average value of a given quantity has been obtained. A notable exception is the publication by Bentley (1973).

After obtaining the smooth spectra from each individual event, there are three possible ways of combining all the different single events, i.e., averaging. The three possibilities are

(i) averaging the auto- and cross-spectra assuming a normal distribution, or (ii) averaging the impedance tensors assuming a lognormal distribution, or (iii) averaging the apparent resistivities assuming a lognormal distribution. The first two averaging techniques are quite convenient for the later necessary data rotations to the principal or fixed directions and for the invariant calculations, while the third is very cumbersome and hence more time consuming for such manipulations. All the previous MT workers in the Edinburgh Geophysics Department, e.g., Rooney (1976), Jones (1977), Mbipom (1980), used the second averaging technique. The first two averaging techniques

are compared here. In each case, the quantities from the different single events satisfying specified criteria were averaged together assuming the relevant distribution stated above and the standard deviations calculated. The criteria which have been used are discussed later. Using the standard deviations and the theory of error propagation, the errors in all the subsequent MT parameters derived from the averages were calculated. Two examples illustrating the results of the comparison between the averaging techniques are presented here. Figures 4.3A,B show at two different sites the apparent resistivities, phases, etc., resulting from the two averaging techniques - the error bars have been omitted for clarity. There is general excellent agreement between the two techniques; the only slight discrepancy is in the neighbourhood of frequency 0.1 Hz where the signal level is generally low. Figures 4.3C,D show the same plots as in Fig. 4.3A, but now plotted separately with their error bars. It can be seen that the error bars are very much larger in the spectra averaging case. This is due to the fact that the standard deviations are often as large as the average spectra values and sometimes even larger. Hence, the simple error propagation formulae are inadequate - a more sophisticated error analysis approach is needed.

Since the electric and magnetic field components vary drastically from time to time, i.e., different signal levels, the underlying spectra vary similarly and this implies an added component of variability. High and low spectral levels are averaged together giving rise to the large

FIGURE 4.3A,B

Comparison (at two different sites) of the AMT/MT plots resulting from spectra and impedance averaging (error bars have been omitted for clarity) - ● and ▲ denote impedance tensor and spectra averaging respectively.

Since the same events have been used in both averaging techniques, the predicted coherence plot is identical for the two cases (+ and □ for the E_x and E_y coherences respectively).

FIGURE 4.3C,D

Same plots as in Fig. 4.3A, but now plotted separately with their error bars (±1 standard deviation).

A

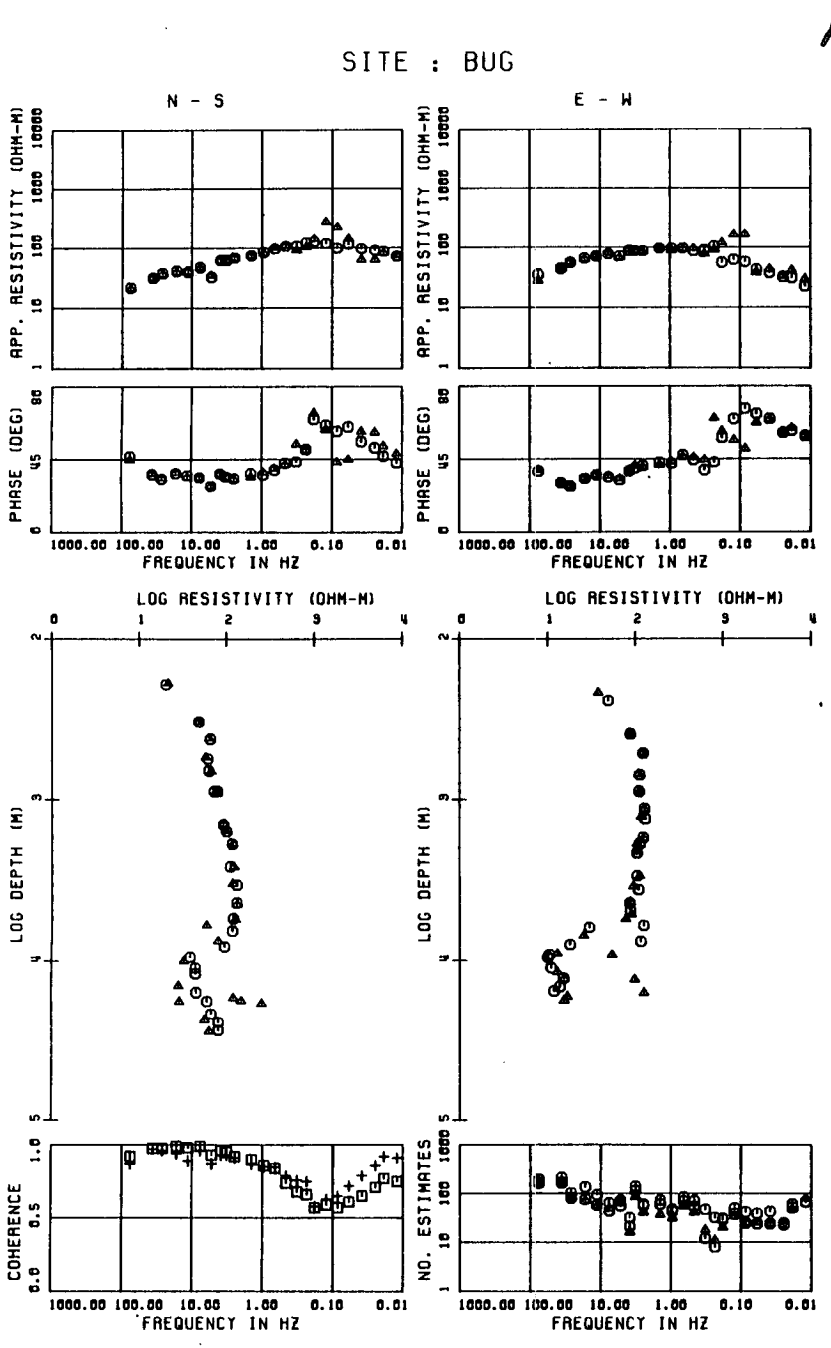
SITE : BUG
N - S
E - W
APP. RESISTIVITY (OHM-M)
PHASE (DEG)
FREQUENCY IN HZ
LOG RESISTIVITY (OHM-M)
LOG DEPTH (M)
COHERENCE
NO. ESTIMATES

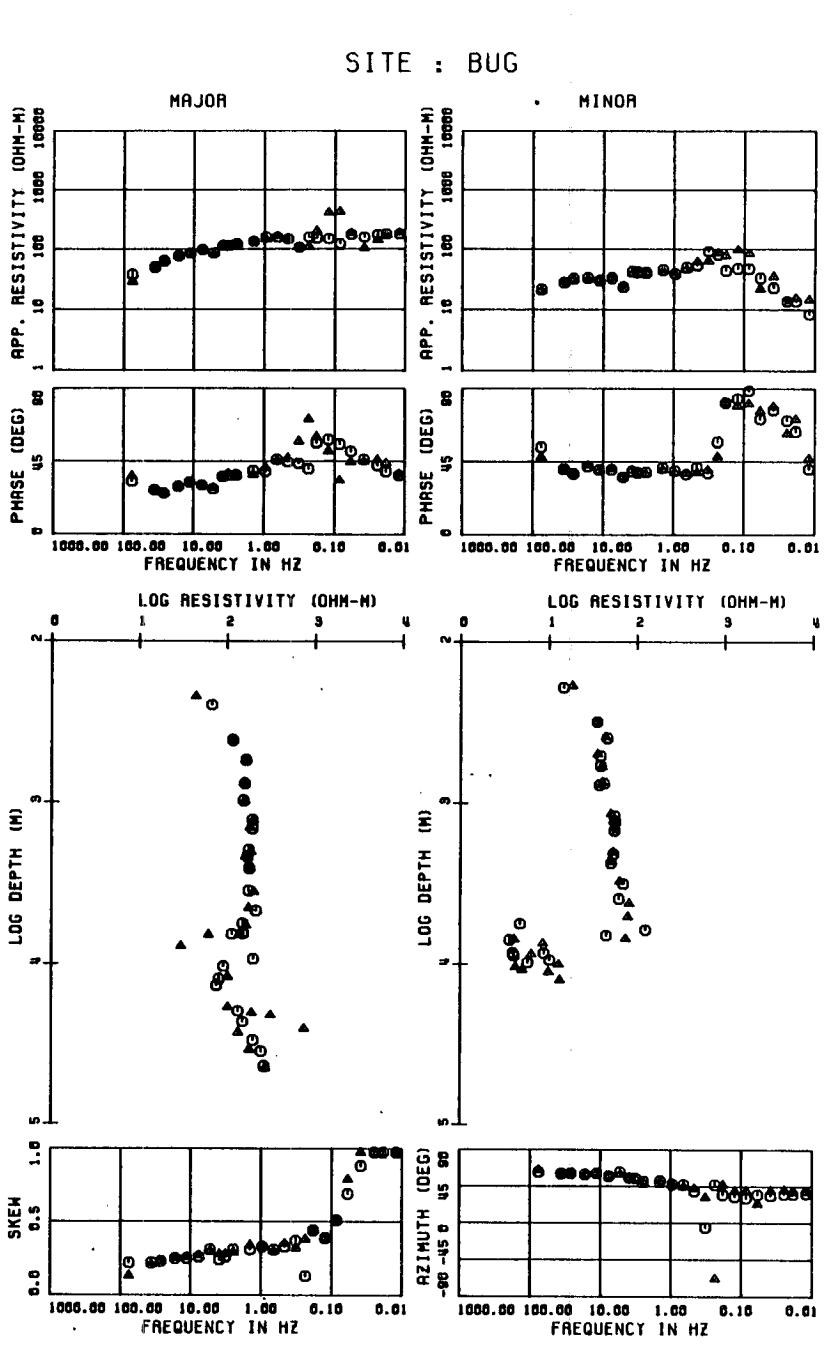
SITE : BUG
MAJOR
MINOR
APP. RESISTIVITY (OHM-M)
PHASE (DEG)
FREQUENCY IN HZ
LOG RESISTIVITY (OHM-M)
LOG DEPTH (M)
SKEW
AZIMUTH (DEG)

701

B

SITE : HUR

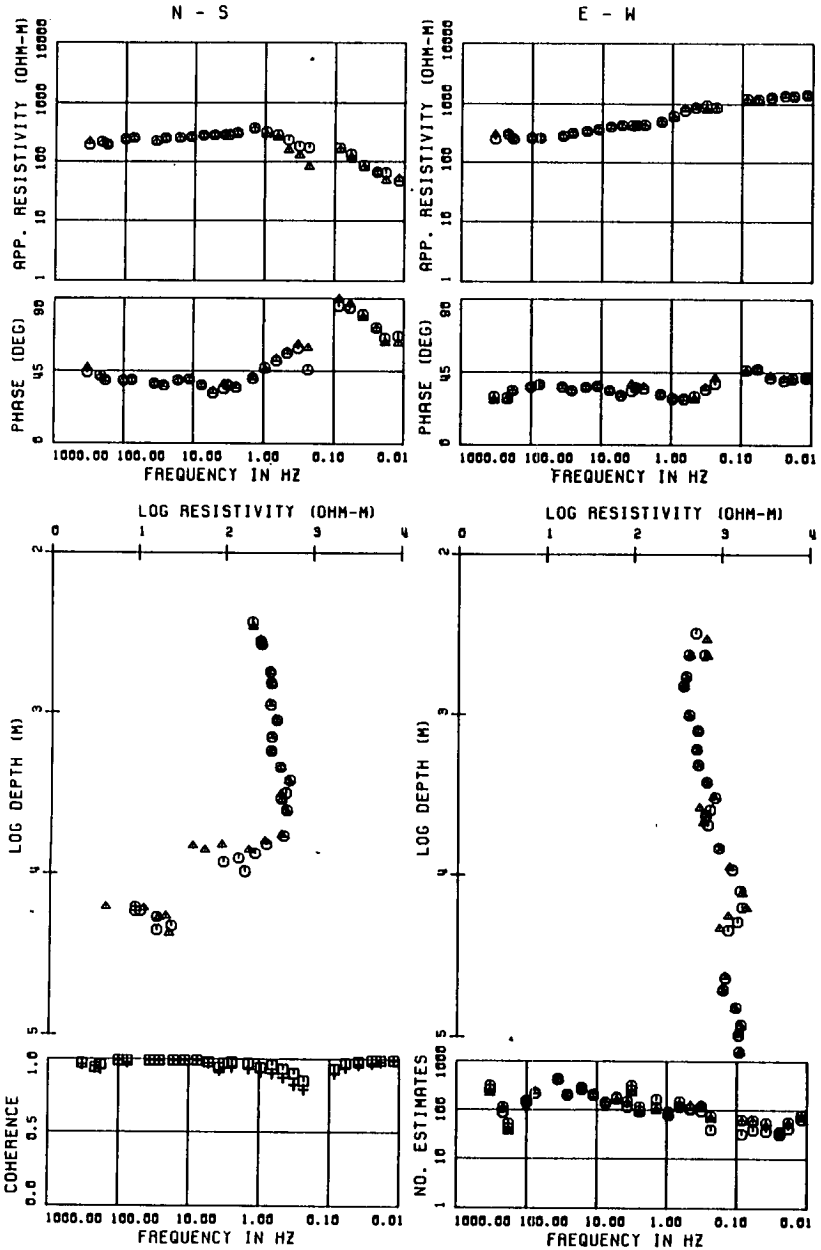

SITE : HUR

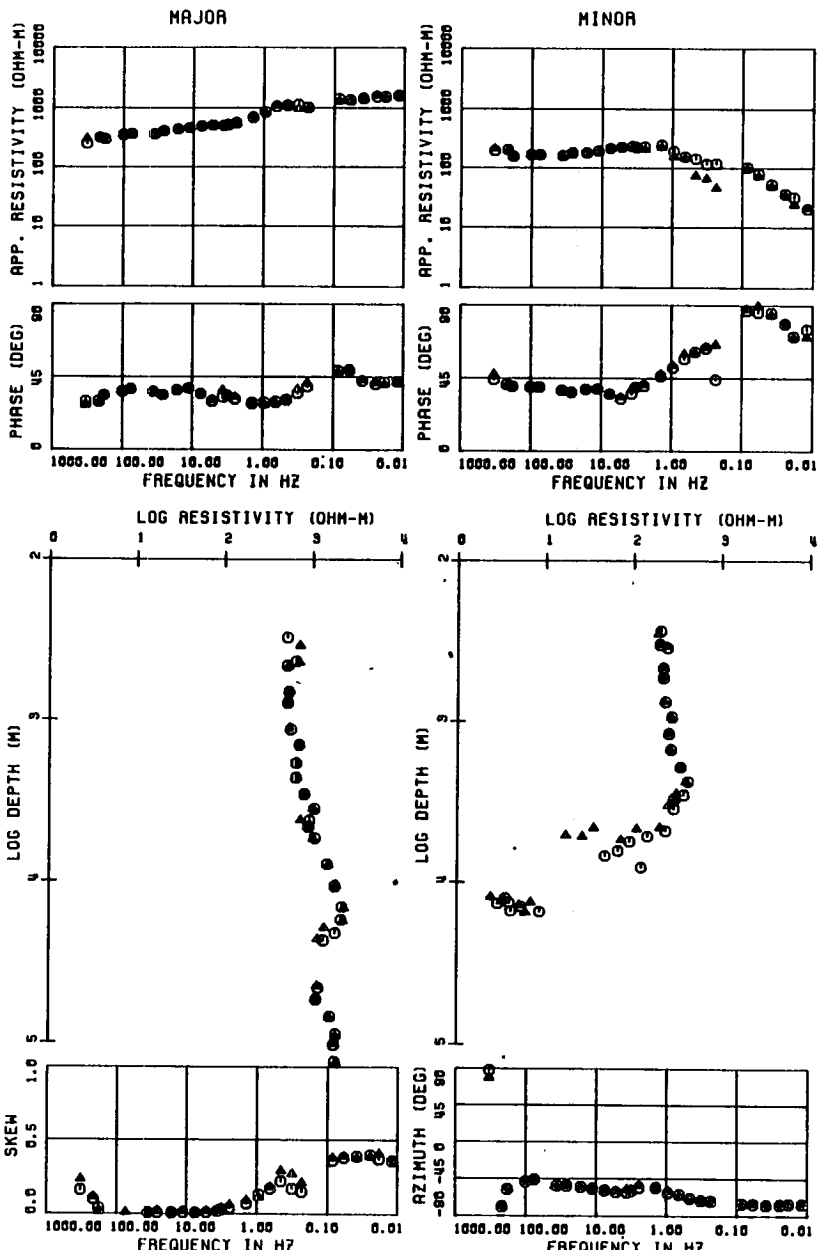

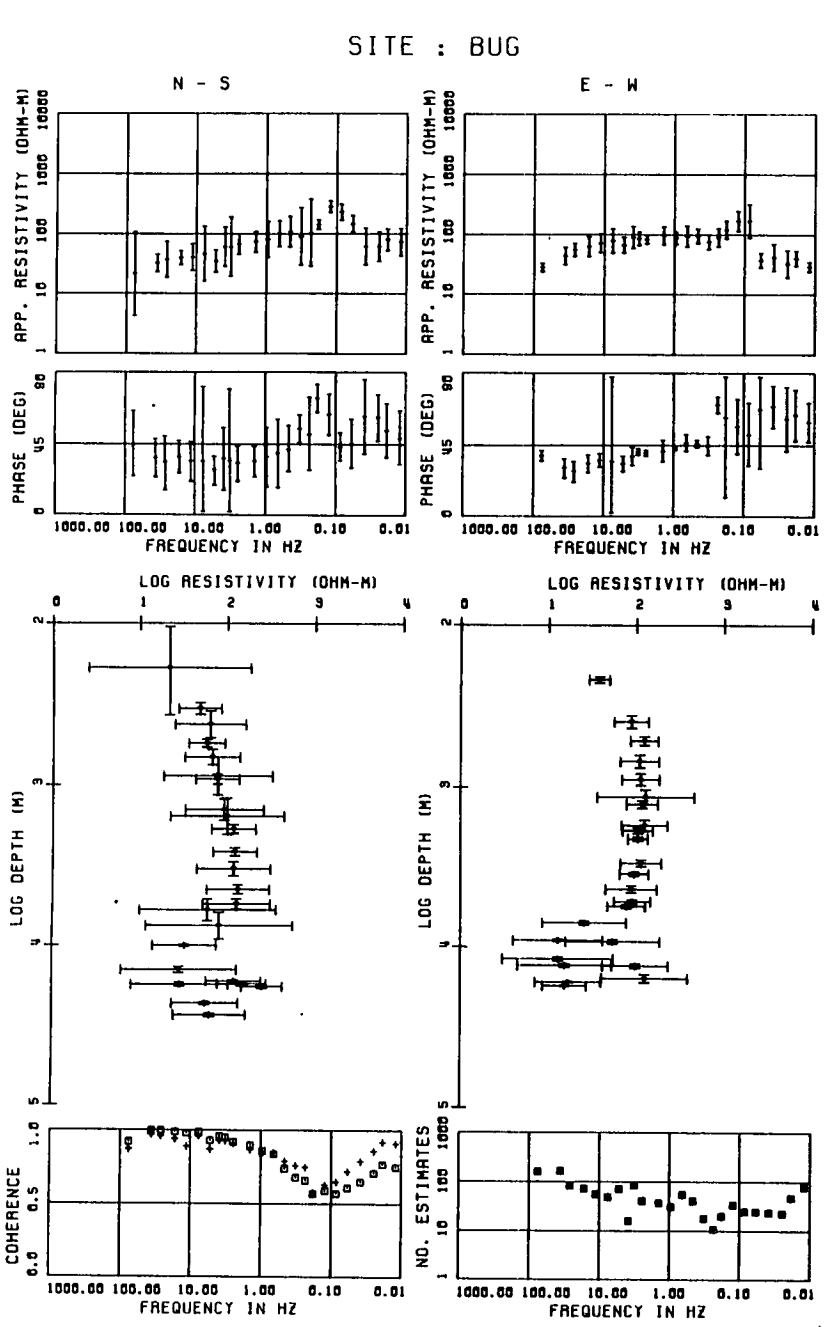
SITE : BUG
N - S
E - W
APP. RESISTIVITY (OHM-M)
PHASE (DEG)
FREQUENCY IN HZ
LOG RESISTIVITY (OHM-M)
LOG DEPTH (M)
COHERENCE
NO. ESTIMATES

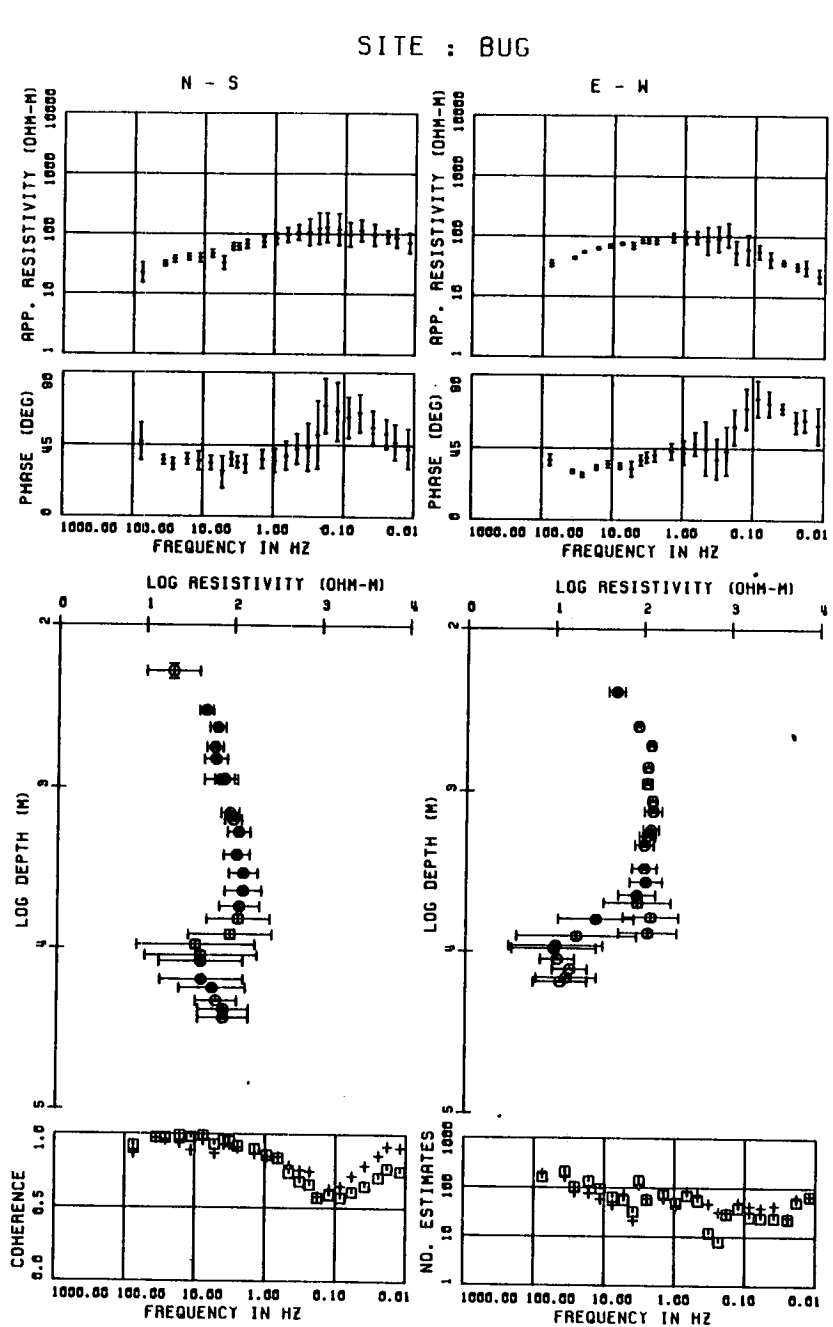
SITE : BUG
N - S
E - W
APP. RESISTIVITY (OHM-M)
PHASE (DEG)
FREQUENCY IN HZ
LOG RESISTIVITY (OHM-M)
LOG DEPTH (M)
COHERENCE
NO. ESTIMATES

L01

D

SITE : BUG

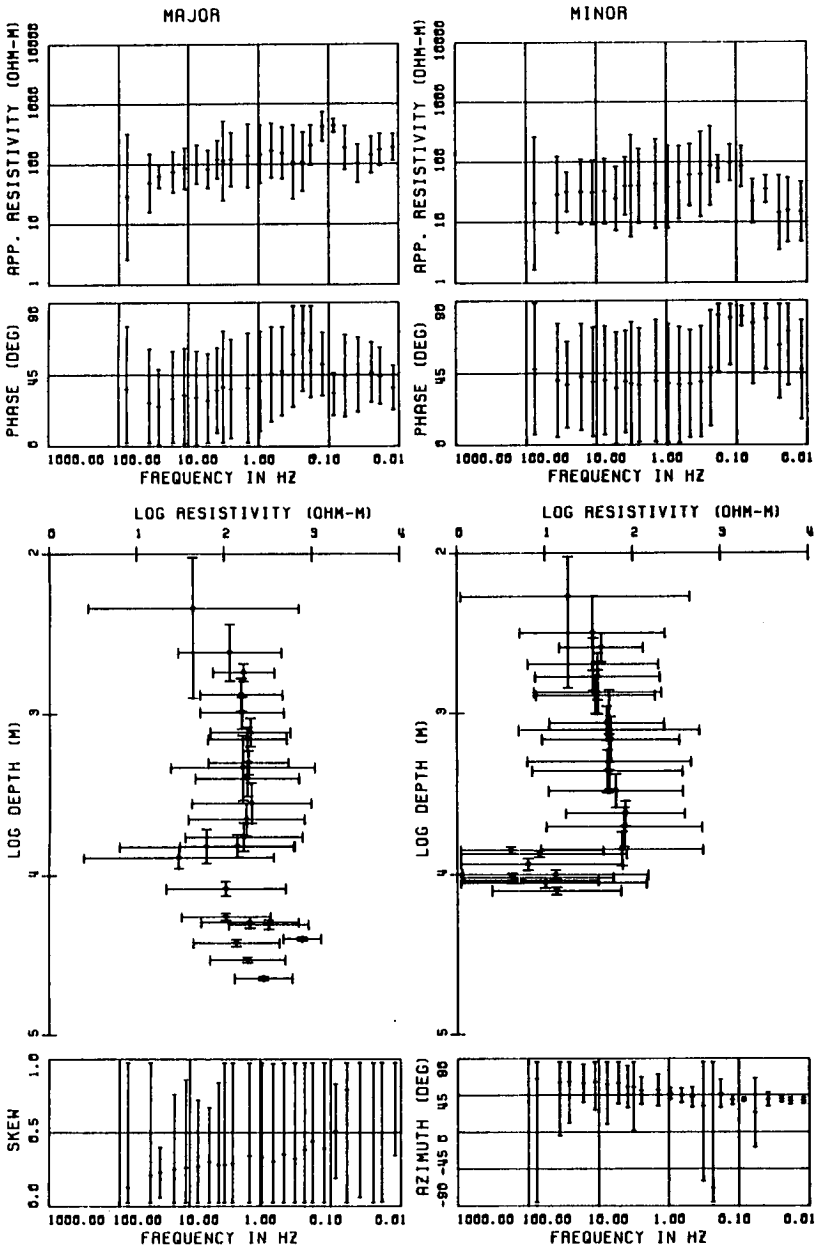

SITE : BUG

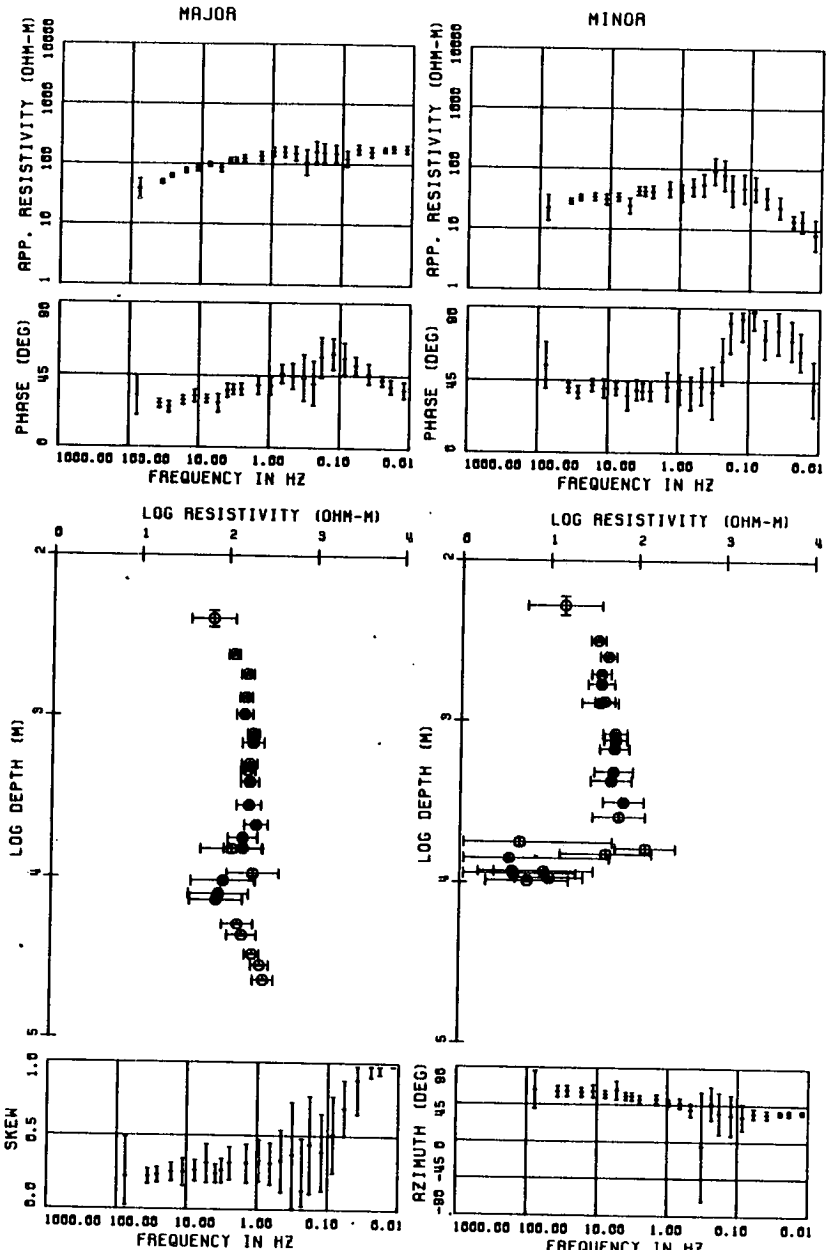

standard deviations. On the other hand, the impedance tensor which is the ratio of the electric to the magnetic field, varies very much less drastically hence accounting for the reasonable amplitudes of the error bars obtained from propagation error formulae. The underlying spectra can be visualized as the product of the true spectra and a random component. How the random component varies from one event to another is unknown and is not easy to determine. Although spectra averaging is no doubt a means of enhancing the signal to noise ratio, its effective use will necessitate some assumptions concerning the random component of the spectra. The latter will add to the normal assumptions already made about the MT technique and in the author's view, this is not very advantageous. Moreover, the impedance tensor is more diagnostic of the subsurface than the individual spectra. Thus, it is concluded that of the three possible averaging techniques in MT, impedance tensor averaging is practically the most convenient. Hence, in the station data averaging, the impedance tensors have been averaged.

4.2.5 Data averaging

The averaging programme read in all the individual analysed events from each data band in turn. Each frequency band was divided into equispaced sub-frequency bands (6/decade on a log scale). The impedance tensors (e.g., Z_{xx}, Z_{xy}, etc., were individually averaged assuming lognormal distribution (Bentley, 1973) and the tipper

coefficients assuming normal distribution. The following criteria were applied :

(i) Coherency rejection : in each sub-frequency band, starting with a predicted coherence value of 0.95 and decreasing in steps of 0.05 to a minimum of 0.80, the percentage of the estimates to be averaged having each of these coherence values and above was noted. The higher coherence value ($\geq$ 0.80) exhibited by more than 50% of the estimates was then used as the acceptable level for the sub-frequency band and all estimates with lower coherences were rejected. The predicted E_x and E_y coherences were used respectively in the case of the averaging of the impedance tensor element pairs $\mathbf{Z}_{xx}$, $\mathbf{Z}_{xy}$ and $\mathbf{Z}_{yx}$, $\mathbf{Z}_{yy}$, while the predicted H_z coherences were used in the tipper coefficient averaging.

(ii) Sign rejection : this is essential since the logarithm of a negative number is undefined. The preferred (i.e., the most frequently occurring) sign (+ or -) of the real parts of the individual impedance elements was found and similarly with the imaginary parts and all the estimates with opposite sign were rejected - no sign rejection for the tipper coefficient averaging and the spectra averaging discussed earlier. In the case of a high quality data set, the sign rejection had no effect.

(iii) Outlier rejection : all estimates lying outside $\pm$2.2 standard deviations from the mean value were rejected and the number of estimates remaining was noted. The new mean and standard deviation were then calculated and the whole procedure was repeated a second time. The purpose

of the outlier rejection was to eliminate extreme values.

On the average, less than 25% of the estimates were rejected after applying all the above criteria in the case of a high quality data set, but more than double in the case of a very noisy data set.

From the mean values of the tipper coefficients, the real and imaginary induction vectors were computed using equation (2.36). Owing to instrumental problems and cultural noise, the recorded vertical magnetic field variations were of very poor quality and hence no useful information was derivable from the induction vectors and they have thus been discarded. Figure 4.4 shows a typical example of the induction vectors obtained in this study.

From the mean values of the impedance tensor elements, subsequent computations included the determination of

(a) apparent resistivities and phases in the measuring directions using equations (2.26a,b);

(b) apparent resistivities and phases in the principal directions (i.e., major and minor) using equations (2.26c,d);

(c) azimuths of the major principal direction using equation (2.25);

(d) skew factors using equation (2.29) and

(e) direct inversion of the apparent resistivity and phase data using the Bostick transform (see the relevant equations in table 2.1).

FIGURE 4.4

Sample plot of the induction vectors obtained in the present study - the azimuths are positive clockwise from the magnetic north which is denoted by zero degree.

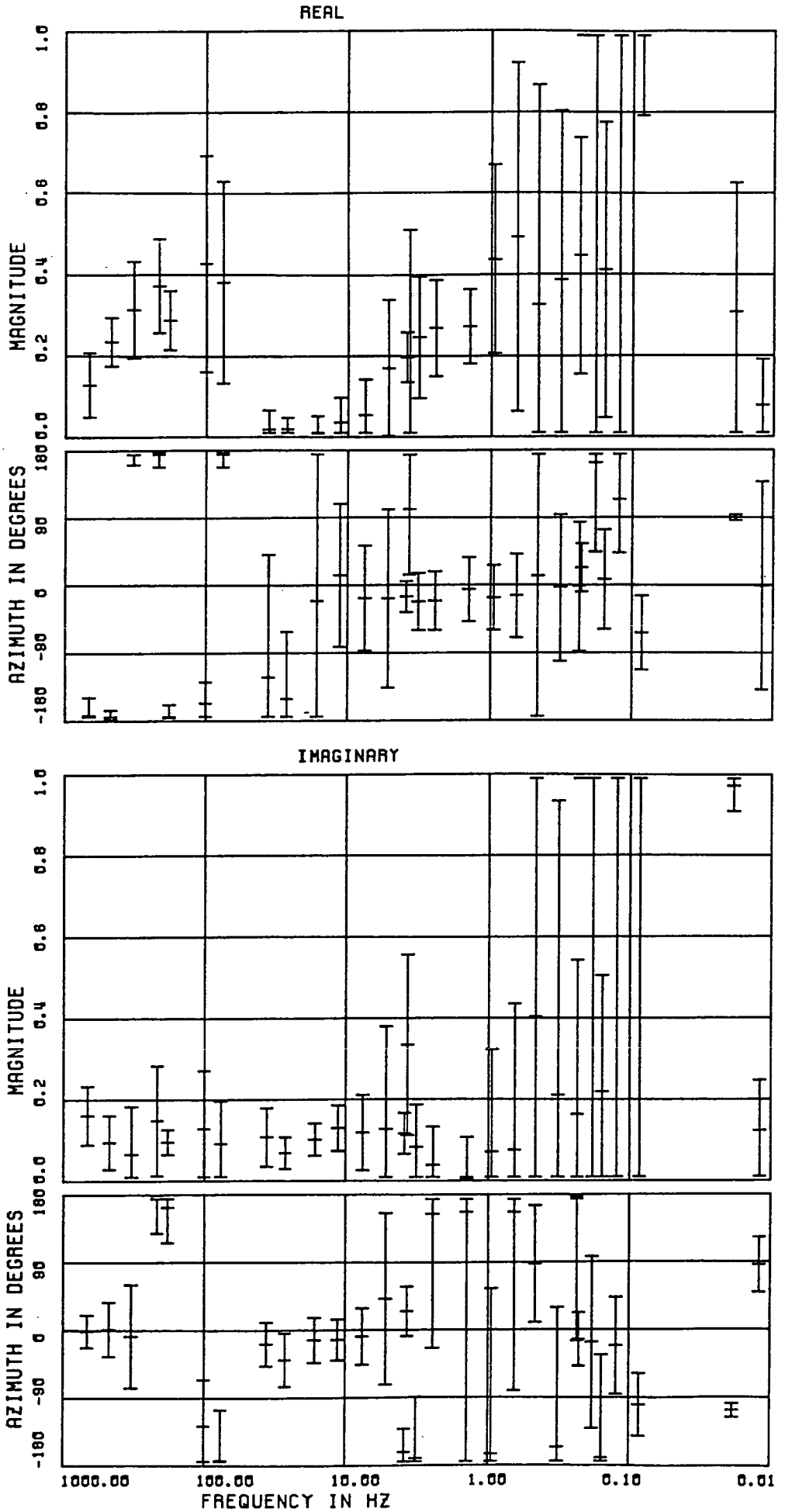
REAL
MAGNITUDE
1.0
0.8
0.6
0.4
0.2
0.0
AZIMUTH IN DEGREES
180
90
0
-90
-180
IMAGINARY
MAGNITUDE
1.0
0.8
0.6
0.4
0.2
0.0
AZIMUTH IN DEGREES
180
90
0
-90
-180
1000.00
100.00
10.00
1.00
0.10
0.01
FREQUENCY IN HZ

4.3 Qualitative approach of extracting results from noisy data

The presence of noise in MT data shows itself in several ways. It may lead to large skew values, but more importantly, very large error bars. The principal directions may vary erratically with period as well as having large error bars as a result of noise. In the case of incoherent noise, the average predicted coherences in the sub-frequency bands will be low and very few estimates will survive after applying the rejection criteria discussed above. Noise can cause considerable scatter in the apparent resistivity and phase plots and segments of these curves may exhibit very abrupt and unrealistic gradients. Some of these enumerated observations can be used in a qualitative sense to reject sub-frequency bands of the processed data and hence extract some useful results from a noisy data set.

As mentioned earlier, there was considerable cultural noise problem at some of the SUF profile sites owing to the inevitable nearness to industrial works. These noise problems were not overcome despite repeat measurements and hence the need to develop a qualitative strategy to minimise these problems. The strategy was based on processing a very large number of events - more than double that used in the case of relatively quiet sites and eliminating sub-frequency bands exhibiting unrealistic apparent resistivity and/or phase gradients, or having large skew error bars, very low average predicted coherences, few number of estimates or exhibiting highly polarised

magnetic polarisation. Without this strategy, it would have been impossible to obtain any results from some of the data bands at some of the profile sites. Figure 4.5 demonstrates the usefulness of this qualitative approach of extracting useful results from noisy data. In (A) and (B), apparent resistivity and phase plots resulting from different recorded events are shown, while the plots resulting from a combination of events (A) and (B) are shown in (C) and (D) shows the plots after applying the above qualitative approach to (C). Far fewer data points than shown in (D) are left if the qualitative approach is applied to either event (A) or (B), thus emphasizing the need to analyse a large number of events at noisy sites. This implies more than one cartridge per data band and hence the necessity for the modification of the analysis programme to facilitate this. Further development of this approach will no doubt enhance the applicability of the AMT/MT technique in very culturally noisy areas. The fact that many events have to be analysed, implies a more lengthy data acquisition time at a noisy site than at a quiet site.

The results of the data analysis are presented in chapter 5. A typical plot of the magnetic and telluric polarisation spreads using all the analysed events is shown in Fig. 4.6.

FIGURE 4.5

Demonstration of the qualitative approach for processing noisy data:-

(A) and (B) show plots using different recorded events;

(C) shows plots resulting from the combination of the events used in (A) and (B), while

(D) shows the plots after applying the qualitative approach to (C).

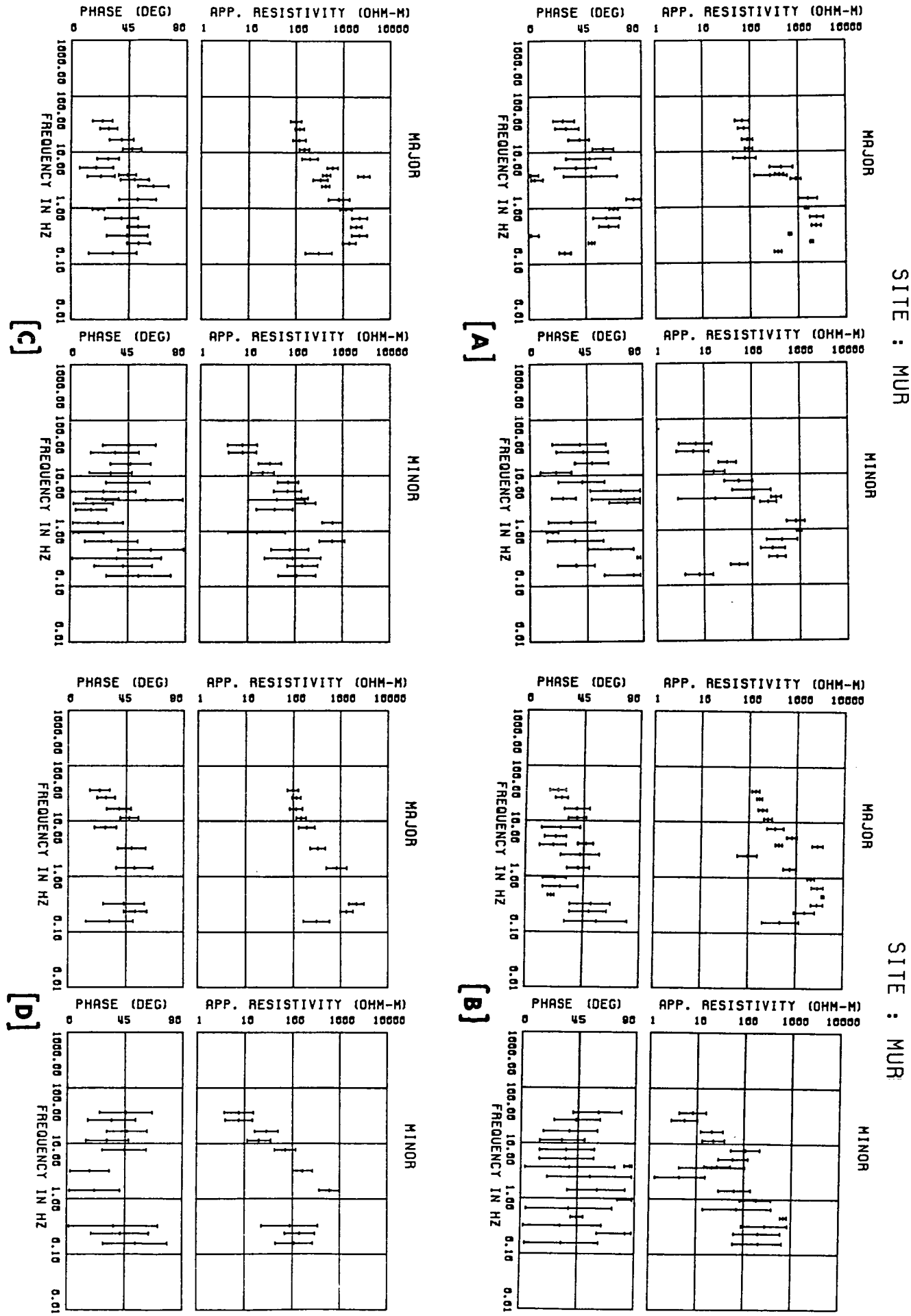
SITE : MUR
[A]
[B]
[C]
[D]
PHASE (DEG)
APP. RESISTIVITY (OHM-M)
FREQUENCY IN HZ
MAJOR
MINOR

FIGURE 4.6

Sample plot of the telluric and magnetic polarisation spreads:-

(A) data band 1 and (B) data band 2; magnetic north, east and west are respectively 0, +90 and -90 degrees.

The numbers, e.g., 1.07, etc., indicate data band 1 and sub-frequency 7 whose frequency is 683 Hz.

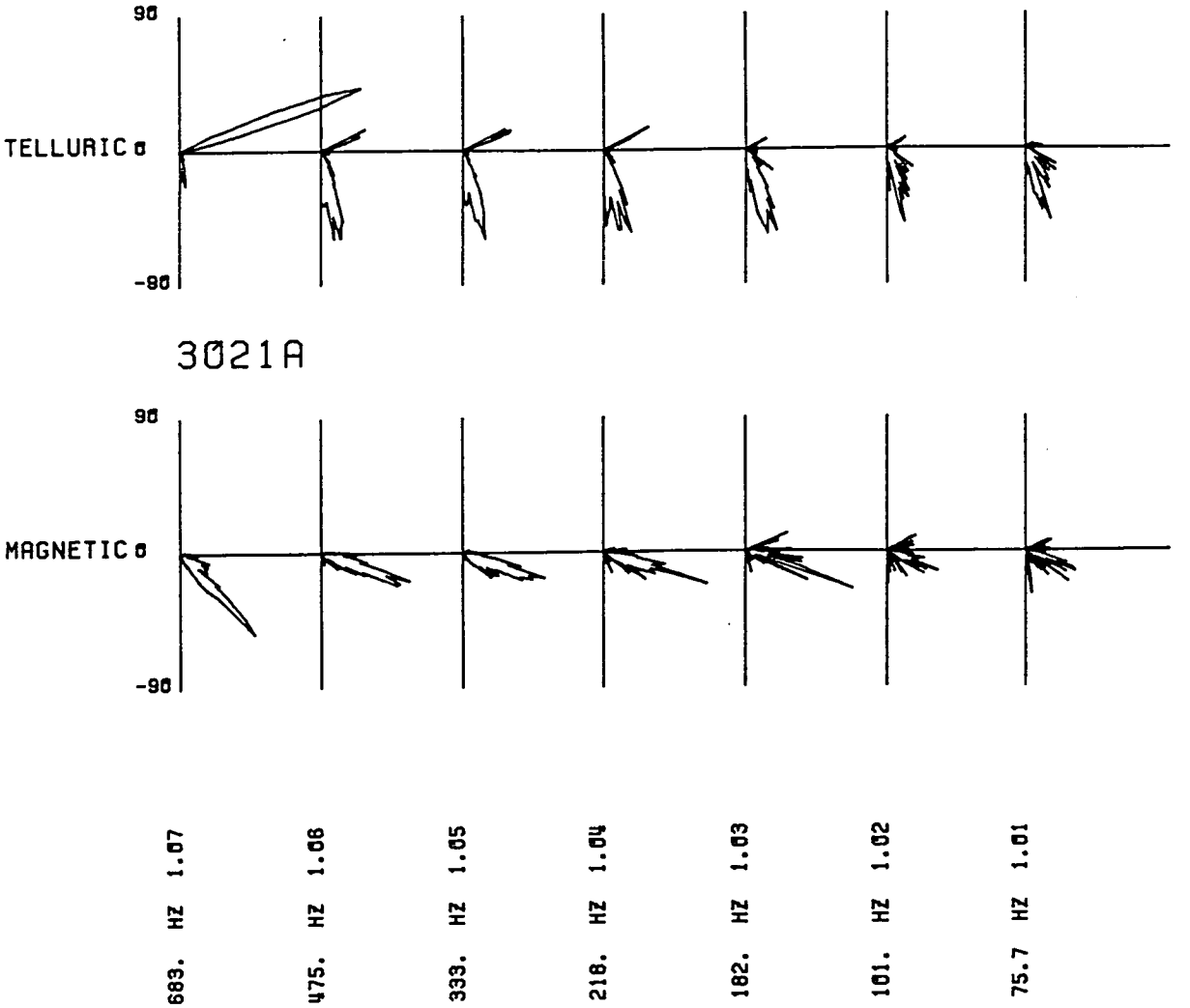
90
TELLURIC σ
-90
3021A
90
MAGNETIC σ
-90
683. HZ 1.07
475. HZ 1.06
333. HZ 1.05
218. HZ 1.04
182. HZ 1.03
101. HZ 1.02
75.7 HZ 1.01

A

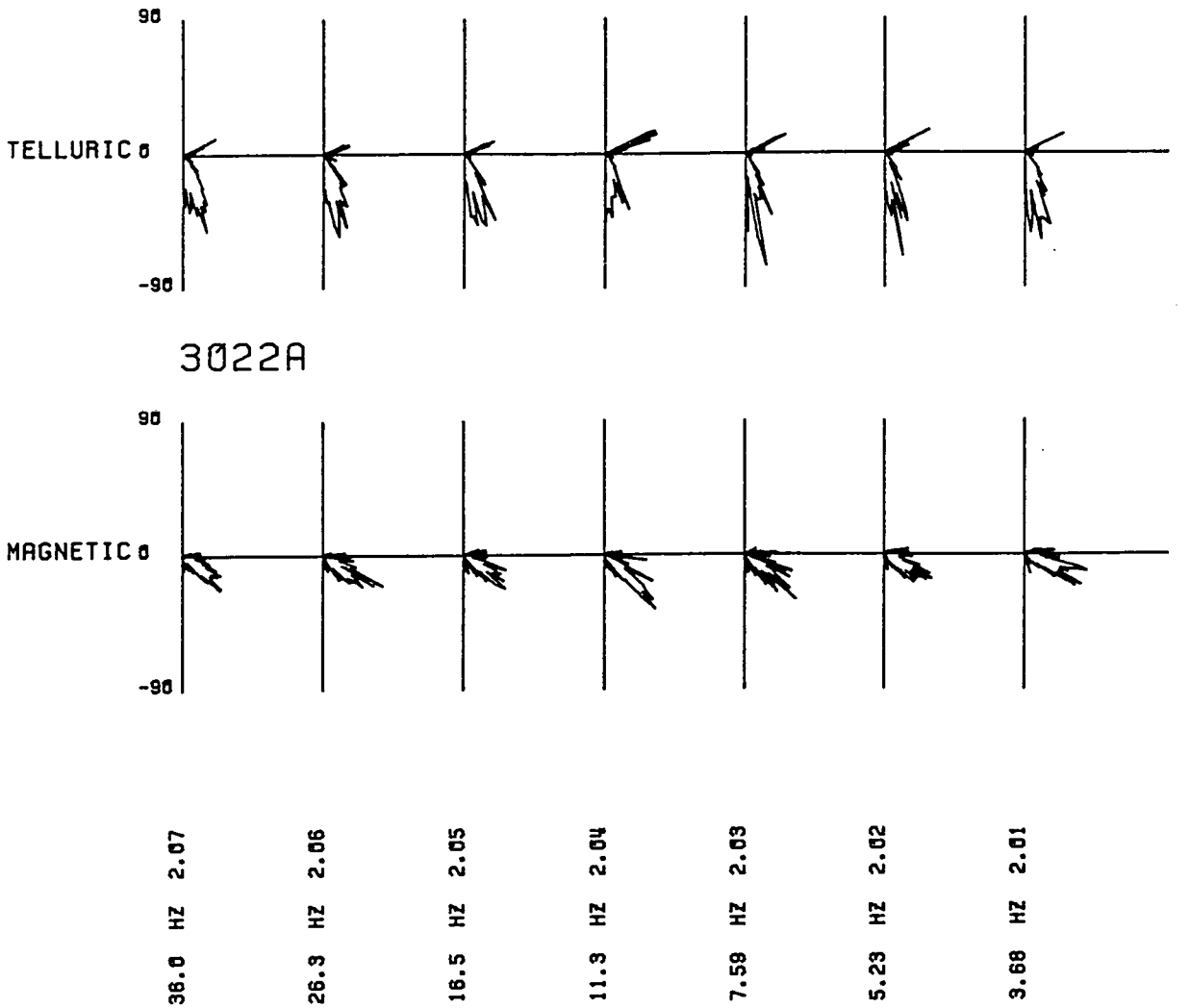
90
TELLURIC 0
-90
3022A
90
MAGNETIC 0
-90
36.0 HZ 2.07
26.3 HZ 2.06
16.5 HZ 2.05
11.3 HZ 2.04
7.58 HZ 2.03
5.23 HZ 2.02
3.68 HZ 2.01

B

CHAPTER 5

DISCUSSION OF RESULTS AND 1D MODELLING

The VLF/R data together with a qualitative discussion are presented in this chapter. The results of the AMT/MT data analysis are also presented at each site in terms of apparent resistivity and phase plots, the corresponding Bostick transform resistivity-depth plots, average predicted coherences, number of estimates, skew and azimuth of the major impedance plots. The azimuths are with reference to magnetic coordinates and 0, 90, -90 degrees denote respectively magnetic north, east and west. A discussion of 1D layered modelling using a Monte-Carlo algorithm is given followed by a discussion of the 2D section obtained from a collation of the various 1D models. A comparison between the Bostick real resistivity-depth plots and the Monte-Carlo layered models shows a very good agreement. The computational time for the Bostick plots is less than 10% of that for the Monte-Carlo models. Thus, the Bostick transform is computationally efficient and is hence advantageous for incorporation in real-time and routine MT analysis as a useful aid to interpretation.

5.1 The VLF/R results

As indicated in section 3.7, at least 10 spot readings of the apparent resistivity and phase were taken at each site where the VLF/R measurements were made. The minimum resistivity and phase readings possible with the VLF/R equipment were 5 ohm-m and 0.5^0 respectively. In Table 5.1a, the averages of all the readings and their standard deviations are shown at each site.

Since the objective of the VLF/R measurements was to provide subsurface resistivity information about the uppermost tens of metres and also because of the more than one decade frequency gap between 16 kHz and the beginning of the AMT data (1 kHz), the VLF/R average data were not appended to the respective AMT/MT data at the modelling stage. Thus, the VLF/R data were used only qualitatively. An average observed VLF/R phase value of 45±2 degrees was interpreted as indicating a constant subsurface resistivity to at least a skin depth and its resistivity value was the measured apparent resistivity. The values at sites WLA, KE2, CHO and CAM satisfy this condition, while those at MUR and BUG only do so approximately. A phase value outside the above range implied two layers within a skin depth of the subsurface. Phase values greater than 47^0, e.g. at SAW, implied the bottom layer was the less resistive layer, while phase values less than 43^0, e.g. at WAN, BER and SCR, implied a more resistive second layer. These qualitative inferences are summarized in Table 5.1b; the skin depths shown are obtained by substituting the average apparent resistivity

TABLE 5.1a

Tabulation of the average VLF/R data and their standard deviations

SITE	AVERAGE		STANDARD DEVIATION	
	RESISTIVITY (ohm-m)	PHASE (deg.)	RESISTIVITY (ohm-m)	PHASE (deg.)
MUR	60	42	10	2
SAW	110	52	10	1
BUG	65	49	5	2
WAN	150	37	20	2
WLA	380	45	25	1
BER	1100	31	60	1
SCR	900	31	85	1
KE2	210	45	20	1
CHO	150	47	15	2
CAM	240	46	15	1

TABLE 5.1b

Qualitative inferences from the VLF/R data

SITE	SKIN DEPTH (m)	INFERENCES
MUR	31	approximately one layer
SAW	42	2 layers; resistor overlying a conductor
BUG	32	approximately one layer
WAN	49	2 layers; conductor overlying a resistor
WLA	78	1 layer
BER	132	2 layers; conductor overlying a resistor
SCR	119	2 layers; conductor overlying a resistor
KE2	57	1 layer
CHO	49	1 layer
CAM	62	1 layer

values in Table 5.1a, transmitter frequency (16 kHz) and μ_0 into equation (2.10a).

The VLF/R data indicate lateral resistivity variation in the top few metres of the subsurface under the SUF profile, but uniform under the Duns area.

5.2 Individual site AMT/MT results

As stated in section 4.1, the Duns sites were projected on to the SUF profile to give a single traverse of 20 sites running from N40^{0}W geographic to S40^{0}E through a distance of 35.3 km. The two remaining sites (WHI, CAI) to the NE of the Duns area were too far to be projected on to the profile and hence were not modelled; the data recordings at these sites were in fact made to demonstrate the AMT technique to undergraduate students during their Christmas 1983 fieldwork exercise.

Starting from the NW towards SE, the AMT/MT results at the various sites are presented (Figs. 5.1a-v) and discussed briefly. Sites MUR to BUG are in the Midland Valley, while the remaining sites are in the Southern Uplands. From surface geology, BUG and WAN are north and south of the SUF respectively, while the Dunbar-Gifford fault (DGF) passes between SAW and BUG (Fig. 1.1).

MUR lies within the Carboniferous millstone grit series. There was considerable noise problem here owing particularly to nearness to a power station and an open pit coal mine. Without the qualitative approach developed and discussed in section 4.3, it would have been impossible

to obtain any AMT results. The apparent resistivity values (Fig. 5.1a) increase from between 10 and 100 ohm-m at the short periods to between 100-1000 ohm-m at the middle periods and decrease to less than 100 ohm-m at the long periods. The phase values vary between 25^0 and 60^0. The skew values are low (< 0.2) above 1 Hz, but tend to increase to about 0.5 at 0.01 Hz. The azimuth of the major impedance is on the average 70^0W of magnetic north.

SPM, SAW and BUG lie within the Carboniferous limestone series. There was a varying degree of noise problem with data band 1 and BUG was the worst affected. At these sites, the apparent resistivity and phase plots as well as their Bostick transform plots (Figs. 5.1b-d) indicate a resistivity depth profile of resistor, conductor, resistor and finally conductor. At SPM, the apparent resistivity values vary between about 30 and 1800 ohm-m and the phase values between about 20^0 and 60^0. At SAW and BUG, the apparent resistivity values vary respectively between 5 and 120 ohm-m; 10 and 200 ohm-m. Their phase values vary between 25^0 and 85^0. At all the three sites, the skew values are on the average less than 0.3, but at SAW and BUG the skews are greater than 0.5 at frequencies below 0.4 Hz. The azimuth of the major impedance is on the average N70^0E at SPM, but there are a few data points with average N75^0W. The average azimuth of the major impedance is about N45^0W at SAW and about N45^0E at BUG.

WAN and WLA are situated within the Ordovician Ashgill and Caradoc series. There was severe noise problem at WAN owing to nearness to a reservoir and electric fencing.

FIGURE 5.1A-V

The AMT/MT results at each of the sites. Along the measuring directions (magnetic N-S and E-W) and the preferred directions (major and minor), the apparent resistivity- and phase-frequency plots and the corresponding Bostick resistivity-depth plots are shown. Also plotted are the average predicted E_x (+) and E_y (▽) coherences of all the analysed events; number of estimates used in the impedance averaging (+ for Z_{xx}, Z_{xy} and ▽ for Z_{yx}, Z_{yy}); skews and the azimuth of the major impedance.

N.B.

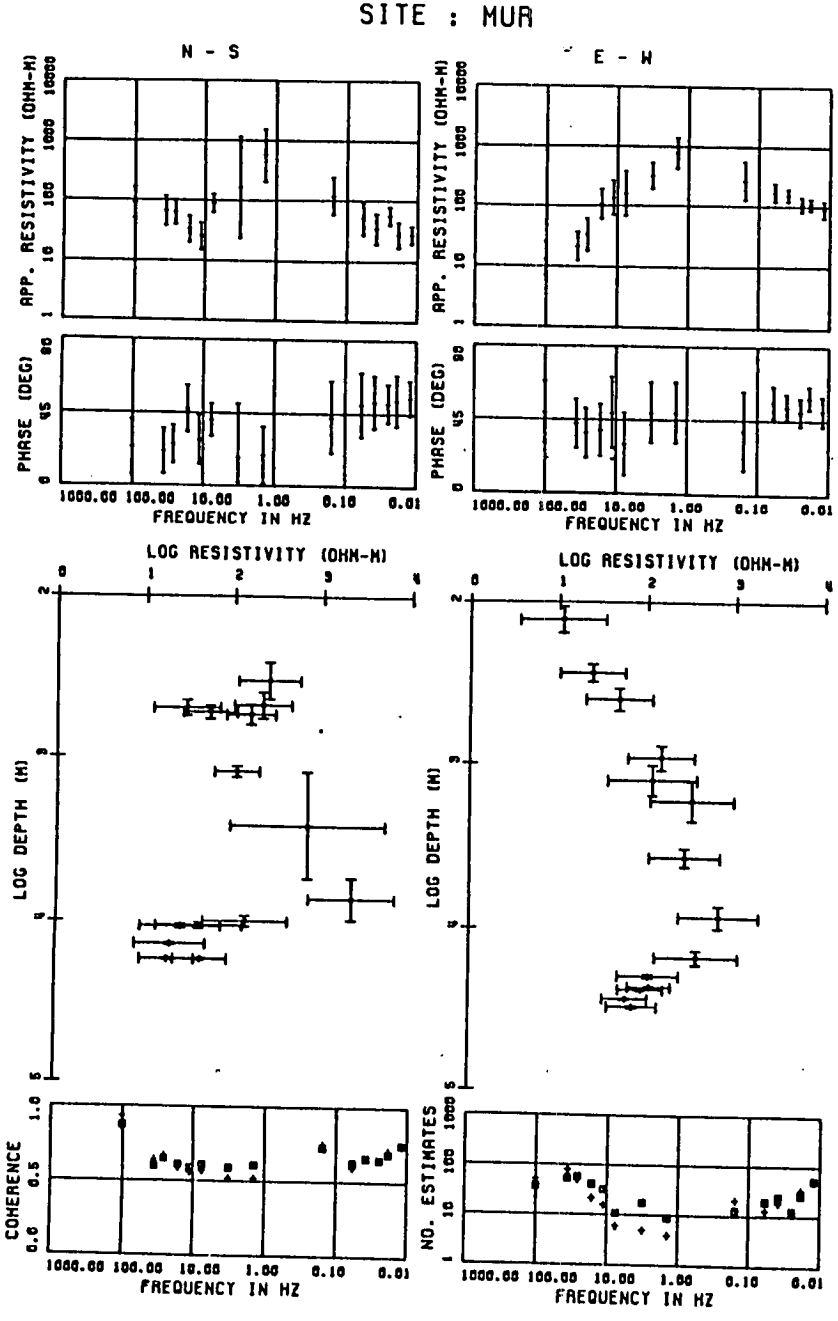
SITE : MUR
N - S
E - W
APP. RESISTIVITY (OHM-M)
PHASE (DEG)
FREQUENCY IN HZ
LOG RESISTIVITY (OHM-M)
LOG DEPTH (M)
COHERENCE
NO. ESTIMATES

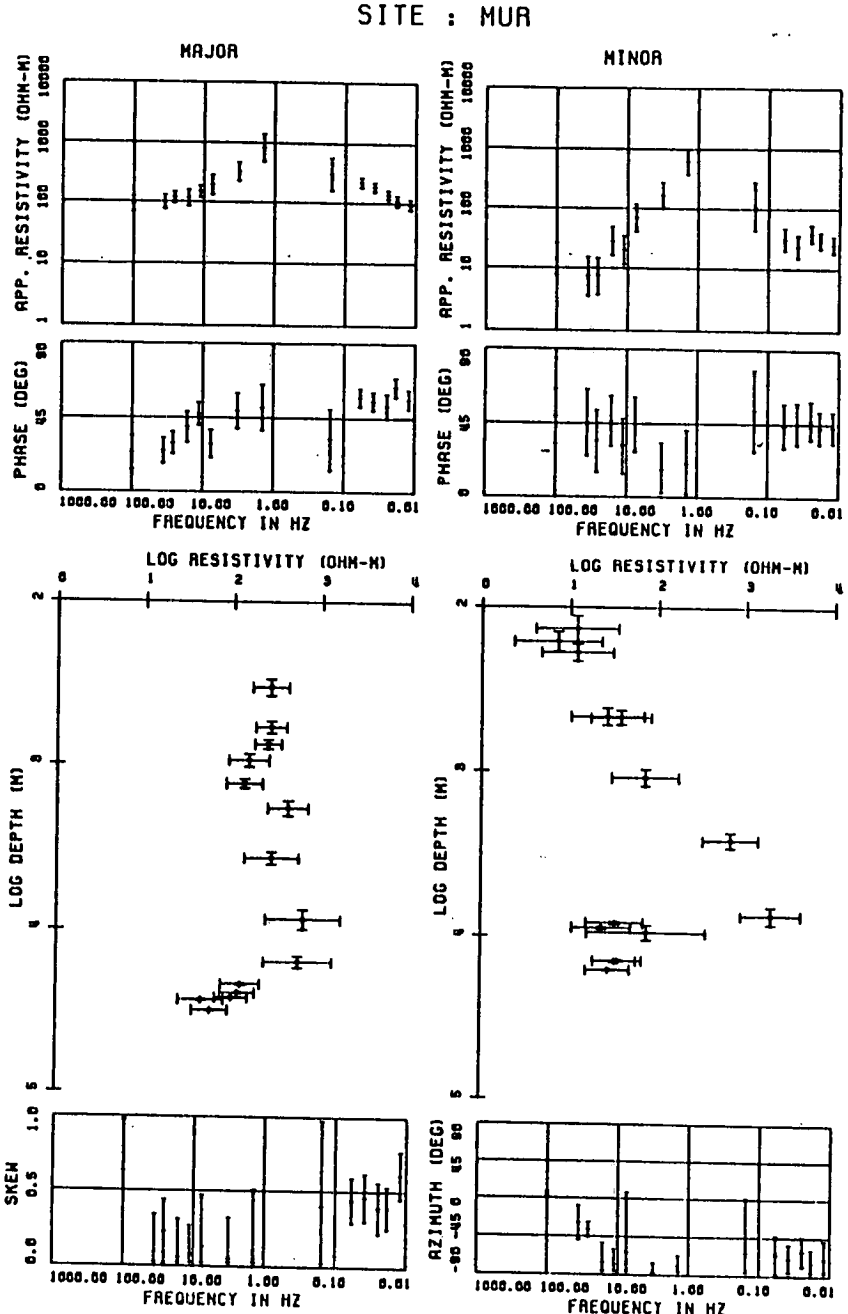
SITE : MUR
MAJOR
MINOR
APP. RESISTIVITY (OHM-M)
PHASE (DEG)
FREQUENCY IN HZ
LOG RESISTIVITY (OHM-M)
LOG DEPTH (M)
SKEW
AZIMUTH (DEG)

Fig. 5.1a

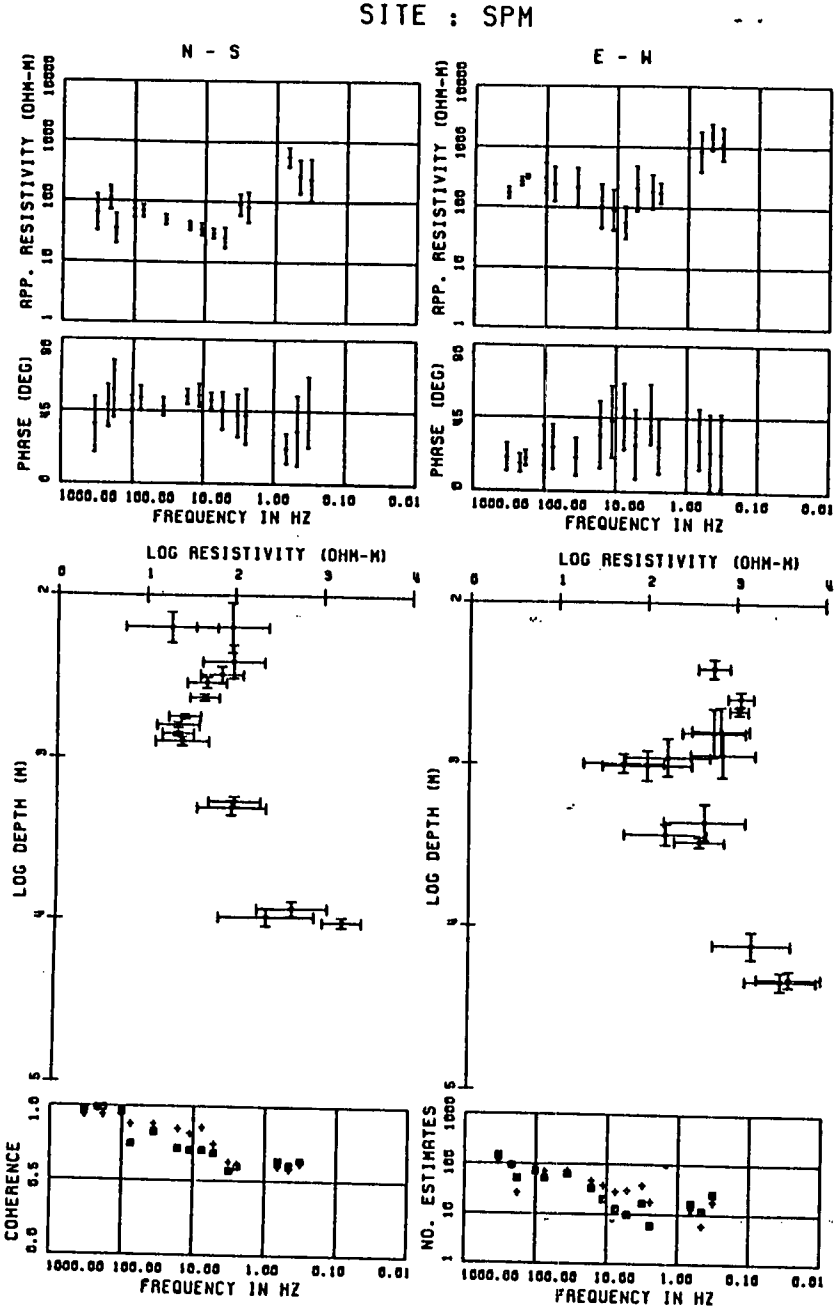
SITE : SPM
N - S
E - W
APP. RESISTIVITY (OHM-M)
PHASE (DEG)
FREQUENCY IN HZ
LOG RESISTIVITY (OHM-M)
LOG DEPTH (M)
COHERENCE
NO. ESTIMATES

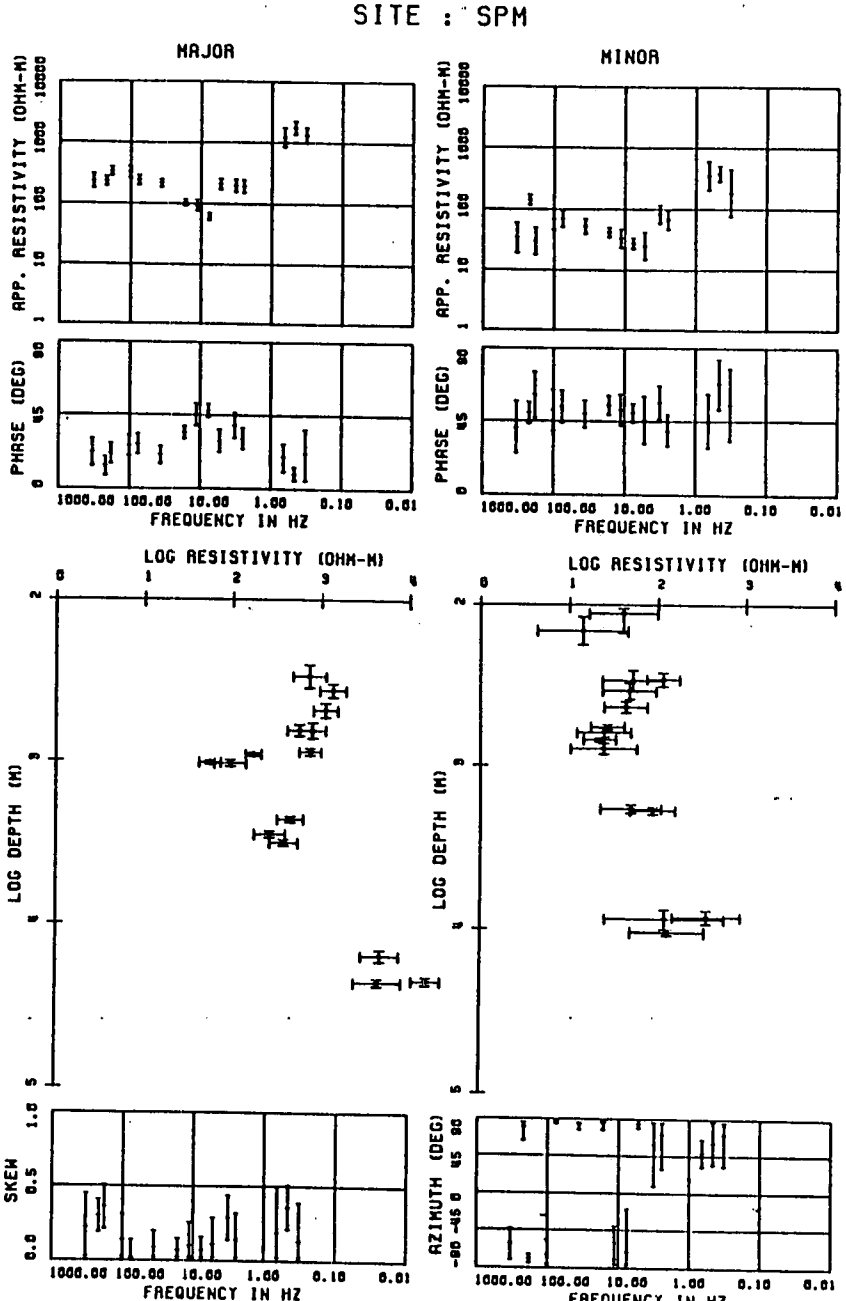
SITE : SPM
MAJOR
MINOR
APP. RESISTIVITY (OHM-M)
PHASE (DEG)
FREQUENCY IN HZ
LOG RESISTIVITY (OHM-M)
LOG DEPTH (M)
SKEW
AZIMUTH (DEG)

Fig. 5.1b

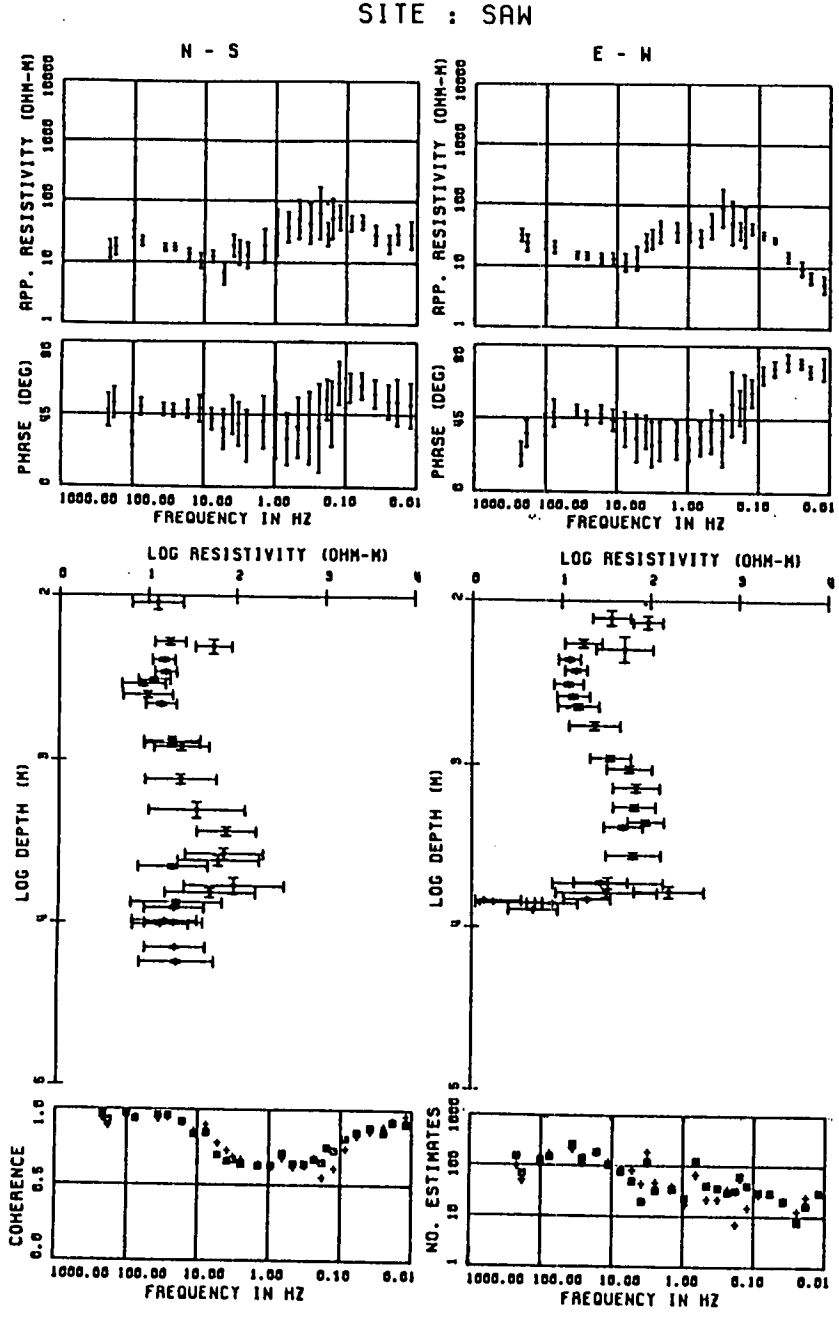
SITE : SAW
N - S
E - W
APP. RESISTIVITY (OHM-M)
PHASE (DEG)
FREQUENCY IN HZ
LOG RESISTIVITY (OHM-M)
LOG DEPTH (M)
COHERENCE
NO. ESTIMATES

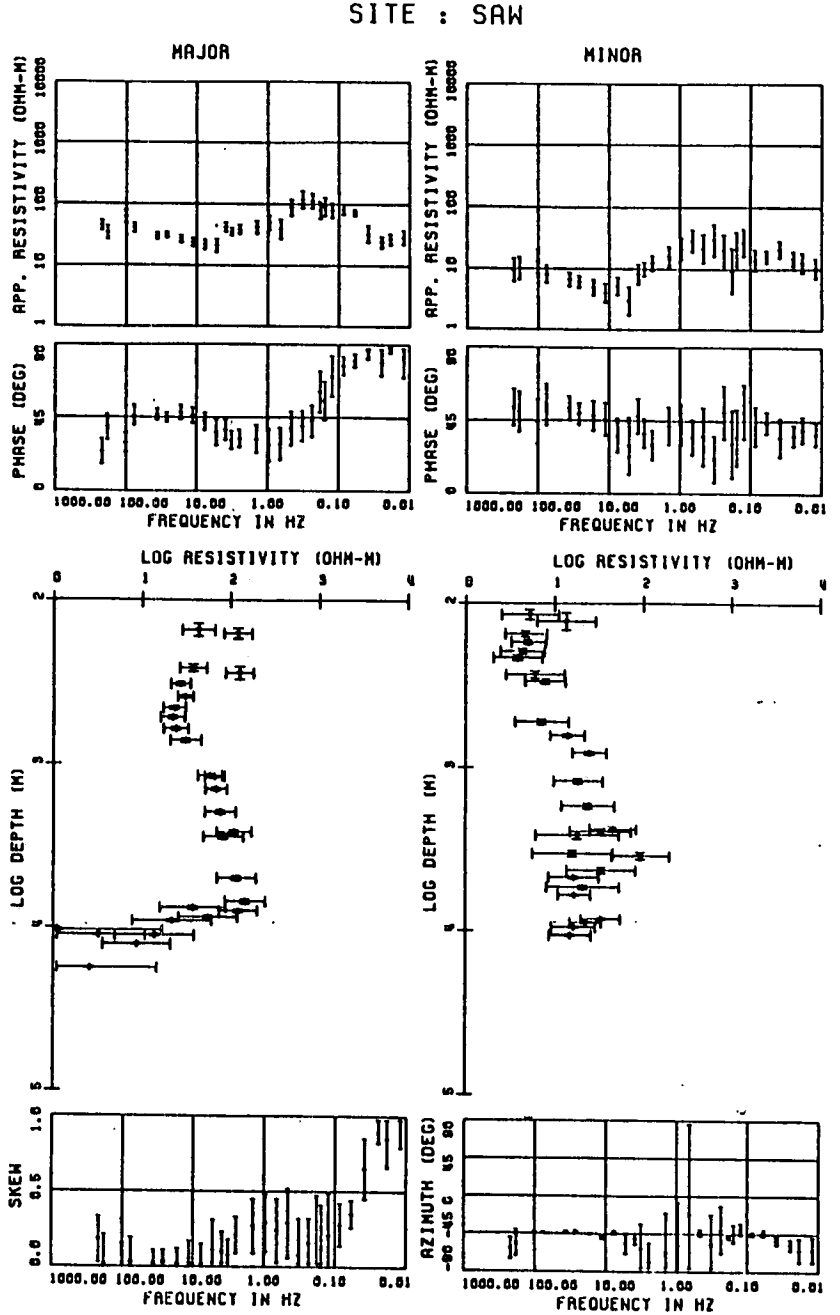
SITE : SAW
MAJOR
MINOR
APP. RESISTIVITY (OHM-M)
PHASE (DEG)
FREQUENCY IN HZ
LOG RESISTIVITY (OHM-M)
LOG DEPTH (M)
SKEW
AZIMUTH (DEG)

Fig. 5.1c

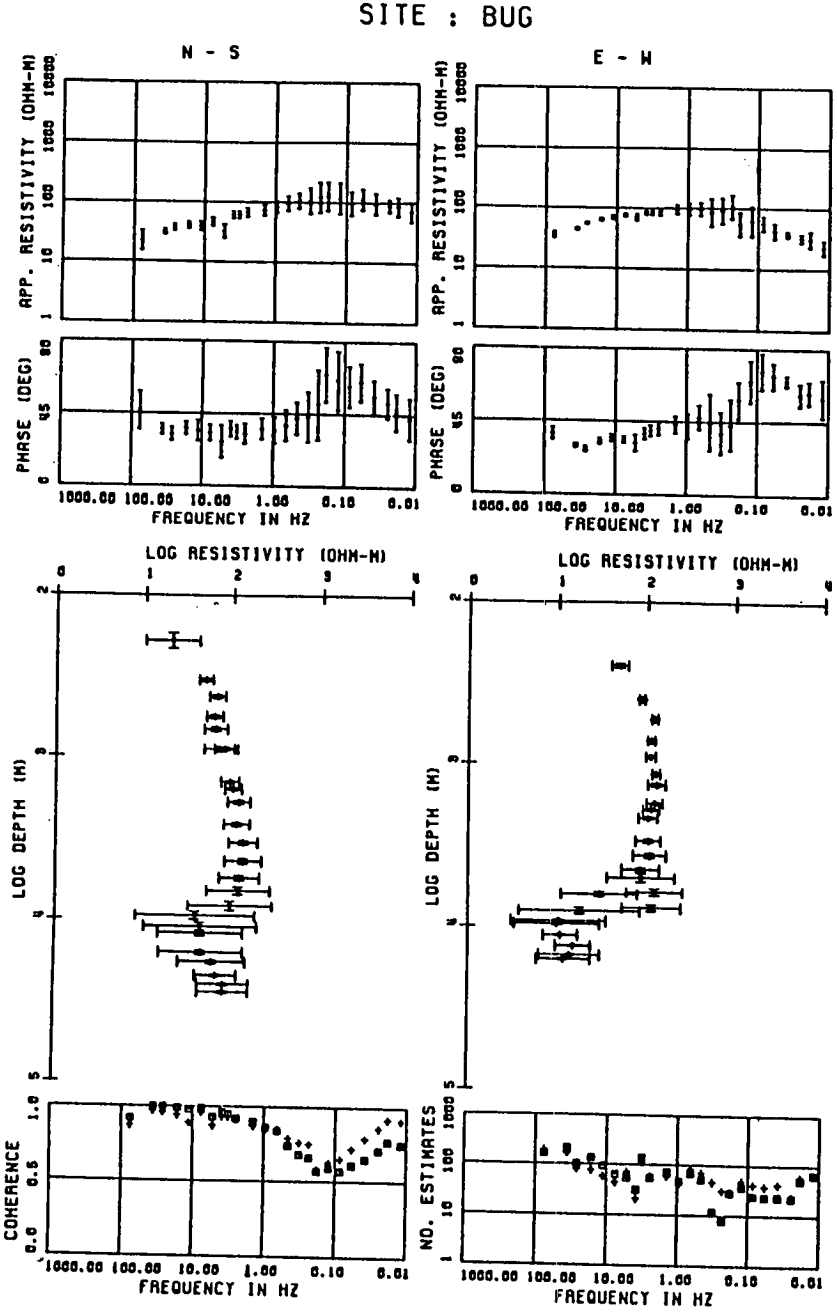
SITE : BUG
N - S
E - W
APP. RESISTIVITY (OHM-M)
PHASE (DEG)
FREQUENCY IN HZ
LOG RESISTIVITY (OHM-M)
LOG DEPTH (M)
COHERENCE
NO. ESTIMATES

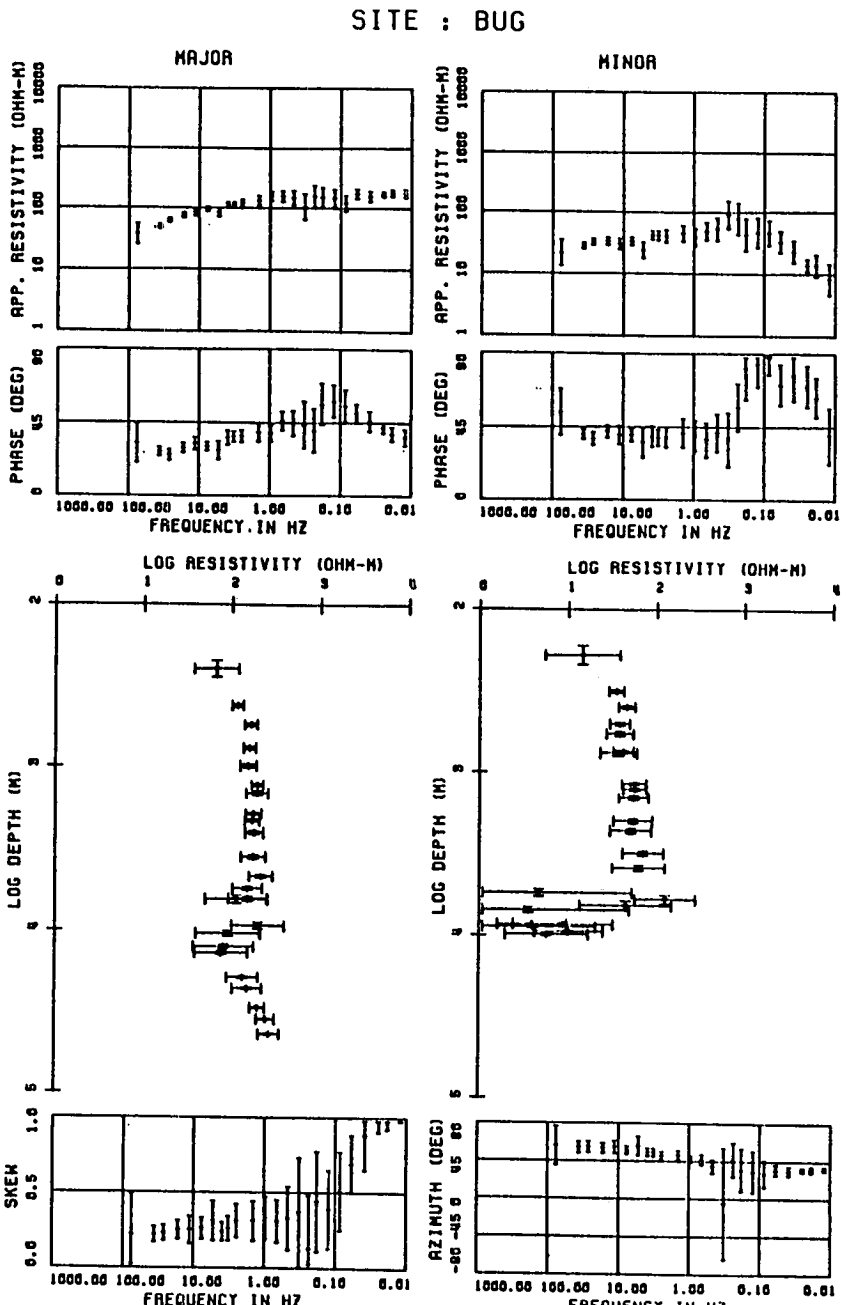
SITE : BUG
MAJOR
MINOR
APP. RESISTIVITY (OHM-M)
PHASE (DEG)
FREQUENCY IN HZ
LOG RESISTIVITY (OHM-M)
LOG DEPTH (M)
SKEW
AZIMUTH (DEG)

Fig. 5.1a

The apparent resistivity and phase plots (Figs. 5.1e,f) indicate a resistivity depth profile of conductor, resistor and then conductor. This resistivity variation with depth can be clearly seen on the Bostick plots. At WAN and WLA, the apparent resistivity values lie respectively in the range 10-1500 and 100-2500 ohm-m, while their respective phase values vary between 10^0 and 85^0. The skew values are less than 0.3, but tend to be larger ($\approx$ 0.5) at the long period. The azimuth of the major impedance tends to increase with increasing period above 2 s, but is on the average N42^{0}E at WAN and N67^{0}W at WLA.

BER and SCR lie within the Silurian Birkhill shale. The noise problem was considerably more severe at SCR than at BER. The apparent resistivity and phase plots (Figs. 5.1g,h) indicate the sequence of surface conductor, resistor and conductor at depth. At BER and SCR, the apparent resistivities are respectively in the range 40-3600 and 20-1500 ohm-m. Their phase values are in the respective range 20^0 - 80^0 and 25^0 - 85^0. The skew values are generally low (< 0.3) and the average azimuth of the major impedance is about N60^{0}W at both sites.

EVE lies within the Silurian Birkhill shale, while all the remaining Duns sites lie within the Devonian Upper Old Red Sandstone series. The apparent resistivity and phase plots as well as the corresponding Bostick plots (Figs. 5.1i-t) show resistivity variation with depth from conductor to resistor to conductor for sites EVE, HRI, HUR, BED and HAL and from resistor to conductor to resistor to conductor for the remaining sites. There was no significant noise

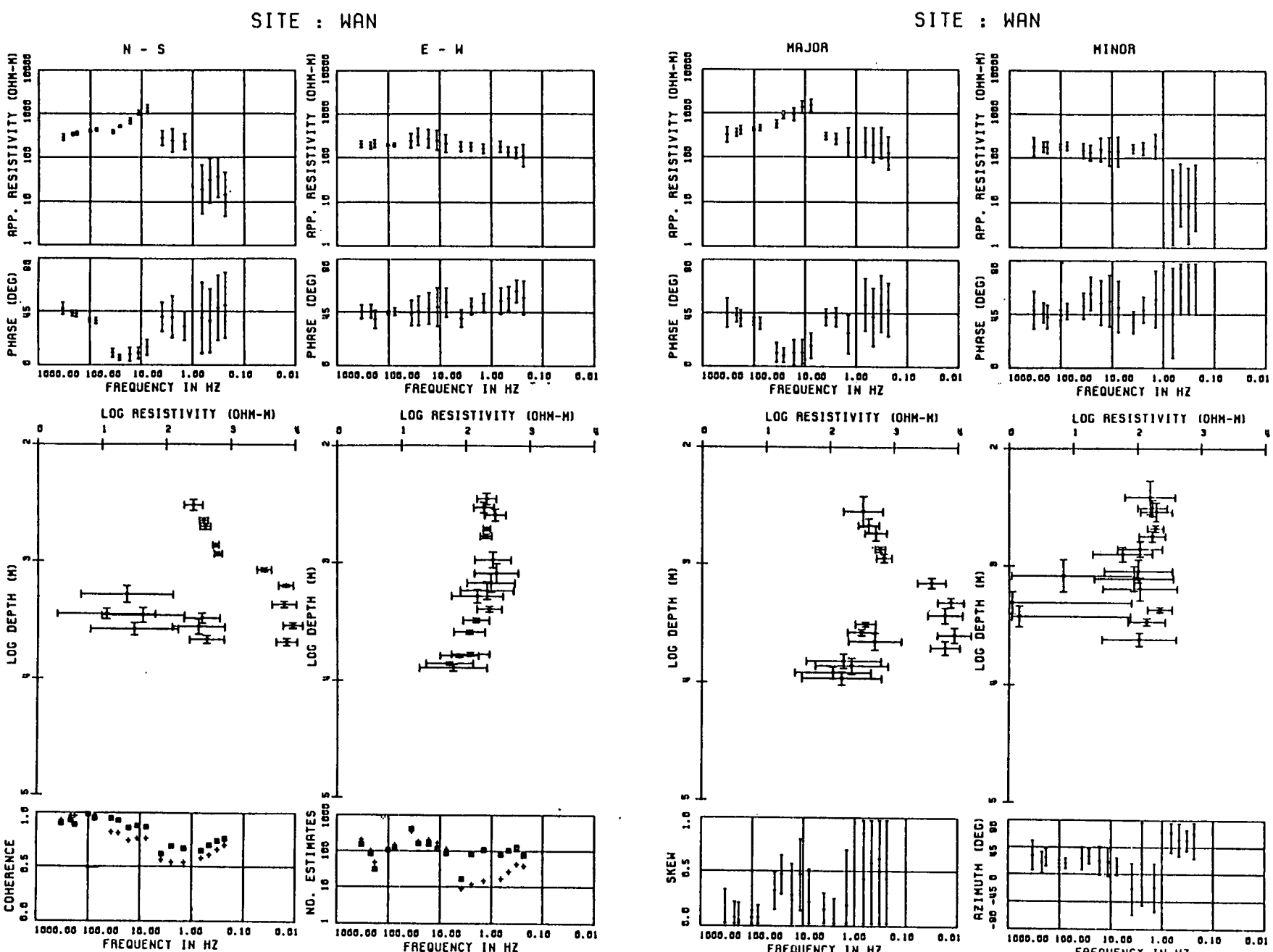
SITE : WAN
N - S
E - W
APP. RESISTIVITY (OHM-M)
PHASE (DEG)
FREQUENCY IN HZ
LOG RESISTIVITY (OHM-M)
LOG DEPTH (M)
COHERENCE
NO. ESTIMATES
SITE : WAN
MAJOR
MINOR
SKEW
AZIMUTH (DEG)

Fig. 5.1e

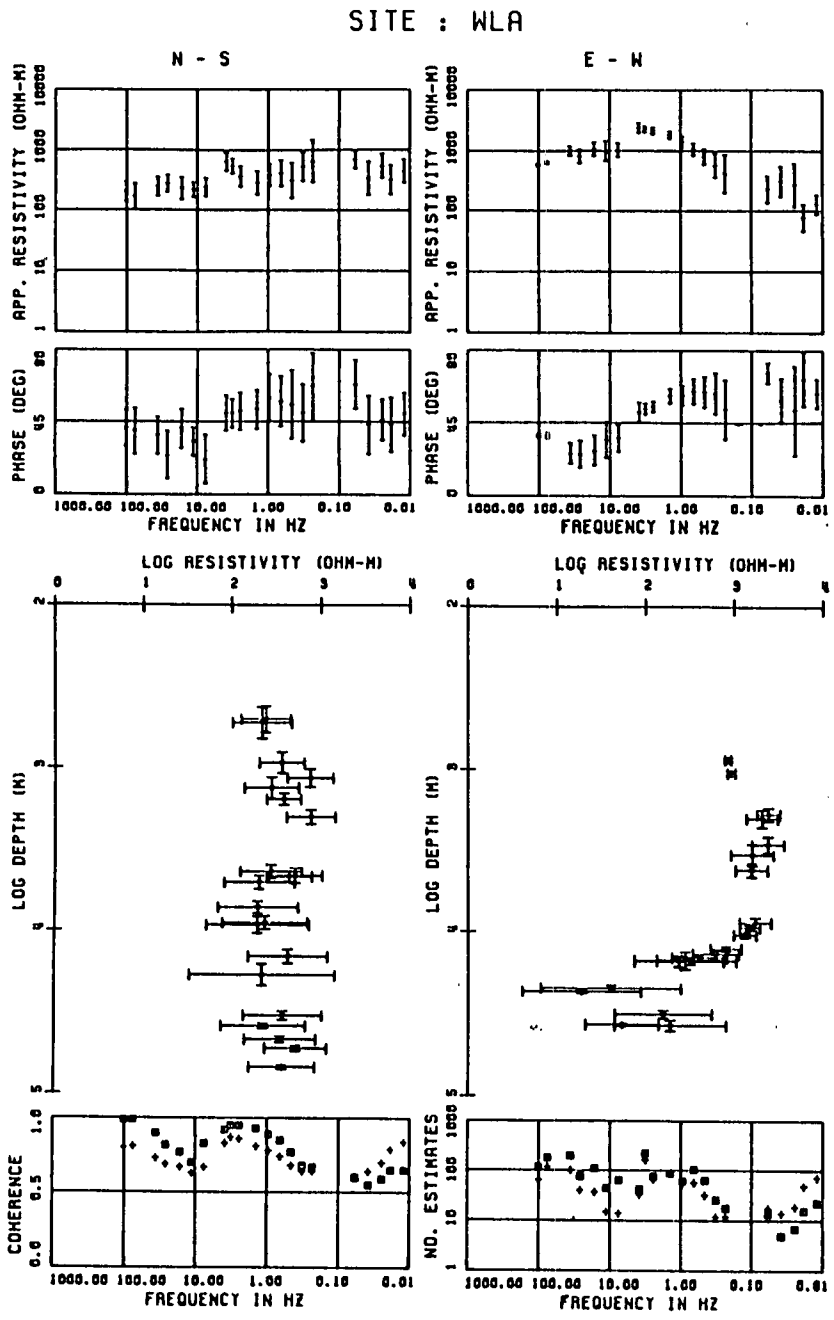
SITE : WLA
N - S
E - W
APP. RESISTIVITY (OHM-M)
PHASE (DEG)
FREQUENCY IN HZ
LOG RESISTIVITY (OHM-M)
LOG DEPTH (M)
COHERENCE
NO. ESTIMATES

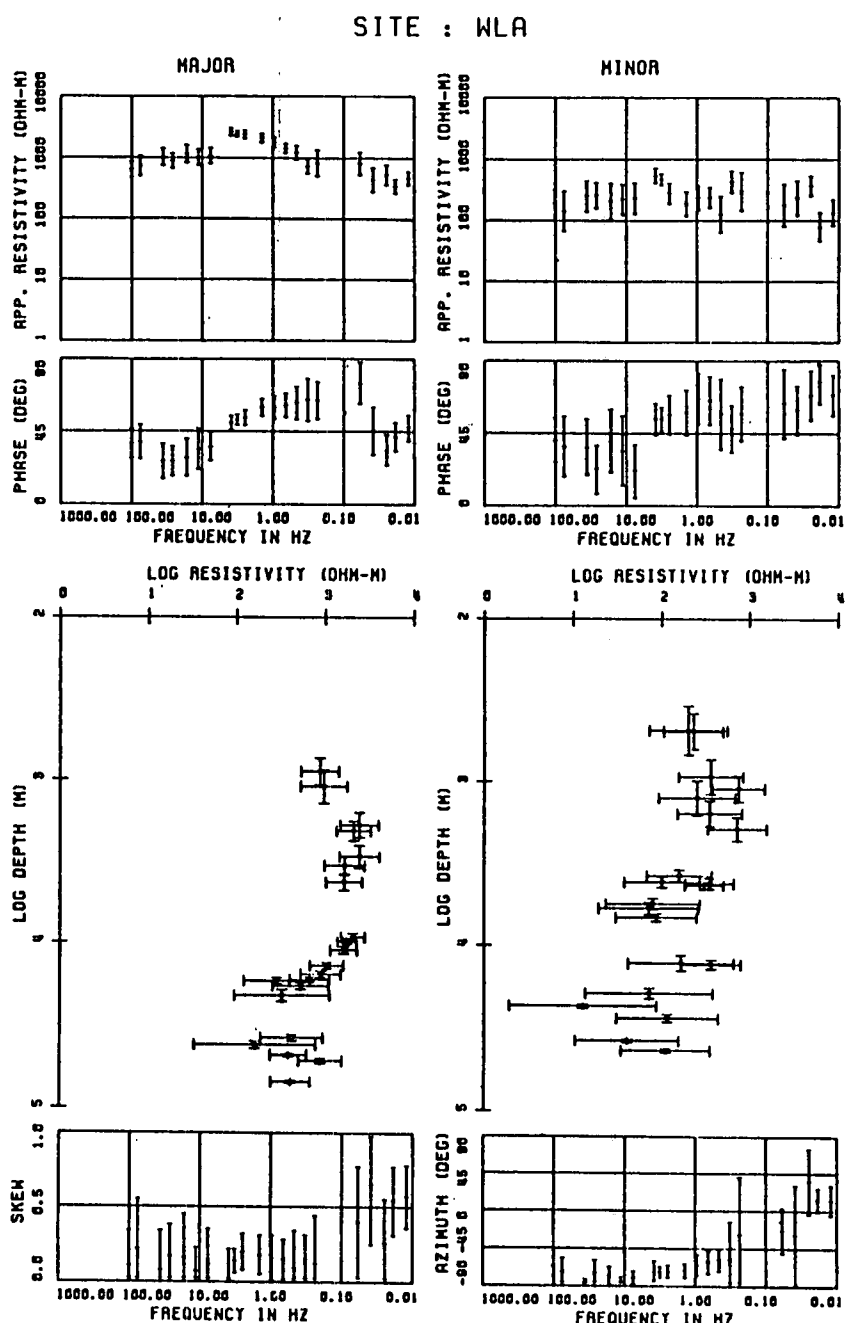
SITE : WLA
MAJOR
MINOR
APP. RESISTIVITY (OHM-M)
PHASE (DEG)
FREQUENCY IN HZ
LOG RESISTIVITY (OHM-M)
LOG DEPTH (M)
SKEW
AZIMUTH (DEG)

Fig. 5.1f

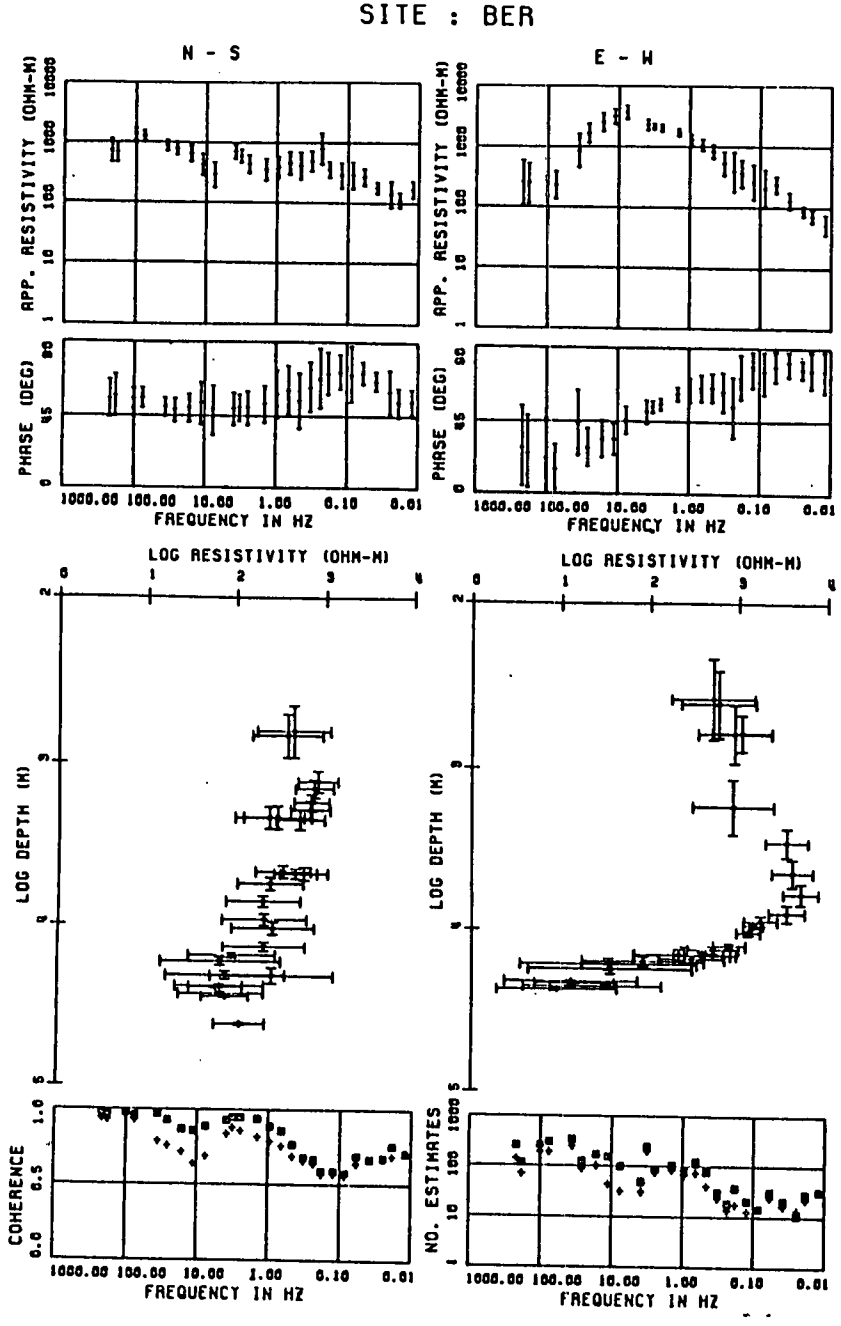
SITE : BER
N - S
E - W
APP. RESISTIVITY (OHM-M)
PHASE (DEG)
FREQUENCY IN HZ
LOG RESISTIVITY (OHM-M)
LOG DEPTH (M)
COHERENCE
NO. ESTIMATES

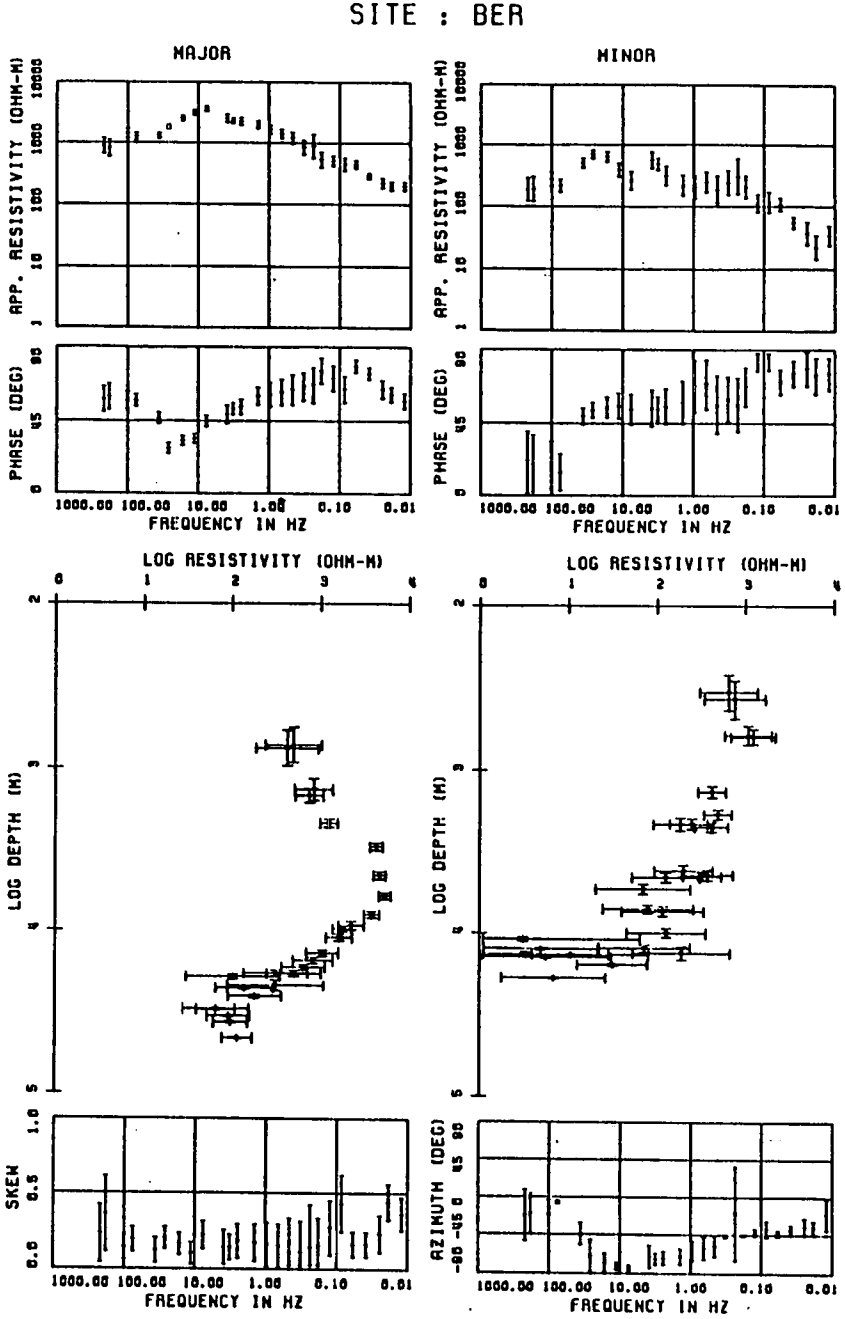
SITE : BER
MAJOR
MINOR
APP. RESISTIVITY (OHM-M)
PHASE (DEG)
FREQUENCY IN HZ
LOG RESISTIVITY (OHM-M)
LOG DEPTH (M)
SKEW
AZIMUTH (DEG)

Fig. 5.18

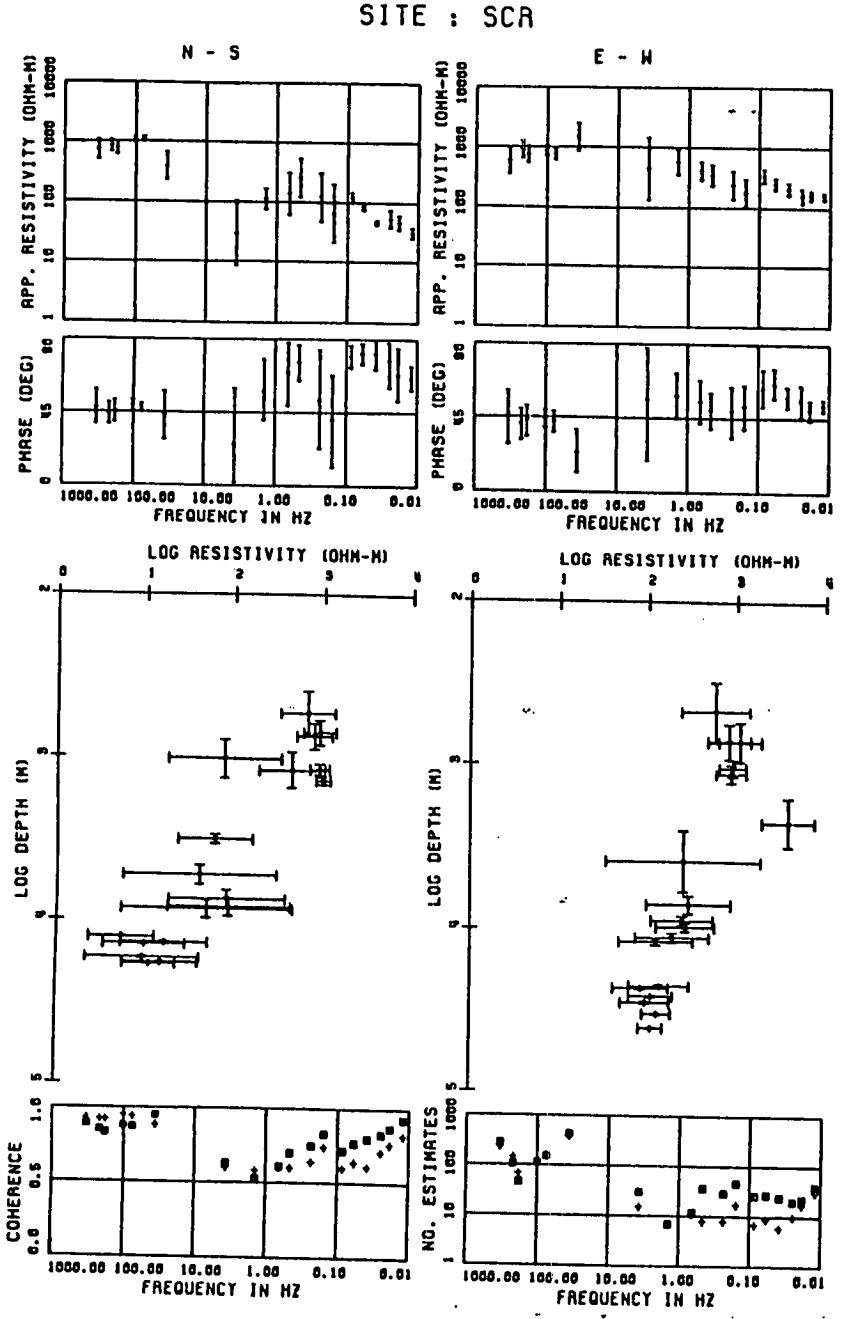
SITE : SCR
N - S
E - W
APP. RESISTIVITY (OHM-M)
PHASE (DEG)
FREQUENCY IN HZ
LOG RESISTIVITY (OHM-M)
LOG DEPTH (M)
COHERENCE
NO. ESTIMATES

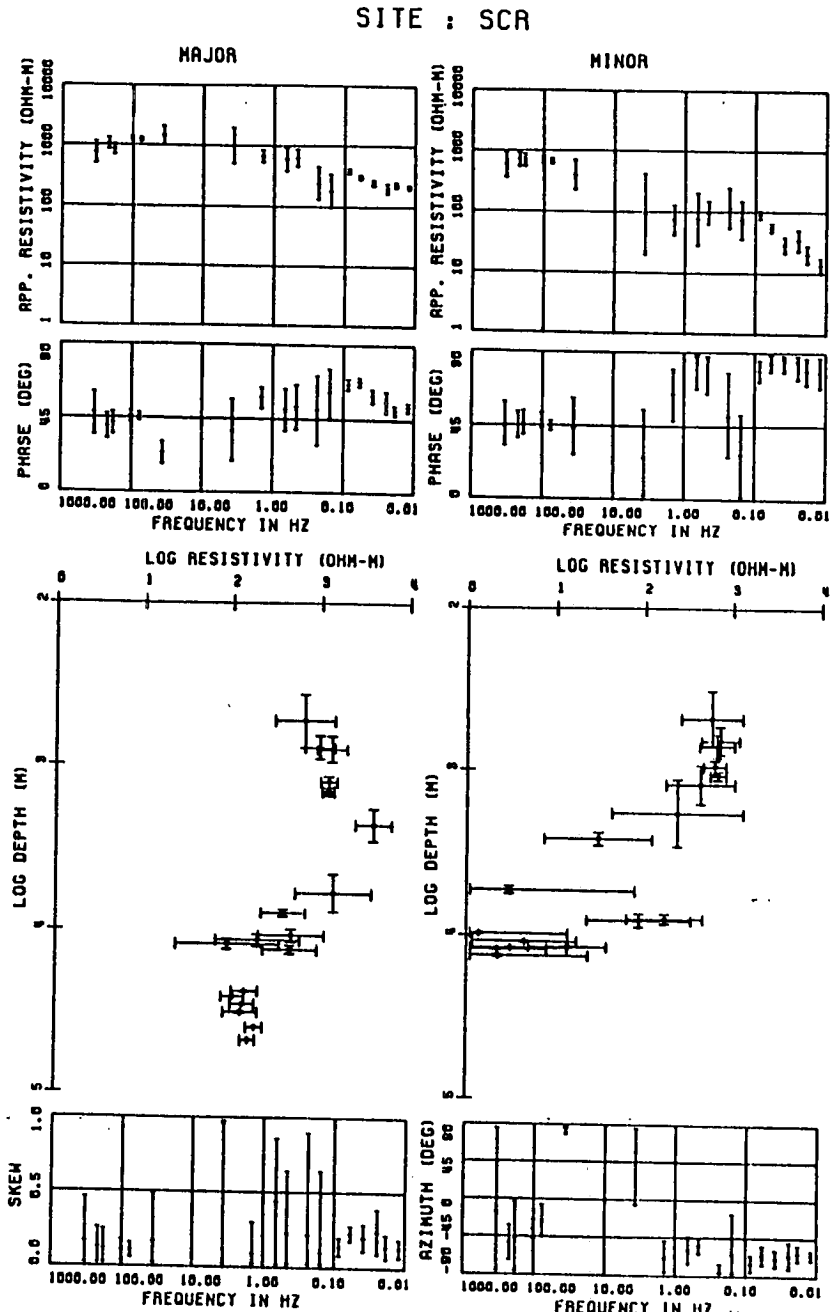
SITE : SCR
MAJOR
MINOR
APP. RESISTIVITY (OHM-M)
PHASE (DEG)
FREQUENCY IN HZ
LOG RESISTIVITY (OHM-M)
LOG DEPTH (M)
SKEW
AZIMUTH (DEG)

Fig. 5.11b

problem except at KE2, CHO and LAN, with the latter being the worst affected. The data at KE2 were recorded during winter when the signal levels were low and thus making the noise effect very significant for data band 3. The band 2 apparent resistivity data at LAN exhibit a very unnatural steep rise that is incompatible with data bands 1 and 3 (Fig. 5.1q) and hence have been eliminated at the modelling stage. This unnatural steep rise is probably due to a local coherent noise, the source of which is unknown.

At EVE, the apparent resistivity values lie in the range 130-550 ohm-m and the phase values between 30^0 and 50^0 (Fig. 5.1i). The skew values are less than 0.1. The average azimuth of the major impedance is $N40^0W$. At HRI, the apparent resistivity values vary between 90 and 800 ohm-m and the phase values between 20^0 and 60^0. The skews are less than 0.2. The average azimuth of the major impedance is $N70^0W$ (Fig. 5.1j).

At HUR, BED and HAL respectively the apparent resistivity values are in the range 20-1600, 40-1100 and 80-740 ohm-m (Figs. 5.1k-m). The phase values are in the range 30^0 - 85^0 at HUR and 25^0 - 70^0 at BED and HAL. The skews are less than 0.1 at the high frequencies, but greater at frequencies below 2 Hz (< 0.4). The average azimuth of the major impedance is $N65^0W$ at HUR and BED and $N72^0W$ at HAL, but increases slightly with decreasing frequency.

At KET, HAR and KE2, the ranges of the apparent resistivity values are respectively 20-300, 10-130 and 5-170 ohm-m and the phases are in the range 25^0 to 75^0 at

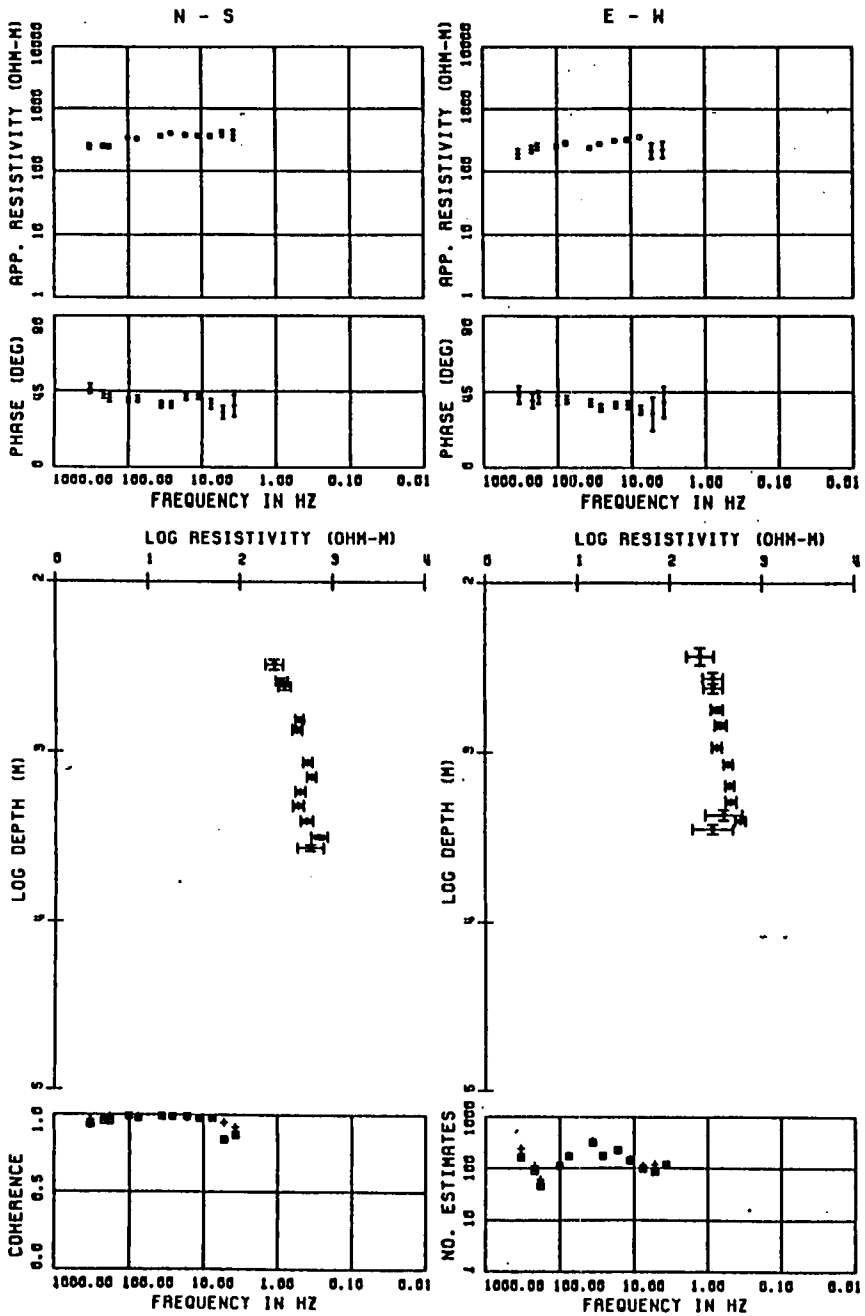
SITE : EVE
N - S
E - W
APP. RESISTIVITY (OHM-M)
PHASE (DEG)
FREQUENCY IN HZ
LOG RESISTIVITY (OHM-M)
LOG DEPTH (M)
COHERENCE
NO. ESTIMATES

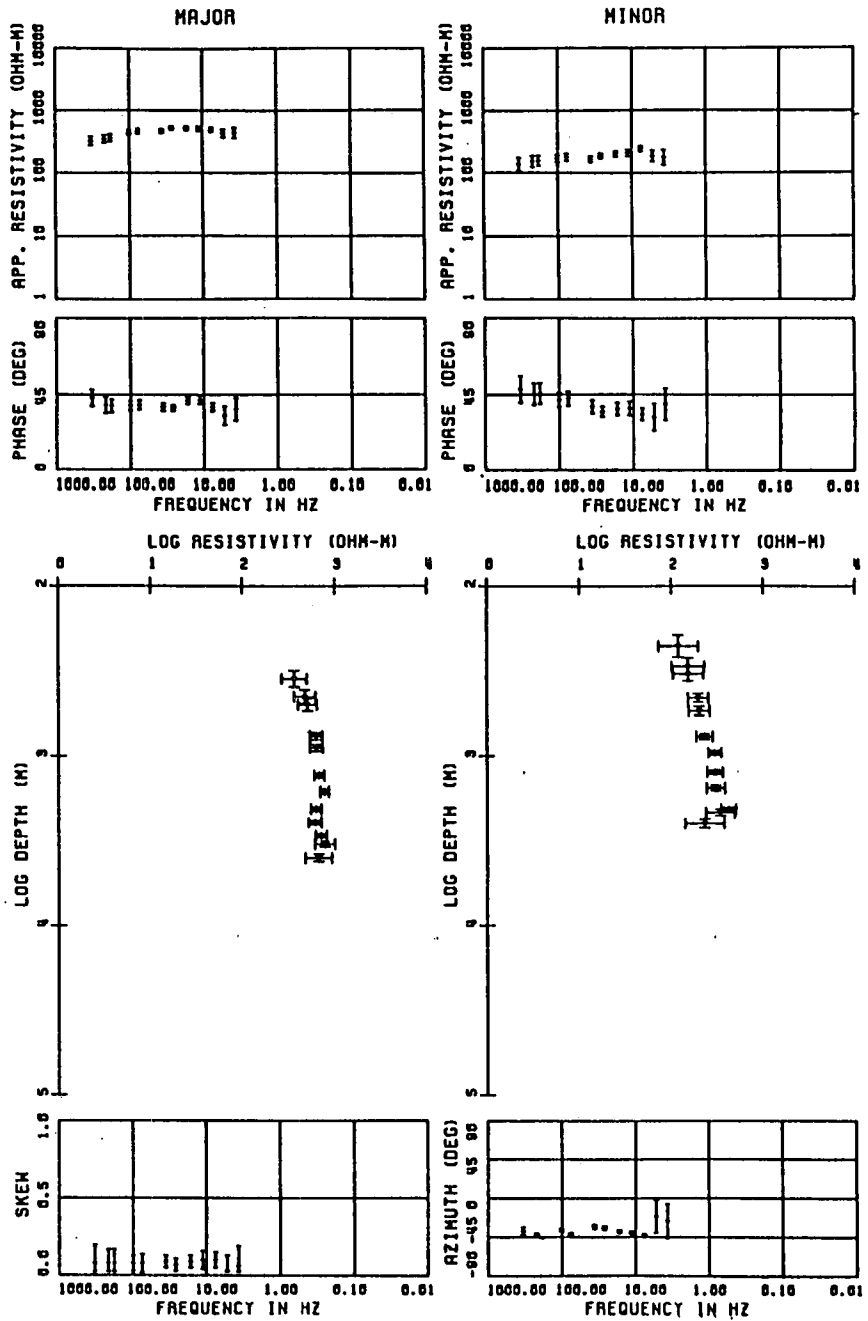
SITE : EVE
MAJOR
MINOR
APP. RESISTIVITY (OHM-M)
PHASE (DEG)
FREQUENCY IN HZ
LOG RESISTIVITY (OHM-M)
LOG DEPTH (M)
SKEW
AZIMUTH (DEG)

Fig. 5.11

Fig. 5.1j

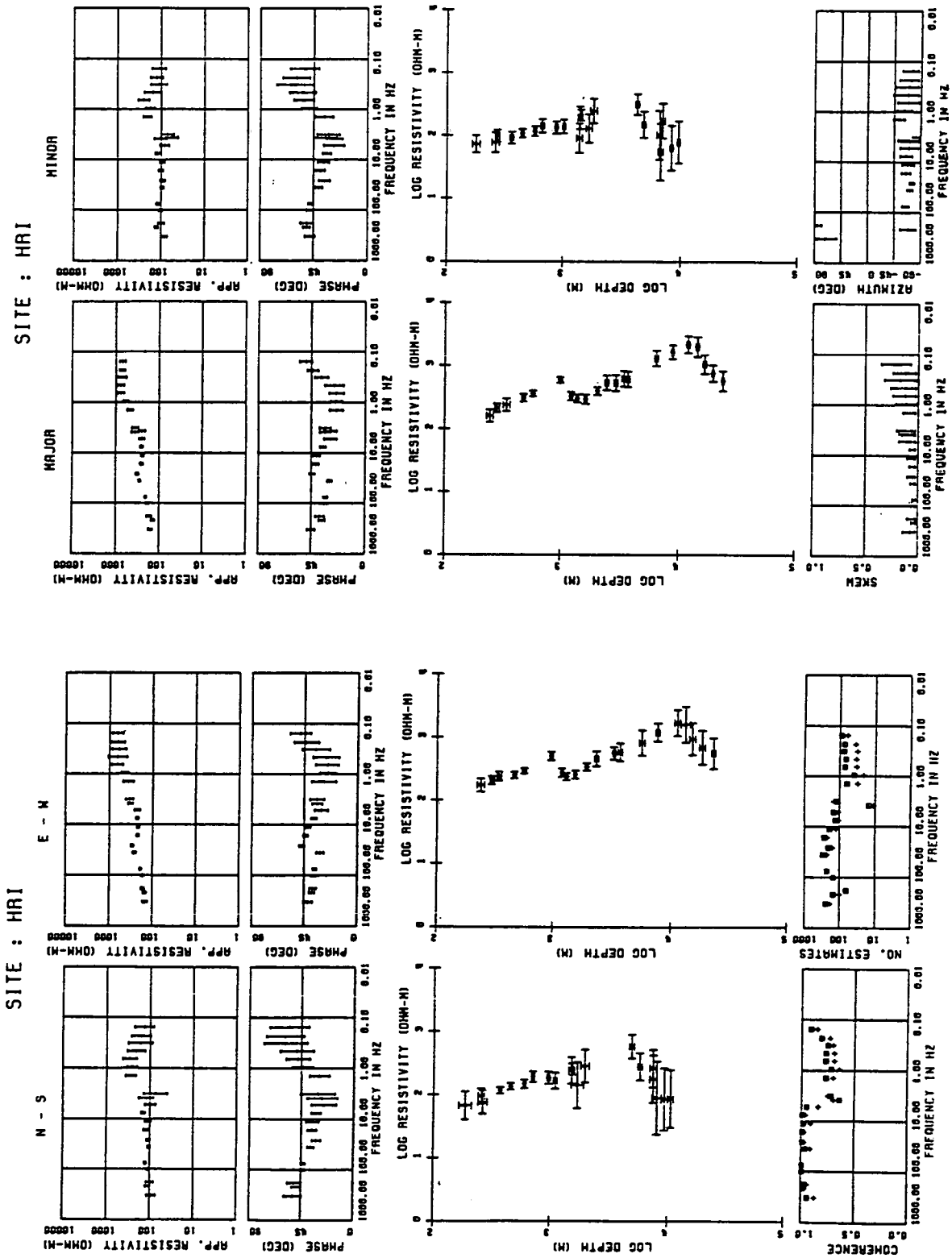
SITE : HRI
MINOR
MAJOR
E - N
N - S
APP. RESISTIVITY (OHM-M)
PHASE (DEG)
FREQUENCY IN HZ
LOG RESISTIVITY (OHM-M)
LOG DEPTH (M)
AZIMUTH (DEG)
SKEW
NO. ESTIMATES
COHERENCE

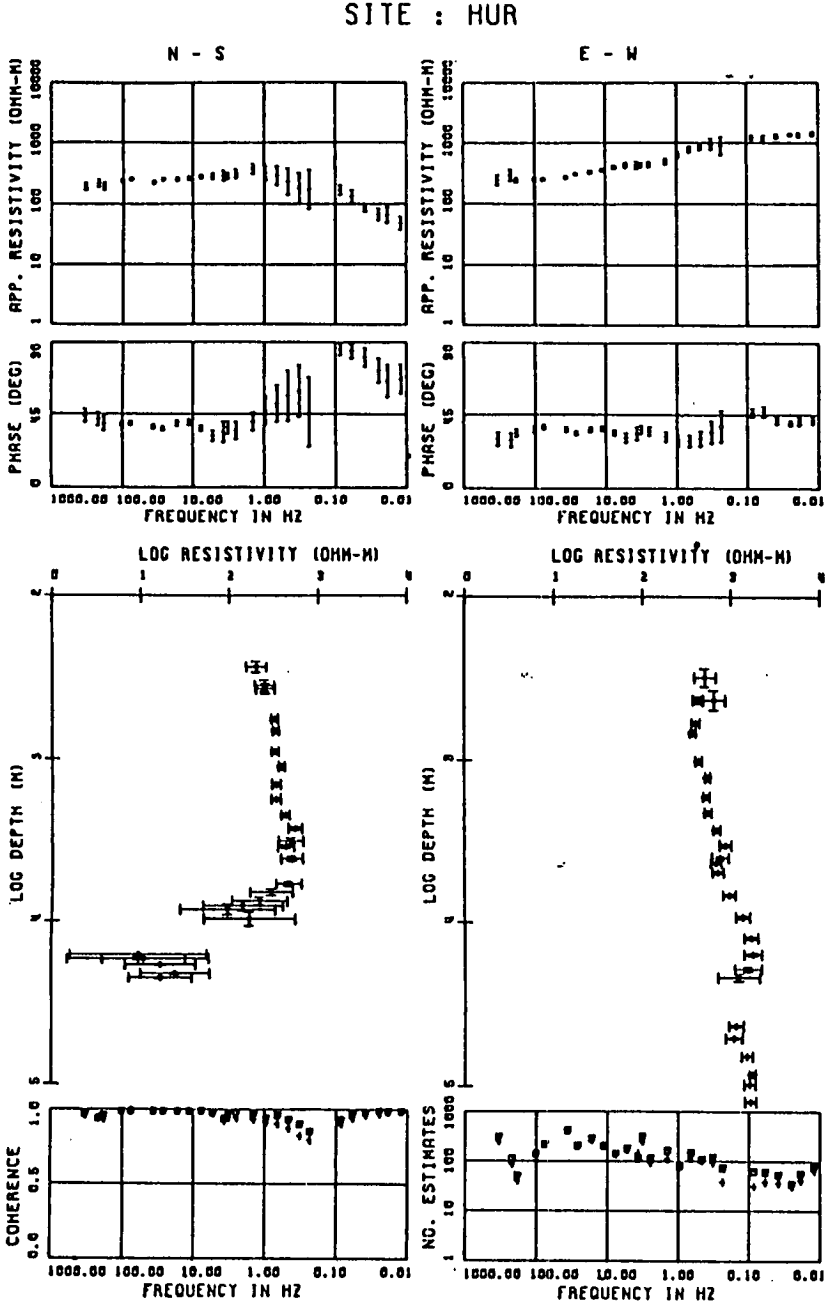
SITE : HUR
N - S
E - W
APP. RESISTIVITY (OHM-M)
PHASE (DEG)
FREQUENCY IN HZ
LOG RESISTIVITY (OHM-M)
LOG DEPTH (M)
COHERENCE
NO. ESTIMATES

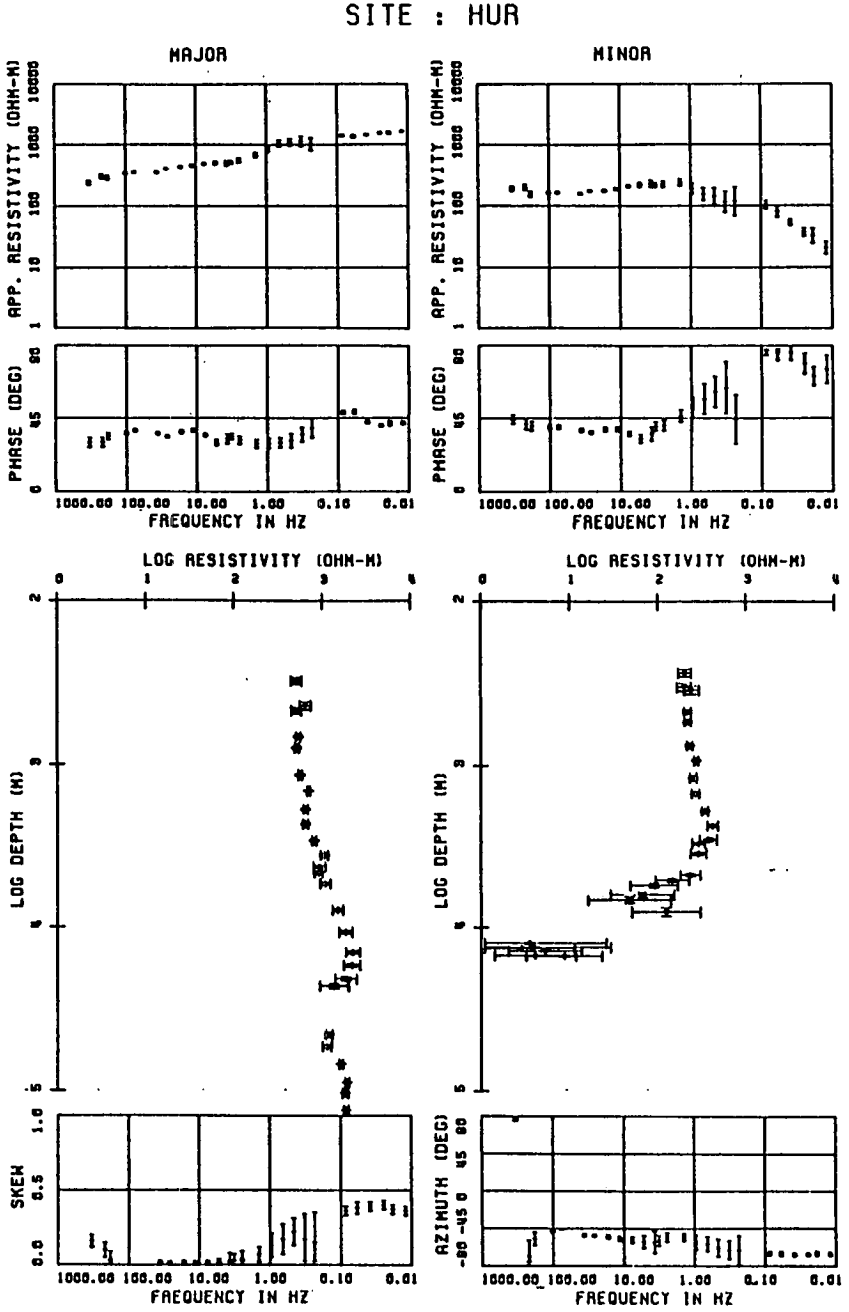
SITE : HUR
MAJOR
MINOR
APP. RESISTIVITY (OHM-M)
PHASE (DEG)
FREQUENCY IN HZ
LOG RESISTIVITY (OHM-M)
LOG DEPTH (M)
SKEW
AZIMUTH (DEG)

Fig. 5.1k

Fig. 5.11

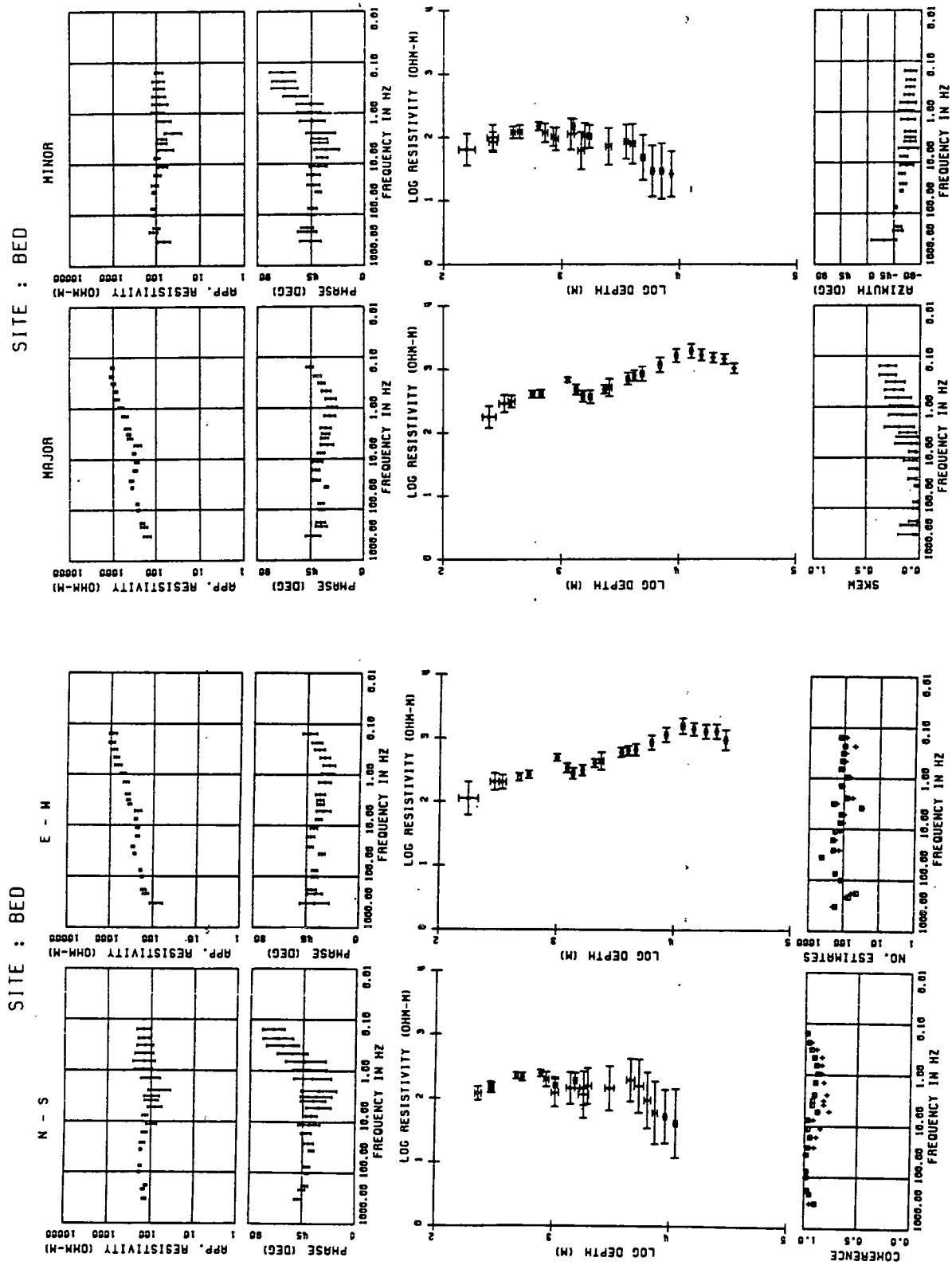
SITE : BED
MINOR
MAJOR
E - W
N - S
APP. RESISTIVITY (OHM-M)
PHASE (DEG)
FREQUENCY IN HZ
LOG RESISTIVITY (OHM-M)
LOG DEPTH (M)
AZIMUTH (DEG)
SKEW
NO. ESTIMATES
COHERENCE

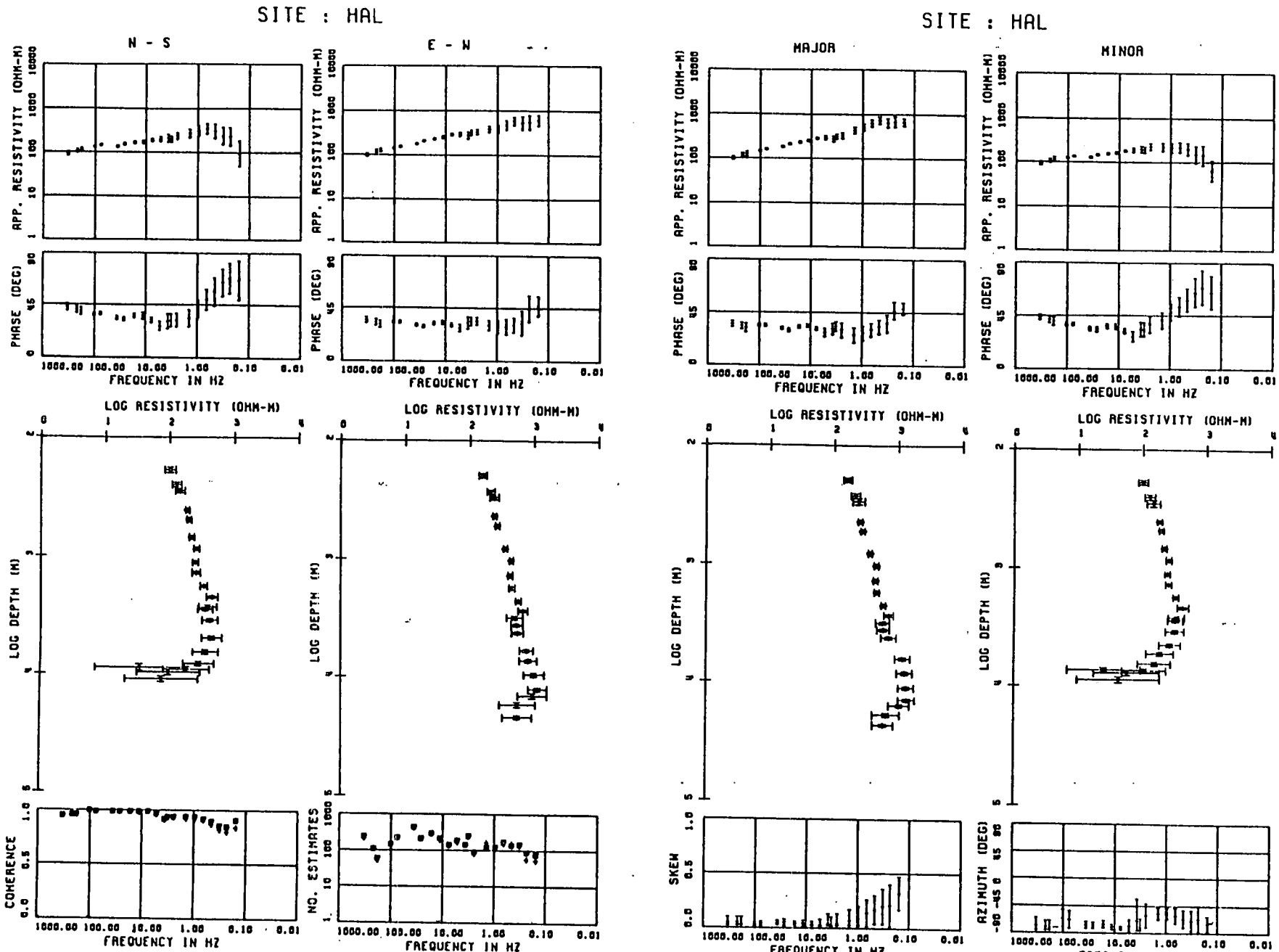
SITE : HAL
N - S
E - W
APP. RESISTIVITY (OHM-M)
PHASE (DEG)
FREQUENCY IN HZ
LOG RESISTIVITY (OHM-M)
LOG DEPTH (M)
COHERENCE
NO. ESTIMATES
SITE : HAL
MAJOR
MINOR
SKEW
AZIMUTH (DEG)

Fig. 5.1m

KET and KE2 and 20^0 to 60^0 at HAR (Figs. 5.1n-p). The skews increase with period, but are generally less than 0.2. The azimuth of the major impedance increases with period; its average value is N64^0W, N50^0W and N80^0E respectively at KET, HAR and KE2.

At LAN and CHO, the apparent resistivity ranges are respectively 10-4400 and 25-1600 ohm-m and the respective phase ranges are 10^0 to 65^0 and 10^0 to 85^0 (Figs. 5.1q,r). The skews at LAN are about 0.5 in data band 2 and less than 0.2 elsewhere, while at CHO they are generally less than 0.2, but larger ($\approx$ 0.4) at the long period. The average azimuth of the major impedance at LAN is N45^0W in band 2 and N55^0E elsewhere. At CHO, the azimuth of the major impedance changes rapidly between 1000 and 100 Hz ($\approx$ N20^0E to N70^0W), but varies slowly at the lower frequencies with an average value of about N60^0W.

At GRE and CAM, the respective resistivity ranges are 70-1000 and 10-1800 ohm-m and the corresponding phase ranges are 15^0 to 65^0 and 15^0 to 80^0 (Figs. 5.1s,t). The skews increase with period, but generally less than 0.3. The azimuth of the major impedance at GRE is approximately E-W between 1000 and 100 Hz and N65^0W elsewhere. At CAM, the azimuth varies considerably with frequency at the high frequencies (>75 Hz), but less rapidly at the low frequencies and its average value is about N70^0W.

CAI lies within the Devonian Lower Old Red Sandstone series, while WHI lies within the Silurian Birkhill shale. The apparent resistivity plots at both sites and the phase plots at CAI show unnatural steep gradient between bands

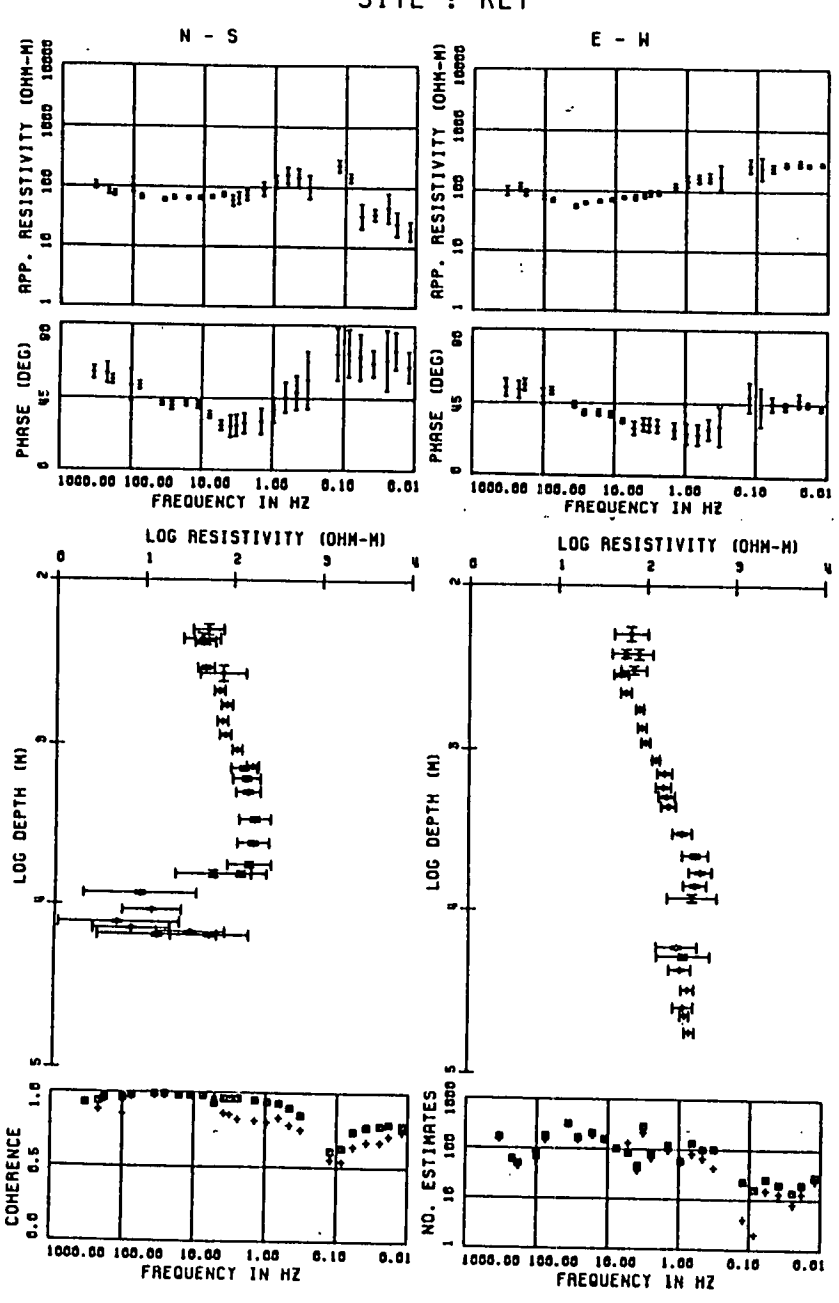
SITE : KET
N - S
E - W
APP. RESISTIVITY (OHM-M)
PHASE (DEG)
FREQUENCY IN HZ
LOG RESISTIVITY (OHM-M)
LOG DEPTH (M)
COHERENCE
NO. ESTIMATES

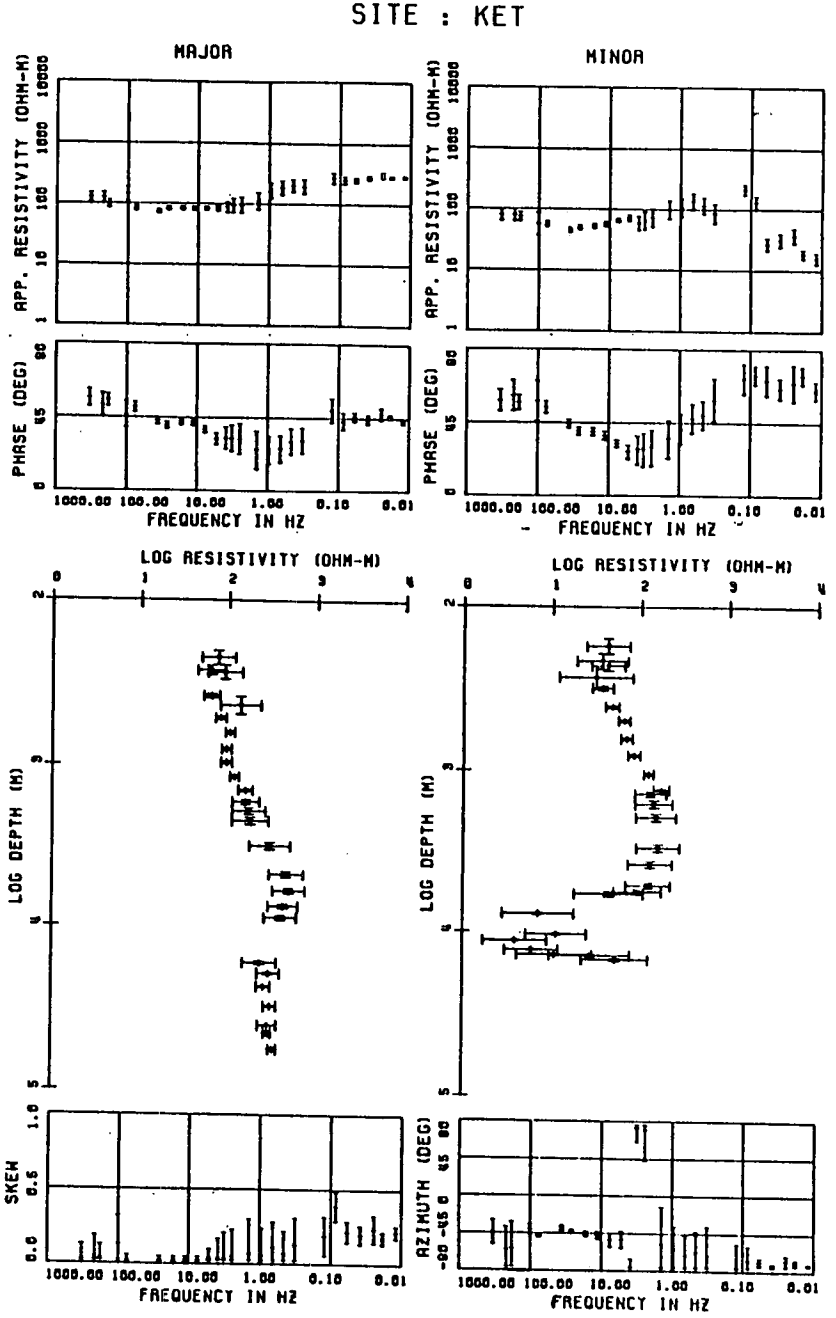
SITE : KET
MAJOR
MINOR
APP. RESISTIVITY (OHM-M)
PHASE (DEG)
FREQUENCY IN HZ
LOG RESISTIVITY (OHM-M)
LOG DEPTH (M)
SKEW
AZIMUTH (DEG)

Fig. 5.1a

Fig. 5.1o

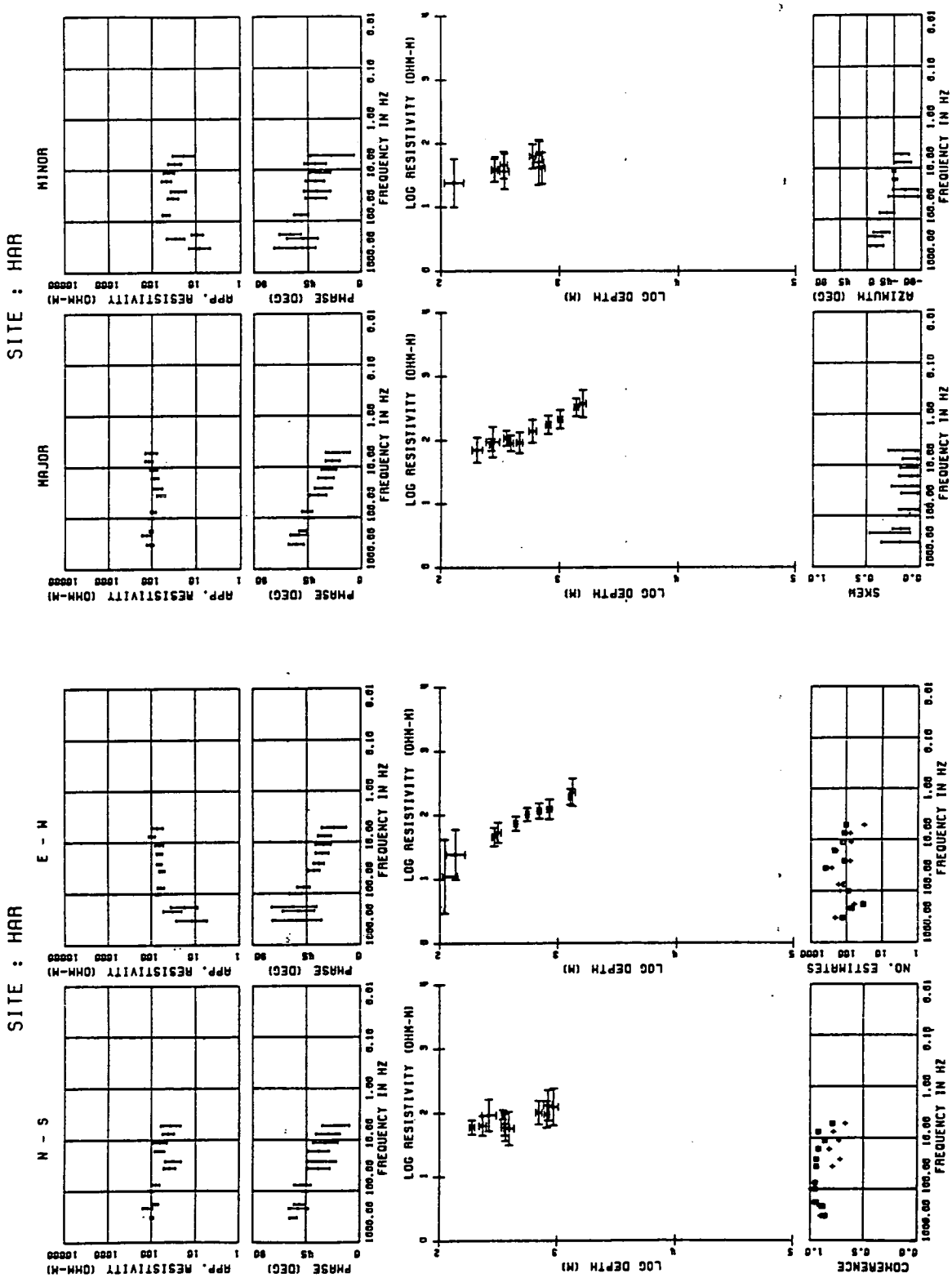
SITE : HAR
MINOR
MAJOR
E - W
N - S
APP. RESISTIVITY (OHM-M)
PHASE (DEG)
FREQUENCY IN HZ
LOG RESISTIVITY (OHM-M)
LOG DEPTH (M)
AZIMUTH (DEG)
SKEW
NO. ESTIMATES
COHERENCE

Fig. 5.1p

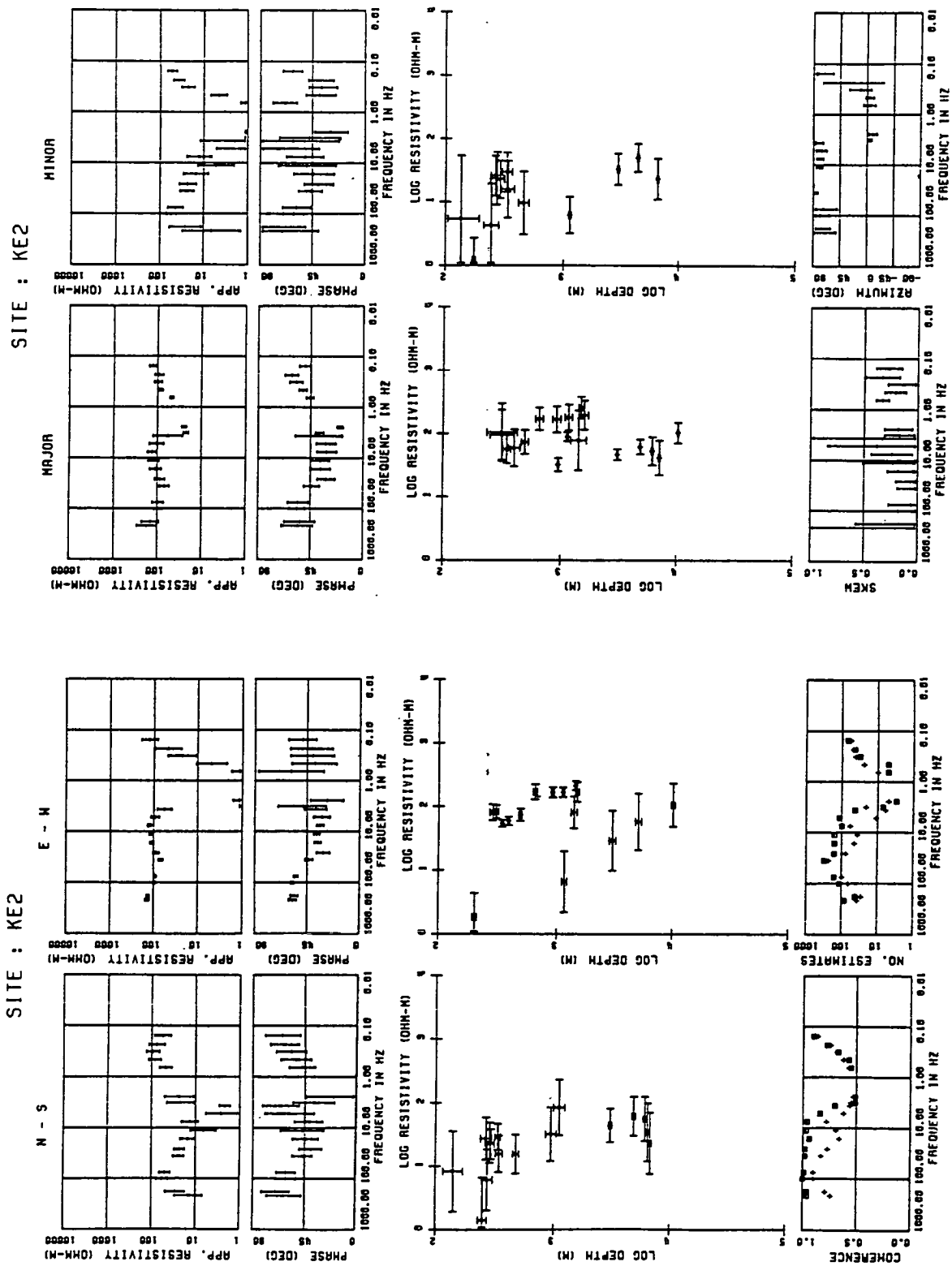
SITE : KE2
MINOR
MAJOR
APP. RESISTIVITY (OHM-M)
PHASE (DEG)
FREQUENCY IN HZ
LOG RESISTIVITY (OHM-M)
LOG DEPTH (M)
AZIMUTH (DEG)
SKEW
SITE : KE2
E - W
N - S
NO. ESTIMATES
COHERENCE

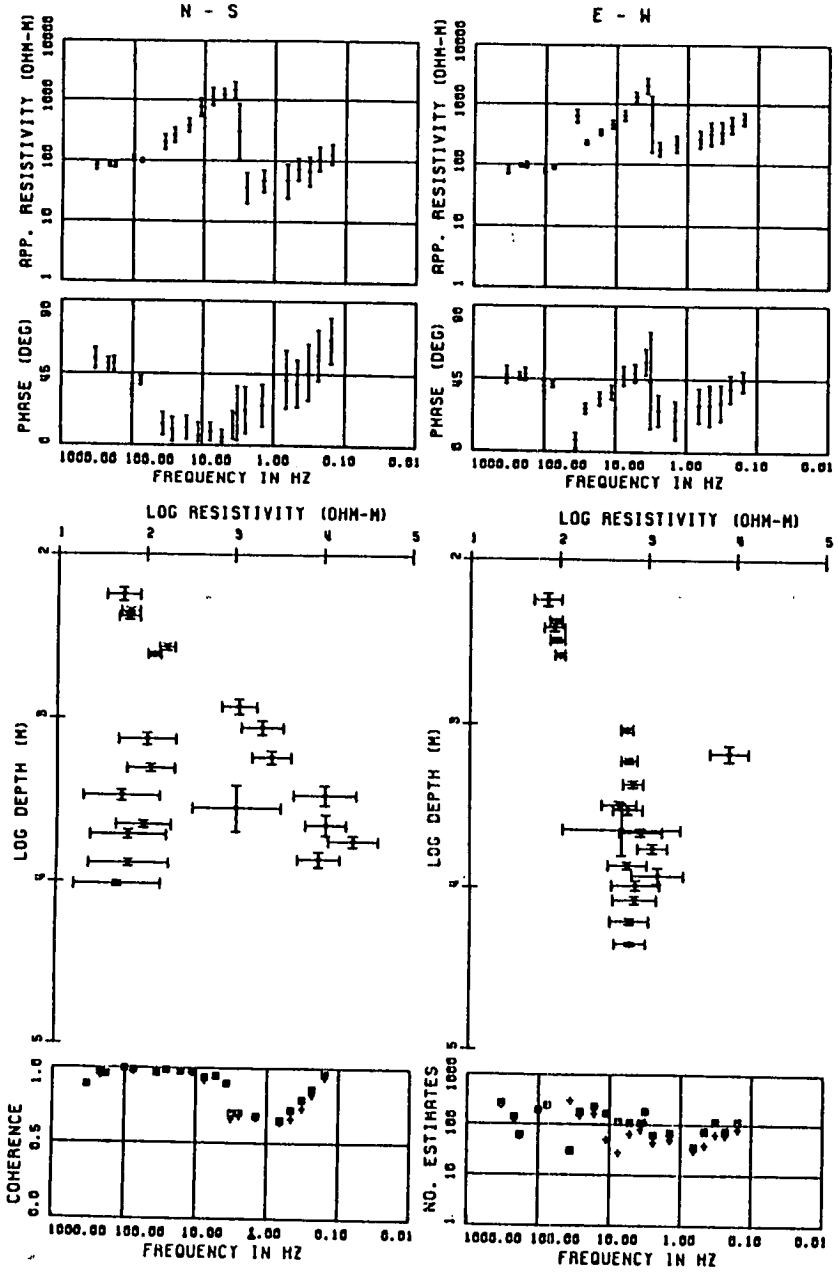
SITE : LAN
N - S
E - W
APP. RESISTIVITY (OHM-M)
PHASE (DEG)
FREQUENCY IN HZ
LOG RESISTIVITY (OHM-M)
LOG DEPTH (M)
COHERENCE
NO. ESTIMATES

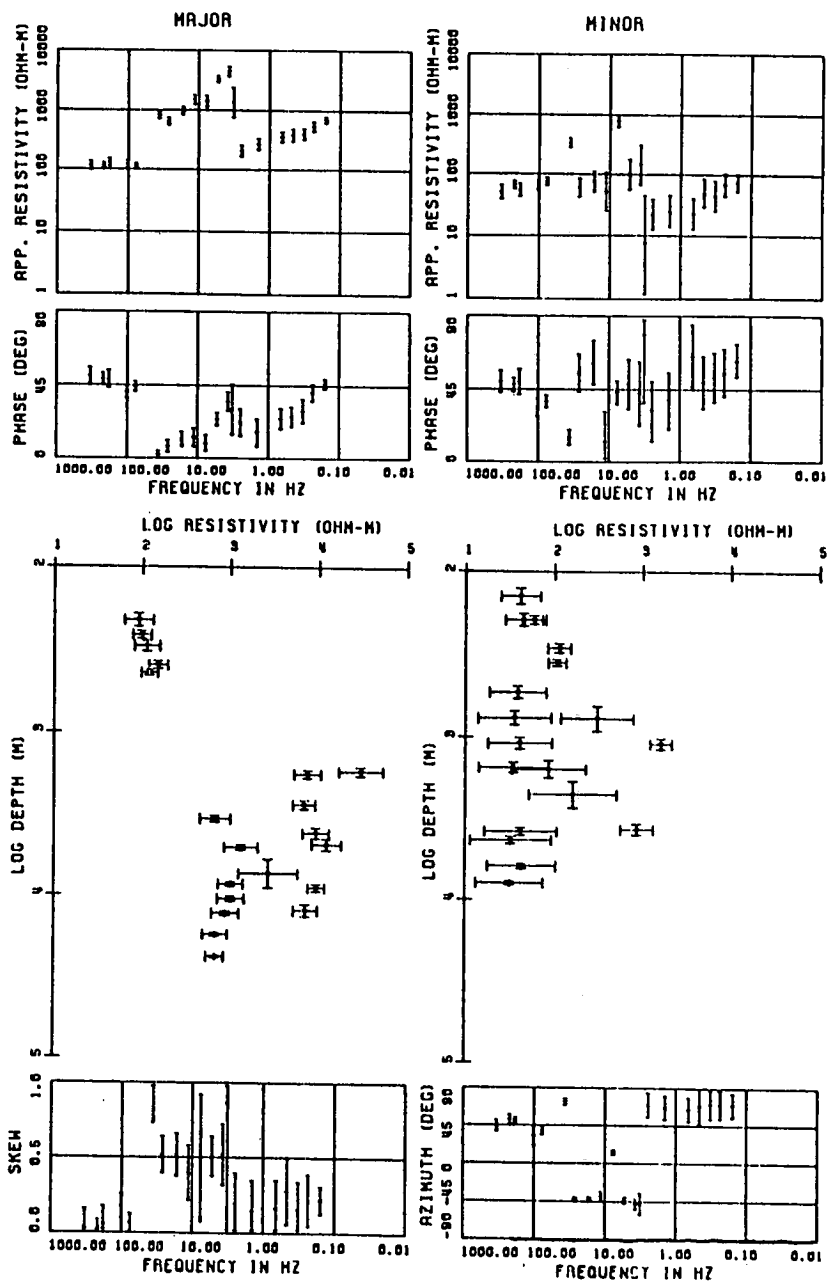
SITE : LAN
MAJOR
MINOR
APP. RESISTIVITY (OHM-M)
PHASE (DEG)
FREQUENCY IN HZ
LOG RESISTIVITY (OHM-M)
LOG DEPTH (M)
SKEW
AZIMUTH (DEG)

Fig. 5.19

Fig. 5.1r

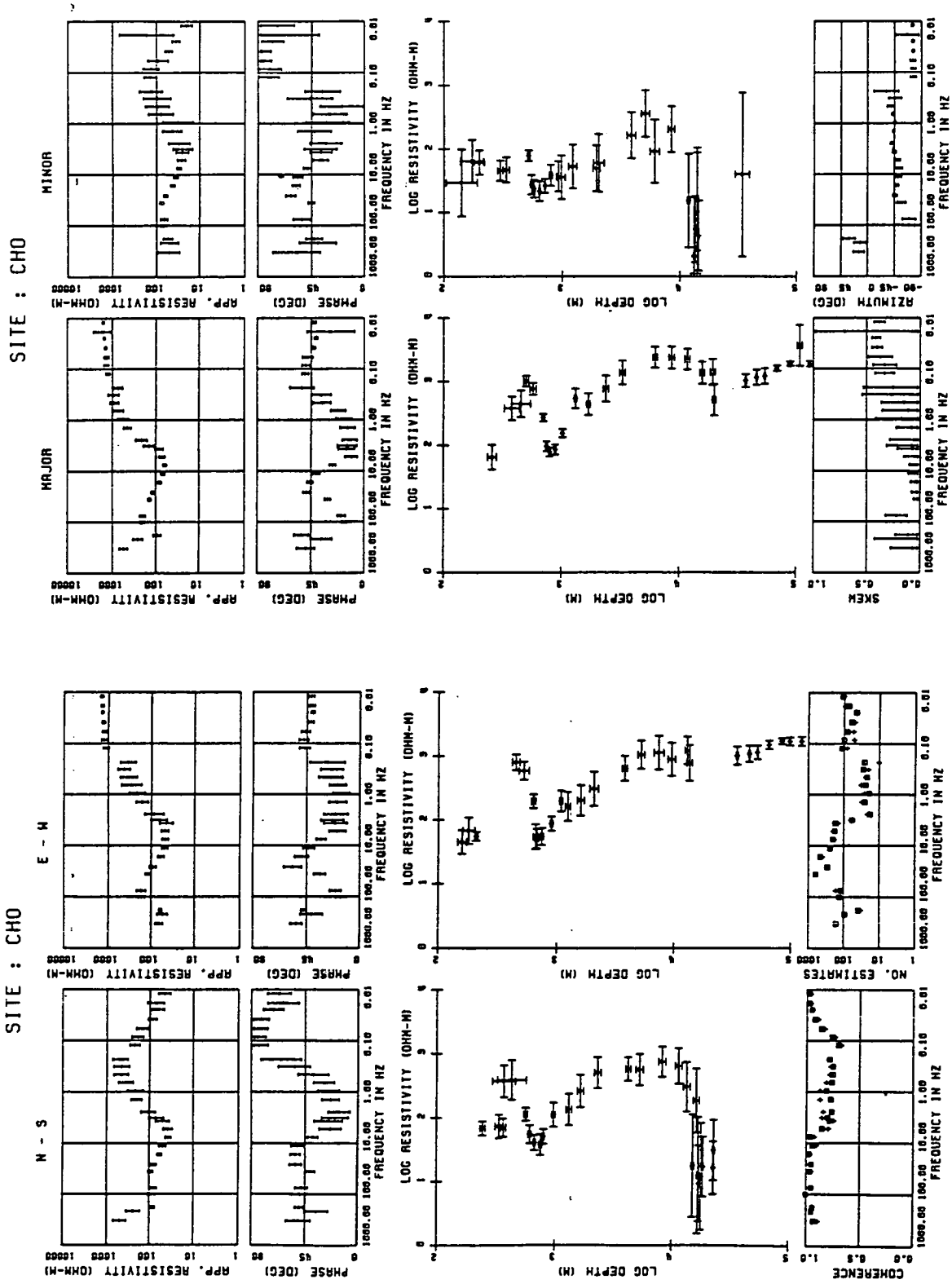
SITE : CHO
MINOR
MAJOR
E - W
N - S
APP. RESISTIVITY (OHM-M)
PHASE (DEG)
FREQUENCY IN HZ
LOG RESISTIVITY (OHM-M)
LOG DEPTH (M)
AZIMUTH (DEG)
SKEW
NO. ESTIMATES
COHERENCE

SITE : GRE
N - S
E - W
APP. RESISTIVITY (OHM-M)
PHASE (DEG)
FREQUENCY IN HZ
LOG RESISTIVITY (OHM-M)
LOG DEPTH (M)
COHERENCE
NO. ESTIMATES

SITE : GRE
MAJOR
MINOR
APP. RESISTIVITY (OHM-M)
PHASE (DEG)
FREQUENCY IN HZ
LOG RESISTIVITY (OHM-M)
LOG DEPTH (M)
SKEW
AZIMUTH (DEG)

Fig. 5.18

Fig. 5.1t

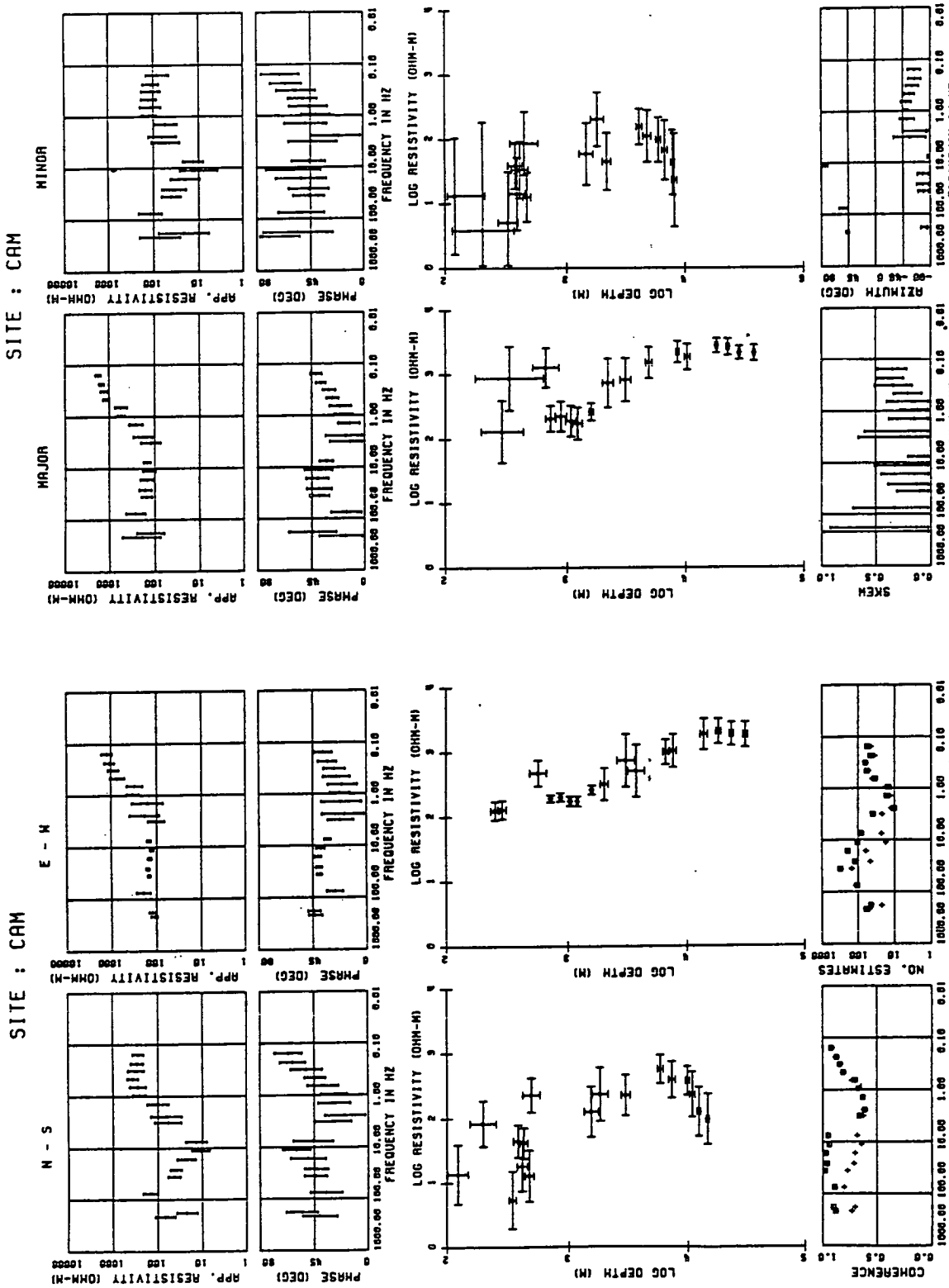
SITE : CAM
MINOR
MAJOR
E - W
N - S
APP. RESISTIVITY (OHM-M)
PHASE (DEG)
FREQUENCY IN HZ
LOG RESISTIVITY (OHM-M)
LOG DEPTH (M)
AZIMUTH (DEG)
SKEW
NO. ESTIMATES
COHERENCE

2 and 3. This may be indicative of local coherent noise. The apparent resistivity and phase plots indicate a near-surface resistor underlain by a conductor, then resistor and finally a conductor. This resistivity variation with depth can be more clearly seen on the Bostick transform plots (Figs. 5.1u,v). The apparent resistivity ranges are respectively 10-800 and 30-30000 ohm-m at CAI and WHI, while their phases are in the range 10^0 to 85^0. The skews are less than 0.1 in bands 1 and 2, but larger ($\approx$ 0.5) in band 3. It seems that the band 3 data are suspect. The azimuth of the major impedance varies considerably with frequency. At CAI and WHI respectively, its average value is $N70^0W$ and $N70^0E$ in band 1, $N50^0W$ and $N60^0E$ in band 2 and about $N25^0E$ in band 3 at both sites.

At most of the sites, the anisotropy is small ($\leqslant$1/2 decade) except at a few sites where it is about 1 decade at periods greater than 10 s. Hence, the observed increase in skew values at the long period may be indicative of a change from an approximately 1D to a 2D structure at depth. Thus, from all the MT results, it can be said that the gross structural features of SE Scotland are 2D. From the apparent resistivity variations in the area, it can be seen that anomalously low apparent resistivity values occur at two zones; one of these is in the neighbourhood of SAW and BUG and the other is at KET, HAR and KE2. It will be seen in the 2D section resulting from a collation of the individual site 1D models as well as in the final 2D model presented later that at these zones the upper/lower crustal conductor rises much nearer the earth's surface

Fig. 5.1u

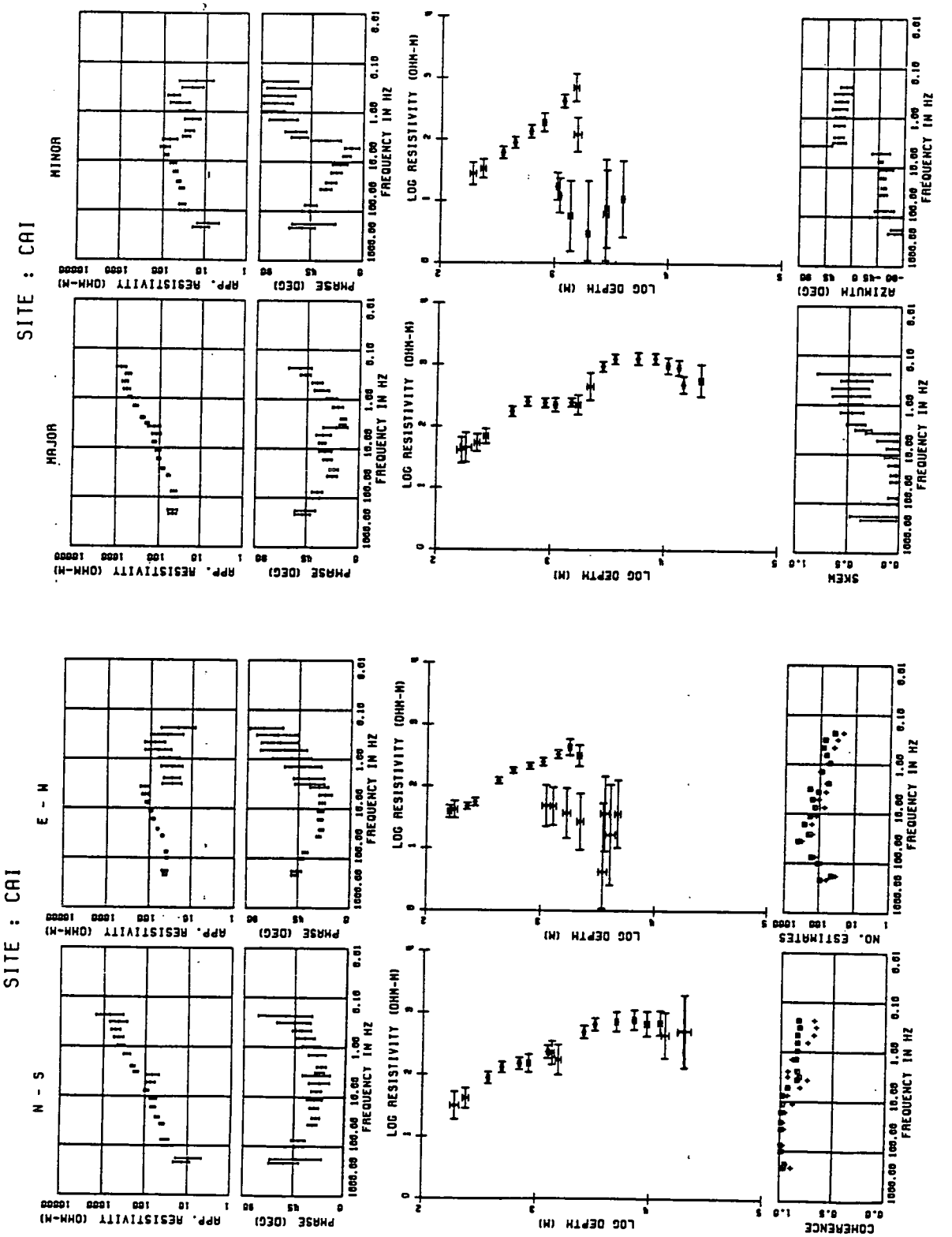
SITE : CAI
MINOR
MAJOR
E - W
N - S
APP. RESISTIVITY (OHM-M)
PHASE (DEG)
FREQUENCY IN HZ
LOG RESISTIVITY (OHM-M)
LOG DEPTH (M)
AZIMUTH (DEG)
SKEW
NO. ESTIMATES
COHERENCE

SITE : WHI
N - S
E - W
APP. RESISTIVITY (OHM-M)
PHASE (DEG)
FREQUENCY IN HZ
LOG RESISTIVITY (OHM-M)
LOG DEPTH (M)
COHERENCE
NO. ESTIMATES

SITE : WHI
MAJOR
MINOR
APP. RESISTIVITY (OHM-M)
PHASE (DEG)
FREQUENCY IN HZ
LOG RESISTIVITY (OHM-M)
LOG DEPTH (M)
SKEW
AZIMUTH (DEG)

Fig. 5.17

compared with the surrounding.

5.3 1D modelling

In any geophysical technique, a necessary step prior to interpretation is the determination of the different relevant earth parameters through modelling. In the case of MT, these parameters are layer resistivity and thickness/depth.

5.3.1 General discussion

The simplest modelling approach is the curve matching technique whereby the MT experimental curves are compared with master curves which have been drawn for various 1D theoretical earth structures. The experimental curves are drawn on the same scale as the master curves. When a satisfactory fit is obtained between the experimental and the master curves, the parameters of this mathematical model are assumed in deriving the real earth parameters for the area in question. This type of indirect approach may sometimes give ambiguous results. A brief discussion of the ambiguities involved in interpretational geophysical work has been given by Roy (1962).

The available published master curves are quite few, e.g., two-layer master curves by Cagniard (1953); three-layer curves by Yungul (1961); two- and three-layer curves by Srivastava (1967). The published master curves are also limited in scope and hence a more versatile extension of

the curve matching technique is the forward modelling technique. In the latter case, an algorithm is used to compute different layered models and by trial and error adjustment of the model parameters, a satisfactory fit is obtained between the calculated model data and the measured MT data. The theoretical model parameters are then assumed as those of the real earth.

Modelling techniques which obtain parameters directly from the measured MT data are the direct inversion techniques. Some approximate direct inversion methods have been discussed in section 2.4. Several 1D MT inversion schemes have been discussed in the literature, e.g., Weidelt (1972), Hermance and Grillot (1974), Summers (1976), Fischer et al. (1981) and Hobbs (1982) among others.

A 1D Monte-Carlo inversion scheme computer programmed by Jones (1977) was used by Jones and Hutton (1979b) in their MT modelling. In the present study, a modified version of this Monte-Carlo inversion scheme has been used and is briefly discussed below.

5.3.2 1D Monte-Carlo inversion

This is an iterative scheme with the following main specifications :

(a) one of three types of data is specified to be modelled, viz, apparent resistivity only, phase only or both;

(b) one of three acceptance criteria is applied in selecting the best model fit, i.e., number of data error bars crossed by the model curve or the sum squared

difference between model and real data or the sum squared error bar weighted difference;

(c) the number of layers to be used in the modelling is specified;

(d) one of three possible variations of layer parameters is specified, viz, either vary depth only, resistivity only or both depth and resistivity and

(e) for each of the layers, starting model parameters P (depth and resistivity) are specified with upper and lower bounds (denoted as P_{min} , P_{av} and P_{max} with P_{av} as the one used in computing the model curve).

The computer programme does 10 iterations. In the first iteration, it computes

$$DIF2 = \log_{10}(P_{max}/P_{av}) \tag{5.1a}$$

$$DIF1 = \log_{10}(P_{av}/P_{min}) \tag{5.1b}$$

It generates 500 random models using the relationship

$$P_i' = P_i 10^{ra} \tag{5.2}$$

where i = 1, number of layers; P_i' is the new parameter value and P_i its previous value; r is a member of a set of random numbers having zero mean and a standard deviation of 1; a=DIF2 if r>0 and a=DIFF1 if r<0 (|r| <1). In the case of the depth parameter, any situation where the depth to a lower interface is less than that to the interface above is rejected. Based on the acceptance criterion, the best 20

models are selected and put in an order table, with the best one at the top. It then finds the mean and standard deviation on a log-scale, the minimum (PMN) and maximum (PMX) of each of the parameters of these 20 best models. This mean value is taken as the new P_{av} and it then computes

$$DIFMAX = \log_{10}(P_{max}/PMX) \qquad (5.3a)$$

$$DIFMIN = \log_{10}(PMN/P_{min}) \qquad (5.3b)$$

DIFMAX and DIFMIN are used in altering P_{max} and P_{min} to new values. These new values of P_{av}, P_{max} and P_{min} are used in starting the second iteration from equation (5.1) above and similarly for the remaining iterations. In each iteration, the order table is updated so that it always contains the best 20 models so far. At the end of the 10 iterations, the best 20 models give a range of acceptable models and hence some indication of the non-uniqueness of the technique.

Another computer programme is then run to plot the 20 models (layered resistivity-depth profiles), their model curves and the modelled (observed) apparent resistivity and phase data. It is sometimes necessary to do some forward modelling to improve the fit between the models and the observed data.

5.3.3 Individual station 1D modelling results

Although the gross structural features of the project area can be said to be 2D, it is instructive as a prelude to 2D modelling to carry out 1D modelling. A 2D section derived from a collation of the individual site 1D models can then be used as the initial starting 2D model. The latter approach is obviously a means of reducing the computing cost of 2D modelling because it is generally very helpful in getting to a satisfactory model faster. Many workers (e.g., Rooney and Hutton, 1977; Jones and Hutton, 1979b; Beblo and Bjornsson, 1980; Stanley, 1984) have fitted 1D model curves to E-polarisation or major apparent resistivities and phases on the ground that these are less distorted by near-surface inhomogeneities than H-polarisation or minor data. This is true in many cases, especially where the strike direction is clearly undisputed. Other workers (e.g., Hutton et al., 1980; Jodicke et al., 1983) have preferred an average of the data. In the latter case no data part is neglected. The two forms of average in frequent use are Z_{eff} and Z_{av} given respectively by equations (2.23a,c) and the corresponding apparent resistivities (ϱ_{eff}, ϱ_{av}) and phases (φ_{eff}, φ_{av}) computed from these. Since Z_{eff} uses all the impedance tensor elements, it is more preferable than Z_{av} which neglects the diagonal elements.

For a 1D structure, ϱ_{av} and ϱ_{eff} are each the same as the apparent resistivity of the medium (ϱ_{xy}), while φ_{av} is the phase of Z_{xy} and φ_{eff} is twice the phase of Z_{xy}. Considering a 2D structure and rotating to the strike and

perpendicular directions, $Z_{xx}=Z_{yy}=0$ and hence from equation (2.23a), $Z_{eff}=(-Z_{xy}Z_{yx})^{1/2}$. The latter is the geometric mean of Z_{xy} and $-Z_{yx}$ (parallel and perpendicular impedance tensor elements respectively), while Z_{av} is the arithmetic mean of the two impedance elements. On the assumption that impedance tensor is lognormally distributed (Bentley, 1973), a geometric mean is thus more appropriate than an arithmetic mean. For this 2D case, it may be noted that the apparent resistivity, ϱ_{av} is not a simple linear average of the parallel and perpendicular apparent resistivities. On the other hand, ϱ_{eff} is the geometric mean of the parallel and perpendicular apparent resistivities and can be interpreted as average scalar resistivity for the 2D structure by analogy with mixtures, where the geometric mean gives an accurate estimate of the physical properties (Madden, 1976). On account of the invariance of the determinant of the impedance tensor [I_1 in equation (2.23a)], ϱ_{eff} is always the geometric mean of the parallel and perpendicular apparent resistivities, irrespective of the orientation of the measuring axes (Ranganayaki, 1984). Thus, for a 2D structure, ϱ_{av} and φ_{av} are inappropriate. However, ϱ_{eff} and φ_{eff} do give correct averages for both 1D and 2D resistivity variations, irrespective of the orientation of the measuring axes (Ranganayaki, 1984). Hence, ϱ_{eff} and φ_{eff} are better averages to use than ϱ_{av} and φ_{av}.

In the present project, the major and minor, the E- and H-polarisation and the invariant (using Z_{eff}) apparent resistivity and phase data have been modelled. In each

case, an optimum number of layers was specified, both layer resistivity and depth were allowed to vary and the number of error bars criterion was used. When necessary, some forward modelling was done to improve the fit of the best 20 models from the Monte-Carlo inversion.

In the modelling exercise, it was found that the minor data were more difficult to model than the major. In fact at some sites, particularly BED, LAN and WAN, it was impossible to get a satisfactory model fit to the minor data with the inversion scheme. However, the H-polarisation data were only slightly more difficult to model than the E-polarisation data. The apparent difficulty was due to the fact that the minor data were considerably more scattered and smaller than the major, while the H-polarisation data were only slightly more scattered than the E-polarisation data. The above evidence thus supports the view that the H-polarisation and minor data are more affected by near-surface inhomogeneities than E-polarisation and major data. At any of the sites, the models resulting from the E-polarisation/major data when compared with those from the H-polarisation/minor data generally indicated similar structure, i.e., the same resistor/conductor sequence. However, the minor/H-polarisation parameter values were generally lower than the corresponding major/E-polarisation values. The major and E-polarisation parameter values were normally very similar and the same can be said of the minor and H-polarisation parameter values. In view of the above, the author is of the same opinion as workers such as Hutton

et al. (1980) and Jodicke et al. (1983) that a kind of average data is more preferable. These authors and Mbipom and Hutton (1983) have modelled ϱ_{av} and φ_{av} resulting from $\mathbf{Z}_{av}$. However, for reasons given earlier, ϱ_{eff} and φ_{eff} data resulting from $\mathbf{Z}_{eff}$ are preferable and hence have been modelled.

Although other data were modelled as indicated earlier, only the models resulting from the invariant data are presented here. Figures 5.2a-j show the 1D layered Monte-Carlo models for the individual sites. In each case, the model curves and the measured apparent resistivity and phase data points with error bars (±1 standard deviation) are shown on the left hand graphs, while the right hand graphs show the layered models and the resistivity-depth data points with error bars (±1 standard deviation) resulting from the direct inversion of the apparent resistivity and phase data using the Bostick transform. These latter resistivity-depth plots will be simply referred to as the Bostick plots. A comparison of the Monte-Carlo layered models with the Bostick plots is given in section 5.4.

5.3.4 Discussion of 1D model results

A simplified 2D section from a collation of the individual site 1D models is shown in two parts for clarity - Fig. 5.3a shows the SUF profile sites and three Duns sites and Fig. 5.3b shows all the Duns sites only. A brief discussion of this 2D section is given here. A detailed discussion of

FIGURE 5.2A-J

1D models of the invariant data (ϱ_{eff}, φ_{eff}) at the individual sites. On the left hand graphs are the model curves and the apparent resistivity and phase data points with error bars (±1 standard deviation), while the right hand graphs show the Monte-Carlo layered resistivity-depth models and the Bostick resistivity-depth data points with error bars (±1 standard deviation).

N.B.

SITES	PAGE	SITES	PAGE
MUR, SPM	162	HUR, BED	167
SAW, BUG	163	HAL, KET	168
WAN, WLA	164	HAR, KE2	169
BER, SCR	165	LAN, CHO	170
EVE, HRI	166	GRE, CAM	171

Fig. 5.2a

SITE : MUR

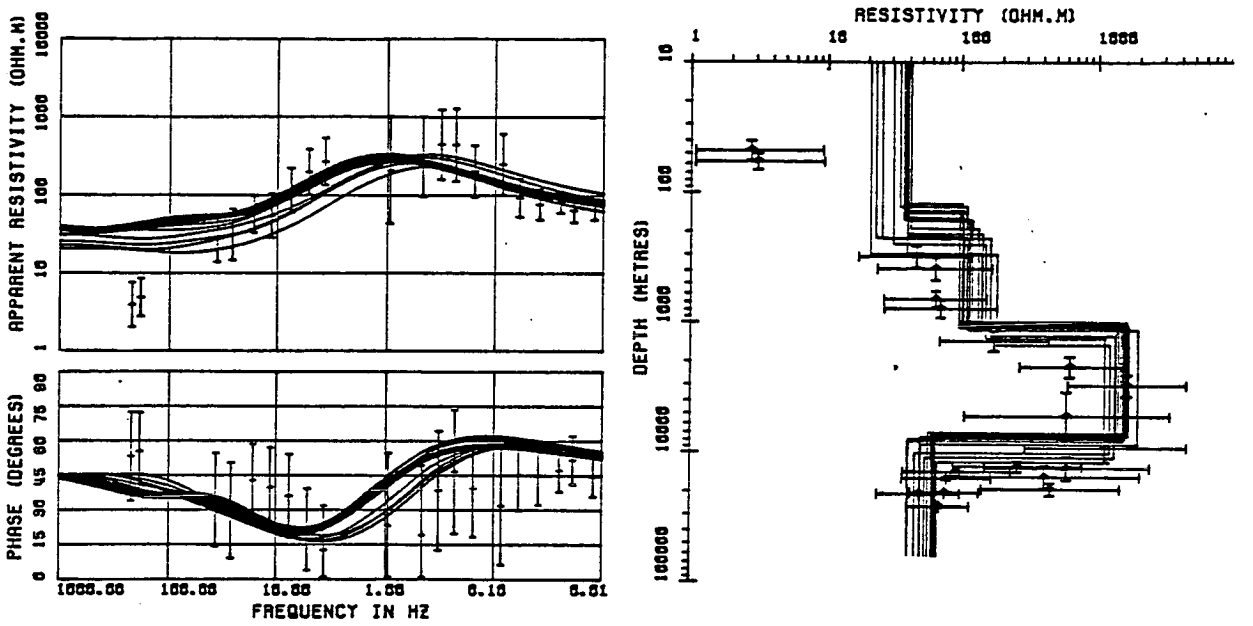

SITE : SPM

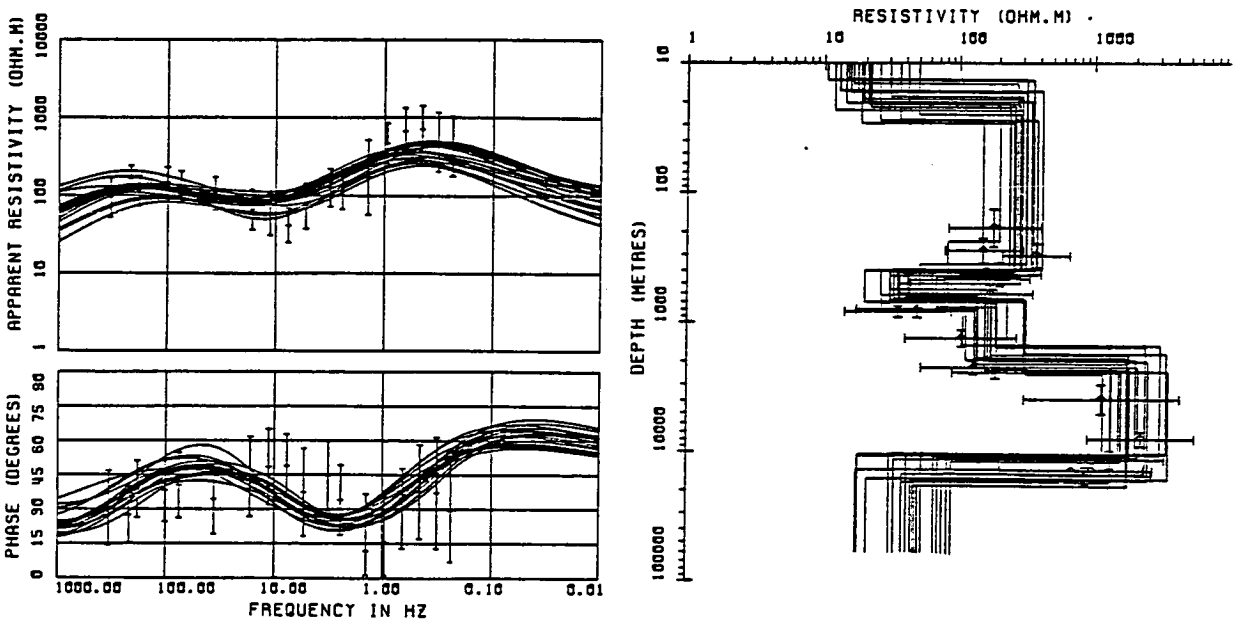

Fig. 5.2b

SITE : SAW

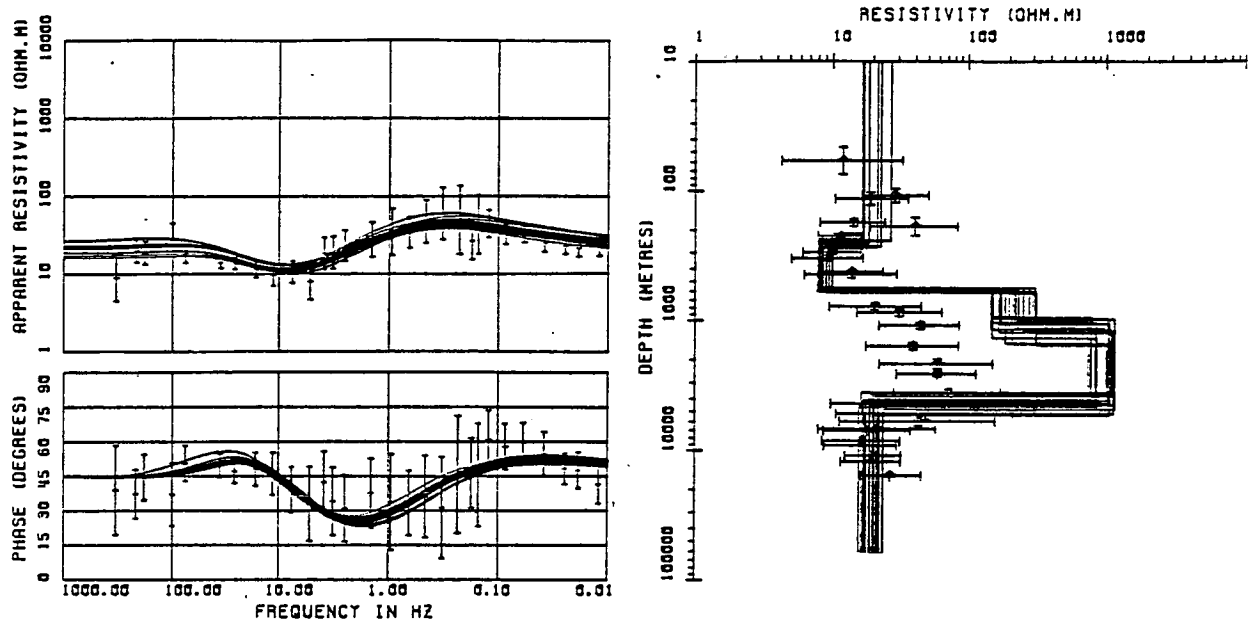

SITE : BUG

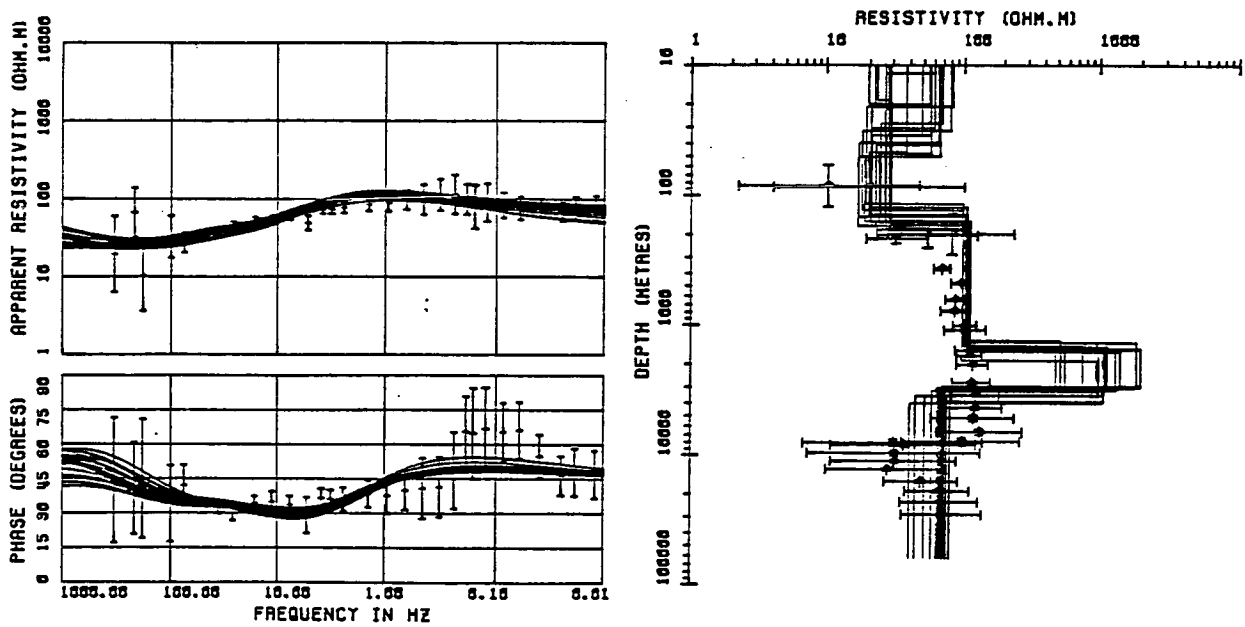

Fig. 5.2c

SITE : WAN

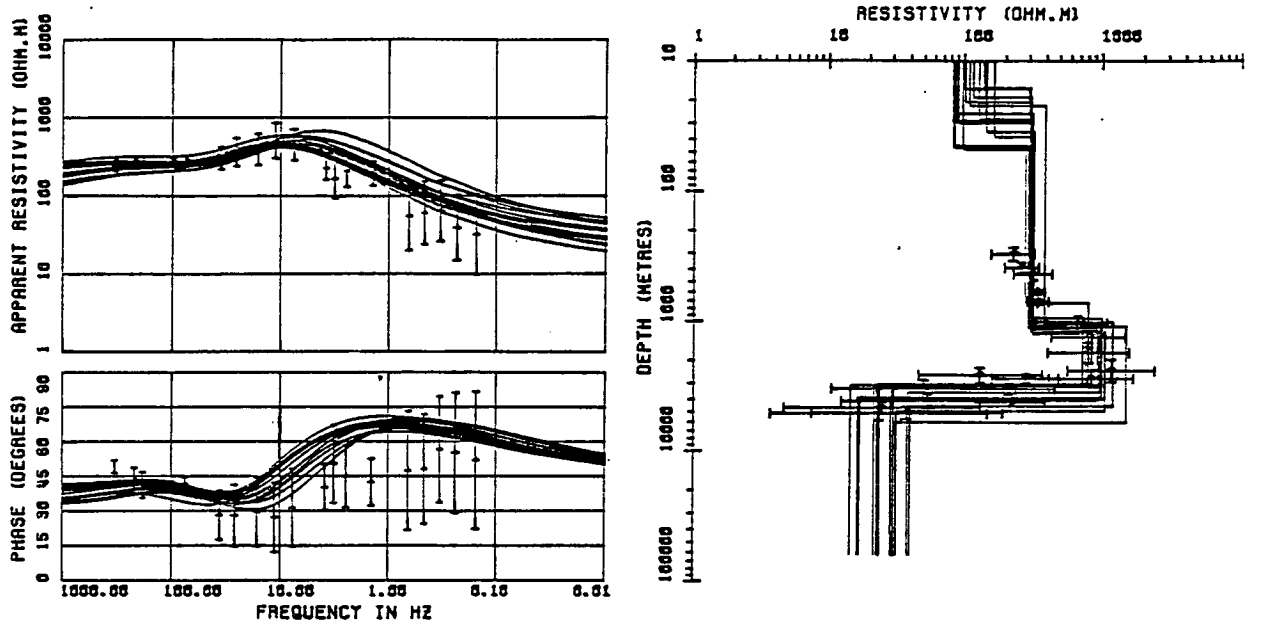

SITE : WLA

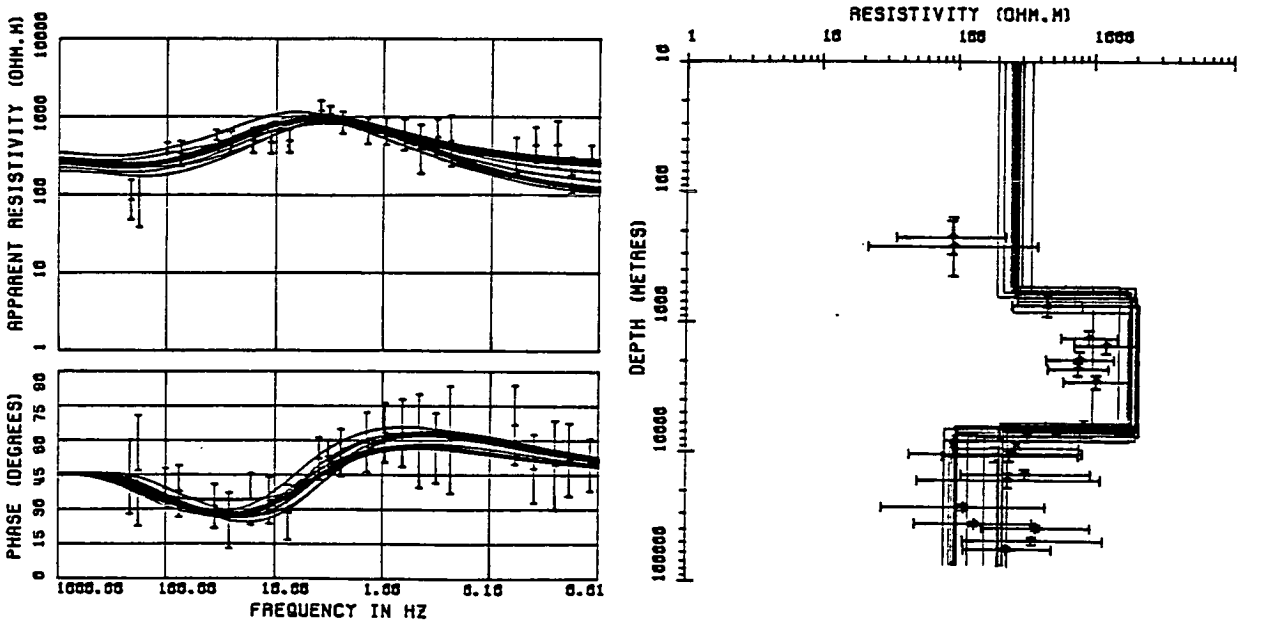

Fig. 5.2d

SITE : BER

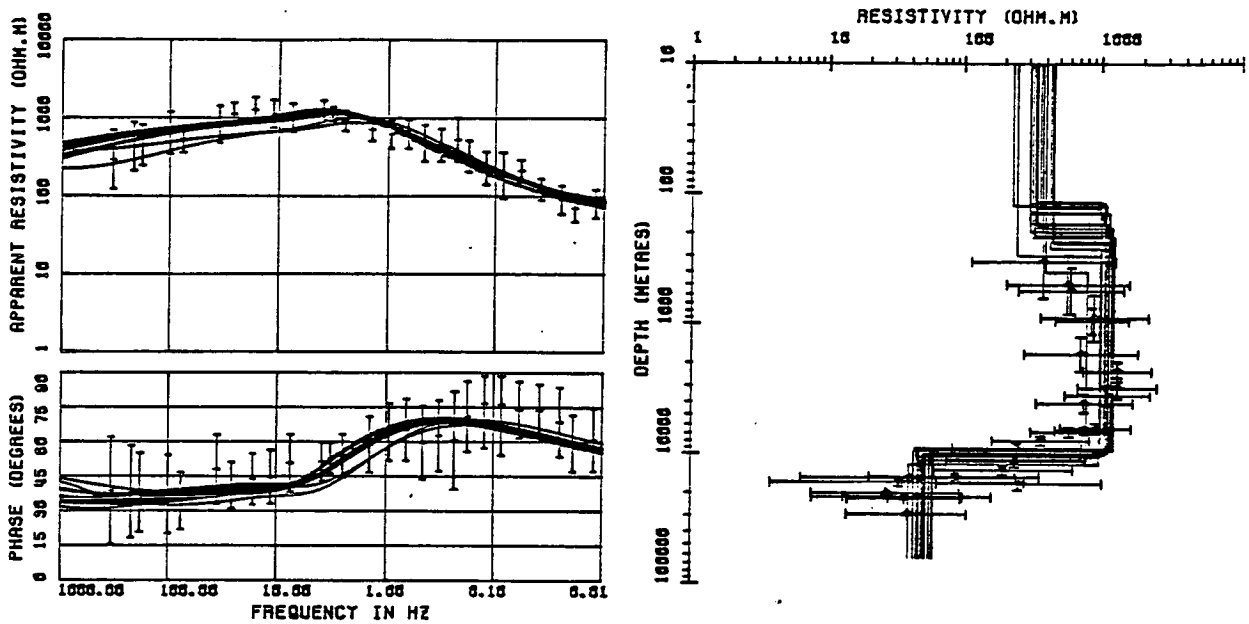

SITE : SCR

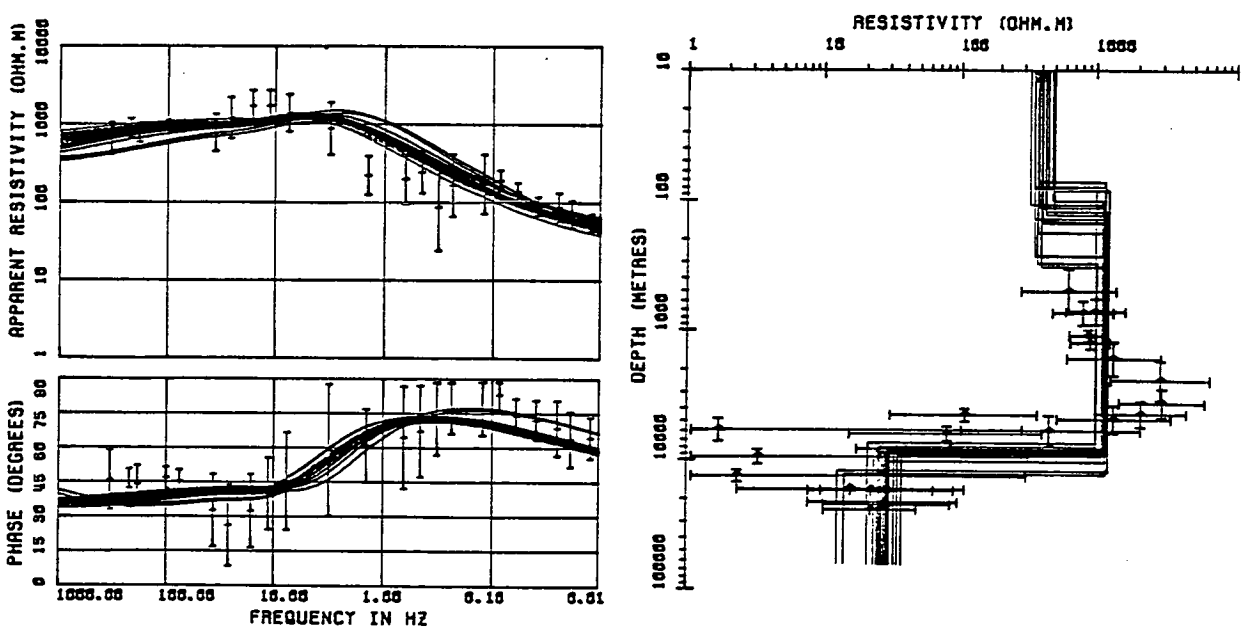

Fig. 5.2e

SITE : EVE

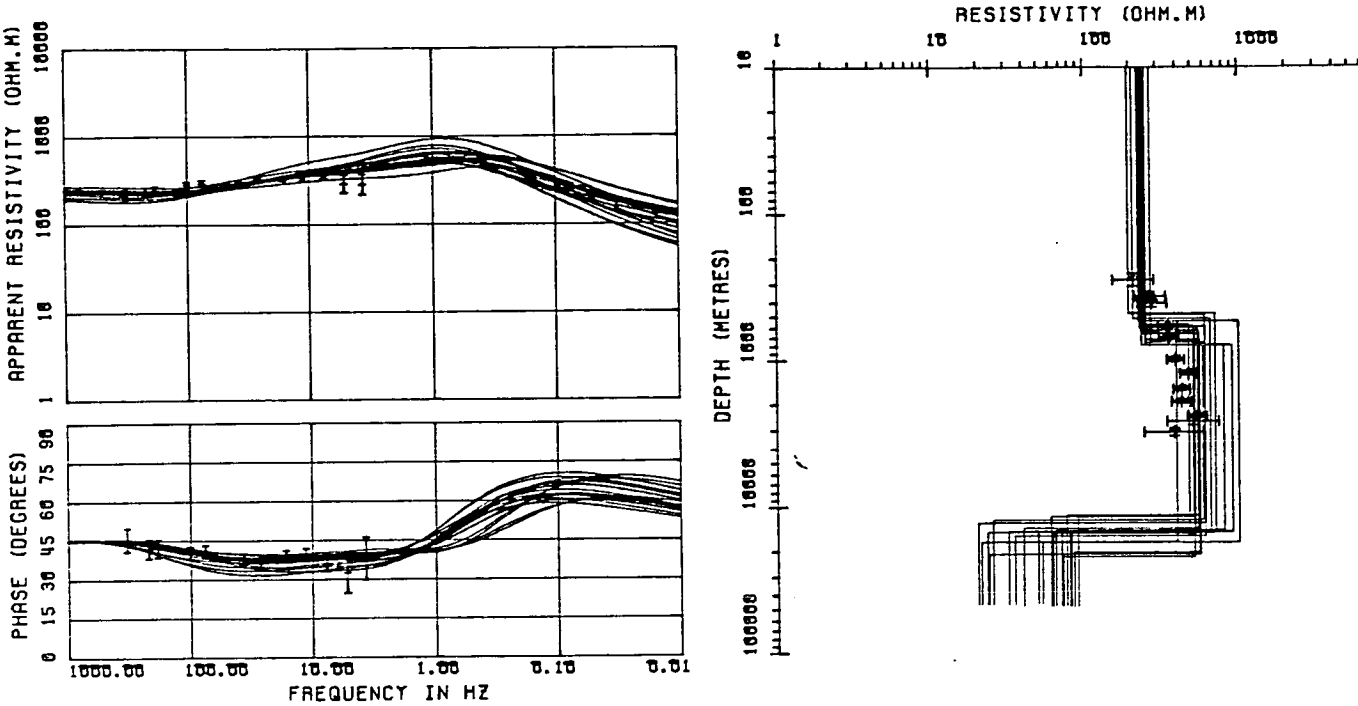

SITE : HRI

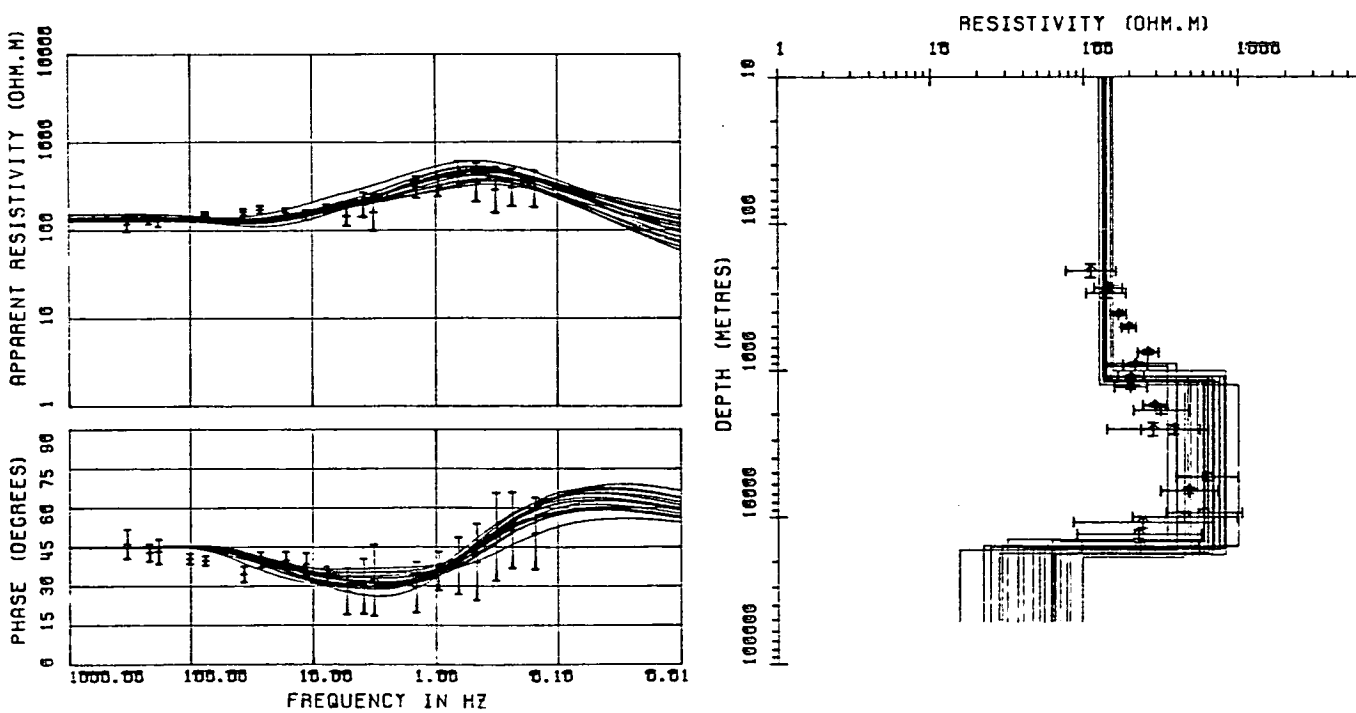

Fig. 5.2f

SITE : HUR

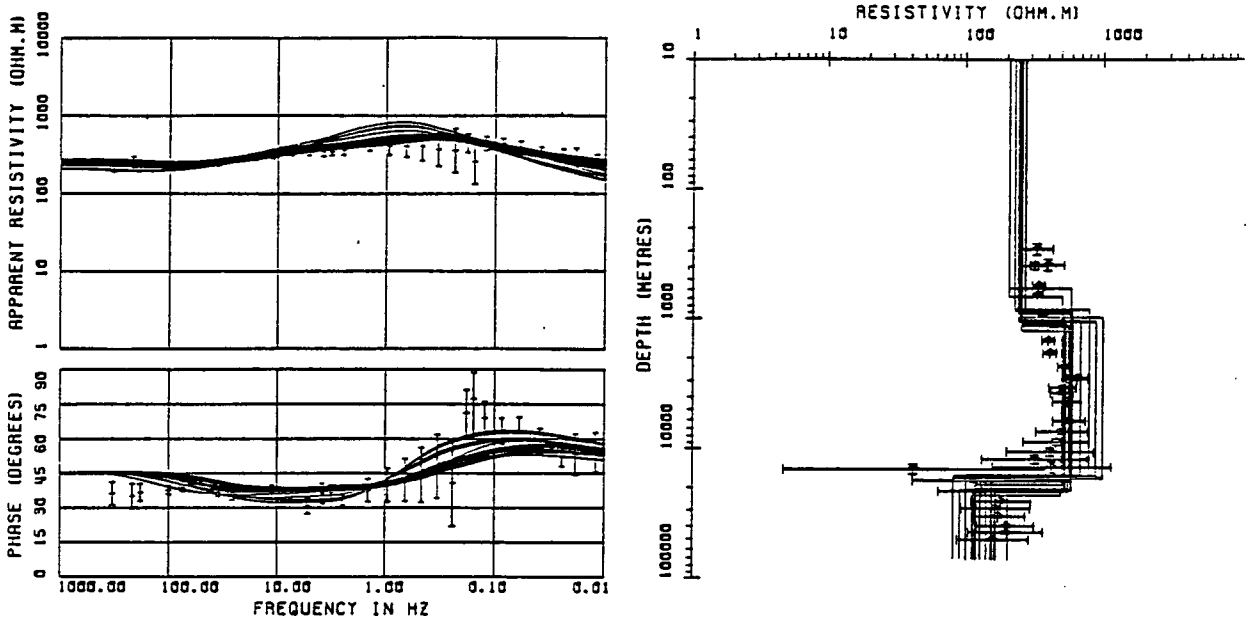

SITE : BED

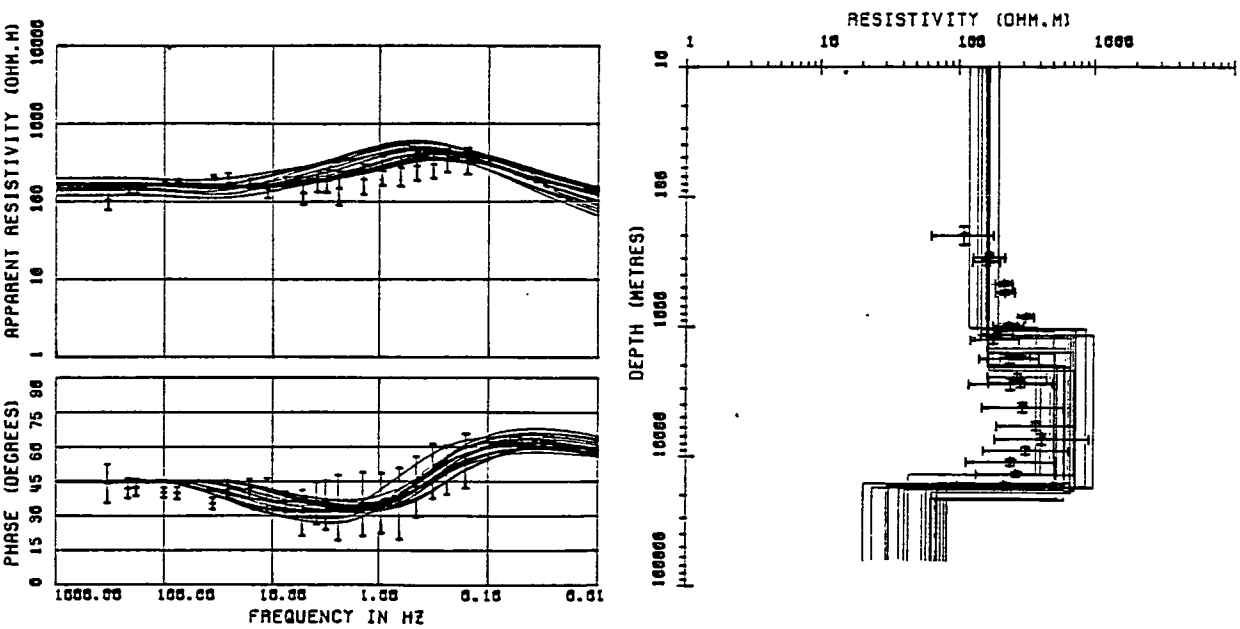

Fig. 5.2g

SITE : HAL

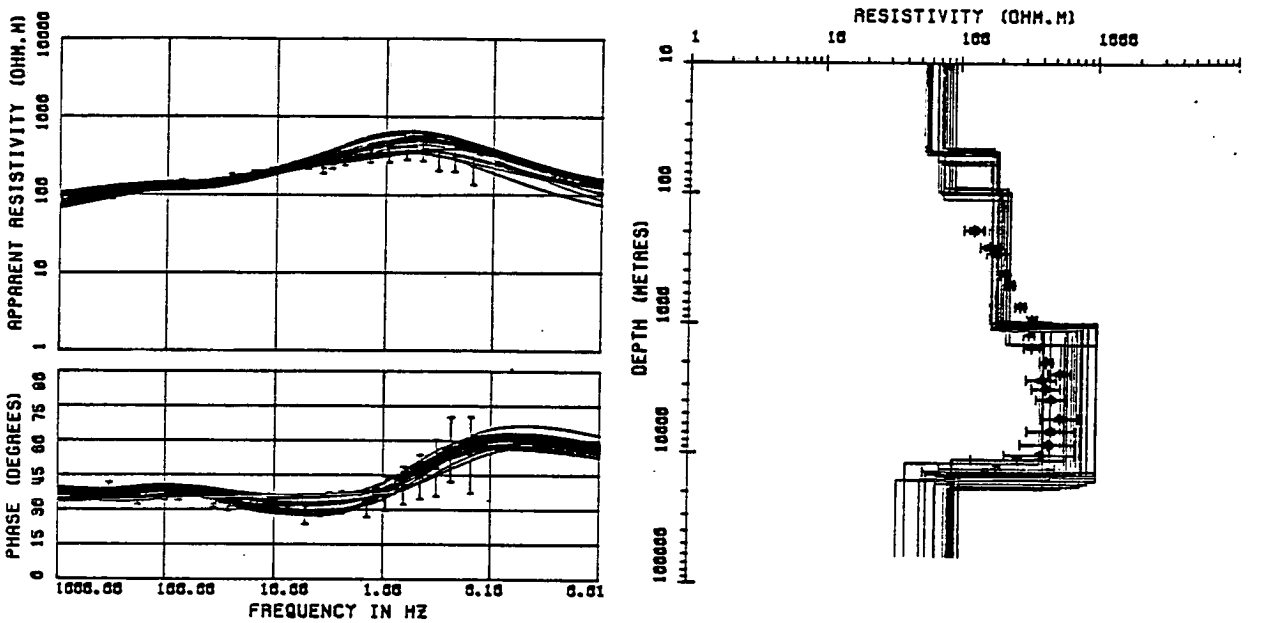

SITE : KET

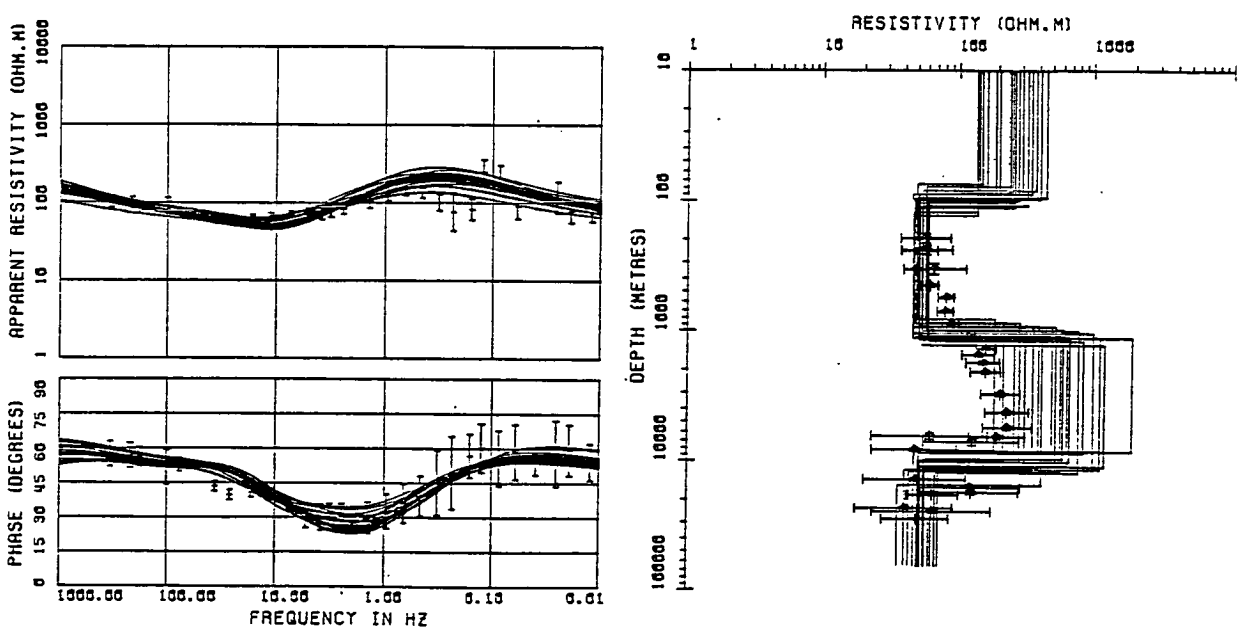

Fig. 5.2h

SITE : HAR

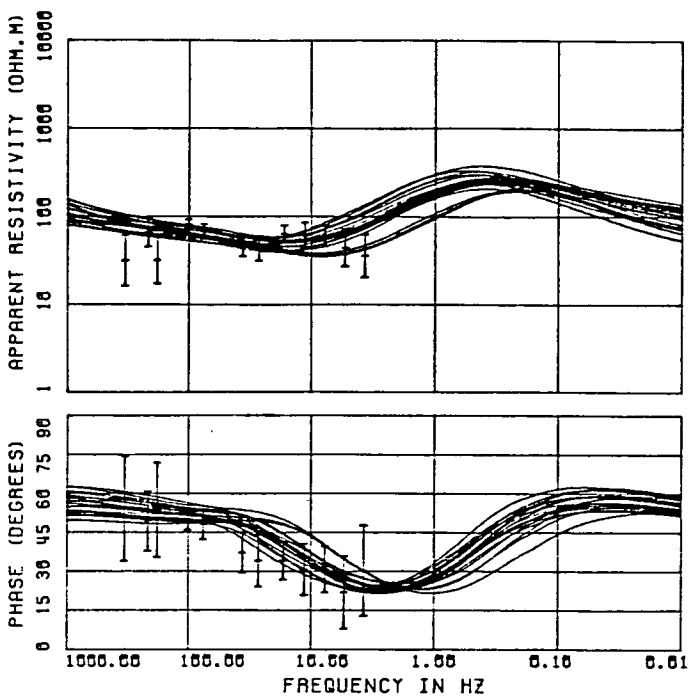

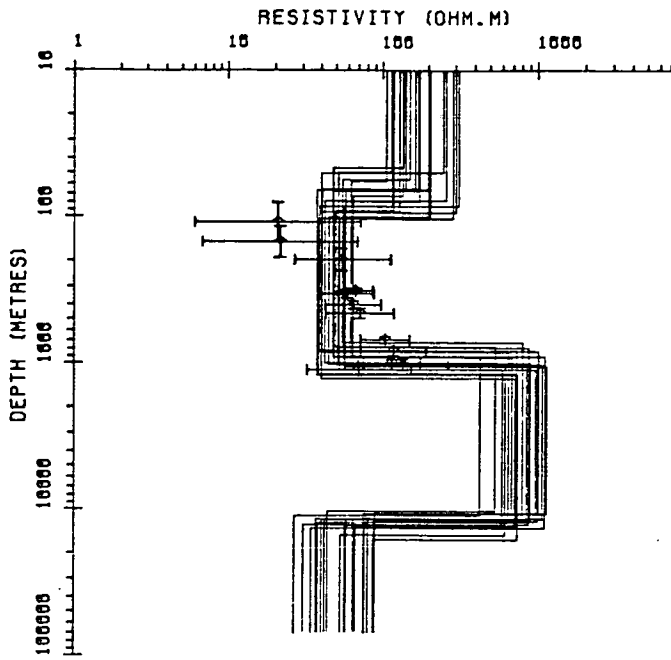

SITE : KE2

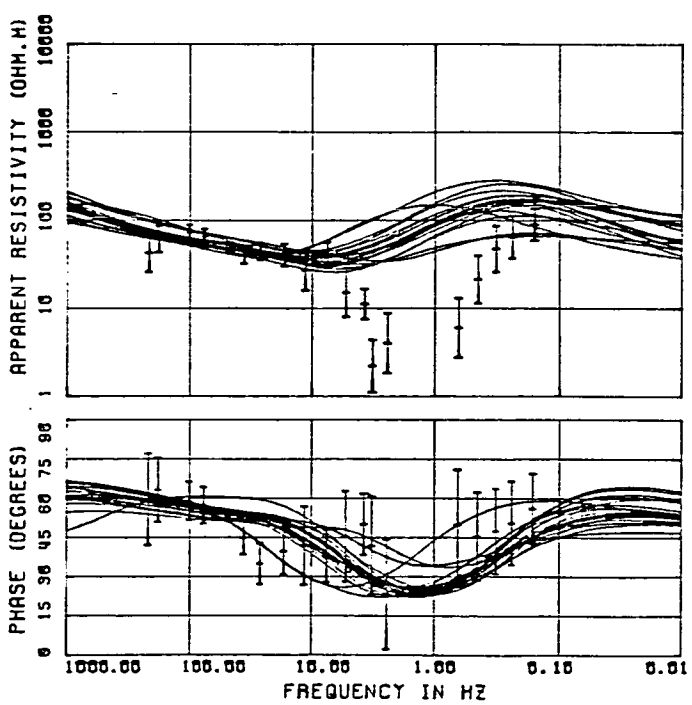

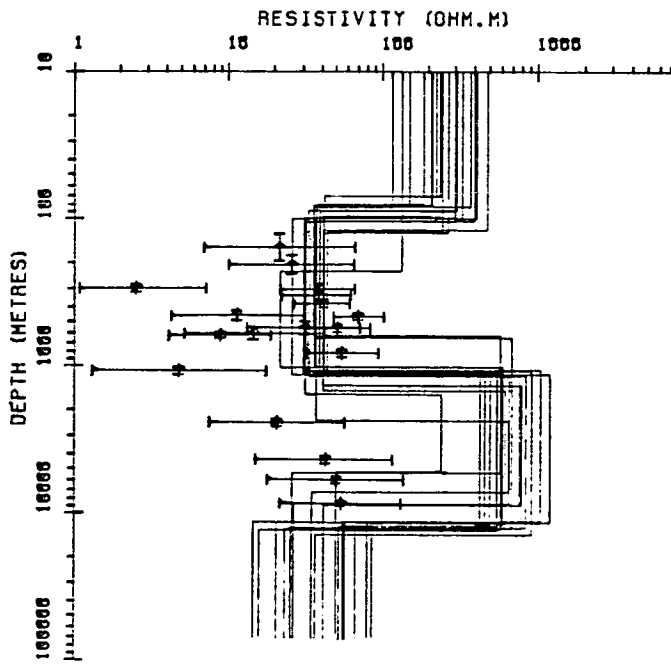

Fig. 5.2i

SITE : LAN

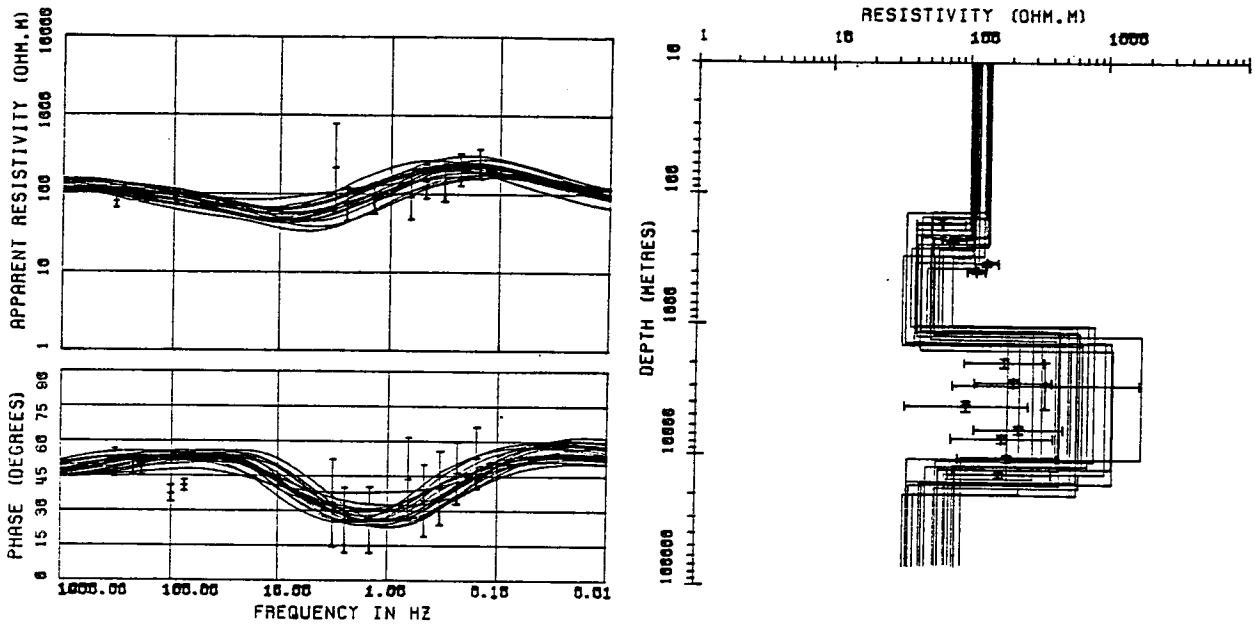

SITE : CHO

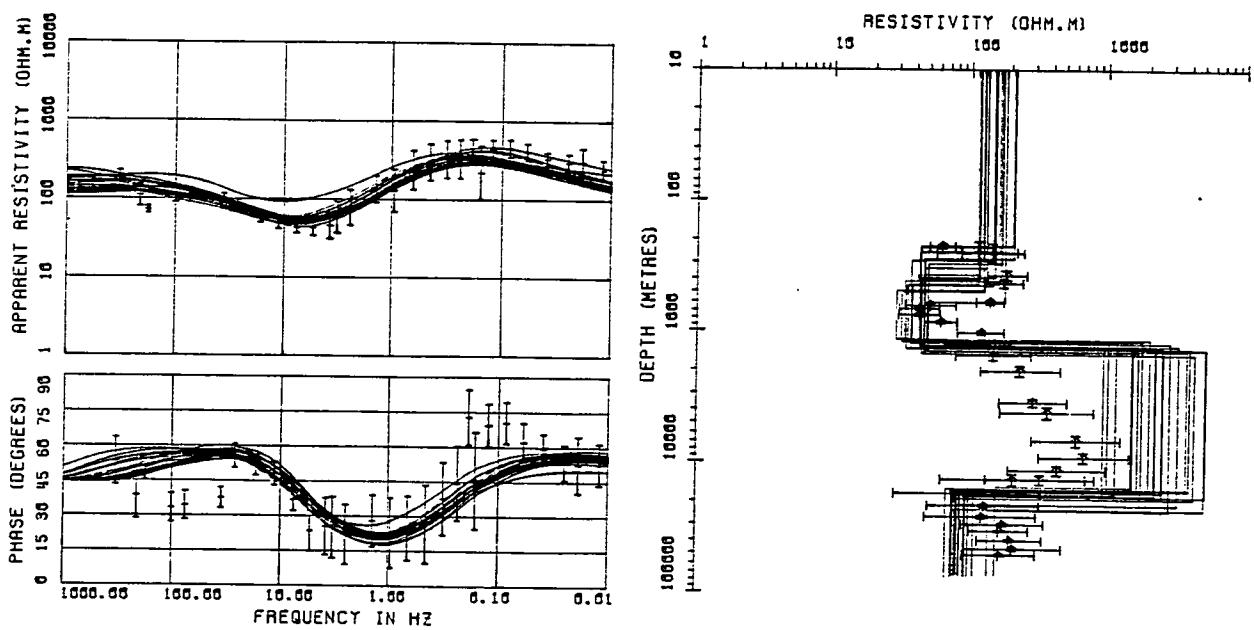

Fig. 5.2j

SITE : GRE

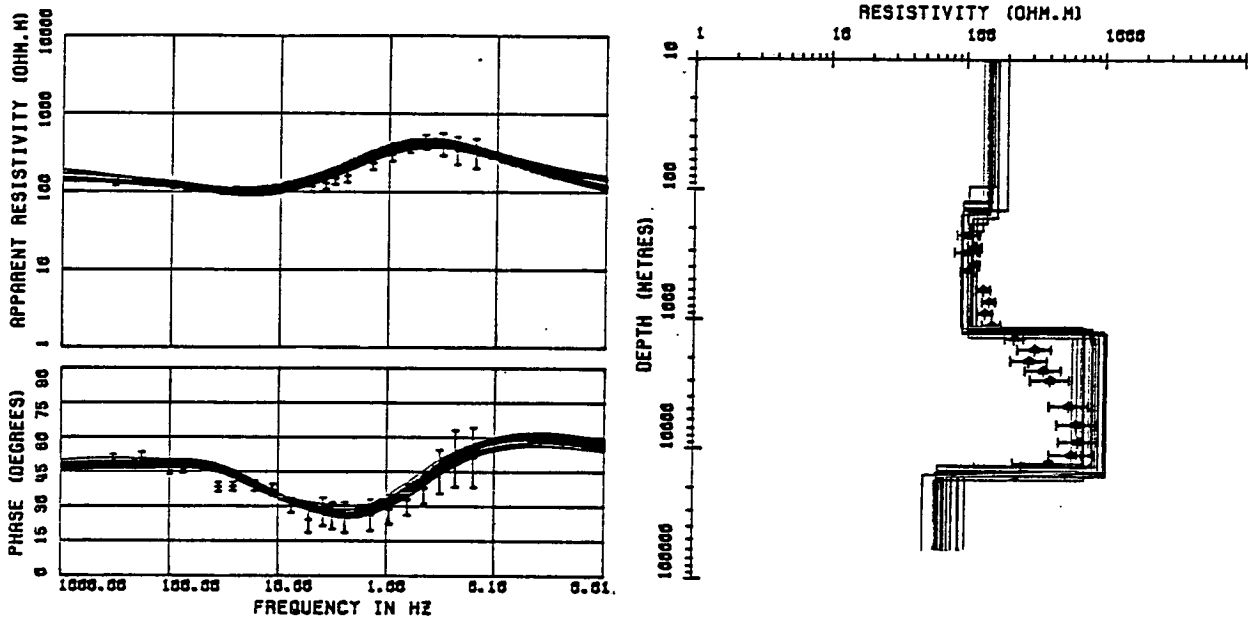

SITE : CAM

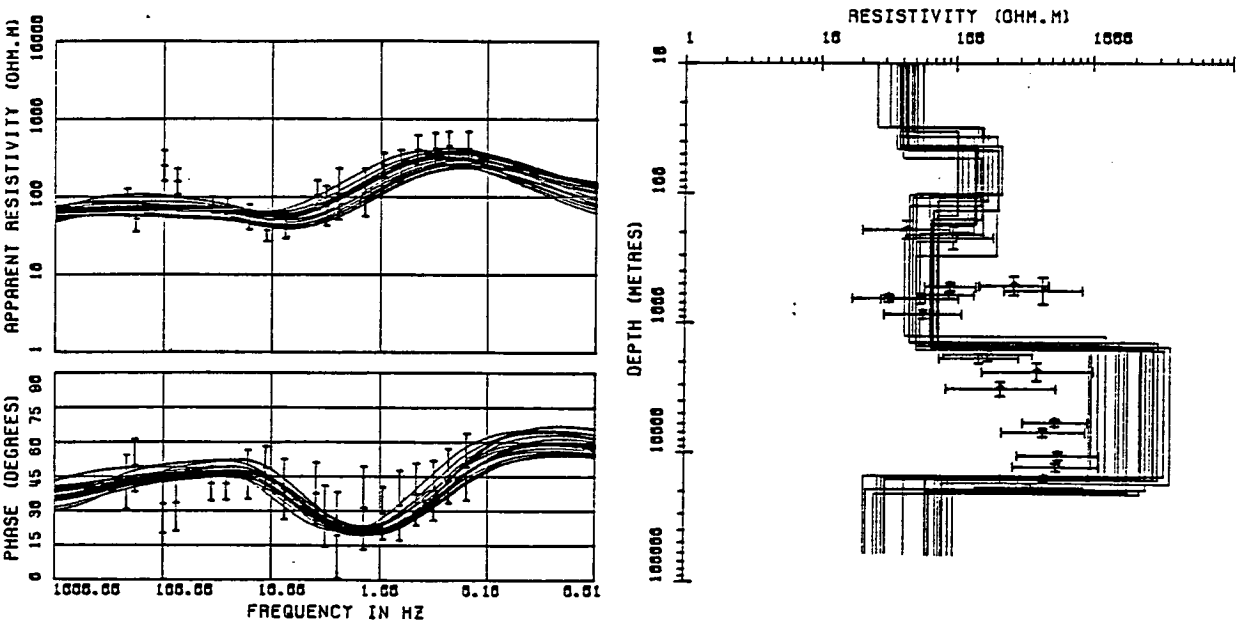

the section shown in Fig. 5.3a has been given by Sule and Hutton (1984).

From Figs. 5.3a,b, it can be seen that two conductive upper layers (< 100 and 100-500 ohm-m) of varying thickness are in evidence. Both layers are interpreted as a conductive sedimentary cover. In Fig. 5.3a, the < 100 ohm-m upper layer thins rapidly from north to south across the SUF with the result that in the Duns area up to just beyond BED it does not feature at all (Fig. 5.3b). From the neighbourhood of KET onwards the < 100 ohm-m layer underlies the 100-500 ohm-m upper layer. The sedimentary cover is thinnest under BER and SCR and thickens north and south of these sites.

The sedimentary cover is underlain by a resistive layer (> 1000 ohm-m), the depth to which is shallowest (< 0.3 km) at BER and SCR, but greater than 1 km further north and south. Beneath the resistive layer is a significant low resistivity layer (< 100 ohm-m) with its upper boundary at depths varying from the upper crust to the lower crust. This confirms the existence of a lower crustal conductor predicted from long period MT studies by Jones and Hutton (1979a,b) and Ingham and Hutton (1982a,b). In addition, Figs. 5.3a,b indicate that this conductor extends into the upper crust. It rises nearer the earth's surface at two zones - in the neighbourhoods of BUG where its depth is shallowest (< 4 km) and KET where its depth is less than 11 km. Outside these zones, the depth to the conductor deepens as one goes farther north and south. It may be noted that the second zone does not show up in Fig. 5.3a with only 3

FIGURE 5.3

A simplified 2D section from a collation of the individual site 1D models -

(a) The SUF profile sites and three Duns sites. DGF and SUF are the Dunbar-Gifford Fault and the Southern Uplands Fault respectively.

Note that there is a 2.5 vertical exaggeration.

(b) All the Duns sites:- the site codes are respectively EVE, HRI, HUR, BED, HAL, KET, HAR, KE2, LAN, CHO, GRE and CAM.

Note that there is a horizontal exaggeration of 2.

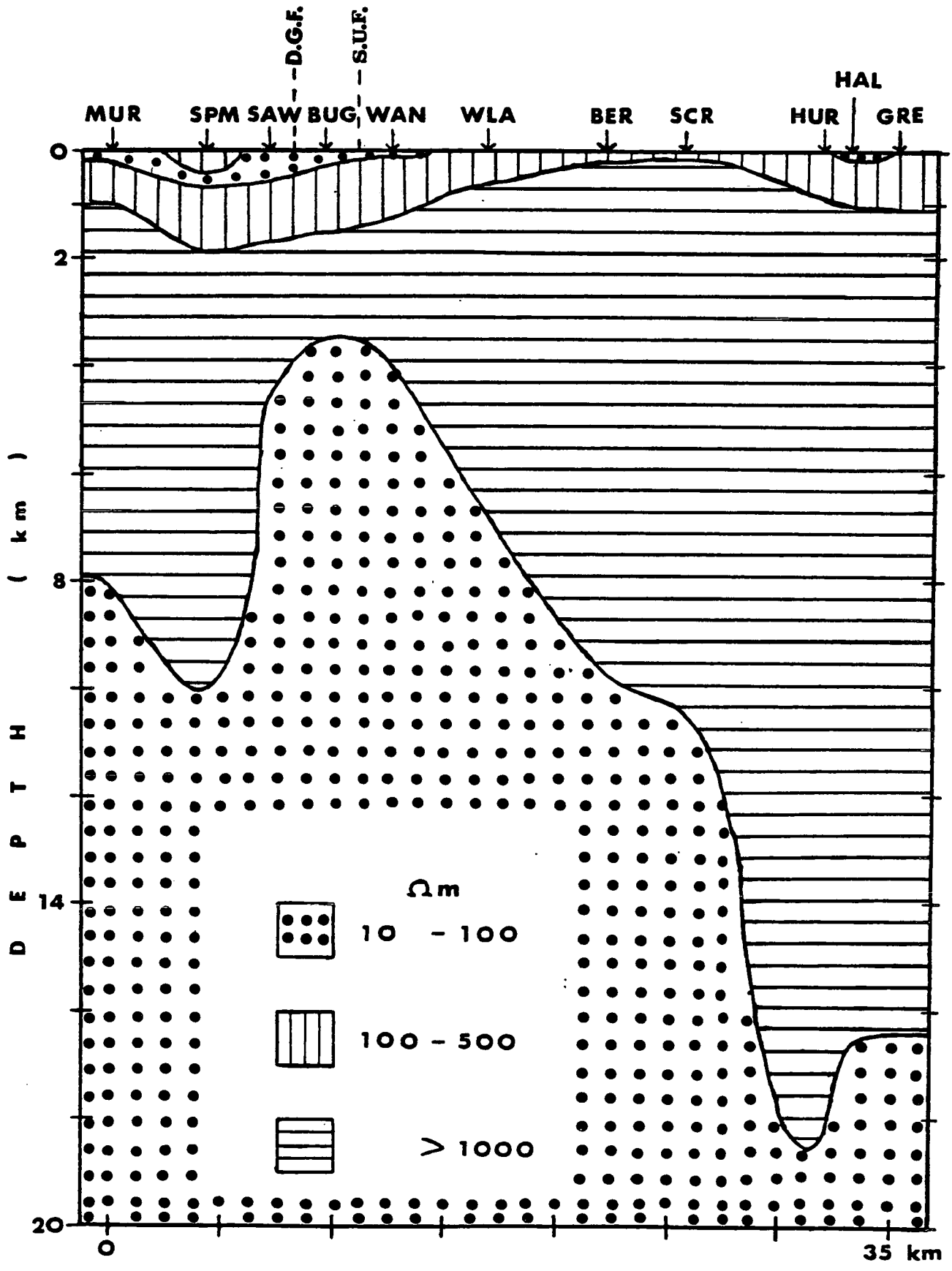
MUR
SPM
SAW
D.G.F.
BUG
S.U.F.
WAN
WLA
BER
SCR
HUR
HAL
GRE
0
2
8
14
20
DEPTH (km)
Ωm
10 - 100
100 - 500
> 1000
0
35 km

(a)

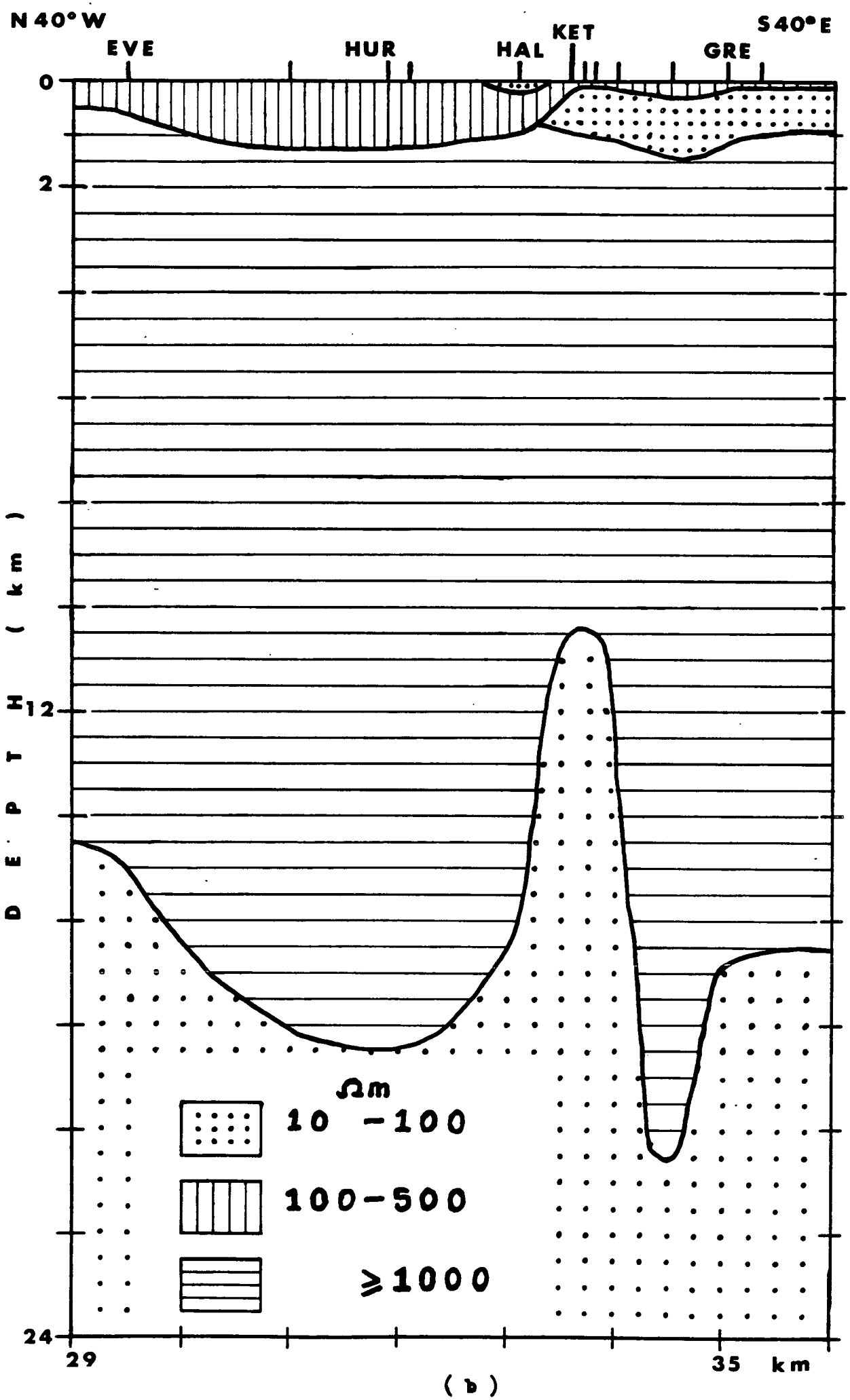
N 40° W
S 40° E
EVE
HUR
HAL
KET
GRE
0
2
12
24
D E P T H (k m)
29
35 km
Ωm
10 -100
100-500
≥1000
(b)

Duns sites, thus underscoring the importance of close station spacings and emphasizing the need for extreme caution in extrapolating structures between widely spaced stations.

The 2D section indicates a significant lateral variation in the electrical conductivity structure of the area. The conductivity structure is more complex north of the SUF than south in good agreement with the more complex surface geology in the Midland Valley than in the Southern Uplands.

It is pertinent to investigate whether or not a very thin and very conductive upper/lower crustal conductor is compatible with the measured AMT/MT data. From Jones and Hutton (1979a,b) and Ingham and Hutton (1982a,b), there is evidence that a resistor (750 and 1250 ohm-m respectively) lies beneath the conductor. In the present study, only the band 4 (MT) data can possibly penetrate this conductor. Hence, at each site where band 4 data were available, the following steps were carried out: (a) the model parameters of the layers above the conductor were kept fixed; then (b) a resistor (1000 ohm-m) was placed beneath the conductor; (c) keeping the conductance of the conductor fixed, the resistivity and thickness of the latter were varied until it was very thin and very conductive and (d) the forward model curves were plotted and compared with the measured data. Figure 5.4 shows examples of the plots at two of the sites. The results from the other sites indicate similar behaviour. Model 1 (one of the best 20 Monte-Carlo models) at each site

FIGURE 5.4

Model curves illustrating how thin and conductive the deepest crustal conductor can be:- model 1 in each case shows this conductor as a half-space for comparison. On the left hand graphs, the model curves are plotted on the apparent resistivity and phase data points, while the layered models are shown on the right with the layer resistivities in ohm-m and depth in m.

On the apparent resistivity and phase data plots, model 1 and 2 curves are indistinquishable except very near 0.01 Hz where model 2 curve lies slightly below curve 1.

SITE : BUG

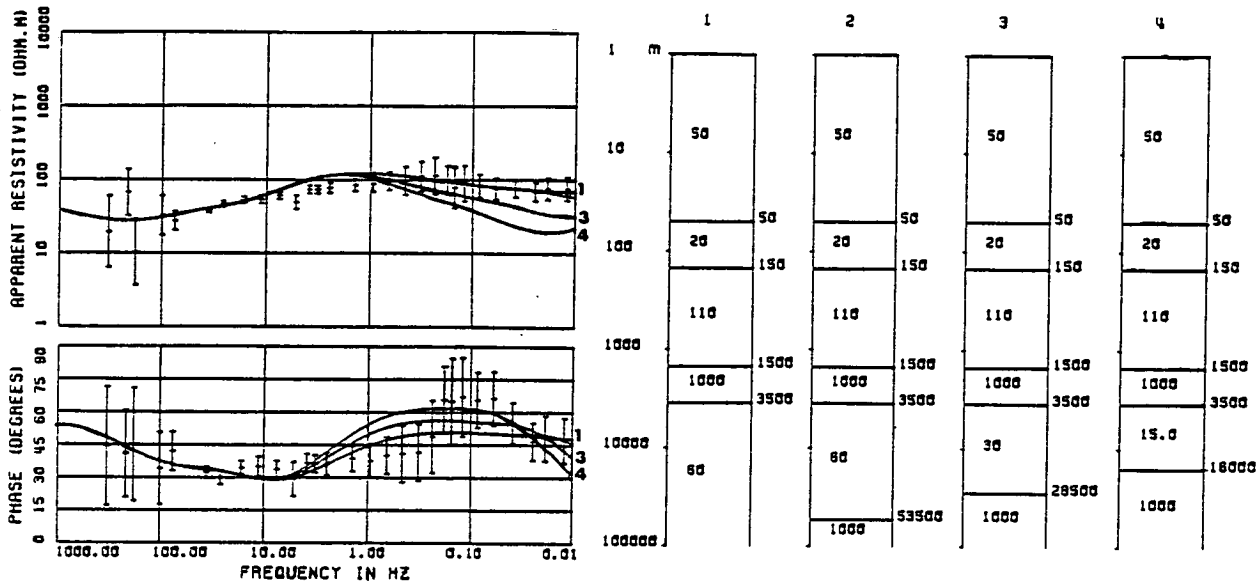

SITE : BER

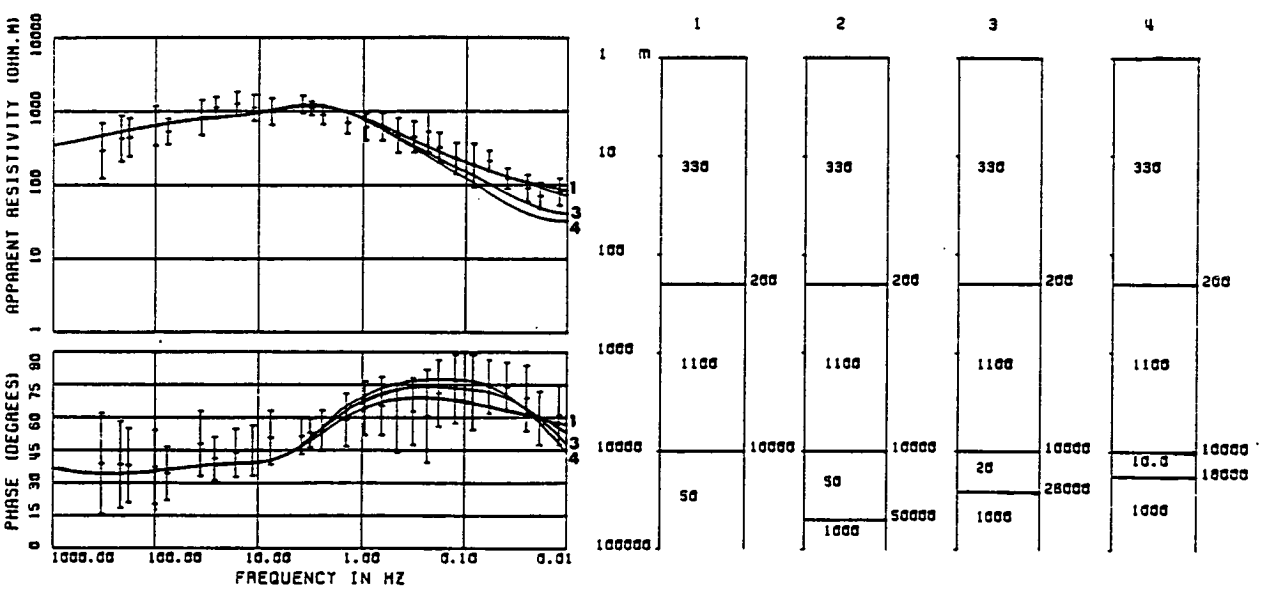

shows for comparison the case when the conductor is a half-space. It can be clearly seen that a very thin and very conductive upper/lower crustal conductor is precluded by the AMT/MT data. Model 1 and 2 plots on the apparent resistivity and phase data are virtually identical except very close to frequency 0.01 Hz, where model curve 2 lies slightly below model curve 1. In the absence of (or omitting) the AMT data and considering only the MT period data used in the present project and including few slightly longer period data, i.e., a very narrow band data set starting from >4 s, it is possible to get a model consisting of a resistive upper crust overlying a thin good conductor and a resistive half-space below to fit such a data set. Hence, it may be emphasized that extreme caution is essential when interpreting a very narrow band data set.

5.4 Comparison of the Bostick plots with the 1D Monte-Carlo layered models

In Figs. 5.2a-j, the best 20 Monte-Carlo layered resistivity-depth models are shown at each of the sites. Also plotted on the same graphs are the continuously varying resistivity-depth profiles derived from applying the Bostick transform to the apparent resistivity and phase data. It can be seen that there is generally a very good agreement between the Bostick plots and the Monte-Carlo 1D models. The agreement is better the higher the quality of the AMT/MT data. Only minor discrepancies can be detected particularly at SAW and BUG. These sites are in

the vicinity of faults (Fig. 1.1). Thus, even in a very complex geological setting and despite the fact that the Bostick transform of the data is only an approximate direct inversion, satisfactory results are obtained.

The computational time for the Bostick transform plots is less than 10% of that for the Monte-Carlo inversion and plots. For any site where the latter are repeated on account of a very poor fit to the data as a consequence of a poor initial starting model, the above percentage is halved. Thus, the Bostick transform is computationally efficient and also simple to use. It transforms the apparent resistivity and the corresponding phase data to real resistivity and depth on a 1 to 1 basis and hence, there is no need to repeat the operation. It also shows the precise sounding depth attained without any inference. It preserves quite clearly the data quality and gives an indication of the homogeneity or otherwise of the subsurface (see Figs. 5.1a-v). In the latter figures, it can be clearly seen that it is more advantageous to present MT data in terms of the Bostick resistivity-depth plots rather than in terms of the conventional apparent resistivity and phase plots. The apparent resistivity and phase plots cannot be easily visualized in terms of the subsurface structure in any quantitative sense (only qualitative deductions are possible), while the Bostick plots characterize the subsurface quantitatively. The conventional formats are generally understood only by EM experts, while the Bostick plots can be readily understood by geologists and geophysicists alike.

The author is in agreement with Goldberg and Rotstein (1982) who have opined that the Bostick form of MT data presentation may help familiarize earth scientists with the results of MT surveys and this may in consequence help overcome the present lack of wide spread use of the MT method in exploration. The author suggests a collation of the Bostick results at the individual sites into a 2D section and a simple contouring of this section. This can show quite clearly the basic subsurface structure and may be equivalent to a time section in seismics. This thus enables easy comparison of the MT and seismic results. The 2D section can also be used as a basis for forming an initial starting model for 2D modelling.

On account of simplicity, it is desirable and useful to incorporate the Bostick transform in real-time MT analysis. Infield MT processing with the Bostick plots will enable data quality and sounding success to be fully assessed before leaving a field site.

Thus, it can be concluded that it is advantageous to incorporate the Bostick transform in real-time and routine MT analysis. It can be a useful interpretation tool. The resulting models will aid the quick assessment of reconnaissance surveys; this is particularly desirable in those surveys involving MT and other geophysical techniques.

CHAPTER 6

COMPARISON OF TECHNIQUES

The Habberjam deep resistivity technique (HAB) and the AMT/MT technique are compared here. A brief description of the HAB technique is given. The 1D models for the Duns area obtained from the two techniques are compared. It can be seen that there is an excellent general agreement in the depth range resolved by HAB. However, the AMT/MT technique provides more information at depth as well as a clear indication of the lateral variation in the electrical conductivity structure within the area. It is demonstrated quite clearly that AMT/MT is a more useful rapid coverage resistivity mapping technique than HAB and hence more suitable for reconnaissance survey. From a detailed evaluation of both techniques from the exploration viewpoint, it is concluded that AMT/MT is more cost- and exploration-effective with a much greater depth and lateral resolution.

6.1 Description of Habberjam deep resistivity technique

The technique will be simply referred to as HAB. A detailed description of HAB has been given by Habberjam (1979) and Habberjam and Thanassoulas (1979).

HAB uses a square array and crossed dipole-dipole arrays. The configurations for the square array are shown in Fig. 6.1a. The additive resistance rule $R_\alpha = R_\beta + R_\gamma$ holds. The centre of the square gives the assignment location (x,y), i.e., the sounding centre, while the side a of the square is the conventional electrode spacing. The array orientation θ is conventionally taken as the direction $1 \rightarrow 4$. Thus, the parameters x, y, a and θ completely specify the square array. The α and β configurations give rise to similar orientations. Hence, in a homogeneous subsurface $R_\alpha = R_\beta$ and $R_\gamma = 0$. The latter is used as a check on the resistance measurements. R_α and R_β may be averaged together to give the mean resistances which are used in an attempt to produce orientationally insensitive earth resistance measurements.

Based on the moving source technique, measurements are conducted in a symmetrical fashion about the sounding centre in two perpendicular directions (the diagonals of a square) up to a maximum spacing of about 5 km (Fig. 6.1b). A square array sounding is initially conducted starting from a spacing of $\sqrt{2}$ m and expanding the square sides incrementally by a factor of $\sqrt{2}$. Usually, up to a maximum of 1024 m spacing, the current AB and potential MN electrodes are disposed among the electrode locations 1 to 4 according to the configurations α, β and γ (Fig. 6.1a), providing resistance measurements R_α, R_β and R_γ.

Beyond 1024 m spacing, collinear dipole-dipole arrays sited along the diagonals of the above square are used. The transmitting and receiving dipoles are collinear, of

FIGURE 6.1

(a) The configurations of the square array sounding.

(b) Extension of the square array sounding using dipole-dipole configurations.

In each case, the position of the sounding centre is denoted by +.

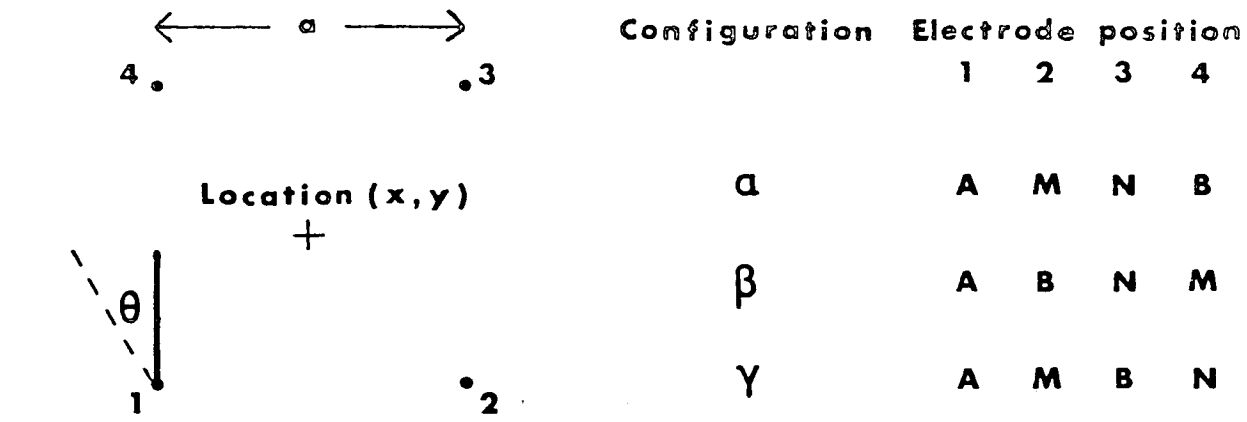
a
4
3
Location (x, y)
θ
1
2
Configuration
Electrode position
1 2 3 4
α A M N B
β A B N M
γ A M B N

[a]

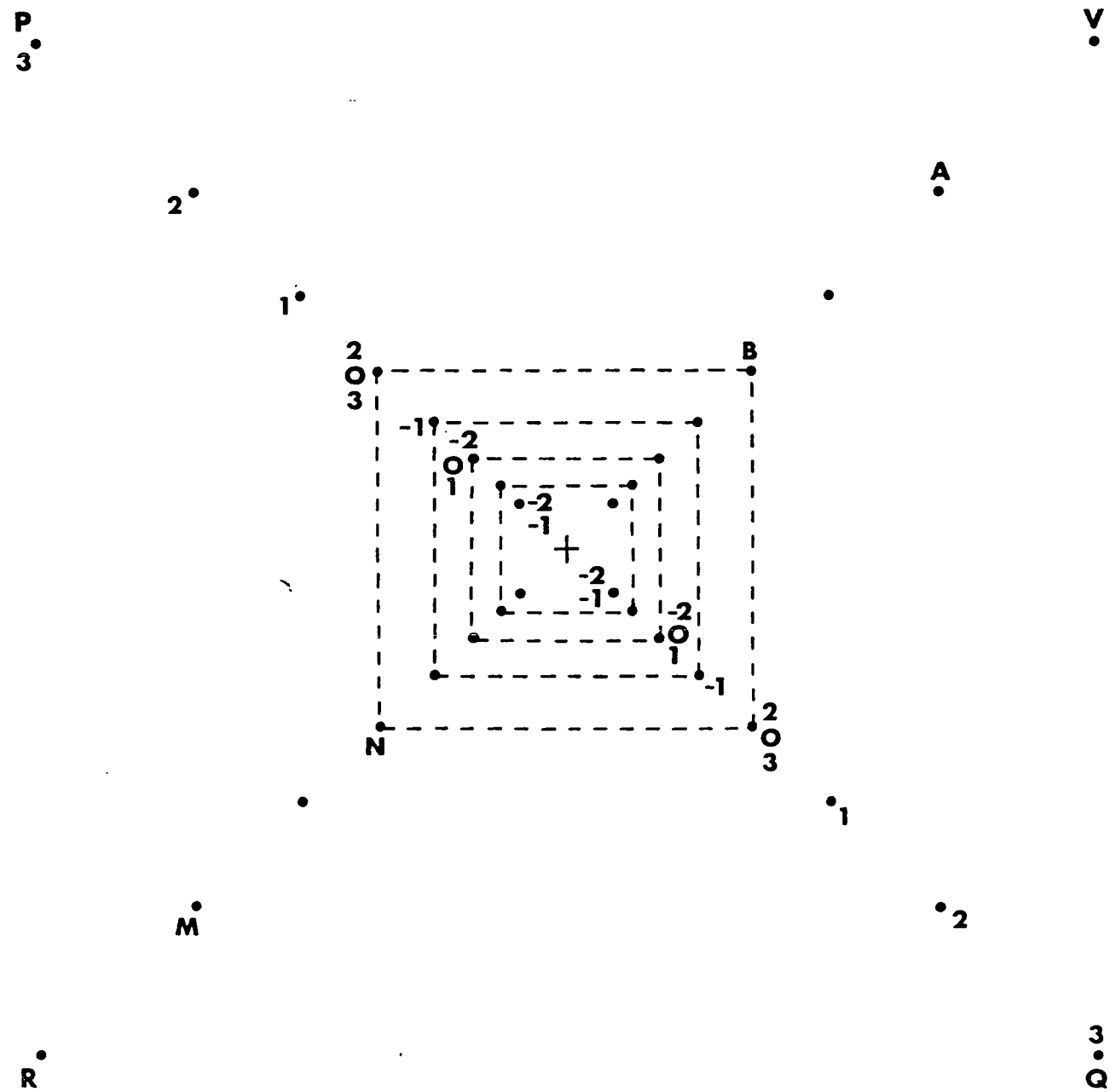
P
3
V
A
2
1
2
O
3
B
-1
-2
O
1
-2
-1
-2
-1
-2
O
1
-1
2
O
3
N
1
M
2
3
R
Q

[b]

equal length and symmetrical with respect to the sounding centre. Figure 6.1b illustrates this extension, where the dots show the electrode locations for successive dipoles. On the PQ diagonal, the dots are labelled by the dipole-dipole numbers -2, -1, 0, 1, etc. Each pair of identical numbers on either side of the sounding centre show current or potential electrode locations. The outer square corresponds to the maximum square array sounding. In order to minimize wire laying and sounding cost, only one dipole-dipole array configuration is used in practice as shown by the current AB and potential MN electrode locations for the dipole-dipole array 2 on the RV diagonal (Fig. 6.1b).

Roxis (1984) has indicated that somewhere between the last dipole positions used above, two equatorial dipole-dipole measurements are made to close the series of collinear dipole-dipole measurements. In one of these measurements, the transmitting and receiving dipoles are located on either side of and symmetrical with respect to the sounding centre and along a direction perpendicular to one of the diagonals of the square. The midpoints of these dipoles are collinear with the sounding centre. The second equatorial dipole-dipole measurement relates to the other diagonal of the square. Roxis (1984) has also indicated that the exact position and length of the equatorial dipoles are not critical, that these additional measurements increase the effective sounding depth and that all the different measurements can be transformed into a single set of square array apparent resistivities in

the case of a 1D earth. He has shown that this transformation is unstable if the equatorial dipole-dipole measurements are missing.

Denoting the measured earth resistance by R in either the square or dipole-dipole array configuration, the square side by a, the dipole lengths AB=MN by p and the dipole separation BN by q, the apparent resistivity for the square array and the collinear dipole-dipole configurations are respectively

$$\varrho_a = 2\pi aR/(2 - \sqrt{2}) \qquad (6.1)$$

$$\varrho_a = 2\pi GR \qquad (6.2)$$

where $G = [q^{-1} + (2p+q)^{-1} - 2(p+q)^{-1}]^{-1}$. The general expression for any four electrode configuration is

$$\varrho_a = 2\pi R/(AM^{-1} - AN^{-1} - BM^{-1} + BN^{-1}) \qquad (6.3)$$

where AB, MN denote respectively the transmitting and receiving electrode positions.

6.2 Comparison of HAB and AMT/MT results

For some years now, it has been the desire of both the Edinburgh and Leeds groups to carry out deep resistivity and AMT/MT measurements in the same area and hence compare the results and the techniques in detail. Hitherto, this has not been possible owing to financial constraints.

However, in 1980 Dr. Habberjam's group at Leeds carried out deep resistivity measurements in the Duns area using Habberjam's square and dipole-dipole array techniques referred to here as HAB for short. The latter was the impetus for the AMT/MT measurements in the Duns area which were made in 1982 and 1983 as part of the project reported here.

Figure 6.2 shows a map of the Duns area, with the geological formation. Also shown on the map are the AMT/MT sites with the different recorded data band combinations identified by appropriate symbols; the HAB measurements have been made along the diagonals of and within the square whose centre is near BED (Fig. 6.2). The square's diagonals 1 → 3, and 2 → 4 will be termed directions 1 and 2 respectively. It can be seen that 5 of the AMT/MT sites lie within the HAB square.

The HAB measurements were conducted using the square array from spacings of $\sqrt{2}$ m up to 3818 m, i.e., the square array was extended beyond the usual 1024 m maximum spacing. Owing to shortage of wire, the maximum spacing used was 3818 m instead of 4096 m required by the $\sqrt{2}$ incremental expansion sequence. Four dipole-dipole measurements were made along each of the directions 1 and 2 with the current transmitter at the north side in the former and east in the latter, i.e., β-configuration only.

The observed deep resistivity sounding data (resistivities and electrode spacings, a) listed in Roxis' thesis (1984) have been taken and plotted by the author. Figure 6.3A shows the apparent resistivity versus electrode spacing plots for

FIGURE 6.2

Map of the Duns area showing the geological formation, AMT/MT sites and the HAB square labelled 1234.

The cross-hatched segment on the inset shows the Duns area.

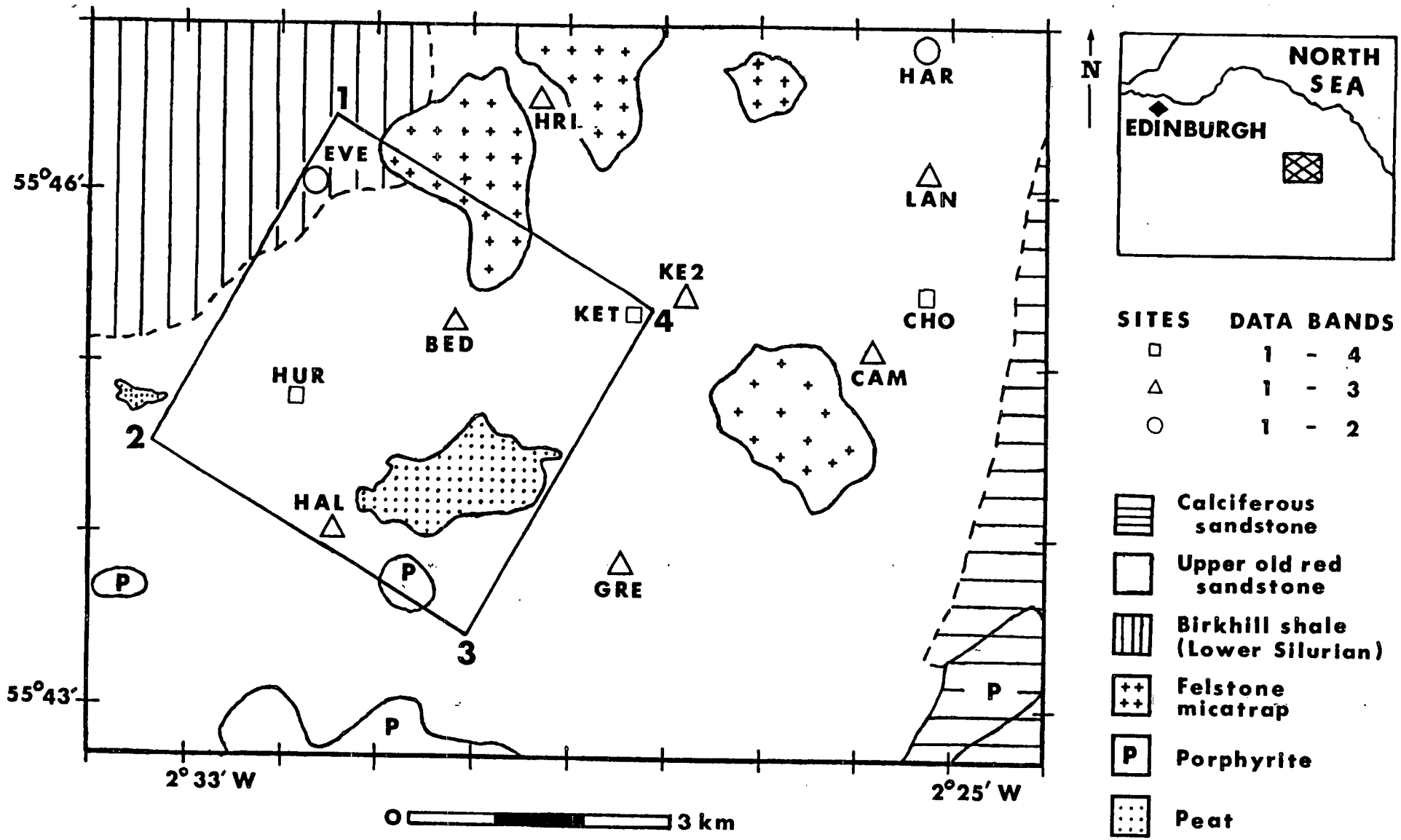
1
2
3
4
EVE
HRI
HAR
LAN
KE2
KET
CHO
BED
HUR
CAM
HAL
GRE
P
55°46′
55°43′
2°33′ W
2°25′ W
0
3 km
N
NORTH SEA
EDINBURGH
SITES
DATA BANDS
1 - 4
1 - 3
1 - 2
Calciferous sandstone
Upper old red sandstone
Birkhill shale (Lower Silurian)
Felstone micatrap
Porphyrite
Peat

FIGURE 6.3

(A) Plots of HAB observed resistivity data for the two orthogonal measuring directions 1 and 2.

(B) The plot of the linear mean HAB observed resistivity data.

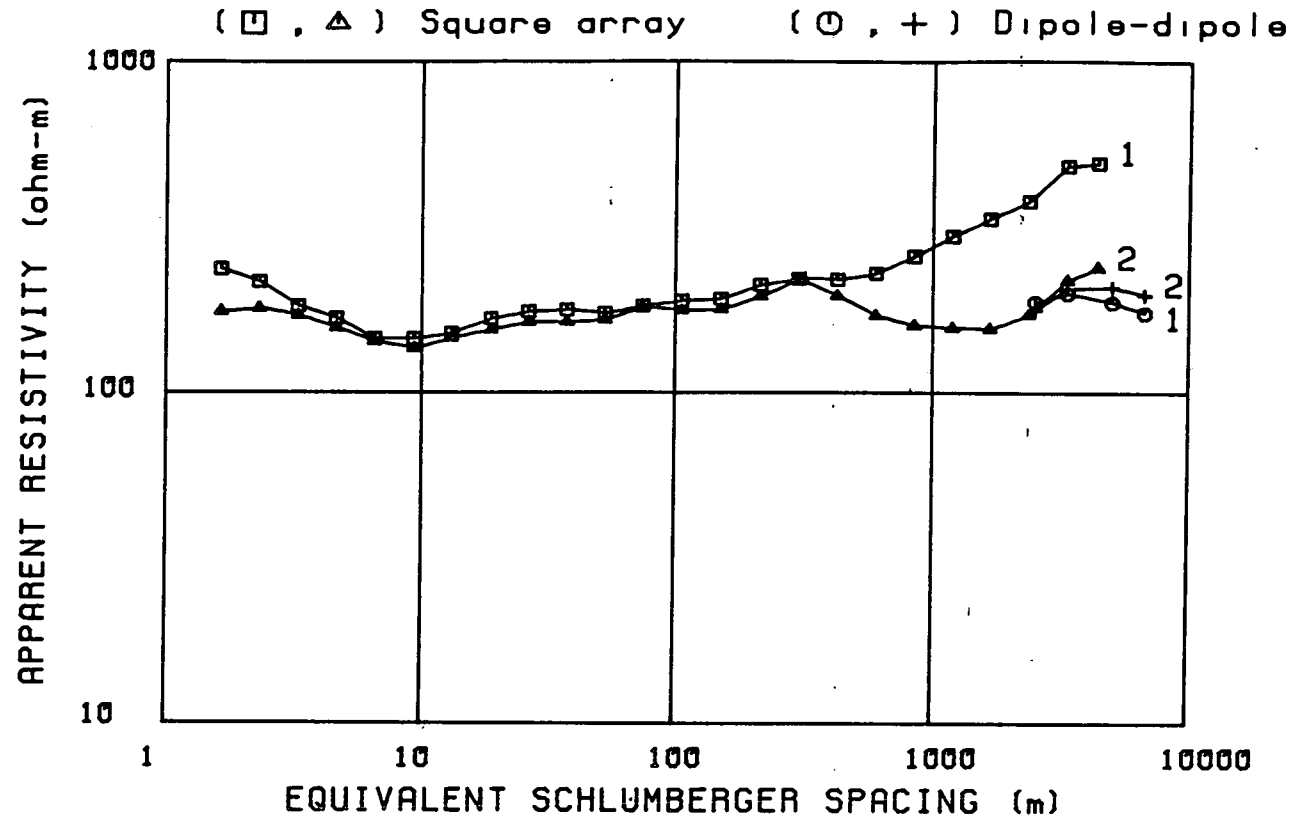
(□ , △) Square array
(○ , +) Dipole-dipole
1000
100
10
APPARENT RESISTIVITY (ohm-m)
1
10
100
1000
10000
EQUIVALENT SCHLUMBERGER SPACING (m)
1
2
2
1

[A]

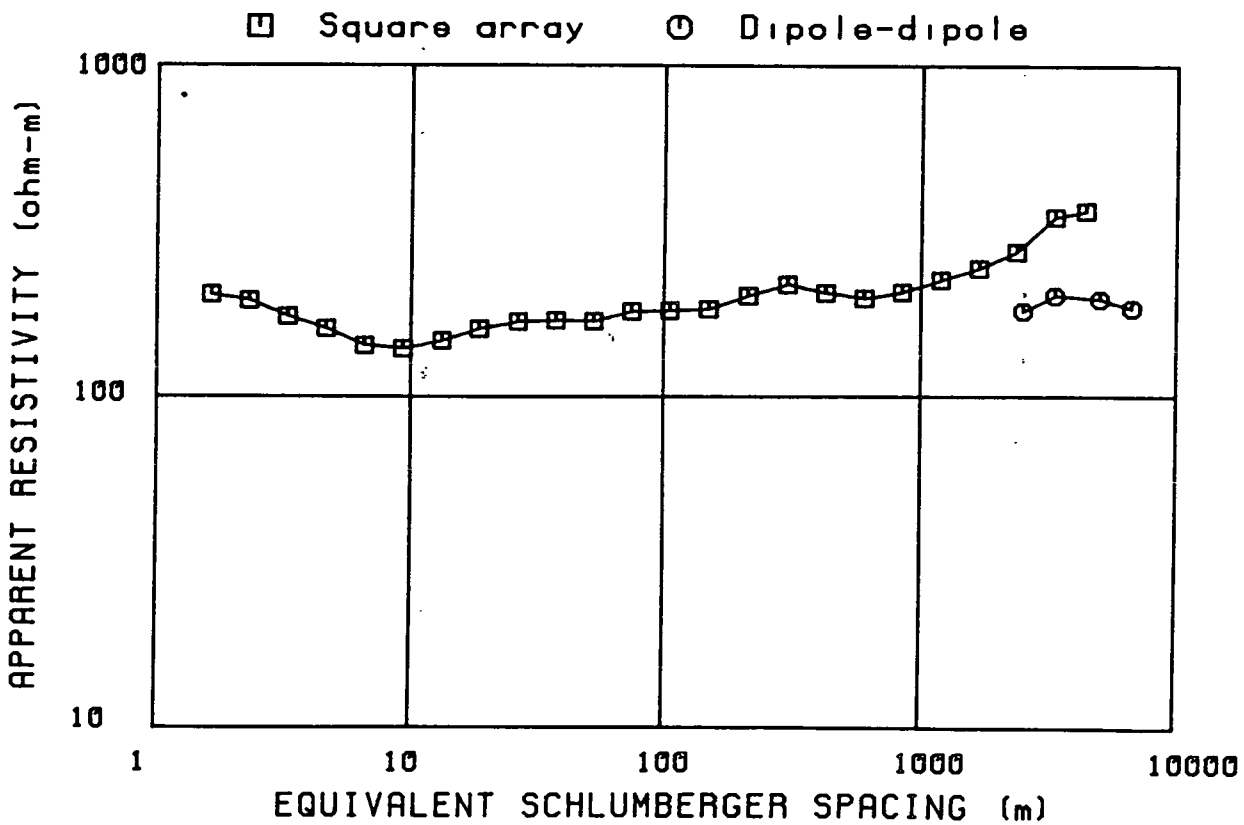
□ Square array
○ Dipole-dipole
1000
100
10
APPARENT RESISTIVITY (ohm-m)
1
10
100
1000
10000
EQUIVALENT SCHLUMBERGER SPACING (m)

[B]

the two measuring directions. The data have been converted to the Schlumberger values by replacing the square side spacings, a, by the equivalent Schlumberger spacings, 1.17a and adopting the square array resistivities as the Schlumberger resistivities in accordance with Habberjam and Thanassoulas (1979). It can be seen that at the large spacings, there is a considerable divergence between the square array data in the two orthogonal directions and also the dipole-dipole data are inconsistent with the square array data (Figs. 6.3A,B). This clearly indicates significant lateral variation. Hence, the fundamental assumption of the deep resistivity technique of a homogeneous 1D structure within a sounding area is clearly violated for Schlumberger spacings greater than 424 m (Fig. 6.3A). Figure 6.3B shows the plot of the linear mean of the observed data.

Tsokas (1980) has presented a series of layered earth models to fit the mean observed data. He has tried 11, 6 and 5 layered models of varying thickness (2-1000 m). Three of his models are shown in Fig. 6.4A. Roxis (1984) has remodelled the mean observed data omitting the dipole-dipole data and has presented a 5 layered model, also shown in Fig. 6.4A. The model data values at the various electrode spacings listed in the respective references have been taken and plotted on the mean observed square data by the author. It can be seen that Tsokas' and Roxis' models are quite similar; they indicate a series of moderately conducting layers (90-200 ohm-m) in the uppermost 1.2 km (approximately) overlying a resistive

FIGURE 6.4

(A) 1D models of the mean HAB resistivity data for the Duns area; the fit of the model curves to the mean observed HAB data is shown in the upper figure and the layered models [1 to 3, Tsokas (1980) and 4, Roxis (1984)] are shown at the bottom with the layer resistivities in ohm-m and depths in m.

(B) A 2D collation of the individual site 1D AMT/MT models for the Duns area; the positions of the sites (EVE, HRI, HUR, BED, HAL, KET, HAR, KE2, LAN, CHO, GRE and CAM) are shown at the top and the horizontal distance in km at the bottom.

There is a horizontal exaggeration of 2.

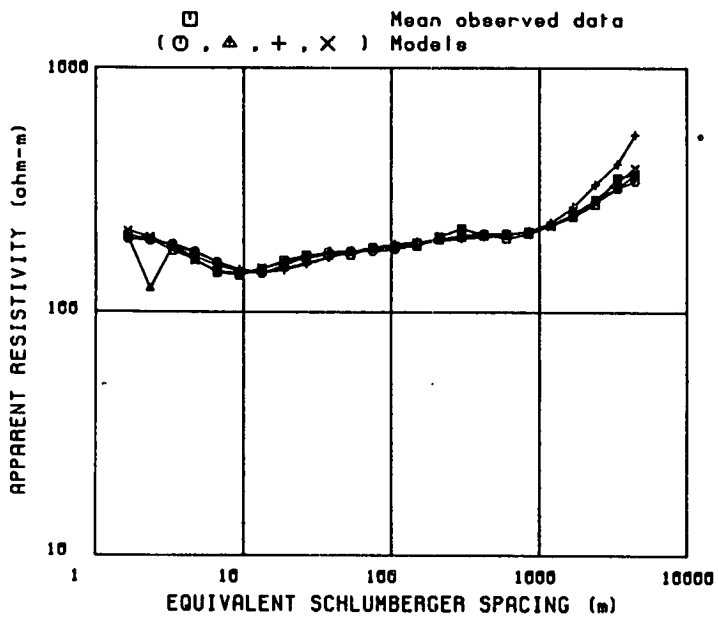
Mean obeerved data
(⊙ , ▲ , + , ×) Models
APPARENT RESISTIVITY (ohm-m)
1000
100
10
1
10
100
1000
10000
EQUIVALENT SCHLUMBERGER SPACING (m)
⊙ , ▲ , + Models 1-3 resp. --> Tsokas
× Model 4 --> Roxis

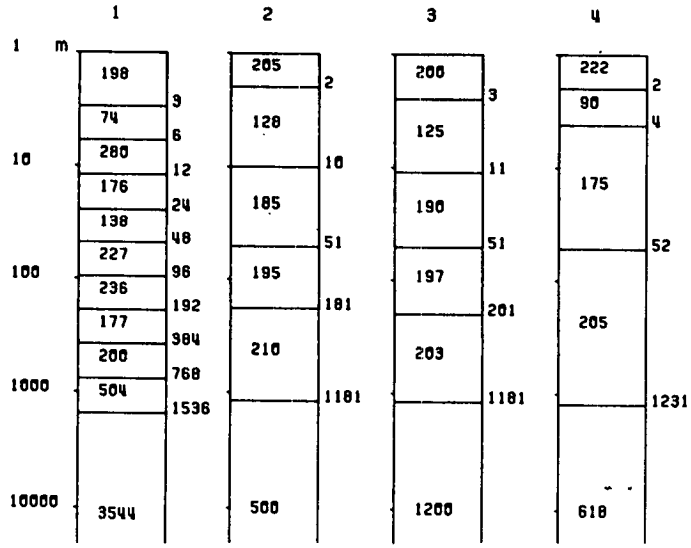
1
2
3
4
1 m
10
100
1000
10000
198
74
280
176
138
227
236
177
200
504
3544
9
6
12
24
48
96
192
384
768
1536
205
128
185
195
210
500
2
16
51
181
1181
200
125
190
197
203
1200
3
11
51
201
1181
222
90
175
205
618
2
4
52
1231

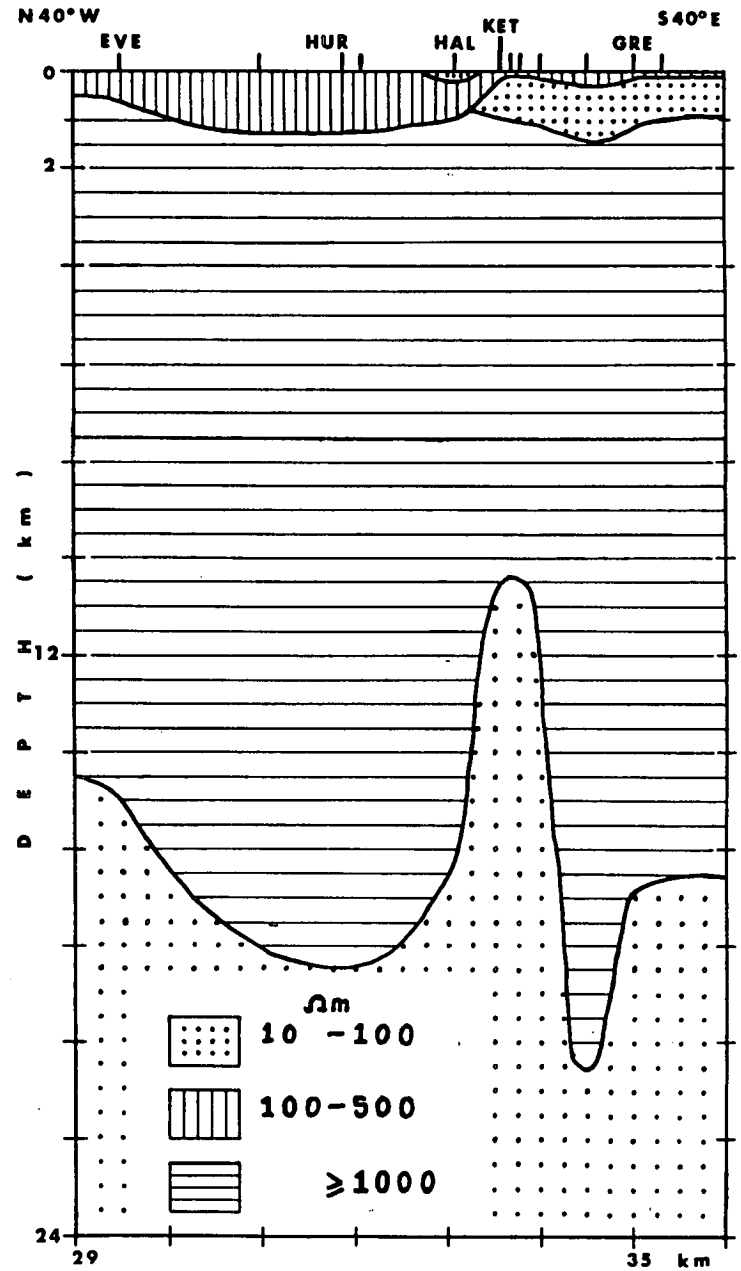
N40°W
S40°E
EVE
HUR
HAL
KET
GRE
0
2
12
24
D E P T H (k m)
Ωm
10 -100
100-500
≥1000
29
35 km

half-space (> 500 ohm-m).

Figures 5.2i,k-n show the 1D AMT/MT models for the five sites which lie within the HAB square (Fig. 6.2). For an easy visual overall picture of the AMT/MT result, it is better to see a collation of the individual 1D AMT/MT models for all the Duns sites in the form of a 2D section shown earlier in Fig. 5.3b and reproduced here in Fig. 6.4B. An anomalous conductivity region within the uppermost 1.5 km in the neighbourhood of KET can be clearly seen in Fig. 6.4B - KET is at the east corner of the HAB square.

It can be clearly observed that there is a general good agreement between the HAB and AMT/MT models within the depth range resolvable by HAB (≈1.2 km). AMT/MT evidently provides more information at depth than HAB and it also depicts more clearly the lateral variation in the electrical conductivity structure of the area. The anomalous conductivity zone delineated by the AMT/MT technique can account for the increasing anisotropy in the HAB data at the large spacings. At the large spacings and with the current transmitter at the east end, the current flow is concentrated around the anomalous zone.

6.3 Evaluation of HAB and AMT/MT techniques

Both techniques are evaluated in detail from the exploration viewpoint. AMT/MT uses a naturally occurring source which is free and needs no special maintenance, while HAB uses an artificial source which costs money and needs some maintenance and hence adds to the cost of any

survey. However, cost apart, an artificial source can sometimes be advantageous because data recording can be done at will, while AMT/MT data recording is impossible during geomagnetically quiet periods and hence leads to a vital loss of exploration crew time. Some assumptions are made about the nature of the natural source, while the nature of the artificial source is known. It may be noted that an artificial source inherently poses some danger to people, animals and the environment in the event of any mishap.

The logistics of AMT/MT are relatively simple, while those of HAB are quite complicated because of the extensive wire laying involved. HAB requires more than one day to determine the array centre, mark out on the ground the positions for the electrodes and lay the wires. At a field site, AMT/MT requires about one hour to set up the equipment. Hence, AMT/MT field operations and data acquisition are by far more rapid than HAB's. Consequently, it is very easy to go back to the same site(s) even after a year to repeat AMT/MT measurements as was done at some of the present project sites, while it is highly impracticable to do the same with HAB.

HAB requires 5 people working morning to evening for about 14 days (i.e., about 70 man-days) to survey an area about 5 km by 5 km. For the same area, AMT/MT measurements at 5 sites will be more than adequate; this will particularly be the case if the fundamental assumption of HAB of homogeneous earth is satisfied. Our AMT/MT equipment requires a maximum of 2 people to set up and

operate. For general exploration purposes and under very favourable field conditions, i.e., geomagnetically active periods and very low level of artificial noise, 1 day per site (i.e., a maximum of 10 man-days for the above 5 sites) will be sufficient to record enough AMT/MT data (bands 1 to 4). If the conditions are unfavourable, however, the number of man-days may double. It may be noted that if a similar sounding depth as HAB is desired, then only data bands 1 and 2 need be recorded and this implies less than 3 hours per site. Thus, AMT/MT requires far less man-days than HAB to survey a given area. The VLF/R and AMT/MT measurements (including repeat measurements, see table 4.1) carried out at 12 sites in the Duns area, extending far beyond the HAB square (Fig. 6.2) took 82 man-days. It might be noted that the total amount of data recorded was far in excess of that in a purely commercial exploration venture. Thus, AMT/MT can be more effectively used than HAB in a rapid low cost survey of a region to map conductivity features and hence locate anomalies.

For a given sounding area, HAB produces one sounding result usually expressed as a Schlumberger apparent resistivity curve, while at each site AMT/MT usually produces apparent resistivity- and phase-frequency curves. A visual observation of these AMT/MT sounding curves can easily reveal lateral resistivity variations in the sounding area.

Lateral inhomogeneity is a very significant drawback of the HAB technique. Lateral inhomogeneity is clearly the reason why HAB data often exhibit wide divergence and

discrepancy particularly at the large electrode spacings. However, it is easy to make several closely-spaced AMT/MT measurements and hence more precise information is possible in areas with a significant lateral inhomogeneity.

The depth of penetration in AMT/MT is much higher than that of HAB. Despite all the field efforts put into HAB measurements, subsurface resistivity information is obtained for less than 1.5 km depth. With less field effort, AMT/MT provides subsurface resistivity information for depths far in excess of 20 km. In AMT/MT, the depth of penetration is limited by the skin effect since the source is effectively at infinity, while in HAB the depth of penetration is constrained by the transmitter-receiver separation. To achieve a comparable AMT/MT depth of penetration, HAB will require a very powerful transmitter and an electrode spacing in excess of tens of kilometres. Such cable lengths are not easy to realize in a reconnaissance survey and are in any case very cumbersome to carry around.

From HAB models, it appears that HAB can resolve a subsurface layer that is only 2 m thick. Hence, HAB will give resistivity values for the very shallow near-surface features (100 m depth or less) with a higher precision than AMT/MT. However, this AMT/MT deficiency may be overcome by supplementing with VLF/R measurements. In areas where conductive contact for electric current is not easy, e.g., areas covered by sand dunes and sandy soils, ice-covered and arid areas, HAB may be inappropriate.

Contamination of AMT/MT data by cultural noise, particularly coherent artificial signals, may be a significant drawback of the technique. When such artificial signals are very strong or close to the measuring site, the desired natural signals may be completely swamped by noise and this makes the recording of good natural signals impossible. Under these circumstances of low natural signal level, HAB is clearly more appropriate.

To transport our AMT/MT equipment from one site to another requires the use of a Landrover, while HAB equipment is carried by people from one point to another within the survey area. Hence, under adverse topographic conditions and in very remote areas, where access by road is difficult, HAB will be more appropriate than AMT/MT.

With more people involved in HAB measurements and the fact that they are virtually milling all over the survey area (laying wire, carrying equipment, etc.), there is more likelihood of environmental damage than in the case of AMT/MT. It may be noted that any possible environmental damage caused by electrical method is by far less than that by seismics.

Since the level and sophistication of computer data processing and modelling are quite varied, it is not easy to compare the two techniques from this standpoint and hence no attempt has been made here to do so.

Thus, from all of the above, it can be easily seen that from the exploration viewpoint where cost- and exploration-effectiveness coupled with simple field logistics are highly desirable, AMT/MT has advantages over HAB.

CHAPTER 7

TWO-DIMENSIONAL NUMERICAL MODELLING

The computer programme for the modified finite difference method of Brewitt-Taylor and Weaver (1976) written by Brewitt-Taylor and Johns (1980) has been used in the numerical 2D modelling of the AMT/MT data carried out in the present study. The Duns sites have been projected on to the SUF profile to give a single traverse of 20 sites extending from N40^{0}W (geographic) to S40^{0}E through a distance of 35.3 km. The data at all the sites have been rotated to a fixed azimuth of N50^{0}E. The latter implies N57^{0}E (geomagnetic) assuming a magnetic declination of 7^{0}W of geographic north. Thus, the E-polarisation direction is parallel to the SUF and H-polarisation perpendicular to it. A brief description of the modelling programme is presented followed by a discussion of the modelling strategy adopted in this study. The result of the modelling is presented in the form of a 2D geoelectrical model for SE Scotland. The fit of the model curves to the observed E- and H-polarisation data at each site is also presented.

7.1 The numerical modelling programme

The modelling programme is based on the modified finite difference technique of computing numerical solutions to 2D induction problems by Brewitt-Taylor and Weaver (1976). The diakoptic computer programme for this technique has been written by Brewitt-Taylor and Johns (1980). The non-diakoptic option of this programme has been used in the 2D modelling carried out in the present study. The theoretical basis of the programme is outlined below.

A right-handed Cartesian coordinate system x, y, z with the +z-axis vertically downwards from the earth's surface is assumed. The unit vector along the x-axis is $\underline{x}$. For the 2D structure, an invariance with x is assumed. For the E-polarisation case ($\underline{E} = E\underline{x}$), equation (2.19a) reduces to

$$\partial^2 E/\partial y^2 + \partial^2 E/\partial z^2 = i\omega\mu_0\sigma E \qquad (7.1)$$

In the case of the H-polarisation ($\underline{H} = H\underline{x}$), equation (2.19b) becomes

$$\sigma(\partial^2 H/\partial y^2 + \partial^2 H/\partial z^2) = i\omega\mu_0\sigma^2 H + (\partial\sigma/\partial y)(\partial H/\partial y) + (\partial\sigma/\partial z)(\partial H/\partial z) \qquad (7.2)$$

Three boundary conditions are common to both E- and H-polarisation cases, viz,

(a) A basic assumption is made that σ is only a function of z as $|y| \rightarrow \infty$, i.e., at large horizontal distances, the induction problem becomes 1D.

(b) By virtue of (a), the total magnetic field above the earth is horizontal, uniform and independent of the subsurface conductivity distribution (e.g. Jones and Price, 1970). Hence, assuming the same inducing field everywhere, the magnetic field H tends to a constant value H_c as $|y| \rightarrow \infty$.

(c) At large depths, the fields are zero, i.e., $H \rightarrow 0$, $E \rightarrow 0$ as $z \rightarrow \infty$.

For the E-polarisation case, two additional boundary conditions are applicable, viz,

(i) Within the earth ($z>0$), the electric field E tends to $E^{\pm}$ and g ($=\mu_0 \omega \sigma$) tends to $g^{\pm}$ as $y \rightarrow \pm\infty$ so that from equation (7.1)

$$\partial^2 E^{\pm}/\partial z^2 = i g^{\pm} E^{\pm} \qquad (7.3)$$

subject to the conditions that $E^{\pm} \rightarrow 0$ as $z \rightarrow \infty$ and from equation (2.20a)

$$(\partial E^{\pm}/\partial z)_{z=0} = -i\omega\mu_0 H_c \qquad (7.4)$$

(ii) At large distances $(y^2+z^2)^{1/2}$ in the region $z<0$, the electric field approximately satisfies

$$E \approx E' - i\omega\mu_0 H_c z + (\Delta E/\pi)\arctan(y/|z|) \qquad (7.5)$$

where $E' = 0.5(E^{+}+E^{-})_{z=0}$ and $\Delta E = (E^{+}-E^{-})_{z=0}$

Apart from the boundary conditions (a) to (c), the additional boundary condition for the H-polarisation case is

that within the earth, $H \rightarrow H^{\pm}$ as $|y| \rightarrow \infty$ so that from equation (7.2)

$$p^{\pm}\partial^2 H^{\pm}/\partial z^2 = iH^{\pm} - (\partial p^{\pm}/\partial z)(\partial H^{\pm}/\partial z) \qquad (7.6)$$

subject to $(H^{\pm})_{z=0} = H_c$ with $p=1/g=1/(\mu_0 \omega \sigma)$

In addition to all the above boundary conditions, the tangential components of the fields ($\underline{E}$ and $\underline{H}$) as well as the normal component of $\underline{H}$ are continuous across conductivity boundaries.

The yz-plane is covered by a mesh of M y-grid vertical lines and N z-grid horizontal lines with the intersection of the grid lines forming the nodes. The 9^{th} z-grid line corresponds to the earth's surface with z=0, i.e., $z_q=0$ for q=9. The plane y=0 passes through the centre of the conductivity model. Thus, the left- and right-hand boundaries and the top and bottom boundaries are respectively $y=y_1$, $y=y_M$, $z=z_1$ and $z=z_N$. The bottom boundary is assumed to lie above a superconducting half-space. The variable node spacings are given by

$$h_m = y_{m+1} - y_m \quad \text{and} \quad k_n = z_{n+1} - z_n \qquad (7.7a)$$

where $1 \leqslant m \leqslant M-1$ and $1 \leqslant n \leqslant N-1$

The region z<0 is free space with $\sigma=0$, i.e.,

$$g_{m,n} = 0 \quad (1 \leqslant n \leqslant q) \qquad (7.7b)$$

Elsewhere, the conductivity values are specified at the

centres of the rectangular elements of the mesh so that $\sigma_{m+1/2,n+1/2}$ is the conductivity at the point $y=y_m+h_m/2$, $z=z_n+k_n/2$ $(1\leqslant m\leqslant M-1,\ q\leqslant n\leqslant N-1)$ and a smooth conductivity variation between the neighbouring values.

Using the central difference formulae, the finite difference representation of equation (7.3), i.e., E-polarisation, at the extreme left and right edges of the model (a,n) where a=1,M respectively is

$$\frac{E_{a,n+1}}{k_n(k_n+k_{n-1})} - \frac{E_{a,n}}{k_n k_{n-1}} + \frac{E_{a,n-1}}{k_{n-1}(k_n+k_{n-1})} = ig_{a,n}E_{a,n}/2 \qquad (7.8)$$

where $q \leqslant n \leqslant N-1$ and

$$g^{\pm} = g_{a,n} = (k_{n-1}g_{a,n-1/2} + k_n g_{a,n+1/2})/(k_n+k_{n-1}) \qquad (7.9)$$

The node (a,n) can be regarded as lying on a sharp boundary between the regions $z_{n-1}<z<z_n$ and $z_n<z<z_{n+1}$ of constant conductivity $\sigma_{a,n-1/2}$ and $\sigma_{a,n+1/2}$ respectively and it can be directly shown that the same finite difference equation (7.8) holds. This result is generalized to 2D E-polarisation case by weighting the conductivity in a similar way to equation (7.9) in both the y- and z-directions. Thus, at nodes (m,n),

$$g_{m,n} = \frac{U_{m,n} + U_{m,n-1} + U_{m-1,n} + U_{m-1,n-1}}{(h_m+h_{m-1})(k_n+k_{n-1})} \qquad (7.10)$$

where $U_{m,n} = h_m k_n g_{m+1/2,n+1/2}$,

$2 \leqslant m \leqslant M-1$ and $q \leqslant n \leqslant N-1$

A similar procedure starting with equation (7.6) leads to a generalized 2D H-polarisation result. Thus, at nodes (m,n)

$$p_{m,n} = \frac{R_{m,n} + R_{m,n-1} + R_{m-1,n} + R_{m-1,n-1}}{(h_m+h_{m-1})(k_n+k_{n-1})} \qquad (7.11)$$

where $R_{m,n} = h_m k_n p_{m+1/2,n+1/2}$,

$2 \leqslant m \leqslant M-1$, $q+1 \leqslant n \leqslant N-1$ and

$$(\partial p/\partial y)_{m,n} = 2\{(h_m+h_{m-1})(k_n+k_{n-1})\}^{-1} \{(R_{m,n}+R_{m,n-1})/h_m - (R_{m-1,n}+R_{m-1,n-1})/h_{m-1}\} \qquad (7.12)$$

$$(\partial p/\partial z)_{m,n} = 2\{(h_m+h_{m-1})(k_n+k_{n-1})\}^{-1} \{(R_{m,n}+R_{m-1,n})/k_n - (R_{m,n-1}+R_{m-1,n-1})/k_{n-1}\} \qquad (7.13)$$

Equations (7.12) and (7.13) simply express the slopes as the linear gradient between the appropriate weighted average values of p.

To solve the H-polarisation problems, it is essential to assign conductivities to the nodes (m,q) and (m,N) [$1 \leqslant m \leqslant M$], treating the surfaces of the earth and the superconductor as sharp boundaries with nodes on their inside faces adjoining the region $0<z<z_N$. It is also assumed that these assigned conductivity values do not vary with z from depths $k_q/2$ up to the earth's surface and $z_N - k_{N-1}/2$ down to the surface of the superconductor, i.e.,

$$(\partial\sigma/\partial z)_{m,q} = 0 = (\partial\sigma/\partial z)_{m,N} \qquad (7.14)$$

(a) E-polarisation finite difference equations

The boundary values at the edges of the grid mesh [$y=y_1$ and $y=y_M$, $0<z<z_N$] are obtained by solving numerically equation (7.8) subject to the boundary condition, equation (7.4), in finite difference form. At all the interior nodes of the mesh, the finite difference representation of equation (7.1) is

$$2k_n(h_m+h_{m-1})^{-1}\{E_{m+1,n} + E_{m-1,n}h_m/h_{m-1}\} + 2h_m(k_n+k_{n-1})^{-1}\{E_{m,n+1} + E_{m,n-1}k_n/k_{n-1}\} = [2k_n/h_{m-1} + 2h_m/k_{n-1} + ih_m k_n g_{m,n}]E_{m,n} \quad (7.15)$$

where $g_{m,n}$ is given by equations (7.7b) and (7.10); $2\leqslant m\leqslant M-1$ and $2\leqslant n\leqslant N-1$.

The magnetic field components can be obtained from E by making use of equation (2.20a). These are computed at points (m+1/2,n+1/2) where the conductivity values are specified, with $1\leqslant m\leqslant M-1$ and $1\leqslant n\leqslant N-1$. Thus,

$$(H_y)_{m+1/2,n+1/2} = (E_{m+1,n}+E_{m,n}-E_{m+1,n+1}-E_{m,n+1})/(2i\omega\mu_0 k_n) \quad (7.16)$$

$$(H_z)_{m+1/2,n+1/2} = (E_{m+1,n+1}+E_{m+1,n}-E_{m,n+1}-E_{m,n})/(2i\omega\mu_0 h_m) \quad (7.17)$$

At the earth's surface, H_z and H_y are given by

$$(H_z)_{m+1/2,q} = (E_{m+1,q} - E_{m,q})/(i\omega\mu_0 h_m) \quad (7.18)$$

$$(H_y)_{m,q} = ik_q k_{q-1}\{\omega\mu_0(k_q+k_{q-1})\}^{-1}\{E_{m,q+1}/k_q^2 - E_{m,q-1}/k_{q-1}^2 - [k_q^{-2}-k_{q-1}^{-2}+ig_{m,q+1/2}/2]E_{m,q}\} \quad (7.19)$$

where $1 \leqslant m \leqslant M-1$ and $q=9$.

(b) H-polarisation finite difference equation

At the earth's surface and everywhere above, H is a constant H_c. Thus, with $1 \leqslant m \leqslant M$

$$H_{m,q} = H_c \tag{7.20}$$

The finite difference representation of equation (7.2) at the interior nodes of the mesh within the earth ($2 \leqslant m \leqslant M-1$, $q+1 \leqslant n \leqslant N-1$) is

$$\begin{aligned} &H_{m+1,n}(p_{m,n}+\gamma_{m,n})\{h_m(h_m+h_{m-1})\}^{-1} + H_{m-1,n}(p_{m,n}+\delta_{m,n}) \\ &\{h_{m-1}(h_m+h_{m-1})\}^{-1} + H_{m,n+1}(p_{m,n}+\alpha_{m,n})\{k_n(k_n+k_{n-1})\}^{-1} \\ &+ H_{m,n-1}(p_{m,n}+\eta_{m,n})\{k_{n-1}(k_n+k_{n-1})\}^{-1} \\ &= H_{m,n}[(\gamma_{m,n}+\delta_{m,n})/(h_m h_{m-1}) + (\alpha_{m,n}+\eta_{m,n})/(k_n k_{n-1}) + i] \end{aligned} \tag{7.21}$$

where $\gamma_{m,n} = p_{m,n} + h_{m-1}(\partial p/\partial y)_{m,n}$,

$\delta_{m,n} = p_{m,n} - h_m(\partial p/\partial y)_{m,n}$,

$\alpha_{m,n} = p_{m,n} + k_{n-1}(\partial p/\partial z)_{m,n}$,

$\eta_{m,n} = p_{m,n} - k_n(\partial p/\partial z)_{m,n}$.

Although the normal component of the electric field varies rapidly but continuously in a smooth transition zone, it is however discontinuous at a plane boundary between two regions of different conductivity. Hence, a central difference formulation of the magnetic field derivatives in equation (2.20b) will yield a consistent sort of average electric field, but whose value is very sensitive to changes

in position. For this reason, the electric field is computed at points (m+1/2,n+1/2) away from possible sharp conductivity variations. Hence, from equation (2.20b)

$$(E_y)_{m+1/2,n+1/2} = \frac{H_{m+1,n+1}+H_{m,n+1}-H_{m+1,n}-H_{m,n}}{2k_n\sigma_{m+1/2,n+1/2}} \qquad (7.22)$$

$$(E_z)_{m+1/2,n+1/2} = \frac{H_{m,n+1}+H_{m,n}-H_{m+1,n+1}-H_{m+1,n}}{2h_m\sigma_{m+1/2,n+1/2}} \qquad (7.23)$$

with $1 \leqslant m \leqslant M-1$ and $1 \leqslant n \leqslant N-1$

On the earth's surface, the horizontal electric field is obtained by expanding H in a Taylor's series downwards from the points (m,q) and on substituting for $\partial H/\partial z$ from equation (2.20b) and $\partial^2 H/\partial z^2$ from equation (7.2) and after making use of equations (7.14) and (7.20), this gives

$$(E_y)_{m,q} = (k_q\sigma_{m,q})^{-1}(H_{m,q+1}-H_c) - i\omega\mu_0 k_q H_c/2 \qquad (7.24)$$

It may be noted that in the H-polarisation case, the z-grids above the earth's surface are redundant and hence if only this polarisation is of interest, then the upper boundary of the numerical grid can be placed at the earth's surface, i.e., q=1.

The computer modelling programme implemented the theory outlined above and the actual running of the programme consisted of detaching an "obey" file for both E- and H-polarisation cases at each of the desired frequencies. After running all the "obey" jobs for the frequencies, another "obey" file was run to compute the model curves

and plot these on the measured E- and H-polarisation apparent resistivity and phase data at each site. After making model parameter changes in the "obey" files, the whole process was repeated.

7.2 The numerical modelling strategy

A simplified 2D section resulting from a collation of the individual site 1D models was shown in two parts in Figs. 5.3a,b. The 2D section in Fig. 5.3a was used as the basis of a starting model for the 2D numerical modelling of the measured AMT/MT data. The structures under the extreme end sites (MUR and GRE) were uniformly extended several kilometres to the left and right respectively. It was desirable to minimize the computing time and cost. The latter depended on the numerical grid size as well as the number of frequencies for which the computer programmes were run. Hence, only 11 sites (all the SUF profile sites and three Duns sites) were considered initially and a y-grid size of 50 and z-grid size of 54 were used. E- and H-polarisation cases were also considered initially only at 6 frequencies (1000, 100, 10, 1, 0.1 and 0.01 Hz). The C.P.U. time for running both polarisations at one frequency with the above grid mesh size was 265 seconds.

The series of y- and z-grid planes with the x-axis as the strike direction divided the extended model area into elementary rectangular cuboids. The relative permittivity and permeability (=1 each) and the conductivity of the cuboids were specified. The plane z=0 (the ninth z-grid)

was the earth's surface and the z-grids spanned -400 to 300 km. The plane y=0 was along the SUF with the y-grids spanning -100 to 100 km. The grid spacings were uneven and more closely spaced near conductivity boundaries.

The model adjustment was first concentrated on the uppermost 1 km so that one or two horizontal boundaries were initially considered under each site and the boundaries and depths were subsequently increased downwards. In other words, the complexity of the model was gradually increased. This strategy is equivalent to fitting the AMT/MT E- and H-polarisation data from the high frequency end towards the long period end. Several different model parameter changes were made in a trial and error fashion. For each model, the finite difference modelling programme was run for both E- and H-polarisation cases for the above six frequencies. To facilitate an easy visual comparison of the model and measured data, a computer programme was written by the author to plot at each site on an A4-size sheet the E- and H-polarisation data (apparent resistivity and phase) side by side and the corresponding model response curves on top. After a visual observation of all the plots along the profile, the model parameters were altered and the whole process was repeated. After a reasonable degree of fit to the data was obtained, two additional frequencies (300 and 0.32 Hz) were added to the initial six. Once a satisfactory degree of fit (i.e., the model curves lay within a smooth envelope of the error bars of the field data) was obtained after trying several models, the remaining Duns sites were

included, the y- and z-grid sizes were increased to 67 and 65 respectively and three more frequencies (25, 3.85 and 0.04 Hz) were considered. The C.P.U. time for running both polarisations at each of the 11 frequencies and using this 67 by 65 grid mesh size was 930 seconds. The computer programmes were run several times for different models until a satisfactory fit to the E- and H-polarisation data at all the sites was obtained. The listing of the initial and final grids used in the modelling is shown in Table 7.1.

The relative magnitudes of the E- and H-polarisation apparent resistivities and the divergence between them as well as the varying shape of the phase curves were used as guides in effecting the model parameter changes. The remarkable feature of the H-polarisation apparent resistivity decreasing sharply as an interface is approached from the more conducting side was found very useful in changing both the lateral positions of interfaces as well as the resistivity contrast across them. For the uppermost 100 m of the subsurface, the qualitative inferences (Table 5.1b) from the VLF/R data were made use of.

Increasing the thickness of a near-surface conductor generally lowered the E- and H-polarisation apparent resistivity curves, but the latter was lowered more appreciably; the phase curves were raised. A similar effect resulted if the conductivity was increased. Conversely, decreasing the thickness or the conductivity raised the apparent resistivity curves and lowered the phase curves; the long period end of the phase curves were much less

TABLE 7.1

Initial and final grid sizes used in the 2D modelling

(a) Initial grid size used

Number of y-grids=50 and z-grids=54

Y-grid values in km

No.	Value	No.	Value	No.	Value	No.	Value	No.	Value
1	-100.00	11	-29.90	21	-3.90	31	5.70	41	23.00
2	-80.00	12	-25.00	22	-3.40	32	8.30	42	24.00
3	-60.00	13	-20.10	23	-2.90	33	10.90	43	25.00
4	-50.00	14	-18.10	24	-2.20	34	12.70	44	26.00
5	-45.00	15	-16.10	25	-1.50	35	14.50	45	30.00
6	-40.00	16	-13.50	26	-0.70	36	16.60	46	40.00
7	-37.00	17	-11.00	27	0.00	37	18.70	47	50.00
8	-35.00	18	-8.80	28	0.70	38	20.90	48	60.00
9	-33.90	19	-6.70	29	1.40	39	21.50	49	80.00
10	-31.90	20	-5.30	30	3.50	40	21.10	50	100.00

Z-grid values in km

1	-400.00	12	0.15	23	0.80	34	2.60	45	11.00
2	-300.00	13	0.20	24	1.00	35	2.80	46	12.00
3	-200.00	14	0.25	25	1.20	36	3.00	47	13.00
4	-100.00	15	0.30	26	1.40	37	3.20	48	15.00
5	-50.00	16	0.35	27	1.50	38	3.80	49	20.00
6	-25.00	17	0.40	28	1.60	39	4.50	50	30.00
7	-5.00	18	0.50	29	1.80	40	4.80	51	40.00
8	-1.00	19	0.55	30	2.00	41	5.00	52	50.00
9	0.00	20	0.60	31	2.20	42	5.20	53	100.00
10	0.05	21	0.65	32	2.40	43	8.00	54	200.00
11	0.10	22	0.70	33	2.50	44	10.00		

TABLE 7.1 (continued)

(b) Final grid size used

Number of y-grids=67 and z-grids=65

Y-grid values in km

No.	Value	No.	Value	No.	Value	No.	Value	No.	Value
1	-100.00	15	-16.10	29	1.40	43	21.10	57	24.00
2	-80.00	16	-13.50	30	3.50	44	21.60	58	24.20
3	-60.00	17	-11.00	31	5.70	45	22.10	59	24.30
4	-50.00	18	-8.80	32	8.30	46	22.30	60	25.00
5	-45.00	19	-6.70	33	10.90	47	22.60	61	26.00
6	-40.00	20	-5.30	34	12.70	48	22.65	62	30.00
7	-37.00	21	-3.90	35	14.50	49	22.70	63	40.00
8	-35.00	22	-3.40	36	16.60	50	22.75	64	50.00
9	-33.90	23	-2.90	37	18.50	51	22.80	65	60.00
10	-31.90	24	-2.20	38	19.30	52	22.90	66	80.00
11	-29.90	25	-1.50	39	20.00	53	23.00	67	100.00
12	-25.00	26	-0.70	40	20.50	54	23.20		
13	-20.10	27	0.00	41	20.90	55	23.50		
14	-18.10	28	0.70	42	21.00	56	23.70		

Z-grid values in km

1	-400.00	14	0.25	27	1.50	40	4.80	53	40.00
2	-300.00	15	0.30	28	1.60	41	5.00	54	45.00
3	-200.00	16	0.35	29	1.80	42	5.20	55	50.00
4	-100.00	17	0.40	30	2.00	43	8.00	56	60.00
5	-50.00	18	0.50	31	2.20	44	10.00	57	70.00
6	-25.00	19	0.55	32	2.40	45	12.00	58	80.00
7	-5.00	20	0.60	33	2.50	46	13.00	59	90.00
8	-1.00	21	0.65	34	2.60	47	15.00	60	100.00
9	0.00	22	0.70	35	2.80	48	18.00	61	120.00
10	0.05	23	0.80	36	3.00	49	20.00	62	150.00
11	0.10	24	1.00	37	3.20	50	25.00	63	180.00
12	0.15	25	1.20	38	3.80	51	30.00	64	200.00
13	0.20	26	1.40	39	4.50	52	35.00	65	300.00

affected than the short period end. On the other hand, if the conductor was deeper then the high frequency portion of the curves were unaffected. Increasing the thickness or resistivity of a surface resistor generally moved both apparent resistivity and phase curves up. The shape of the phase curves varied with both the layer resistivity contrasts and the layer thicknesses.

7.3 2D geoelectrical modelling results

Following the numerical 2D modelling procedure outlined above, the resulting final 2D geoelectrical model for the project area is shown in Fig. 7.1 using the y- and z-grid numbers along the horizontal and vertical axes respectively. The site locations are indicated by vertical bars at the top of the graph; the site names are listed in order in Table 4.1. The fault positions (DGF and SUF) are also shown on the graph. Boundaries with insignificant resistivity contrast across them are shown by dotted lines. The actual grid values (final) in km are shown in Table 7.1. The fit of the model curves to the observed E- and H-polarisation apparent resistivity and phase data at each of the sites is shown in Figs. 7.2a-j.

The features depicted by the 2D model are as follows:

(a) The uppermost 2 km of the subsurface under sites starting from WAN and northwards, i.e., mainly in the Midland Valley are more complex (more resistivity boundaries) than in the Southern Uplands. Thus, there is a significant lateral conductivity variation across the project

FIGURE 7.1

2D geoelectrical model in terms of grid scale - the grid values are listed in Table 7.1. The block resistivities are in ohm-m and the boundaries with insignificant resistivity contrast across them are indicated by dotted lines.

DGF and SUF are the Dunbar-Gifford and the Southern Uplands Faults respectively.

The site locations are indicated by vertical bars at the top of the graph - the site names are listed in order in Table 4.1; the site codes are respectively MUR, SPM, SAW, BUG, WAN, WLA, BER, SCR, EVE, HRI, HUR, BED, HAL, KET, HAR, KE2, LAN, CHO, GRE and CAM.

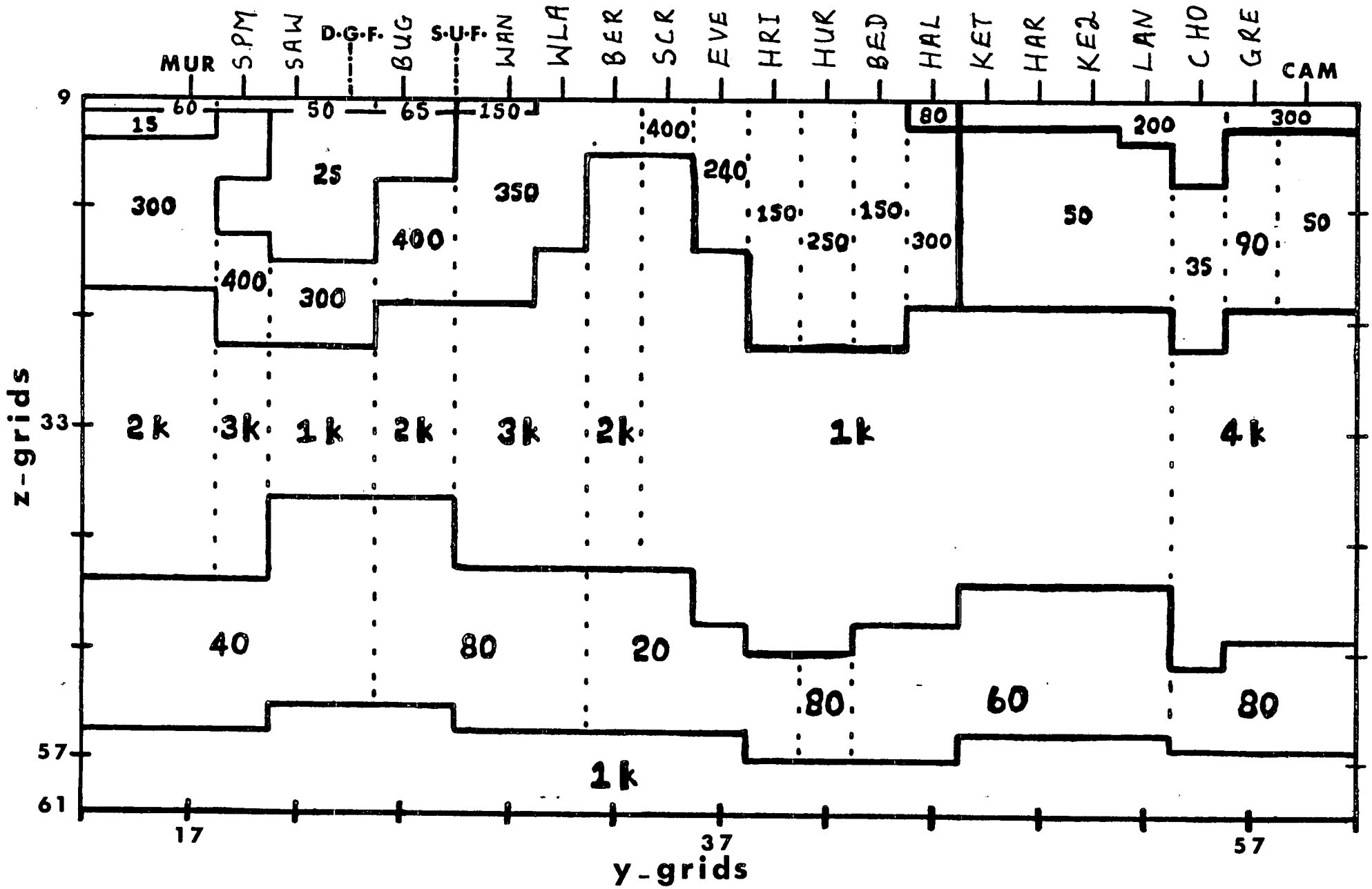
MUR
S.PM
SAW
D.G.F.
BUG
S.U.F.
WAN
WLA
BER
SCR
EVE
HRI
HUR
BED
HAL
KET
HAR
KE2
LAN
CHO
GRE
CAM
9
33
57
61
z-grids
17
37
57
y-grids
60
50
65
150
80
15
25
300
400
350
400
240
150
150
250
300
50
200
300
35
90
50
400
300
2k
3k
1k
2k
3k
2k
1k
4k
40
80
20
80
60
80
1k

area.

(b) The model indicates a 50 m thick layer 1 with resistivity <100 ohm-m under MUR to BUG and 150 ohm-m under WAN. This is compatible with the VLF/R data. At MUR, this layer is underlain by a good conductor (15 ohm-m) extending to a depth of 150 m and below this is a moderately conducting layer (300 ohm-m) extending to a depth of 800 m. At SPM, layer 1 is underlain by three layers; a moderately conducting layer (300 ohm-m) to a depth of 300 m, a good conductor (25 ohm-m) to a depth of 550 m and a moderately conducting layer (400 ohm-m) to a depth of 1.5 km. At SAW and BUG, layer 1 is underlain by two layers; a good conductor (25 ohm-m) to 650 and 300m depths respectively and a moderately conducting layer (400 ohm-m) to 1.5 and 1 km respectively. At WAN, layer 1 is underlain by a moderately conducting layer (350 ohm-m) to a depth of 1 km.

(c) Sites WLA and BER are moderately conducting (350 ohm-m) for the uppermost 600 and 200 m respectively. Sites SCR and EVE are moderately conducting (400 and 240 ohm-m) to depths of 200 and 600 m respectively. HRI, HUR and BED are all moderately conducting (150-250 ohm-m) from the surface to a depth of 1.5 km. From HAL to CAM, two layers exist in the uppermost 1 or 1.5 km. At HAL, there is a 100 m upper layer with resistivity < 100 ohm-m overlying a moderately conducting layer (300 ohm-m) which extends to a depth of 1 km. From KET to CAM a moderately conducting layer (200-300 ohm-m) of thickness 100-300 m overlies a good conductor (< 100 ohm-m) whose

FIGURE 7.2A-J

2D model curve fit to the observed E- and H-polarisation data at the individual sites.

N.B.

SITES	PAGE	SITES	PAGE
MUR, SPM	220	HUR, BED	225
SAW, BUG	221	HAL, KET	226
WAN, WLA	222	HAR, KE2	227
BER, SCR	223	LAN, CHO	228
EVE, HRI	224	GRE, CAM	229

Fig. 7.2a

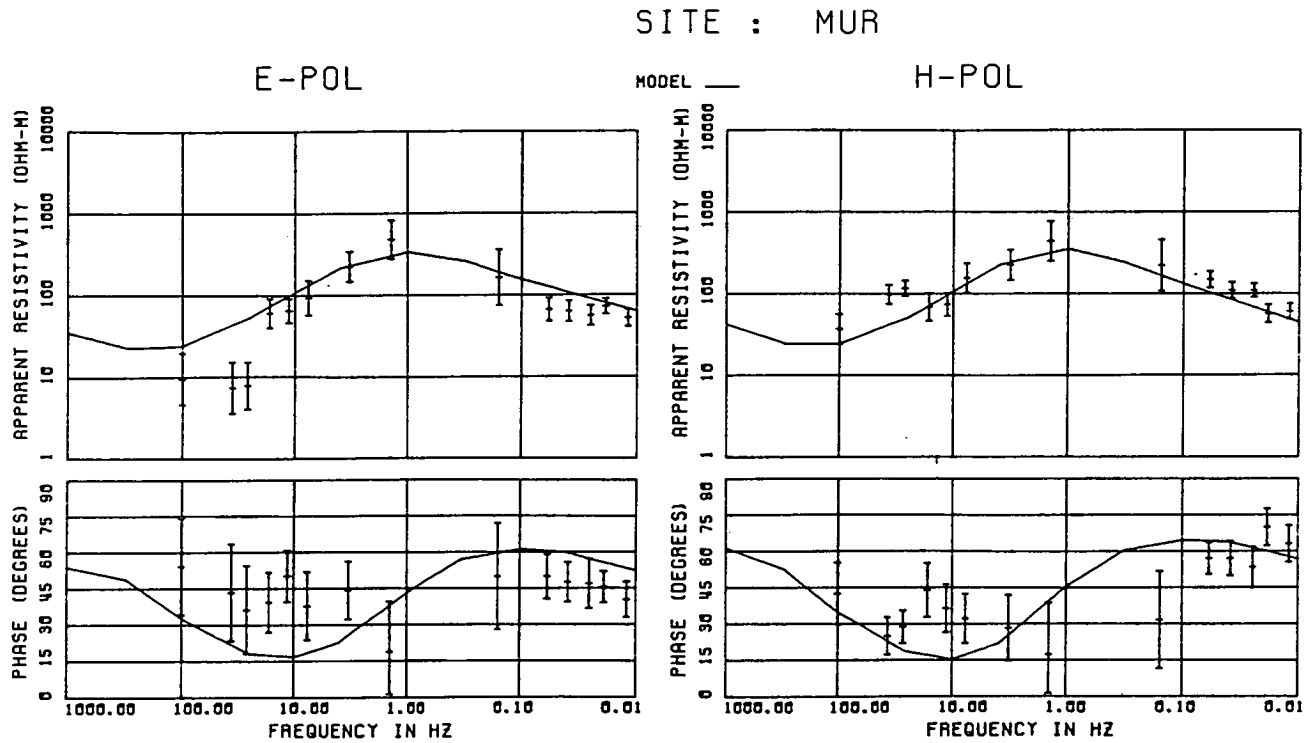
SITE : MUR
E-POL
MODEL
H-POL
APPARENT RESISTIVITY (OHM-M)
1
10
100
1000
10000
PHASE (DEGREES)
0 15 30 45 60 75 90
1000.00 100.00 10.00 1.00 0.10 0.01
FREQUENCY IN HZ

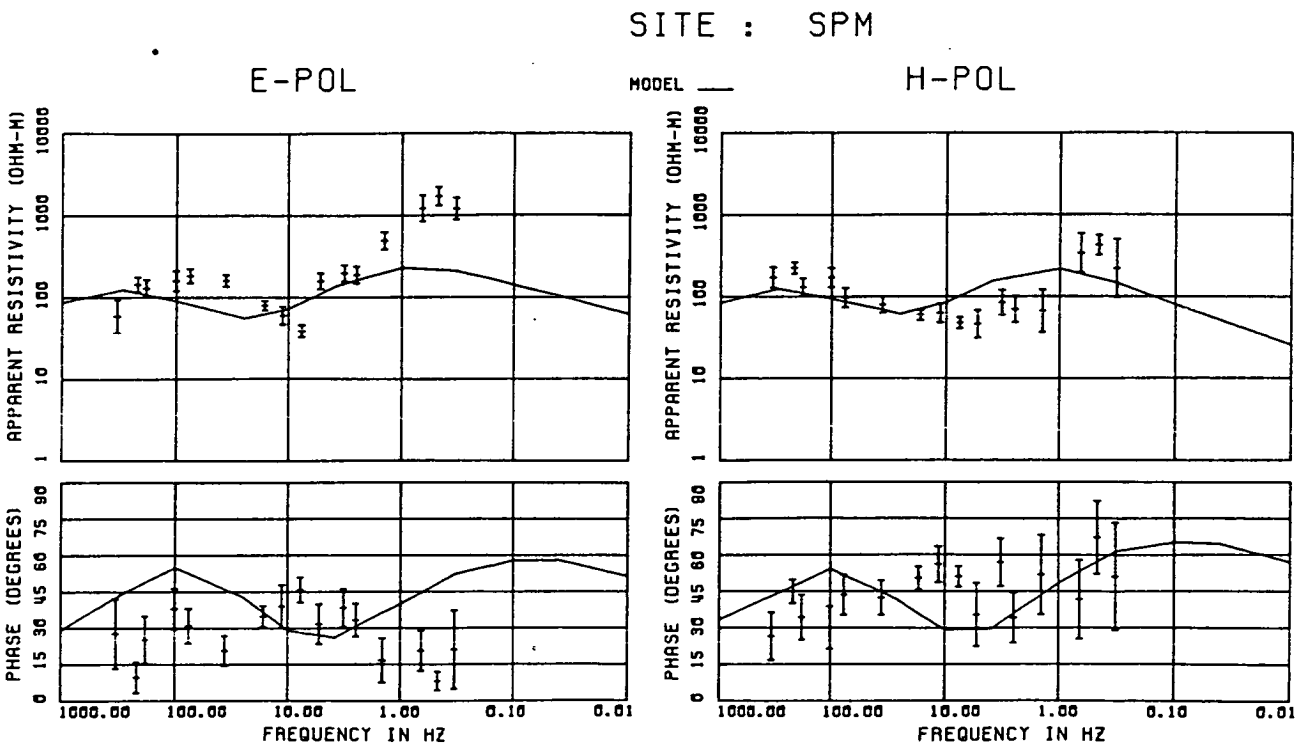
SITE : SPM
E-POL
MODEL
H-POL
APPARENT RESISTIVITY (OHM-M)
1
10
100
1000
10000
PHASE (DEGREES)
0 15 30 45 60 75 90
1000.00 100.00 10.00 1.00 0.10 0.01
FREQUENCY IN HZ

Fig. 7.2b

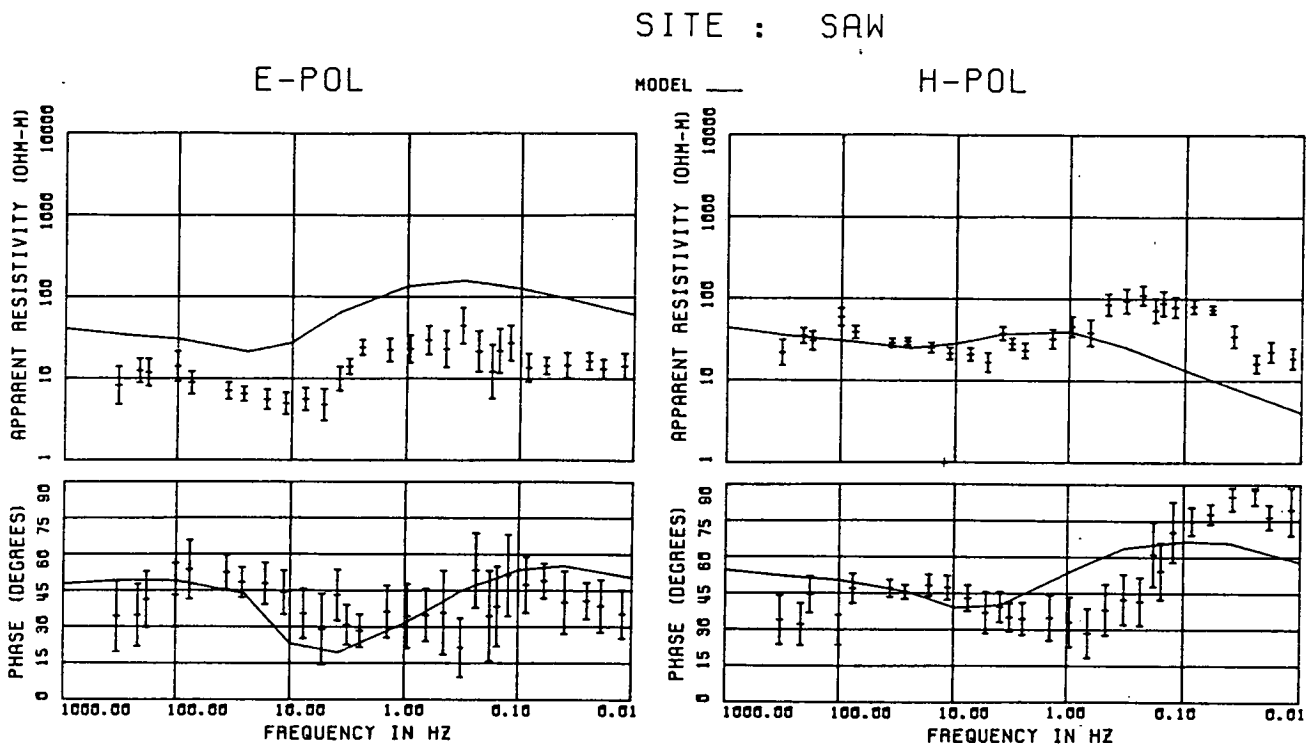
SITE : SAW
E-POL
MODEL
H-POL
APPARENT RESISTIVITY (OHM-M)
1
10
100
1000
10000
PHASE (DEGREES)
0
15
30
45
60
75
90
1000.00
100.00
10.00
1.00
0.10
0.01
FREQUENCY IN HZ

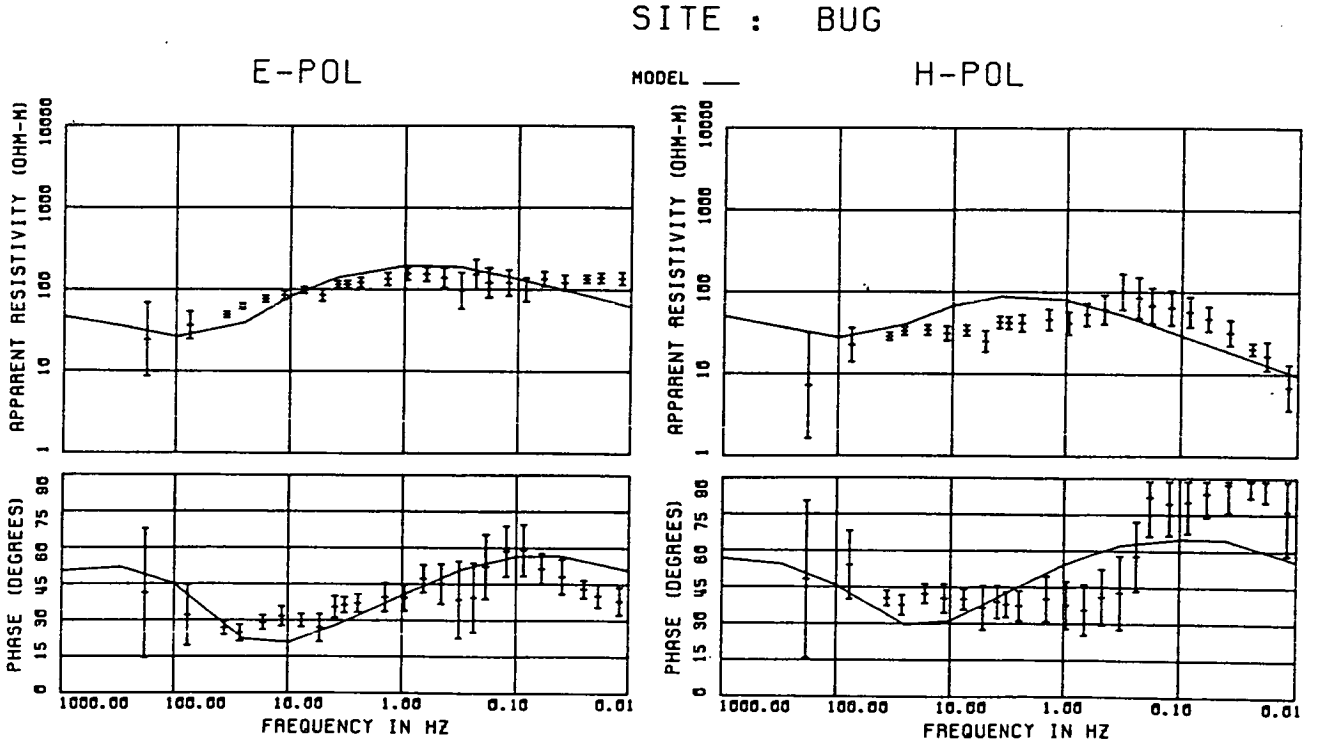
SITE : BUG
E-POL
MODEL
H-POL
APPARENT RESISTIVITY (OHM-M)
1
10
100
1000
10000
PHASE (DEGREES)
0
15
30
45
60
75
90
1000.00
100.00
10.00
1.00
0.10
0.01
FREQUENCY IN HZ

Fig. 7.2c

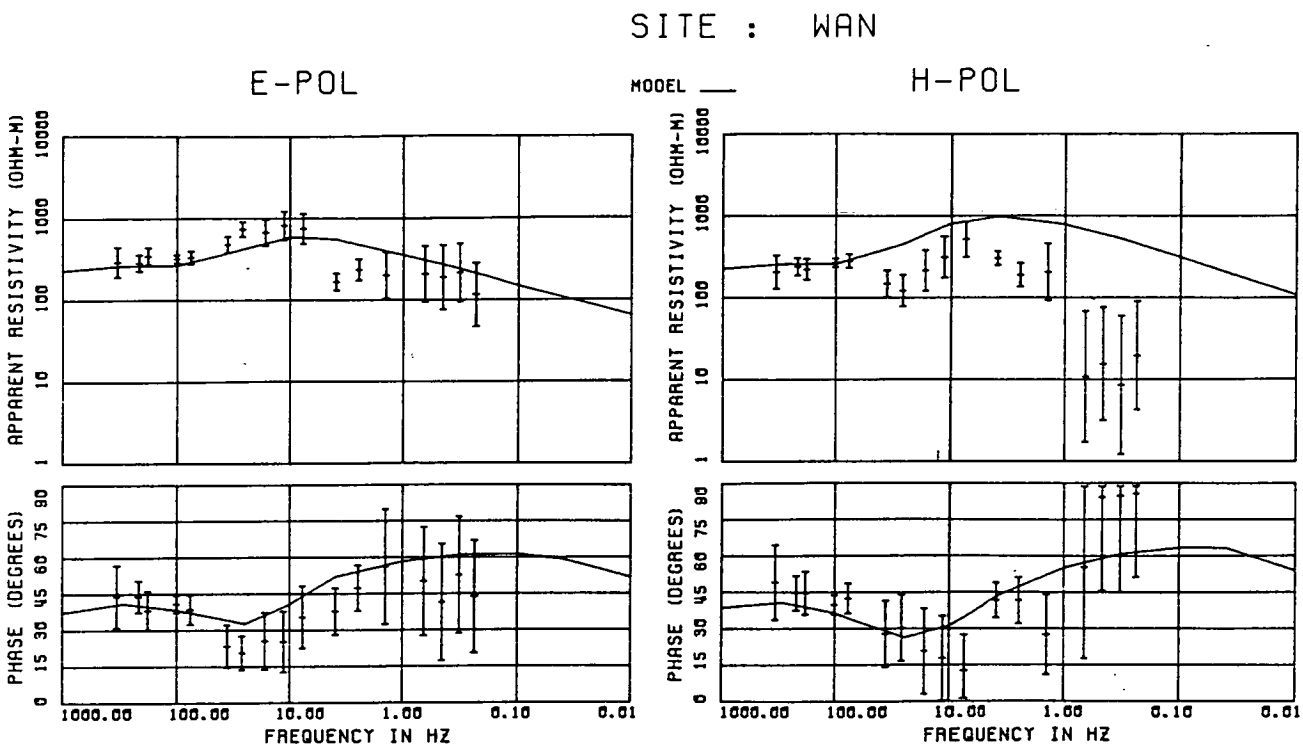
SITE : WAN
E-POL
MODEL
H-POL
APPARENT RESISTIVITY (OHM-M)
1
10
100
1000
10000
PHASE (DEGREES)
0 15 30 45 60 75 90
1000.00 100.00 10.00 1.00 0.10 0.01
FREQUENCY IN HZ

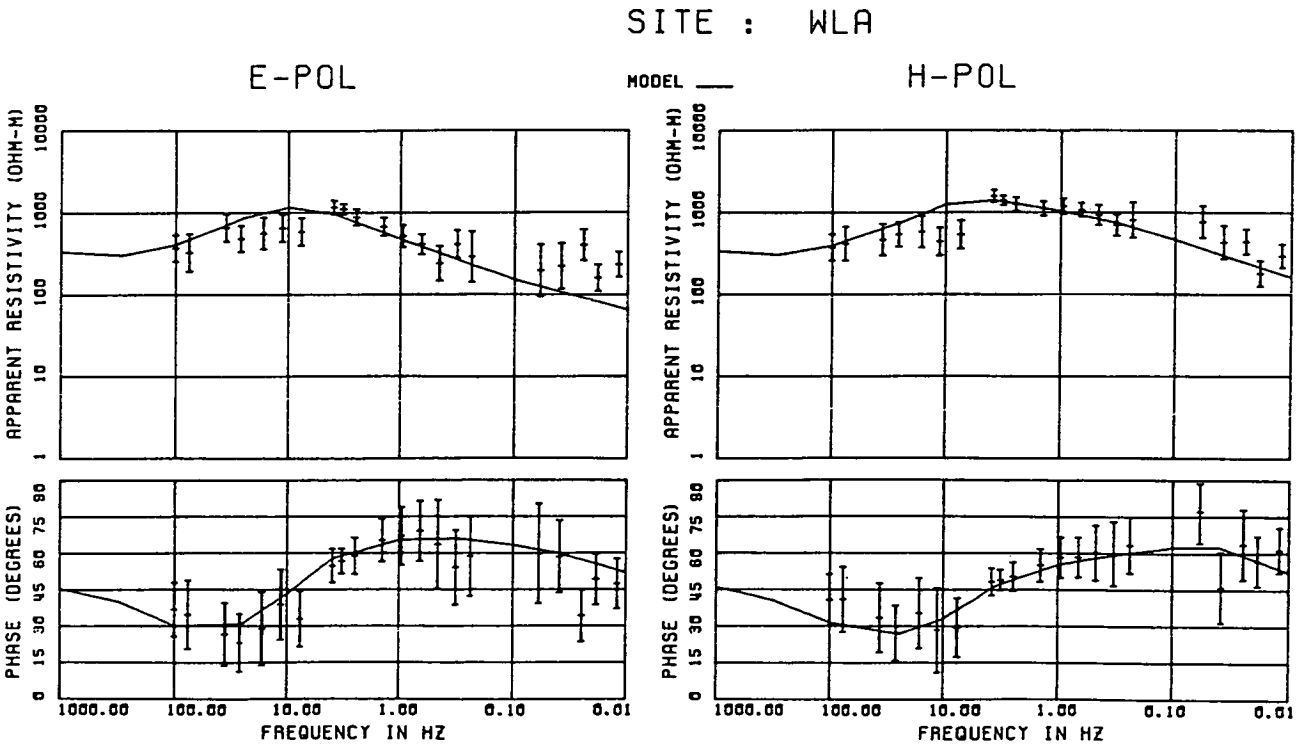
SITE : WLA
E-POL
MODEL
H-POL
APPARENT RESISTIVITY (OHM-M)
1
10
100
1000
10000
PHASE (DEGREES)
0 15 30 45 60 75 90
1000.00 100.00 10.00 1.00 0.10 0.01
FREQUENCY IN HZ

Fig. 7.2d

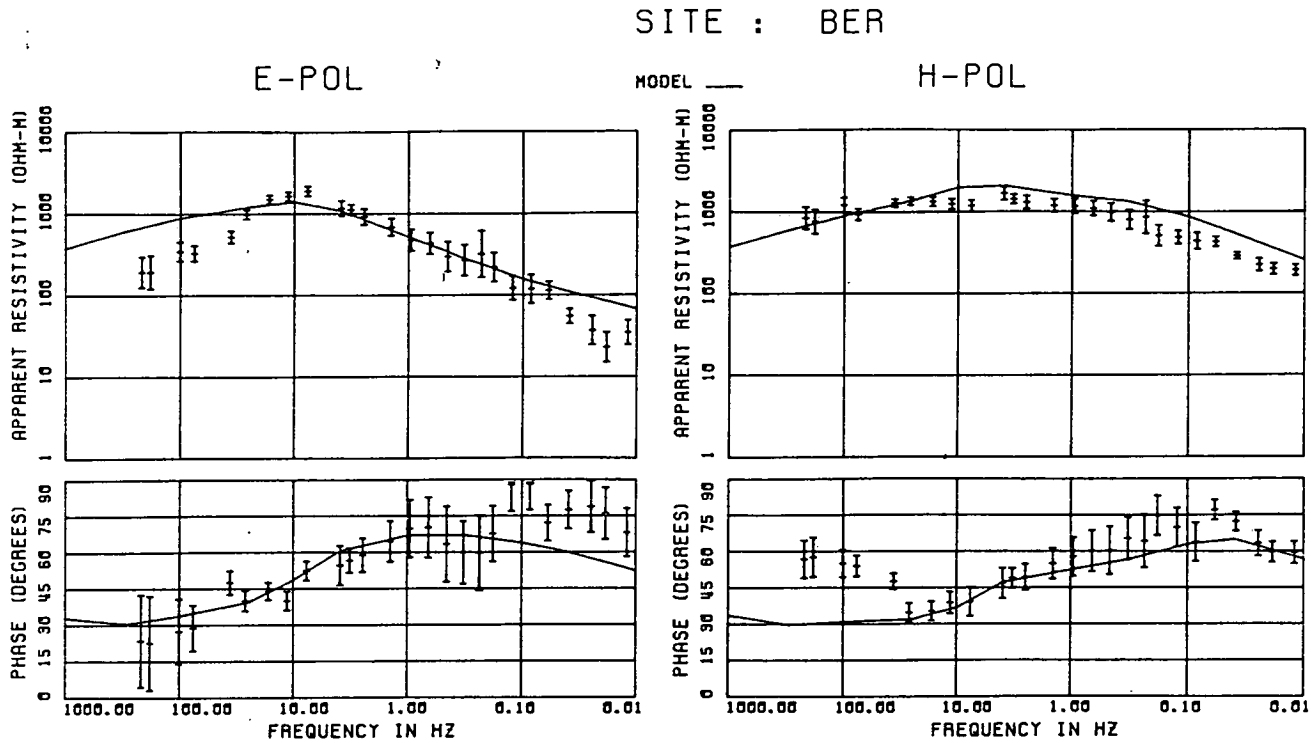
SITE : BER
E-POL
MODEL
H-POL
APPARENT RESISTIVITY (OHM-M)
PHASE (DEGREES)
FREQUENCY IN HZ

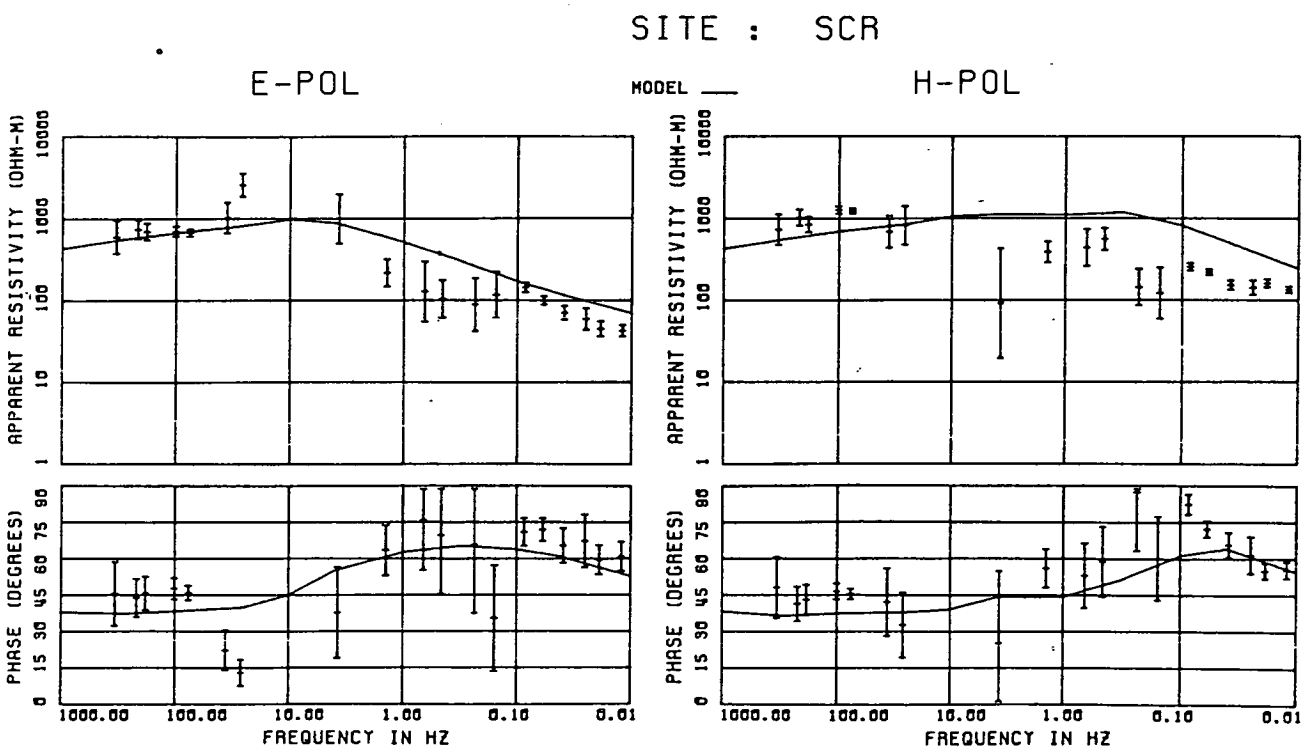
SITE : SCR
E-POL
MODEL
H-POL
APPARENT RESISTIVITY (OHM-M)
PHASE (DEGREES)
FREQUENCY IN HZ

Fig. 7.2e

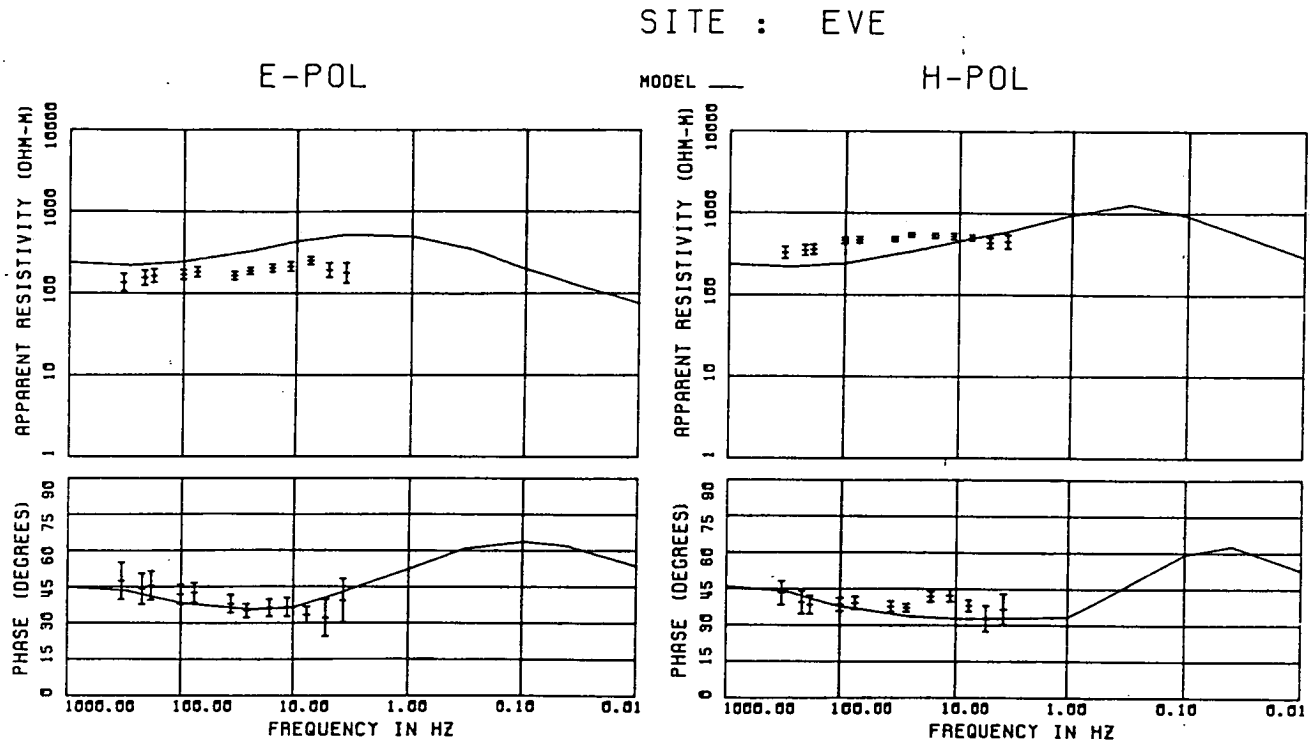
SITE : EVE
E-POL
MODEL
H-POL
APPARENT RESISTIVITY (OHM-M)
1
10
100
1000
10000
PHASE (DEGREES)
0 15 30 45 60 75 90
1000.00 100.00 10.00 1.00 0.10 0.01
FREQUENCY IN HZ

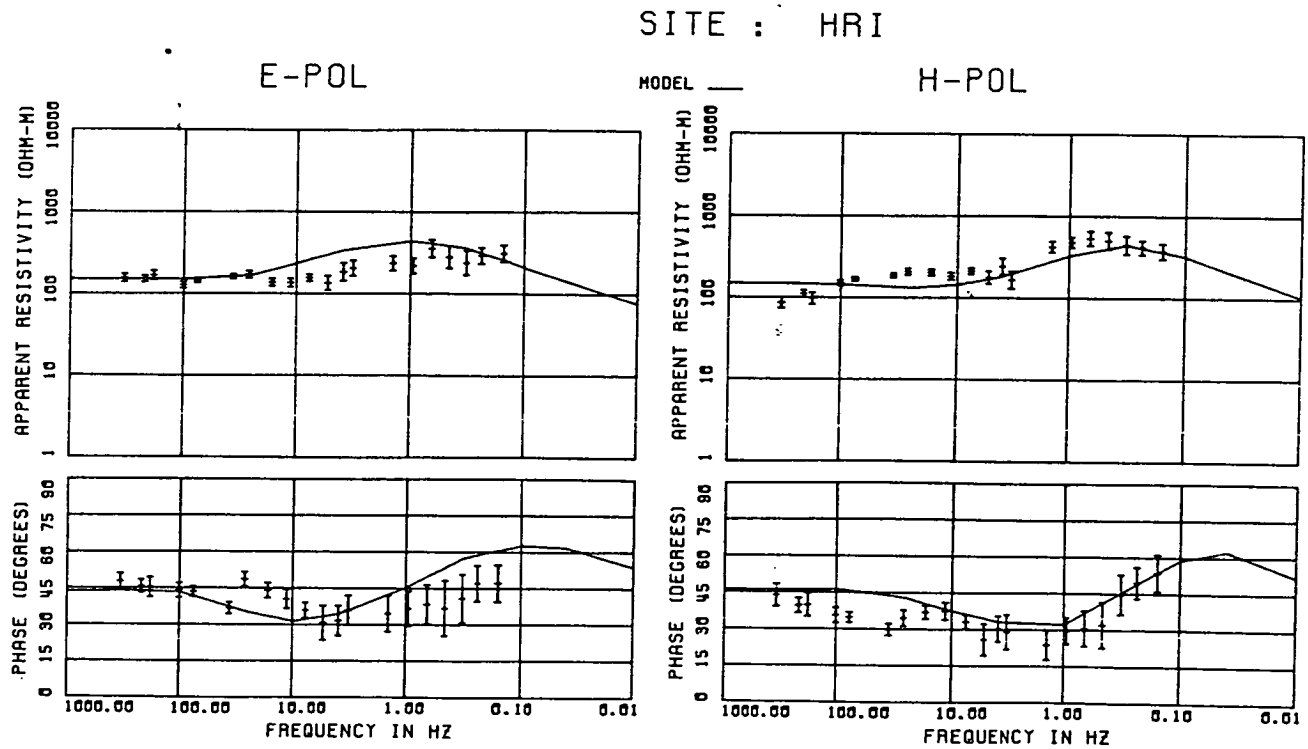
SITE : HRI
E-POL
MODEL
H-POL
APPARENT RESISTIVITY (OHM-M)
1
10
100
1000
10000
PHASE (DEGREES)
0 15 30 45 60 75 90
1000.00 100.00 10.00 1.00 0.10 0.01
FREQUENCY IN HZ

Fig. 7.2f

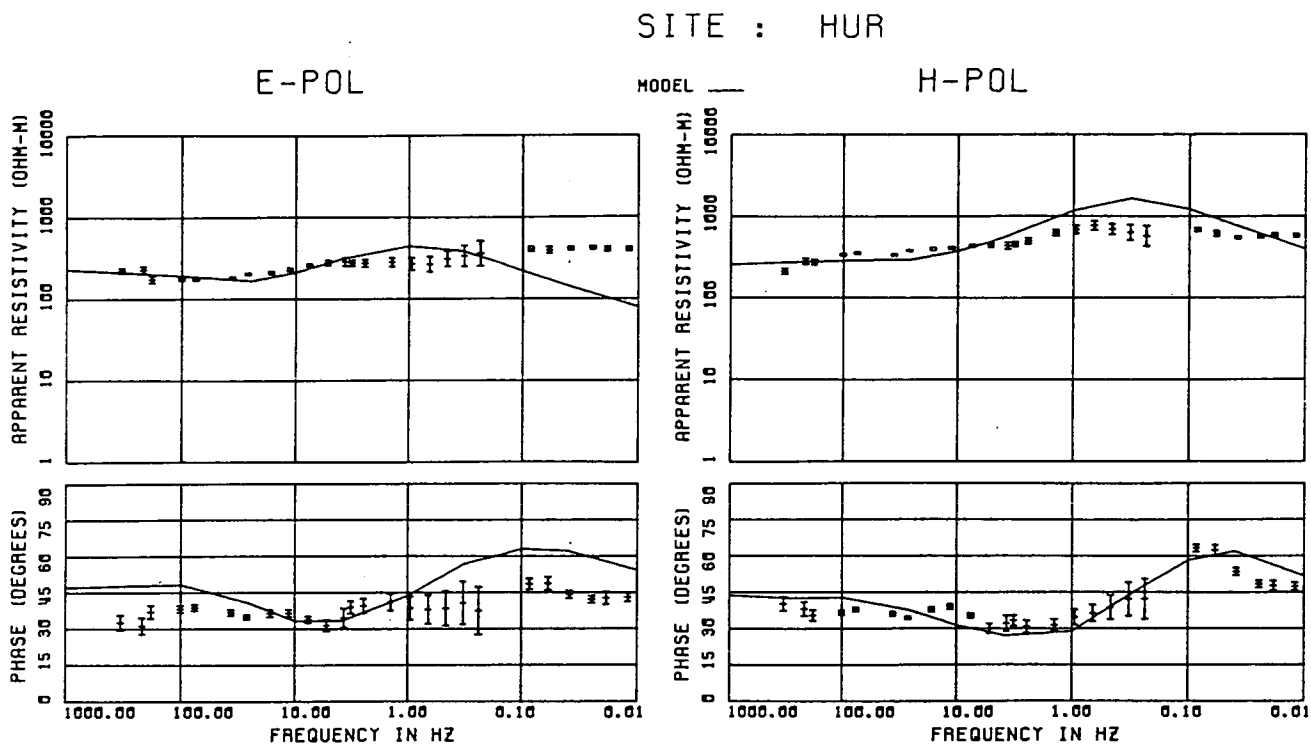
SITE : HUR
E-POL
MODEL
H-POL
APPARENT RESISTIVITY (OHM-M)
PHASE (DEGREES)
FREQUENCY IN HZ

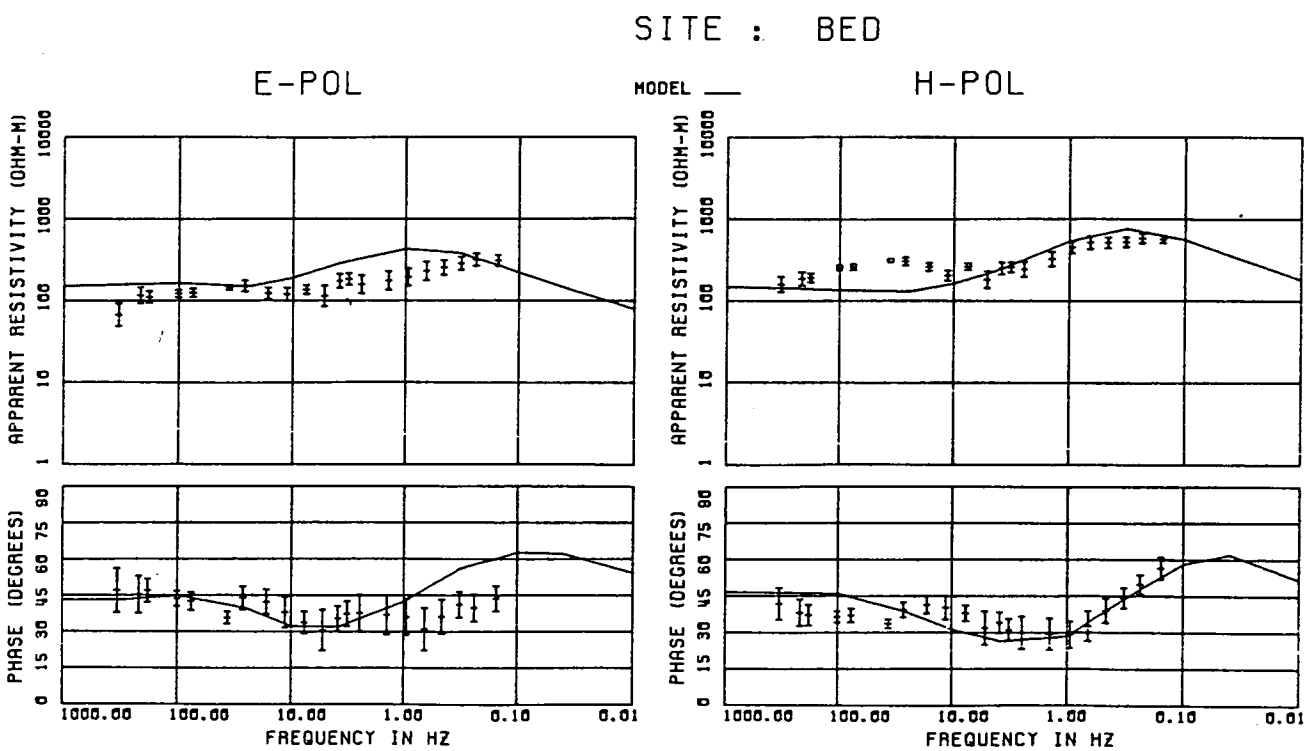
SITE : BED
E-POL
MODEL
H-POL
APPARENT RESISTIVITY (OHM-M)
PHASE (DEGREES)
FREQUENCY IN HZ

Fig. 7.2g

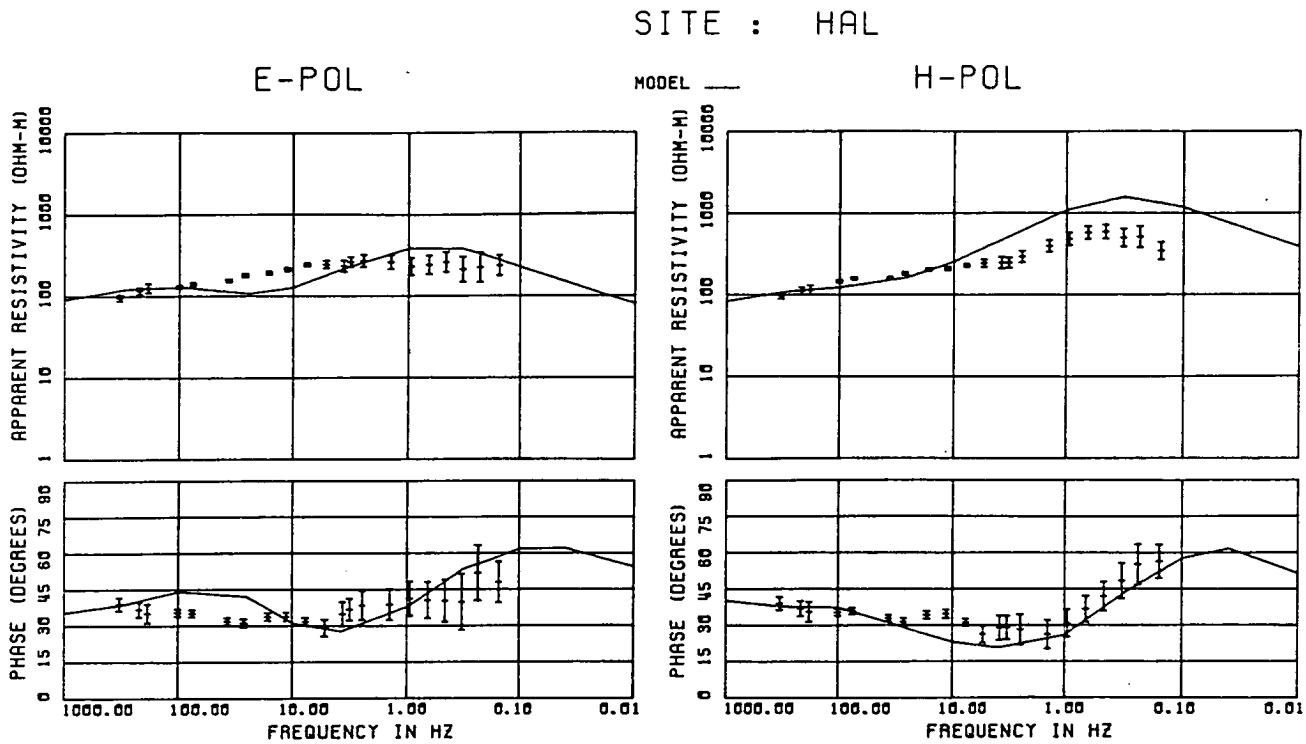
SITE : HAL
E-POL
MODEL
H-POL
APPARENT RESISTIVITY (OHM-M)
1
10
100
1000
10000
PHASE (DEGREES)
0 15 30 45 60 75 90
1000.00 100.00 10.00 1.00 0.10 0.01
FREQUENCY IN HZ

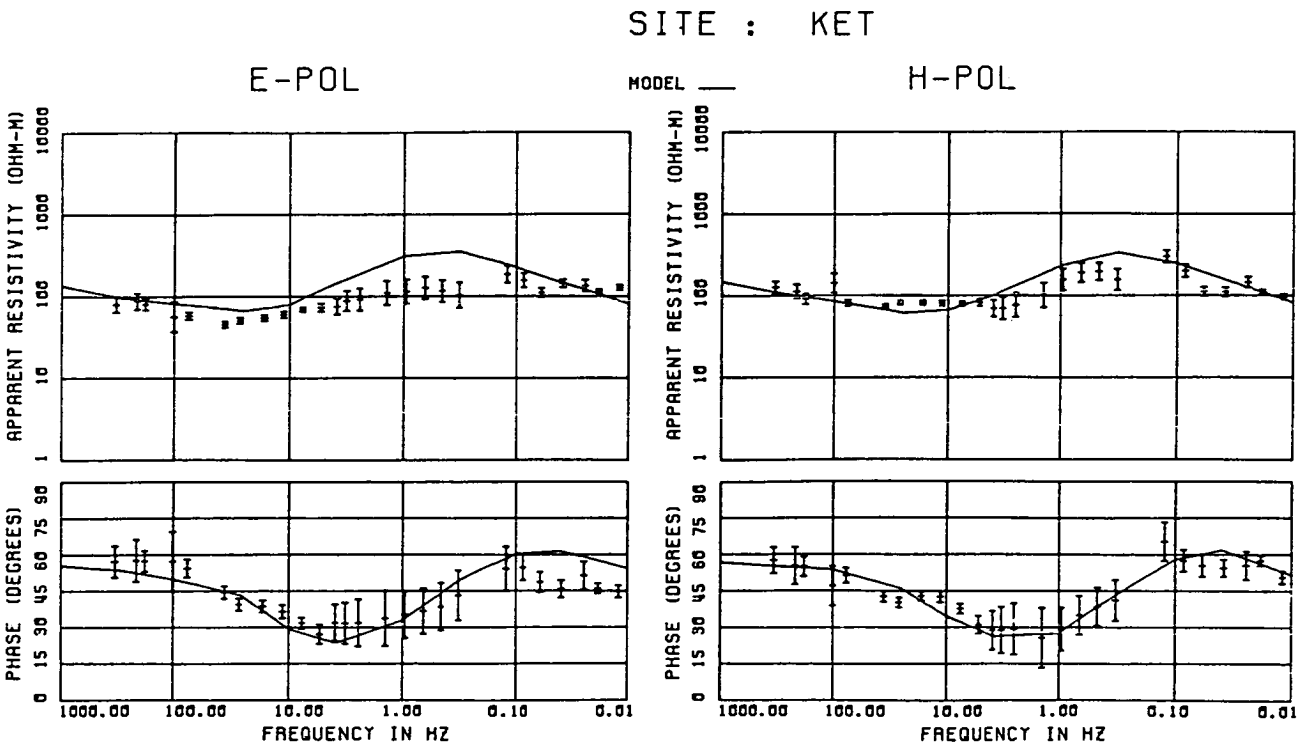
SITE : KET
E-POL
MODEL
H-POL
APPARENT RESISTIVITY (OHM-M)
1
10
100
1000
10000
PHASE (DEGREES)
0 15 30 45 60 75 90
1000.00 100.00 10.00 1.00 0.10 0.01
FREQUENCY IN HZ

Fig. 7.2h

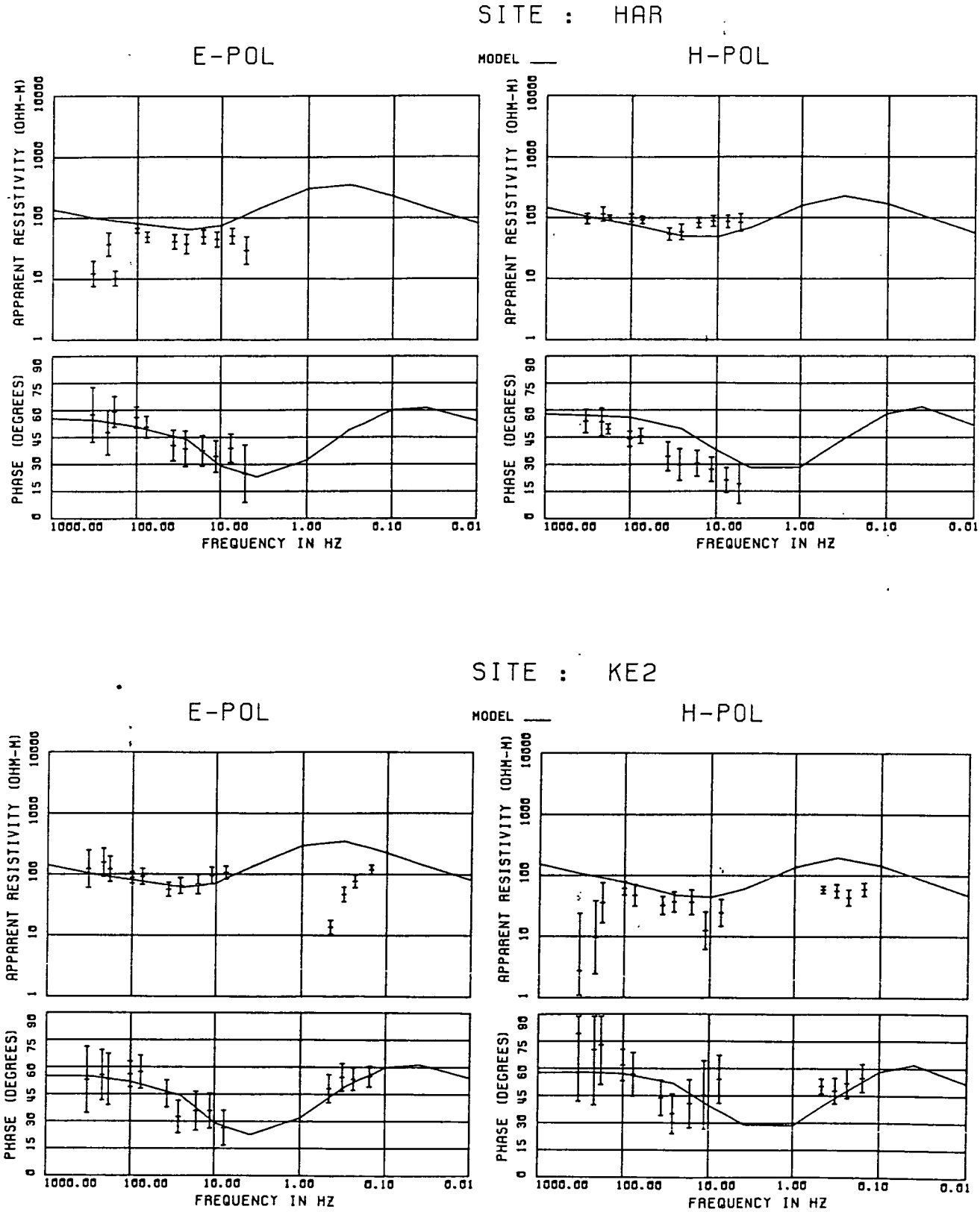
SITE : HAR
E-POL
MODEL
H-POL
APPARENT RESISTIVITY (OHM-M)
1
10
100
1000
10000
PHASE (DEGREES)
0
15
30
45
60
75
90
1000.00
100.00
10.00
1.00
0.10
0.01
FREQUENCY IN HZ
SITE : KE2
E-POL
MODEL
H-POL
APPARENT RESISTIVITY (OHM-M)
PHASE (DEGREES)
FREQUENCY IN HZ

Fig. 7.2i

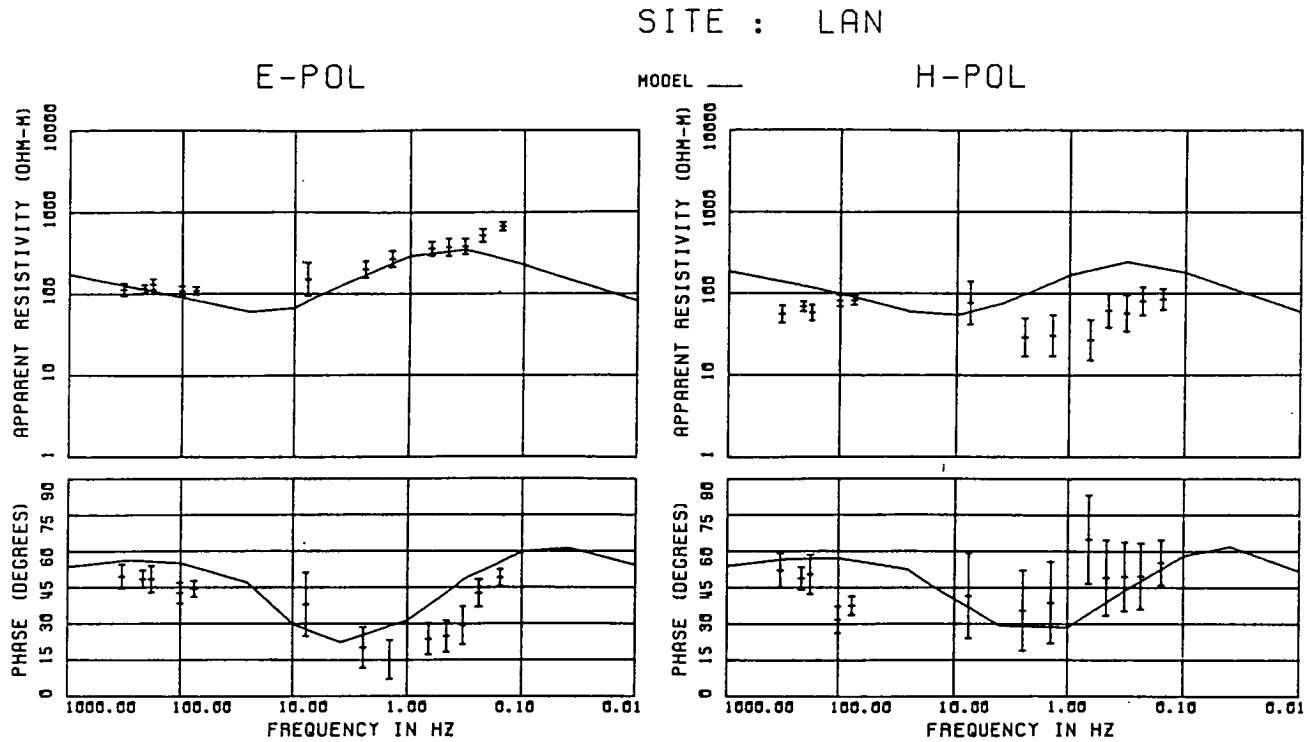
SITE : LAN
E-POL
MODEL
H-POL
APPARENT RESISTIVITY (OHM-M)
1
10
100
1000
10000
PHASE (DEGREES)
0
15
30
45
60
75
90
1000.00
100.00
10.00
1.00
0.10
0.01
FREQUENCY IN HZ

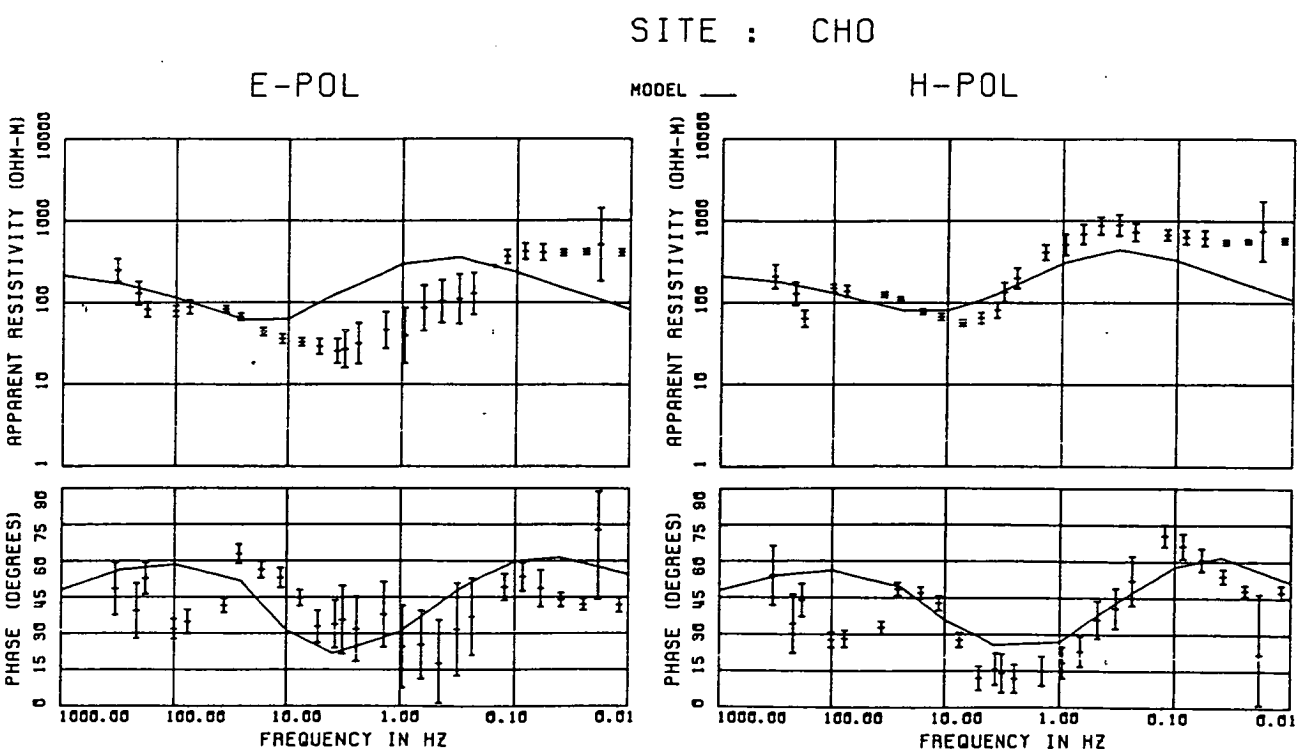
SITE : CHO
E-POL
MODEL
H-POL
APPARENT RESISTIVITY (OHM-M)
1
10
100
1000
10000
PHASE (DEGREES)
0
15
30
45
60
75
90
1000.00
100.00
10.00
1.00
0.10
0.01
FREQUENCY IN HZ

Fig. 7.2j

SITE : GRE

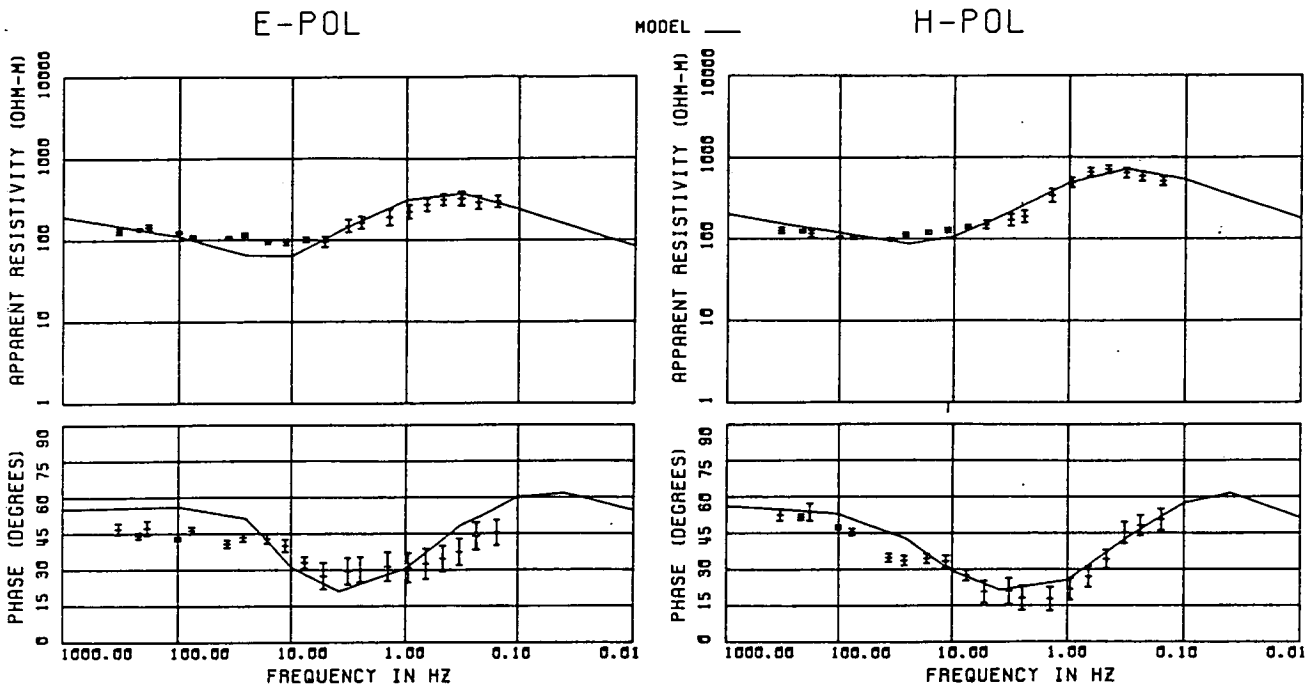

SITE : CAM

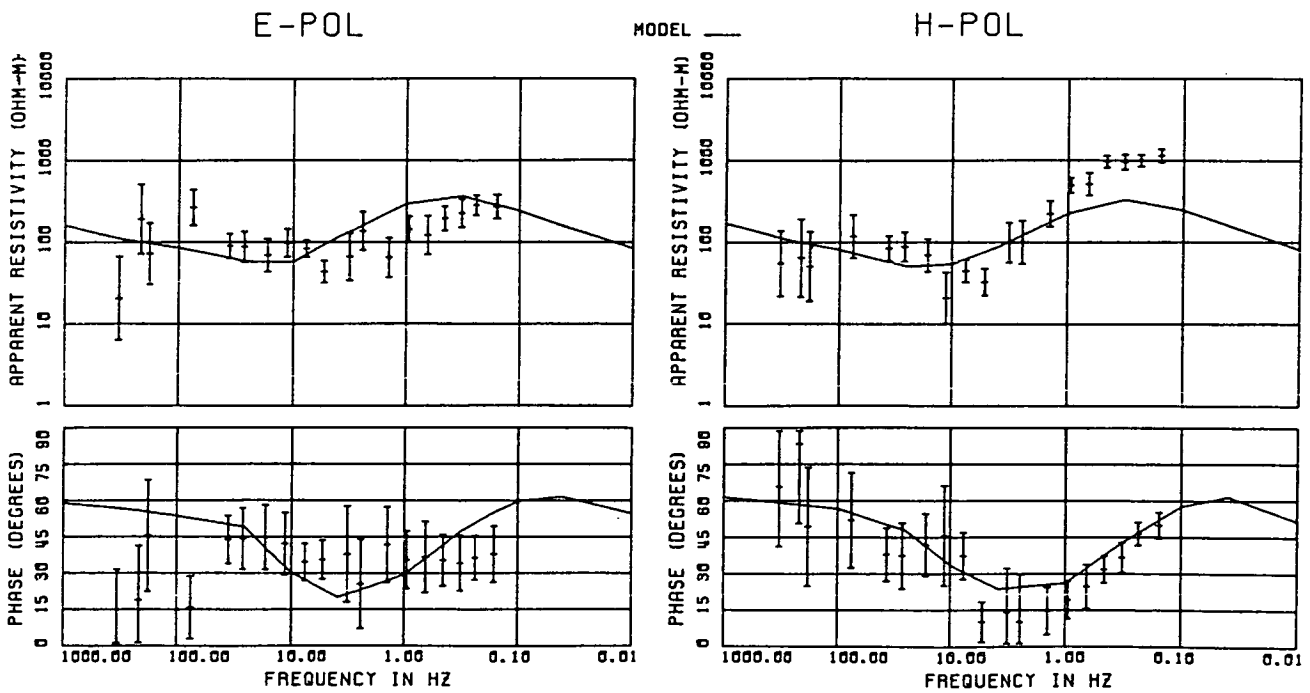

base is between 1 and 1.5 km). Both layers are thickest under CHO. All the above moderately conducting layers and the good conductors together form basin-like structures north of BER and south of SCR.

(d) A resistive layer (> 1000 ohm-m) underlies all of the above. This layer is thinnest (< 3 km) in the neighbourhood of SAW and BUG and it is almost outcropping at the surface at sites BER and SCR. It is about 9 km thick under MUR at the northwest end of the profile and about 17 km thick under CAM at the southeast end.

(e) A good conductor of resistivity less than 100 ohm-m underlies the resistive layer. The depth to this conductor is 10 km under MUR and SPM, about 4 km under SAW and BUG, 8 km under WAN, WLA, BER and SCR, 15 km under EVE, 20 km under HRI and HUR, 15 km under BED and HAL, 10 km under KET, HAR, KE2 and LAN, 25 km under CHO and 18 km under GRE and CAM. Thus, the conductor rises nearer to the earth's surface in the neighbourhood of SAW and BUG and also in the locations of KET, HAR, KE2 and LAN, while north and south of these zones, it deepens. The conductor is much nearer the surface in the neighbourhood of SAW and BUG than in the second zone. As pointed out earlier, the measured apparent resistivity values in these two zones are anomalously low by comparison with other sites.

(f) Beneath the conductor is a resistive layer of resistivity 1000 ohm-m. The depth variation to this layer is very similar to that to the overlying conductor. This resistive layer is not actually penetrated by the longest period used in this project, i.e., the period is not long

enough to resolve the thickness and resistivity of this layer. Hence, the depth to it indicated by the 2D model (Fig. 7.1) is the minimum possible value. Removing this layer and hence assuming the overlying conductor to be a half-space, gives a poorer fit than shown in Figs. 7.2a-j only to the few long period (T>40 s) E- and H-polarisation apparent resistivity and phase data. The presence of this resistive layer is clearly manifested by the previous longer period MT studies in the region (Jones, 1977 and Ingham, 1981) and the 1000 ohm-m used and kept fixed in the present model is in fact the linear average of the values obtained by these authors.

Considering the plots shown in Figs. 7.2a-j, it can be clearly seen that the overall fit of the model curves to the measured E- and H-polarisation apparent resistivity and phase data is generally very good. The only obvious exception is site SAW. Despite the fact that several different parameter values under the site have been tried, none of these has produced a good fit to both polarisation data simultaneously. It has been found that a very good fit is possible for either, but very poor fit for the other. The parameter values producing a good fit to the E-polarisation apparent resistivity data, give rise to an H-polarisation model curve that is much lower than the measured apparent resistivity data. On the other hand, the parameters producing a good fit to the H-polarisation apparent resistivity data, give rise to an E-polarisation model curve that is much higher than the corresponding measured apparent resistivity data. It may be noted that

the average of the model curves shown in Fig. 7.2b is a good fit to the average of the E- and H-polarisation measured data. The difficulty of getting a good fit to both polarisation data simultaneously may be overcome by rotating the impedance tensors to a much different angle from that used at the other sites. There is no obvious convincing evidence to support such a change in the angle of rotation. It is however possible that this apparent inconsistency between the E- and H-polarisation data may be due to the effect of noise in the data, but the exact noise source is unknown. Enquiries from the farmer on whose farm the site is situated and from others in the area in early 1985 have indicated that the site was a previous rubbish dump for the village. The presence of ferrous scrap visible at the surface may well extend to depth and hence, may grossly distort the magnetic field.

Splitting the uppermost 50 m under sites BER and SCR into a conductor ($\approx$ 100 ohm-m) underlain by a resistor ($>$ 1000 ohm-m) will produce a better fit to the observed high frequency data, particularly the E-polarisation apparent resistivity and the H-polarisation phase data. This will necessitate finer grids with spacing less than 50 m near the earth's surface. This is not considered pertinent until high quality data of frequencies greater than 600 Hz are available. Similarly, putting a conductor ($\approx$ 100 ohm-m) in the uppermost 50 m under HUR gives an improved fit to the high frequency E-polarisation phase and if thinner than 50 m, the fit will improve further. A much improved fit to the E-polarisation long period band 4 data is obtained at

HUR by making the whole crust and upper mantle under it resistive, but this leads to poorer fits to the H-polarisation data at the neighbouring sites north and south. Hence, an entirely resistive crust and upper mantle under HUR does not seem plausible. Similarly under CHO, making the base of the resistor deeper and hence the conductor thinner improves the fit to the long period data, particularly the E-polarisation data.

From the trial and error approach discussed earlier, the model parameters (layer resistivities and depths to the interfaces) at each of the sites have been varied and from these, the possible ranges of these parameters are shown in Table 7.2. The parameters (RHO denotes layer resistivity and DEP the depth to an interface) at each site are numbered starting from the top surface. There are more parameters for the sites in the Midland Valley than in the Southern Uplands and any inapplicable parameters at any site are left blank. For site SPM, the uppermost layer 1 of resistivity 40-80 ohm-m and thickness ≤50 m has been omitted in Table 7.2 to enable the convenient layout of the table and hence the listed parameter numbering actually starts from layer 2 downwards. As explained earlier, the depth values to the deepest resistor indicated in the table are only the lower bounds, while the resistivity value has been kept fixed. An acceptable fit here implies that the model curves lie within a smooth envelope of the error bars of the E- and H-polarisation data. The parameter ranges shown in Table 7.2 are the extreme values such that the model curves for any given site just fit one of the

TABLE 7.2

Bounds of 2D model parameters

SITES	RHO 1	DEP 1	RHO 2	DEP 2	RHO 3	DEP 3	RHO 4	DEP 4	RHO 5	DEP 5	RHO 6
	(ohm-m)	(km)	(ohm-m)	(km)	(ohm-m)	(km)	(ohm-m)	(km)	(ohm-m)	(km)	(ohm-m)
MUR	40 - 80	0.05-0.10	5 - 25	0.10-0.20	200 - 500	0.60-1.20	1.0k-4.0k	8 - 12	20 - 60	> 50	1.0k
SPM	200 - 400	0.10-0.40	15 - 30	0.50-0.70	300 - 500	1.00-2.00	2.0k-5.0k	8 - 12	20 - 60	> 50	1.0k
SAW	10 - 80	< 0.05	5 - 50	0.50-0.80	100 - 400	1.00-2.00	1.0k-2.0k	2.6 - 5.0	20 - 70	> 40	1.0k
BUG	40 - 80	0.05-0.10	10 - 40	0.10-0.40	200 - 400	0.50-1.50	1.0k-3.0k	2.6 - 5.0	40 - 100	> 40	1.0k
WAN	80 - 200	< 0.05	300 - 400	0.60-1.20	1.0k-4.0k	5.2 - 12	30 - 80	> 50	1.0k		
WLA	300 - 400	0.40-0.80	2.0k-4.0k	5.2 - 10	80 - 150	> 50	1.0k				
BER	200 - 450	0.10-0.40	1.0k-3.0k	8 - 12	10 - 30	> 50	1.0k				
SCR	350 - 500	0.10-0.30	0.8k-1.5k	8 - 12	10 - 30	> 50	1.0k				
EVE	150 - 400	0.40-1.00	1.0k-1.5k	13 - 18	10 - 80	> 50	1.0k				
HRI	120 - 200	1.00-2.00	1.0k-2.0k	18 - 20	10 - 80	> 70	1.0k				
HUR	200 - 300	1.00-2.00	1.0k-1.5k	18 - 25	60 - 250	> 70	1.0k				
BED	120 - 200	1.00-2.00	1.0k-1.5k	15 - 20	40 - 80	> 70	1.0k				
HAL	80 - 120	0.05-0.15	150 - 400	0.60-1.40	1.0k-1.5k	13 - 18	40 - 80	> 70	1.0k		
KET	150 - 300	0.05-0.15	30 - 70	0.70-1.50	0.8k-1.2k	8 - 12	40 - 80	> 50	1.0k		
HAR	100 - 300	0.05-0.15	30 - 70	0.50-1.50	0.8k-1.2k	8 - 12	40 - 80	> 50	1.0k		
KE2	150 - 300	0.05-0.15	25 - 60	0.70-1.50	0.8k-1.2k	8 - 12	40 - 80	> 50	1.0k		
LAN	120 - 250	0.10-0.20	25 - 70	1.00-1.50	1.0k-2.0k	8 - 15	40 - 80	> 50	1.0k		
CHO	150 - 300	0.20-0.40	20 - 50	1.20-2.20	3.0k- 10k	20 - 30	80 - 150	> 60	1.0k		
GRE	250 - 350	0.05-0.15	80 - 120	0.70-1.20	2.0k-5.0k	15 - 20	60 - 100	> 60	1.0k		
CAM	150 - 400	0.05-0.20	30 - 70	0.70-1.50	3.0k-6.0k	15 - 25	60 - 100	> 60	1.0k		

polarisations but poor for the other and without significantly affecting the fit at neighbouring sites. Outside the stated ranges, the model fit to the data at any site is definitely very poor for at least one of the polarisations. A simplified 2D model on the real physical scale reflecting these ranges is shown in Fig. 7.3a, while the uppermost 25 km of the subsurface is shown in Fig. 7.3b for clarity of the near-surface features. The interface depth ranges are shown on the plots by vertical arrows.

Fig. 7.3c shows for comparison with Fig. 7.3b a simplified 2D section (previously shown in two parts as Figs. 5.3a,b) from a collation of the individual site 1D models of the invariant data (ϱ_{eff} and φ_{eff}). It can be clearly seen that the 2D model and the 2D section exhibit very similar features. The main inferences of the 2D section are thus confirmed by the 2D numerical model. This thus supports the view that even in tectonically complicated regions, a series of 1D models can yield valuable information about the subsurface conductivity structure. This is certainly true if the sites are sufficiently close and the invariant data (ϱ_{eff}, φ_{eff}) are modelled. Hence, 1D modelling of a 2D structure is worth while and it is justifiable to collate the individual 1D models into a 2D section at least as a crude approximation of the structure. It may also be noted that using such a 2D section as a starting model for 2D modelling saves computing time.

The close agreement between the 2D model and the 2D section in as far as any geophysical inferences which can

FIGURE 7.3

(a) A simplified 2D geoelectrical model for SE Scotland. Note that there is a horizontal exaggeration of 3.

(b) Uppermost 25 km of the 2D model.

(c) A collation of the individual site 1D models into a simplified 2D section for comparison with Fig. 7.3b.

On each of the plots, DGF and SUF are the Dunbar-Gifford and the Southern Uplands Faults respectively; the site locations are indicated by vertical bars at the top (for the site names listed in order, see Table 4.1; the site codes are respectively MUR, SPM, SAW, BUG, WAN, WLA, BER, SCR, EVE, HRI, HUR, BED, HAL, KET, HAR, KE2, LAN, CHO, GRE and CAM) and the horizontal distances in km are shown at the bottom.

Fig. 7.3a

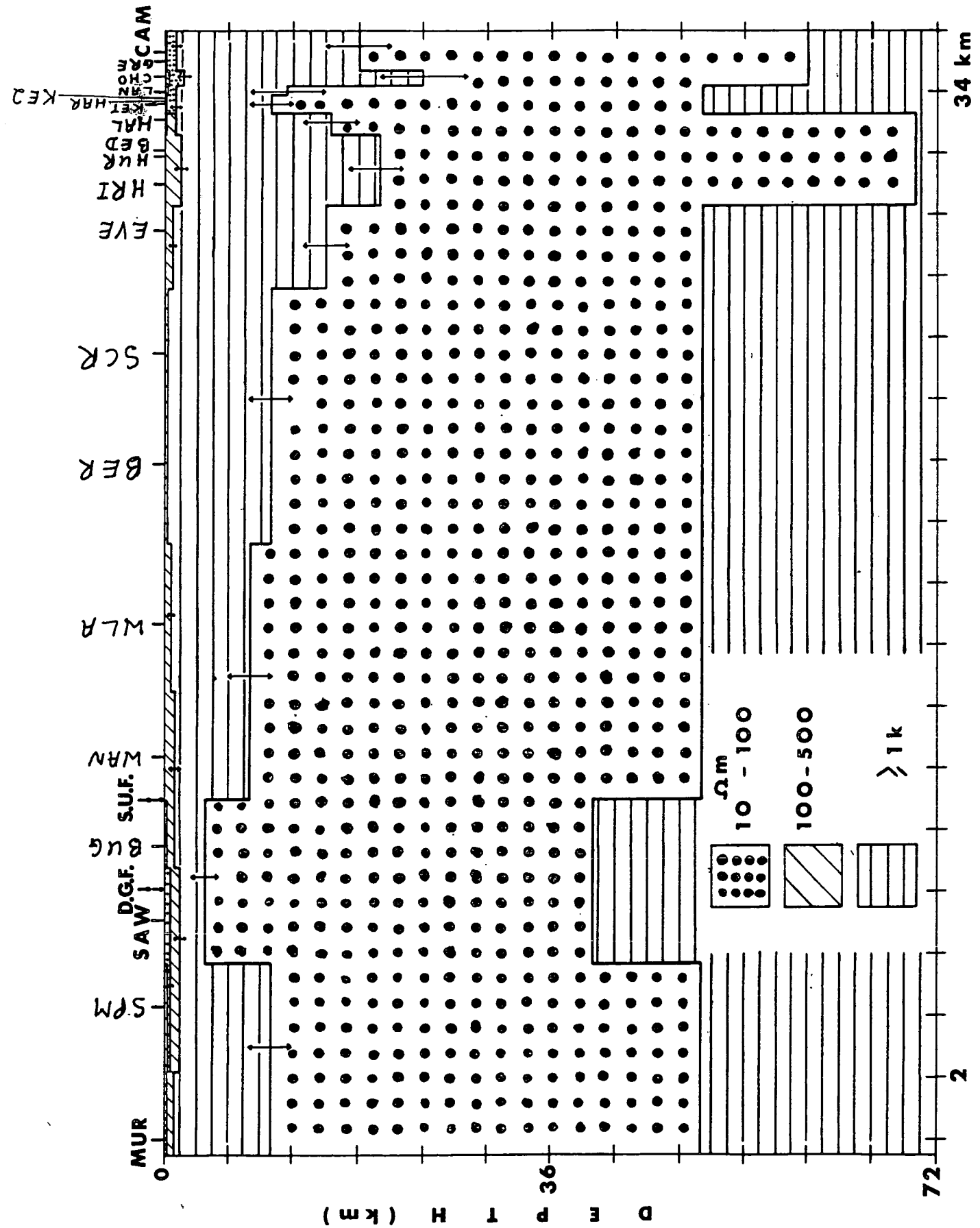
CAM
CRE
CHO
LAN
KET
HAR
KEJ
HAL
BED
HUR
HRI
EVE
SCR
BER
WLA
WAN
S.U.F.
BUG
D.G.F.
SAW
SPM
MUR
34 km
2
Ωm
10 - 100
100-500
≥ 1k
0
36
72
D E P T H (km)

Fig. 7.3b

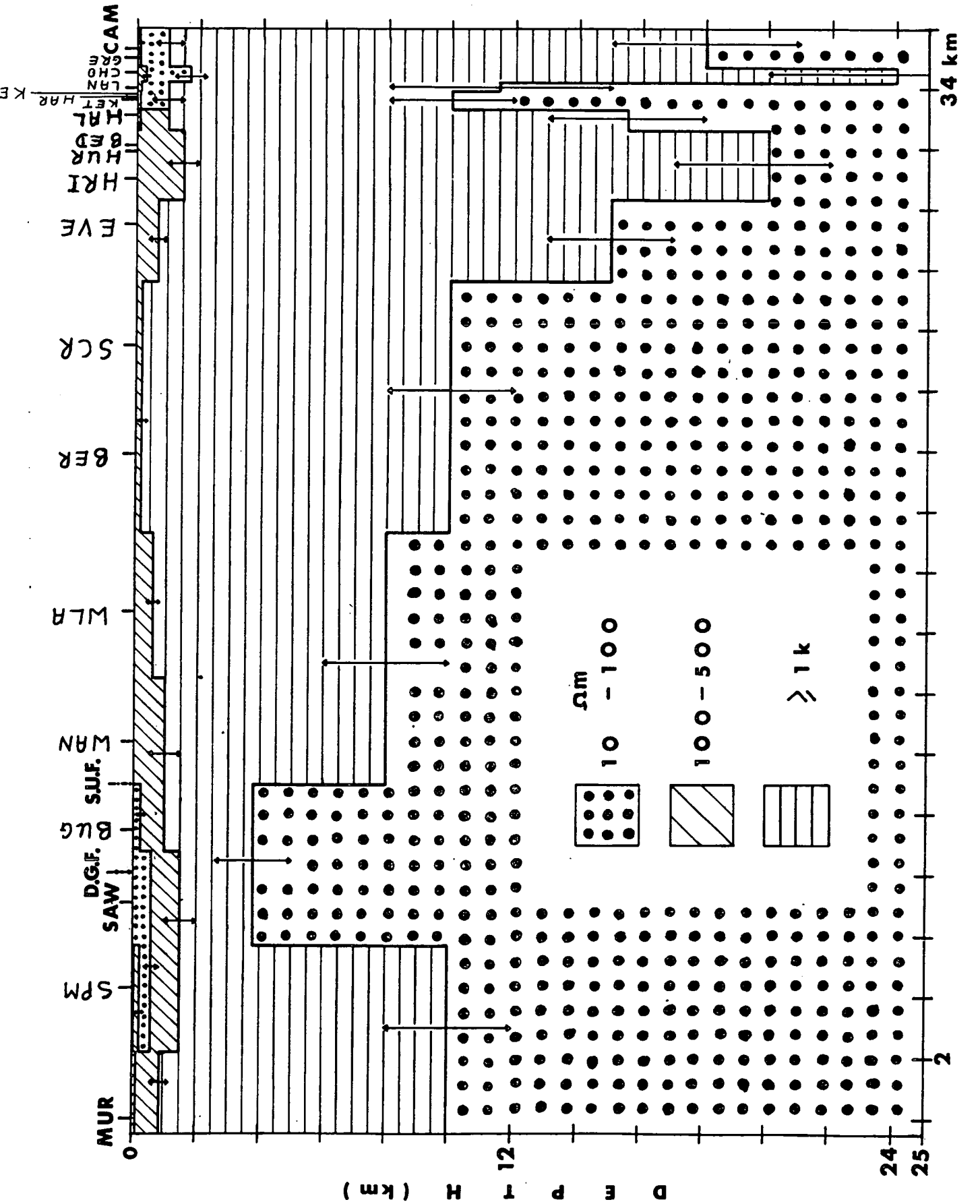
CAM
GRE
CHO
LAN
KET HAR KE
HRL
BED
HUR
HRI
EVE
SCR
BER
WLA
WAN
SUF.
BUG
D.G.F.
SAW
SPM
MUR
34 km
2
0
12
24
25
D E P T H (km)
10 - 100 Ωm
100 - 500
≥ 1 k

Fig. 7.3c

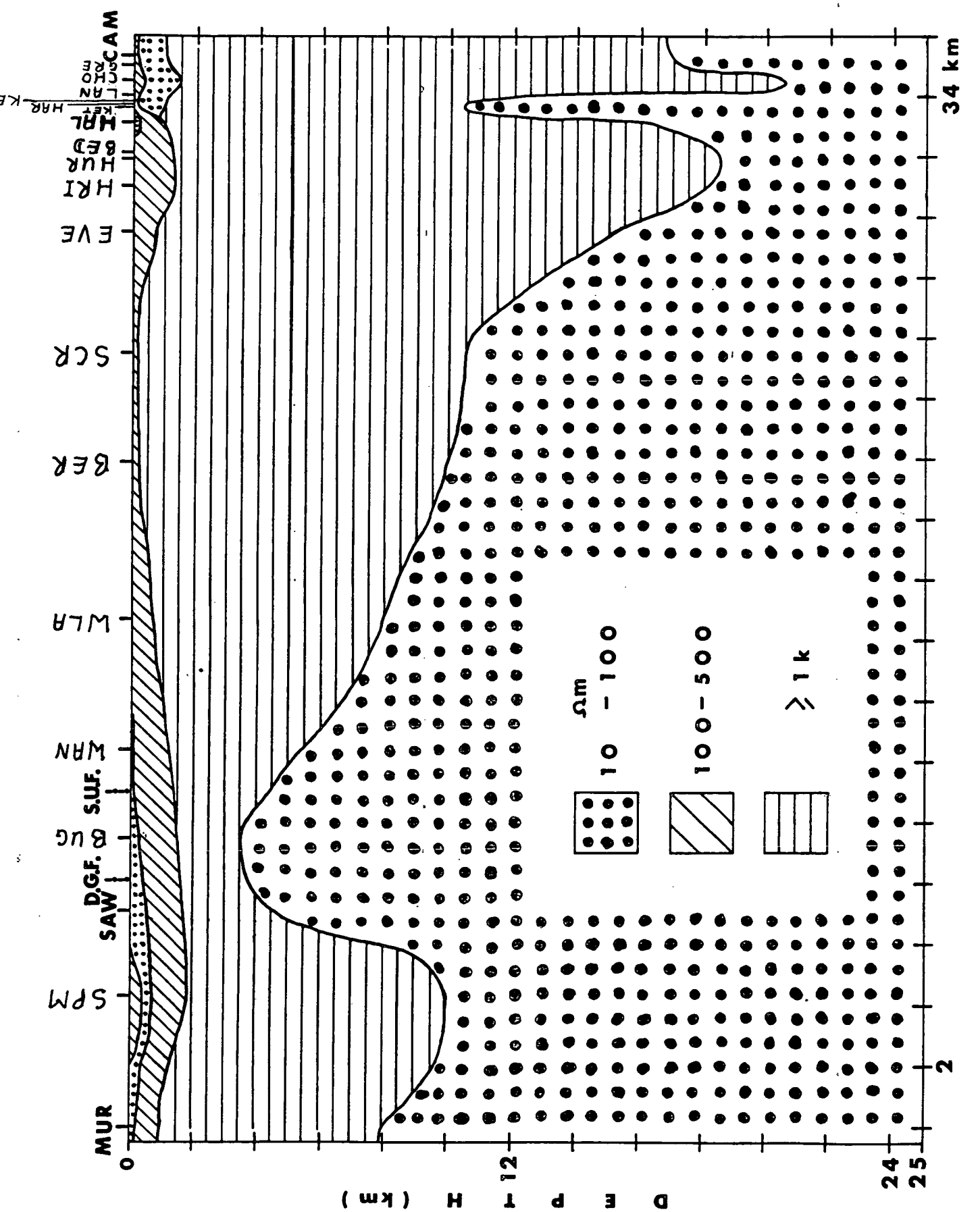
CAM
CHO
RE
LAN
HAR
KET
HRL
BED
HUR
HRI
EVE
SCR
BER
WLA
WRN
SUF.
BUG
D.G.F.
SAW
SPM
MUR
34 km
2
0
12
24
25
D E P T H (km)
Ωm
10 - 100
100 - 500
≥ 1k

be made calls to question whether the effort needed for 2D modelling is economically justifiable. It is suggested here that 1D modelling of the E- and H-polarisation data may be used additionally to provide some bounds on the 2D section derived from the 1D models of the invariant data. In Figs. 7.3a-c, the site locations are shown by vertical bars at the top and the horizontal distance at the bottom; the site names are listed in order in Table 4.1.

CHAPTER 8

INTERPRETATION, CONCLUSIONS AND SUGGESTIONS FOR FUTURE WORK

To highlight the interpretation, a detailed comparison is made between the 2D geoelectrical model of the present project and models proposed by other workers in the region. Examples from other areas elsewhere with similar results are given. The general causes of enhanced electrical conductivities in the earth are discussed. The possible causes which can account for the high conductivity zone in the upper/lower crust and the upper mantle in SE Scotland are outlined. The plausible composition of the conductor as partly serpentinized basalt is proposed here. It is suggested that the neighbourhood of SAW and BUG and the axis of an elongated magnetic variation anomaly where the conductor rises nearest to the earth's surface (<4 km) may be associated with ancient subduction and hence related to the Iapetus suture as first discussed by Sule and Hutton (1984). This conducting zone is also suggested here as being responsible for the magnetic variation anomaly; this thus provides a hitherto unknown near-surface conductor coincident with the anomaly. Suggestions are put forward for further detailed work in South Scotland which will enable more definite knowledge of the subsurface structure and its composition and hence may make possible the definitive assessment of the

tectonic implications of a geoelectrical model for the region.

8.1 Comparison of the 2D geoelectrical model with other results

8.1.1 Comparison with other geophysical models of South Scotland

A number of geological, seismic, gravity and EM induction data are available for South Scotland. The good agreement between the present AMT/MT result in the Duns area and that of Habberjam technique within the uppermost 1.2 km of the subsurface resolved by the latter has already been fully discussed in chapter 6. As indicated earlier, the more complex geoelectrical structure in the Midland Valley than in the Southern Uplands is in good accord with the more complex surface geology. The rapid thinning of the sedimentary cover in the geoelectrical model from north to south across the SUF and its thickening southwards from beyond sites BER and SCR are also in good agreement with geology.

The Spilmersford Borehole (National Grid reference 34570 66902) is about 0.5 km almost due east of site SPM. Davies et al. (1974) have assigned the uppermost 25 m of the 934 m deep borehole to the Lower Limestone Group and the remaining sequence to the Calciferous Sandstone Measures except for the bottom 2 m which may belong to the Upper Old Red Sandstone facies. Within the sedimentary sequence

of Lower Carboniferous age, the borehole indicates interbedded lavas (dominantly olivine-basalts), tuffs and agglomerates from 287 m to 544 m depth, beneath which is a sill intrusion 115 m thick and minor intrusions and tuff bands at greater depths (McAdam, 1974). In the present geoelectrical model, the interpreted sedimentary cover, which is more than 1 km thick at SPM and its layering are thus in good agreement with the borehole information.

The first deep refraction seismic profile across South Scotland is that of LISPB and a section (after Bamford et al., 1978) of this in the neighbourhood of the SUF is shown in Fig. 8.1. It may be pointed out at the outset that the LISPB profile is at an appreciable distance (>40 km) to the west of the present AMT/MT profile. The upper surface of the conducting layer in the Southern Uplands is in good agreement with the seismic boundary between the Pre-Caledonian basement and the lower crust. More significantly is the fact that the seismic profile has not resolved the zone beneath the neighbourhood of the SUF. This zone is resolved by the MT and is highly conducting.

Recently available are the off-shore deep reflection seismic profiles of the British Institutions' Reflection Profiling Syndicate - BIRPS - (Brewer et al., 1983 and Brewer and Smythe, 1984). Fig. 8.2a shows the Western Isles and North Channel (WINCH) off-shore seismic traverse of BIRPS. The relevant sections for the present purpose are segments EF and HG. The former is across strike, while the latter is along strike. The line drawings (Brewer et al., 1983) of the unmigrated WINCH data for these segments

FIGURE 8.1

Seismic refraction cross-section (part of LISPB) across the SUF (after Bamford et al., 1978). The inset shows the entire LISPB line.

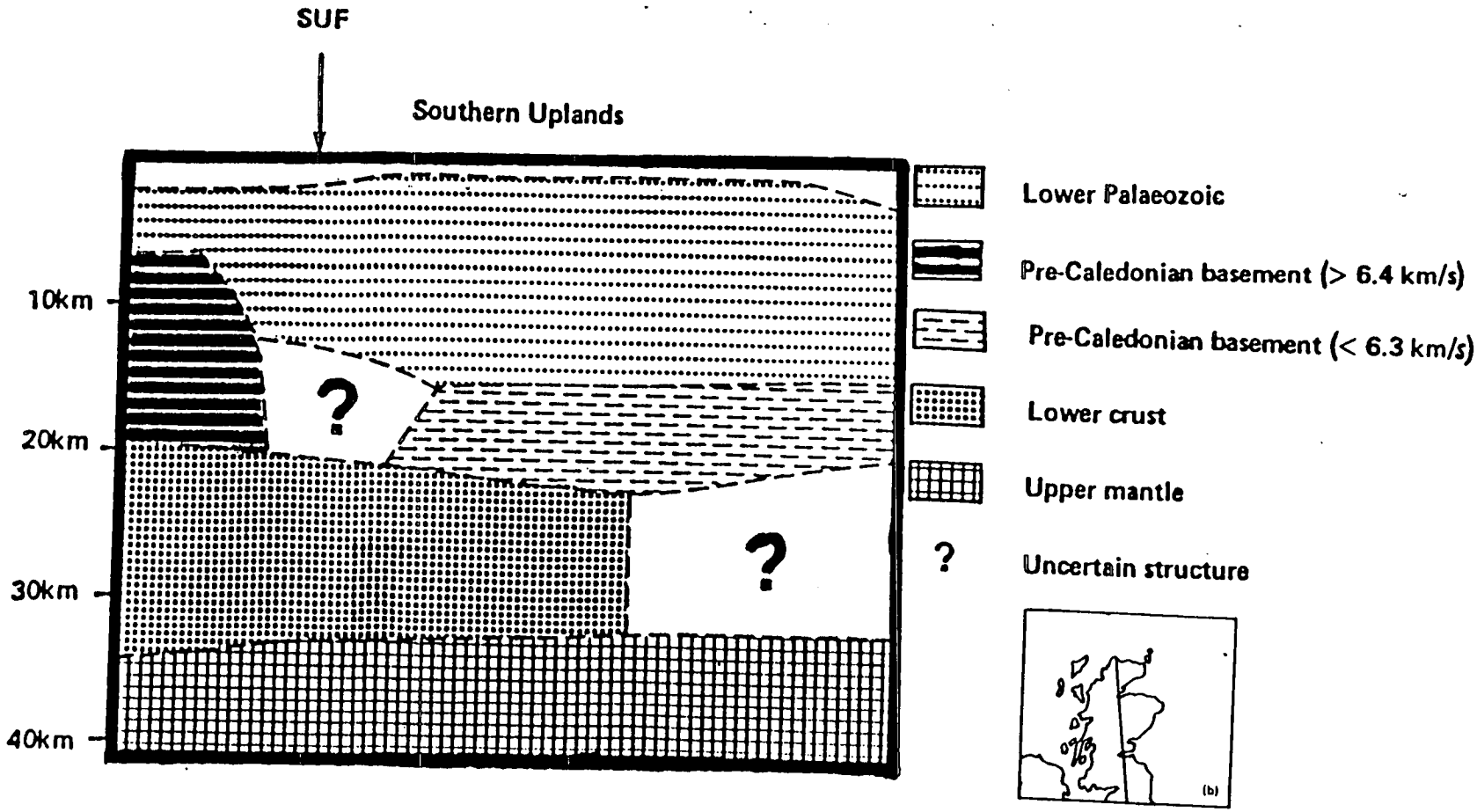
SUF
Southern Uplands
10km
20km
30km
40km
?
?
Lower Palaeozoic
Pre-Caledonian basement (> 6.4 km/s)
Pre-Caledonian basement (< 6.3 km/s)
Lower crust
Upper mantle
?
Uncertain structure
(b)

FIGURE 8.2

(a) Location of the WINCH off-shore reflection seismic profile - the letters alongside the profile refer to the various segments.

(b) The line drawings of the unmigrated data for segment EF.

(c) The line drawings of the unmigrated data for segment HG.

To convert time to approximate depth in km, multiply seconds by 3 in the crust and by 4 in the mantle (after Brewer et al., 1983).

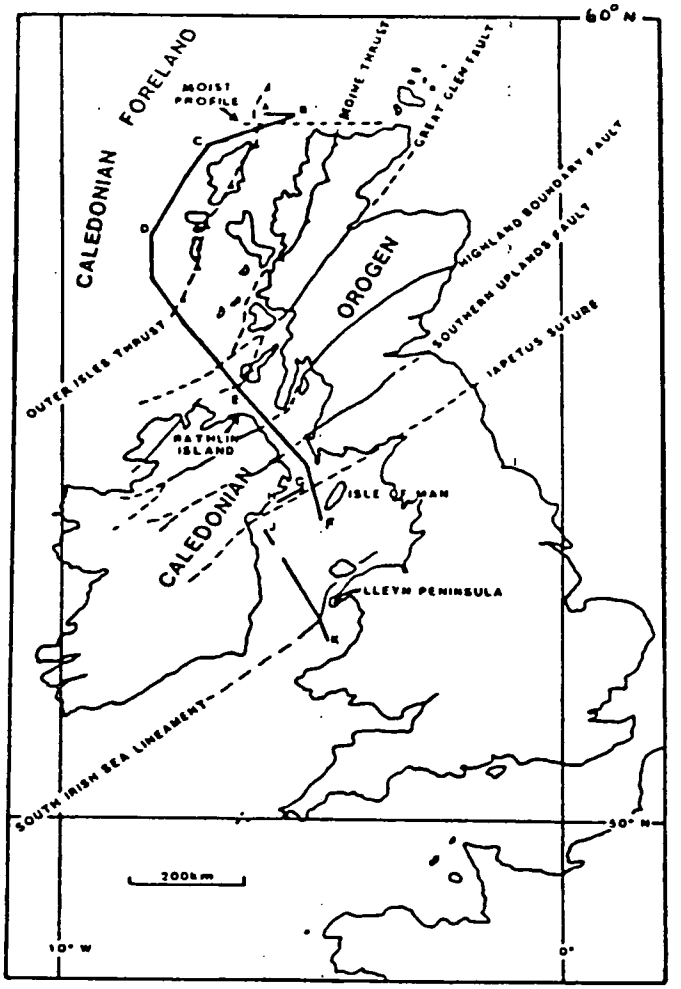
60° N
MOIST PROFILE
MOINE THRUST
GREAT GLEN FAULT
CALEDONIAN FORELAND
CALEDONIAN OROGEN
HIGHLAND BOUNDARY FAULT
SOUTHERN UPLANDS FAULT
OUTER ISLES THRUST
IAPETUS SUTURE
RATHLIN ISLAND
ISLE OF MAN
CALEDONIAN
LLEYN PENINSULA
SOUTH IRISH SEA LINEAMENT
50° N
200km
10° W
0°

[a]

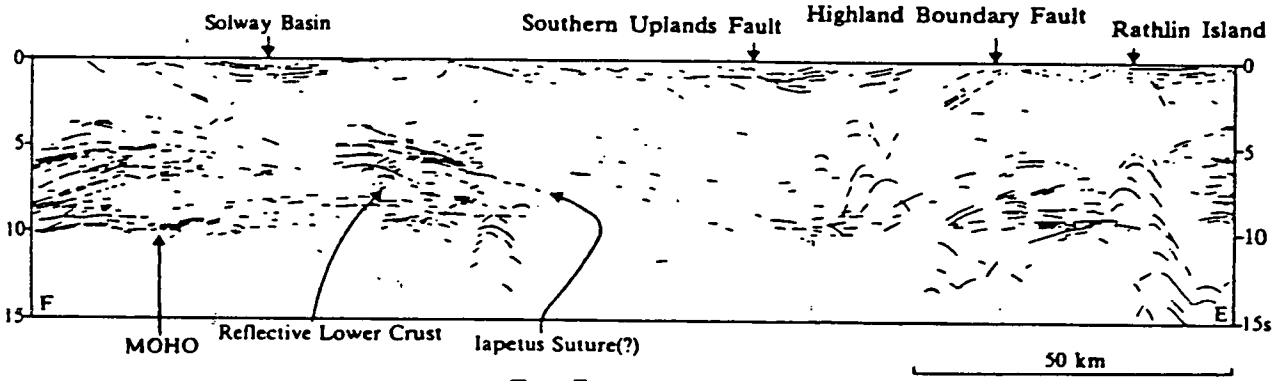
Solway Basin
Southern Uplands Fault
Highland Boundary Fault
Rathlin Island
0
5
10
15
F
E
15s
MOHO
Reflective Lower Crust
Iapetus Suture(?)
50 km

[b]

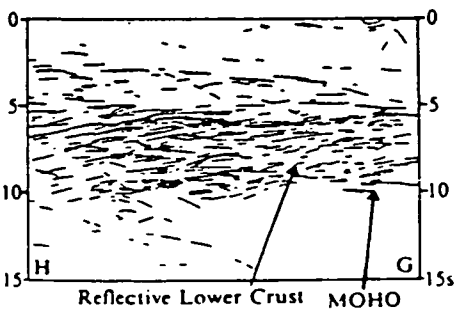
0
5
10
15
H
G
15s
Reflective Lower Crust
MOHO

[c]

are shown in Figs. 8.2b,c. A striking feature of Fig. 8.2b is that most of the Southern Uplands is virtually seismically transparent, while in Fig. 8.2c along strike, very pronounced upper and lower crustal reflectors can be clearly seen. The lack of across strike seismic resolution of features in the Southern Uplands may be due to the inability of sufficient seismic energy to penetrate the overlying sedimentary cover in this section of the traverse or may be there are steep boundaries with no contrast in seismic character across them.

The upper/lower crustal and upper mantle conductor in the 2D model confirms the existence of a lower crustal and upper mantle conductor predicted from long period MT studies by Jones and Hutton (1979a,b) and Ingham and Hutton (1982a,b). Figure 8.3a shows part of the 2D model of Ingham and Hutton (1982a); the section (PEN to YAR) lies to the west of the present study area (Fig. 1.1). Figure 8.3b shows the plots of the 1D models for SAL and PRE of Jones and Hutton (1979b). SAL is adjacent to site SPM of the present study, while PRE is northeast of the Duns area (Fig. 1.1). The present study clearly delineates the upper boundary of the conductor which hitherto has been poorly resolved in the previous studies. The present study also indicates that the conductor extends to the upper crust and the lateral depth variation to the conductor is clearly depicted.

From hypothetical event analysis, Bailey and Edwards (1976) and Hutton and Jones (1980) have located the axis of a major magnetic variation anomaly (AB) in South Scotland

FIGURE 8.3A

A section of the 2D conductivity model for South Scotland from long period MT data (after Ingham and Hutton, 1982a).

FIGURE 8.3B

1D conductivity models for SAL and PRE from long period MT data (after Jones and Hutton, 1979b); the depths are in km and the layer resistivities in ohm-m.

FIGURE 8.3C

Zero contour of the in-phase part of the vertical magnetic field produced by a unit amplitude horizontal field directed along the magnetic north (9^{0}W) - (after Banks et al., 1983). AB is the South Scotland magnetic anomaly, CDE an additional magnetic anomaly and XY is the SUF AMT/MT profile of the present study.

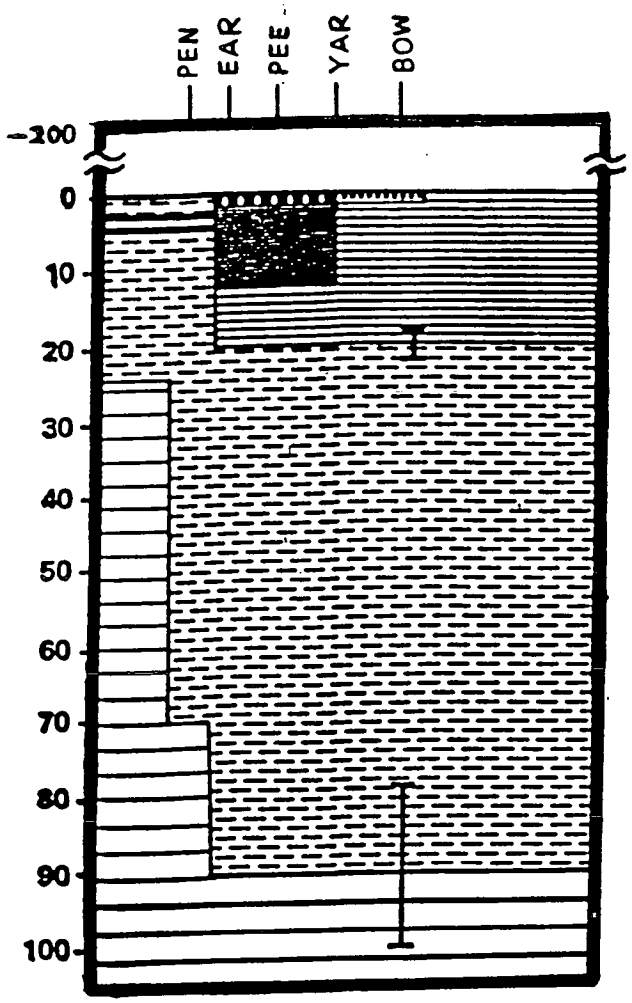

[a]

30–100
100–300
300–1000
1000–3000
3000–10000
> 10000
resistivities in ohm-m

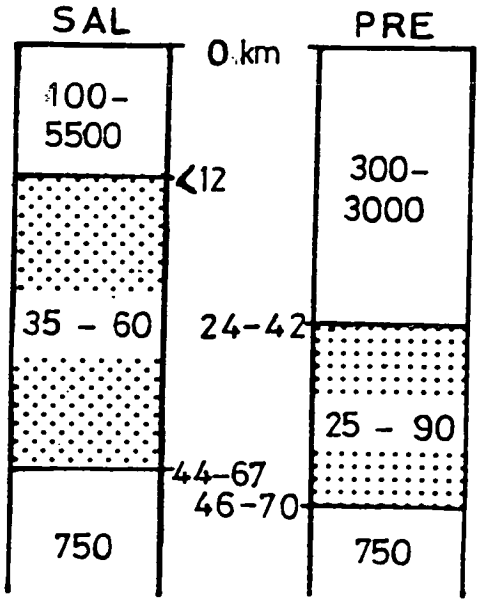

[b]

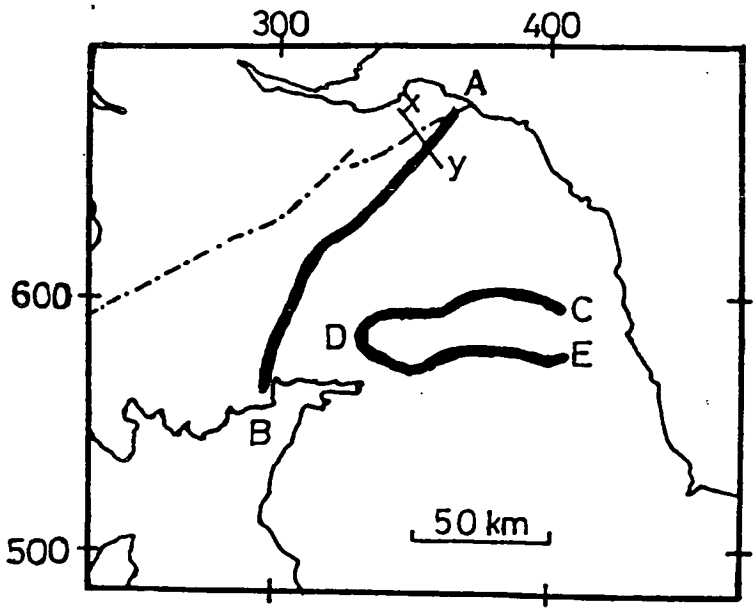

[c]

and Banks et al. (1983) an additional one (CDE) in the vicinity of the southern boundary of the Northumberland Basin (Fig. 8.3c); the SUF profile of the present study is denoted by XY on this figure. The intermediate zero Z-contour (CD) on this figure may be interpreted as resulting solely from the combined effect of the two anomalies AB and DE. All these authors and more recently Haak and Hutton (1985) have drawn attention to the probable association of the South Scotland anomaly AB with the Iapetus suture. The present study indicates that the crustal/mantle conductor rises up to less than 4 km of the earth's surface in the neighbourhood of sites SAW and BUG (Fig. 7.3a,b). It is tentatively suggested that this conductivity feature may be associated with ancient subduction and hence related to the Iapetus suture as first discussed by Sule and Hutton (1984). This conducting zone is also suggested here as being responsible for the South Scotland anomaly AB; this thus provides a hitherto unknown near-surface conductor coincident with anomaly AB. The possible correlation between old plate margins and conductivity anomalies has been discussed by Law and Riddihough (1971). A noteworthy piece of evidence also supporting the proposition that the conductivity feature is associated with the Iapetus suture is that very low resistivity values (a few ohm-m) in the lower crust have been reported in the neighbourhood of the axis of the Carpathian and other magnetic variation anomalies in regions identified as plate boundaries (see for example, Cerv et al., 1984; Zhdanov et al., 1984; Jankowski et al.,

1985). It is acknowledged that it is equally possible in this zone for the conductivity feature to be associated with the SUF. It is thus of considerable interest that similar AMT/MT profile studies be undertaken across the anomaly AB and the SUF to the southwest of the present study to investigate whether the structure of Fig. 7.3a,b is continuous along the anomaly axis and hence confirming the above proposed speculation or it is a feature associated primarily with the SUF itself. If this tentative proposition were confirmed, then AMT/MT can be used to locate and map the entire extent of the suture.

Figure 8.4a shows the Bouguer gravity anomaly map of SE Scotland (Lagios and Hipkin, 1982) with a contour interval of 10 gu (=1 mgal $=10^{-5}$ ms^{-2}). The solid circles plotted on their gravity profile AB indicate the AMT/MT sites of the SUF profile. Figure 8.4b shows their interpretation of the gravity profile AB. Lagios and Hipkin (1982) have postulated that a massive granite batholith underlies the greater part of the eastern Southern Uplands. Since granite is generally resistive, hence the intuitive candidate in the 2D geoelectrical model is the resistive layer (> 1000 ohm-m) which underlies the sediments throughout the profile. This was the inference made in our paper (Sule and Hutton, 1984) where it was indicated that the resistive layer of the 2D section might be compatible with the buried granite batholith proposed from the gravity studies, but that their predicted thickness and depth to this batholith were substantially different from those indicated by our AMT/MT study thus necessitating further

FIGURE 8.4

(a) Bouguer gravity anomaly map of SE Scotland - the contour intervals are 10 gu (=1 mgal = 10^{-5} ms^{-2}) - (after Lagios and Hipkin, 1982). The solid circles on their gravity profile AB show the 8 SUF AMT/MT profile sites of the present study.

(b) Their interpretation of gravity profile AB. On the figure, the black layer represents olivine basalt; LT denotes lavas, trachytes, tuffs and agglomerates; d^2 Limestone series, d^1 Calciferous sandstone series and c^3 Upper Devonian.

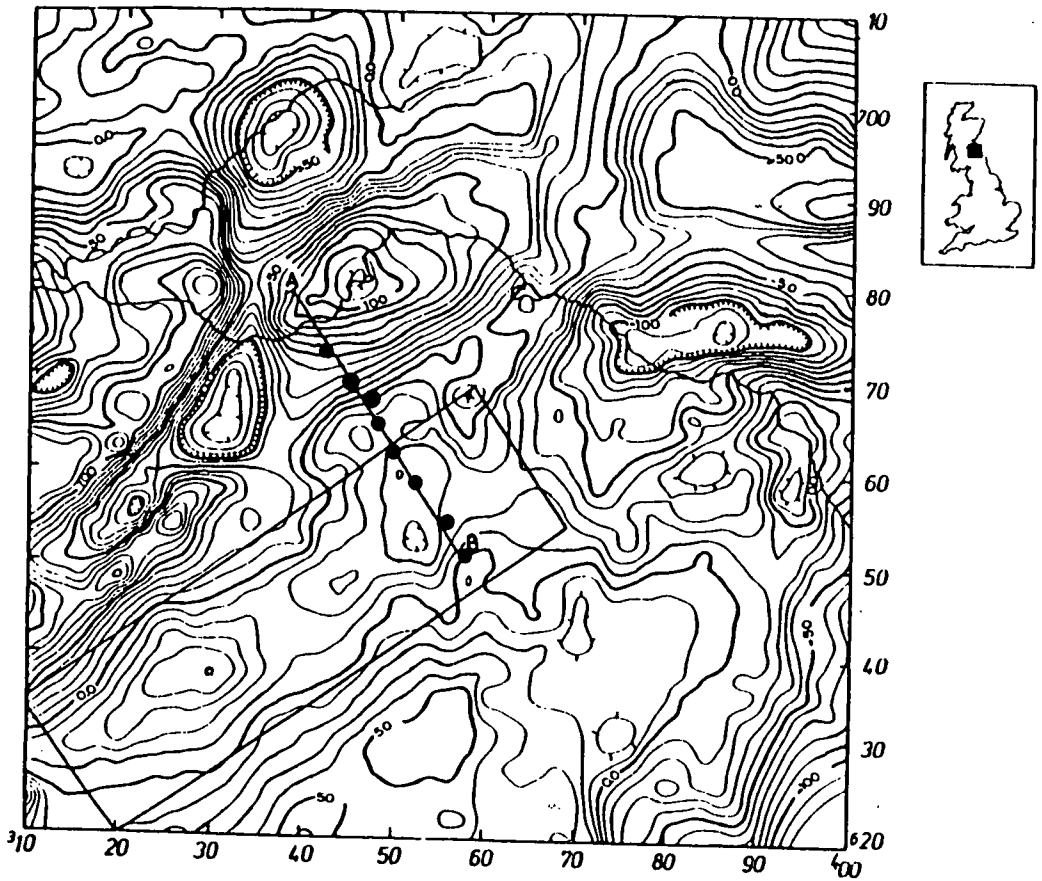
A
B
10
20
30
40
50
60
70
80
90
100
700
90
80
70
60
50
40
30
620
400

[a]

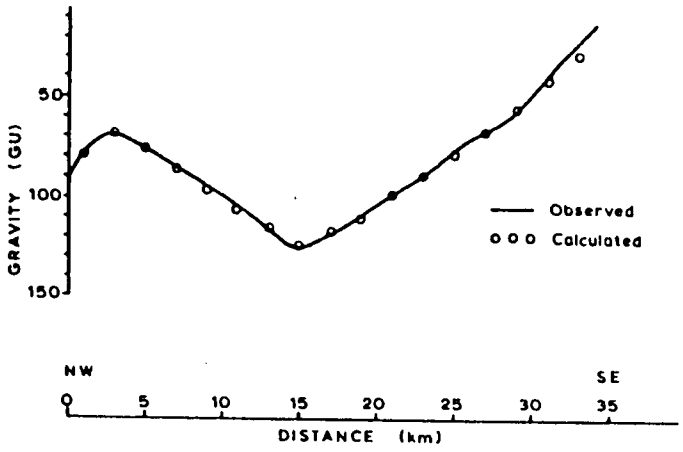
GRAVITY (GU)
50
100
150
Observed
Calculated
NW
SE
0
5
10
15
20
25
30
35
DISTANCE (km)

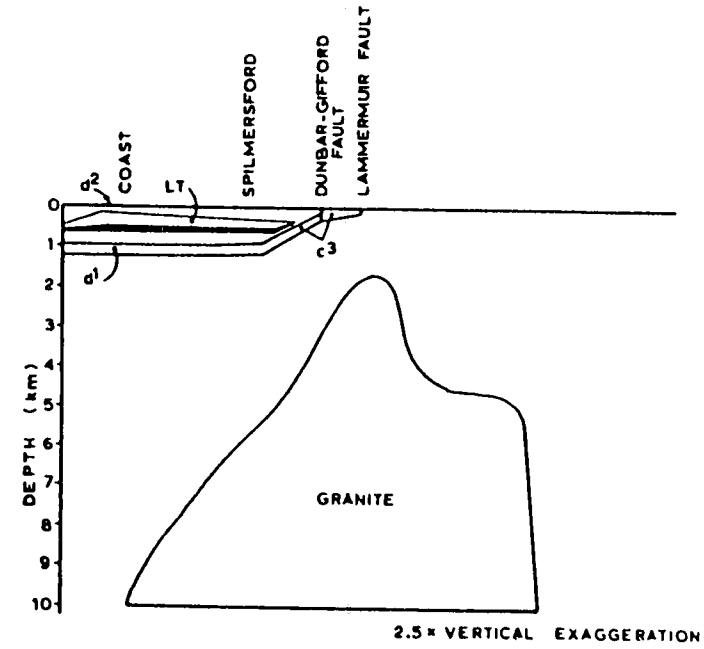
COAST
LT
SPILMERSFORD
DUNBAR-GIFFORD FAULT
LAMMERMUIR FAULT
a2
a1
c3
DEPTH (km)
0
1
2
3
4
5
6
7
8
9
10
GRANITE
2.5× VERTICAL EXAGGERATION

[b]

investigation of this interpretation. However, it can be seen that the shape of their batholith is more similar to that of the conducting layer than the overlying resistor, while the depths from the gravity studies are comparable with the lower limits of the varying depths to the conductor indicated by the conductivity model. The similarity can be more clearly seen by comparing Figs. 8.4b and 5.3a. The gravity interpretation satisfies the observed negative gravity anomaly implying low density, the little or no seismic velocity contrast with the surroundings having velocities less than 6 kms^{-1} as indicated by LISPB and the generally smooth and weak aeromagnetic signature in eastern Southern Uplands (Fig. 8.5). This does not however satisfy the geoelectrical model unless it is a wet granite which will indicate the presence of fluid, e.g., water. Hyndman and Hyndman (1968) have indicated that water saturated granites at lower crustal depths and temperatures can give rise to high conductivity. Although the gravity model does not resolve beyond 10 km depth, however, with the conducting layer extending up to 40 km depth and even deeper at some locations, a wet granite composition at the mantle depth may run into a severe problem which can be overcome by limiting the wet granite to only the crust and a different composition in the mantle. Further discussions of other reasons arising particularly from the new seismic evidence in contrast with LISPB which may militate against granite composition are given in section 8.3 below.

FIGURE 8.5

Aeromagnetic map of SE Scotland (part of sheet 11, after Bullerwell, 1968). The solid circles show the 8 SUF AMT/MT profile sites and 3 of the Duns sites.

690
630
320
390

The resistive layer of the geoelectrical model with its varying thickness along the profile correlates very well with the Lower Palaeozoic greywackes from surface geology; this layer almost outcrops at the surface in the neighbourhood of BER and SCR.

8.1.2 Evidence from geophysical models from elsewhere

Geological and geophysical evidence now abounds from the work of several authors e.g., Hyndman and Cochrane (1971), Cochrane and Hyndman (1974), Edwards and Greenhouse (1975), Kurtz and Garland (1976), Phillips et al. (1976), Cochrane and Wright (1977), McKerrow and Cocks (1977) and Jones and Hutton (1979b) among others, in support of the similarity between the tectonic history of South Scotland and the Atlantic coast of North America. The good agreement between the results of Jones and Hutton (1979b) and the present 2D model has already been discussed. An MT study in eastern Canada (Kurtz and Garland, 1976) shows that a conducting lower crust overlies the resistive upper mantle in the Grenville Shield, while to the southeast in the Appalachian regions, a resistive lower crust overlies a conducting upper mantle. The authors have proposed that the boundary marking the change in the resistivity character may be related to the site of the Iapetus. It is important to note that the change in the conductivity pattern (transition zone) does not coincide with the Logan's Line which is the Shield boundary. Hence, the inference in the present study that the conductivity

feature in the neighbourhood of SAW and BUG is probably not associated with the SUF seems justifiable.

Dragert et al. (1980) have reported from their MT measurements in the Pemberton Volcanic Belt of British Columbia a good conductor (< 100 ohm-m) underlying a highly resistive (> 10000 ohm-m) crystalline complex at a depth of about 20 km. They have ascribed the cause of the enhanced conductivity to be due to hydration or partial melting.

Shallow good conducting zones similar to that in the 2D geoelectrical model of the present study have been reported by several workers mainly from MT, GDS and magnetometer array studies at many places of different tectonic environments. The following are some examples. The North American Central Plains anomaly (Camfield et al., 1971) is believed to be due to graphitic schists within a Proterozoic metamorphic belt and possibly related to a Proterozoic plate boundary (Camfield and Gough, 1977). The Southern Cape Conductive Belt crossing the southern tip of Africa from west to southeast (Gough et al., 1973; De Beer and Gough, 1980) is hypothesised as consisting of partly serpentinized basalt accumulated at the top of a Proterozoic subduction (De Beer et al., 1982). This is discussed further in section 8.3 below. De Beer et al. (1976,1982b) reporting respectively on the 1972 and 1977 magnetometer array studies in part of southern Africa have detected an anomalous zone at lithospheric depths crossing western Zimbabwe, Botswana and the Damara Orogenic Belt of South West Africa. This zone is believed to mark the

southwestward extension of the African Rift system along old weak zones in the lithosphere (De Beer et al., 1975). The resistivity structure in the Damara Belt has also been investigated by means of deep Schlumberger soundings (Van Zijl, 1977). Figure 8.6a shows the location of the 1972 magnetometer array and the position of the conductive structure detected by it (De Beer et al., 1976). Figure 8.6b shows geoelectrical sections across the Damara Belt based on the deep Schlumberger soundings (De Beer et al., 1982b) - (i) the transverse resistance (thickness-resistivity product) of the upper crust and (ii) the resistivity-depth section. The latter indicates that the conductive structure of resistivity less than 20 ohm-m is only 3 km below the earth's surface at some localities and is deeper elsewhere. The upper crust outside the conductive structure is resistive. Apart from the wider lateral extent of this conductor, its shape is remarkably very similar to that under the SUF profile in the present study particularly in the neighbourhood of SAW and BUG - compare Fig. 8.6b with Figs. 5.3a and 7.3a-c. Other examples of conductive zones are in the Gregory Rift Valley, Kenya (Banks and Ottey, 1974; Rooney and Hutton, 1977); in Iceland (Hermance and Garland, 1968; Hermance, 1973b; Beblo and Bjornsson, 1980); in the Rio Grande Rift Valley (Hermance and Pedersen, 1980); in the Carpathians (Adam, 1980; Jankowski et al., 1985); in the Adirondack Precambrian shield region of northern New York State (Connerney et al., 1980); in the Rhenish Massif, Germany (Jodicke et al., 1983); in Eyre Peninsula, South Australia (White and Milligan, 1984)

FIGURE 8.6

(a) The location of the 1972 magnetometer array in South West Africa, Botswana and Zimbabwe and the position of the conductive structure it detected (De Beer et al., 1976). The dots indicate the magnetometer stations.

(b) Geoelectrical sections across the Damara Belt, South West Africa. Transverse resistance (thickness-resistivity product) of the resistive upper crust (upper figure) and resistivity-depth section (bottom figure). The position of the conductor as detected by the 1977 magnetometer array is shown. AIM, OMB, etc., denote some of the magnetometer stations, while ES1, ES2, etc., are the positions of the deep Schlumberger sounding centres. The symbol c indicates a conductive substratum of undetermined resistivity (De Beer et al., 1982b).

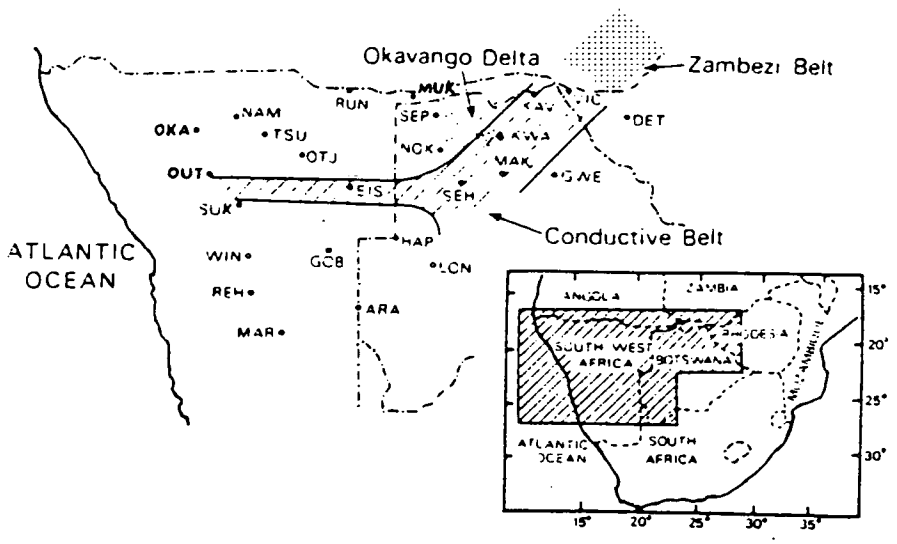
Okavango Delta
Zambezi Belt
Conductive Belt
ATLANTIC OCEAN
MUK
RUN
SEP
NAM
OKA
TSU
OTJ
NGK
MAK
DET
GWE
OUT
EIS
SEH
SUK
WIN
GCB
HAP
LCN
REH
ARA
MAR
ANGOLA
ZAMBIA
SOUTH WEST AFRICA
BOTSWANA
ATLANTIC OCEAN
SOUTH AFRICA
15°
20°
25°
30°
35°

[a]

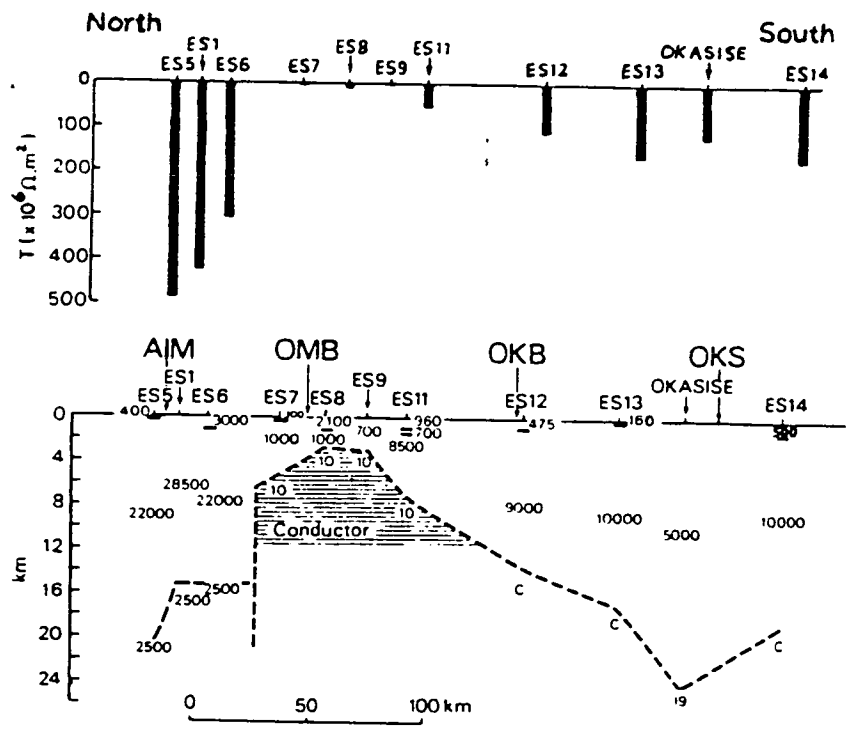
North
South
ES1
ES5
ES6
ES7
ES8
ES9
ES11
ES12
ES13
OKASISE
ES14
T (x 10⁶ Ω.m²)
0
100
200
300
400
500
AIM
OMB
OKB
OKS
400
3000
2100
960
1000
1000
700
700
8500
475
160
10
28500
22000
9000
10000
5000
Conductor
2500
km
4
8
12
16
20
24
0
50
100 km

[b]

and east of Broken Hill, New South Wales, Australia (Cull, 1985).

Thus, the geoelectrical model of the present study is not only in good agreement with the previous results in South Scotland, but it also exhibits features which are similar to those reported from studies in other regions.

8.2 Causes of high electrical earth conductivity

From a detailed discussion of laboratory measurements of electrical conductivity by Brace (1971) and Dvorak (1975) and global electrical conductivity models by Keller et al. (1966) and Banks (1969,1971) among others, conductivity is expected to increase on the average with depth owing to its dependence on porosity, pressure, temperature and other parameters. Consequently, the crust is expected to be resistive and the mantle conductive and a good example for this is part of the Canadian Appalachians (Kurtz and Garland, 1976). However, regions of higher conductivity than average in the crust, termed anomalous, have been identified and some examples of these have been enumerated above. Hence, the need to explore the causes of such anomalous conductivities.

There are a number of reviews on the correlation between conductivities and other geophysical parameters by authors such as Uyeda and Rikitake (1970); Law and Riddihough (1971); Gough (1973) and Garland (1975) among others. There are several factors which can contribute to electrical conductivity variations in the upper mantle, e.g.,

temperature, compositional changes, phase changes, pressure and partial melting. However, the main causes of high conductivity values in general have been categorised (Stanley et al., 1977) as

(a) mineral or electronic conduction; (b) electrolytic conduction; (c) partial melting and (d) the effects of rock alterations.

(a) Mineral or electronic conduction in rocks is the migration of charge carriers through the solid lattice and is basically the same process as in a typical semiconductor. It is generally not very important at temperatures below 700^0C. Thus, at characteristic crustal temperatures electronic conduction is not a significant cause of high conductivity in the crust. This is clearly borne out by Brace's (1971) calculation of the maximum and minimum effects of electronic conduction in several different types of rocks. At greater depths than the crust, with the higher temperature, electronic conduction (semiconduction) is probably significant.

(b) Electrolytic conduction is as a result of the presence of conducting pore fluids in rocks. This conduction process is dependent on mobility, concentration and degree of dissociation of ions in the solvent, rock porosity, prevailing pressure and fluid salinity. Archie's (1942) Law gives the empirical relation in simple form for electrolytic conduction in terms of bulk conductivity as

$$\sigma_r = \sigma_f \eta^k \qquad (8.1)$$

where σ_r is the overall rock conductivity, σ_f the pore fluid conductivity, η the porosity and k is between 1 and 2. The most deciding factor is the porosity. From the calculated variation of the porosity of continental, sub-continental and oceanic rocks with depth by Dvorak (1975) and from Hermance's (1973b) calculation of how temperature and pressure effects on porosity control the pore fluid conductivity variation with depth, electrolytic conduction appears to be significant only at depths less than about 15 km. However, Berdichevsky et al. (1972) have stated that water can be released from hydrated minerals during metamorphism. Their estimated percentage of water in minerals of amphibolitic facies is 1-5 and that the water is released by dehydration at the boundary with granulitic facies. The released water, which is intergranularly distributed, may significantly reduce the rock resistivity.

Thus, even though electrolytic conduction may be very small in the lower crust owing to closure of cracks and pores by pressure, mineral dehydration may give rise to low resistivities in the lower crust.

(c) Partial melting of rocks caused by enhanced temperatures in the upper mantle and localized areas of the lower crust can increase the electrical conductivity considerably. Hyndman and Hyndman (1968) have pointed out that partial melting occurs during the advanced stages of metamorphism and that the presence of water can significantly lower the starting temperature of melting. Conductivity measurements on basalts at 28 kb by Khitarov et al. (1970), although not extending above the liquidus

temperatures, indicate that melting can cause an abrupt conductivity increase of 1 to 2 orders of magnitude. The experimental work of Presnall et al. (1972) has also shown an increase of two orders of magnitude in the conductivity of synthetic basalt in the melting interval between 1130^0 and 1265^0C. Similar results have also been reported by Shankland and Waff (1977).

Although hot springs and abnormally high heat flows are surface manifestations of conductivities caused by partial melting, the lack of surface features does not necessarily rule out partial melting. Berdichevsky et al. (1972) have opined that as little as 1-2% of liquid phase, although too small to give rise to these surface manifestations, is sufficient to provide a significant conducting pathway through the rock. Waff (1974) has indicated from theoretical viewpoint that beyond the melting point and with the degree of melting greater than a critical value, the bulk conductivity of the mantle depends on the properties of the liquid phase. Waff has also stated that if the melt is in the form of isolated pockets, the bulk conductivity is close to that of the parent rock, but if the melt is interconnected, then the bulk conductivity may be increased by several orders of magnitude by even very small melt fractions. Based on network model calculations, Waff's estimate of the bulk conductivity is $2c\sigma/3$, where c is the melt fraction and σ is the melt conductivity.

(d) The alteration of rocks may also give rise to high electrical conductivities (Stanley et al., 1977) in a similar way as fluid conduction. The lining of the pore walls by

alteration products can provide low resistance pathways and any pore fluids present may be sealed into the rock. The latter provides another mechanism whereby fluid can be retained at depths (> 20 km) in the lower crust and even beyond and hence give rise to enhanced conductivities either by electrolytic conduction or by lowering the melting temperature.

Localized mineralisation can give rise to high conductivity on a small scale. Anomalous conductivity enhancement can be caused by the accumulation of highly conducting minerals like graphite, pyrite or magnetite. A review of laboratory studies on the variation of conductivity with temperature in rocks and minerals has been given by Shankland (1975).

8.3 Significance and plausible composition of the conductive zone of the 2D geoelectrical model

From the above discussions of the general causes of enhanced electrical conductivities, a number of deductions can be made about the possible causes which can give rise to the upper/lower crustal and upper mantle conductor depicted by the 2D geoelectrical model of SE Scotland. The most probable cause of the upper mantle conductor is partial melting resulting from enhanced temperatures in the mantle. Partial melting may also contribute in part to the cause of the lower crustal conductor; Schwarz et al. (1984) have interpreted their low crustal resistivities in the Andes in Northern Chile as being due to partial melting.

From Waff's (1974) expression for bulk conductivity already referred to, partial melt fractions of only 1.5% and 7.5% will suffice to produce bulk resistivities of 100 and 20 ohm-m respectively assuming 1 ohm-m for the melt conductivity.

It is highly unlikely that the upper crustal conductor is as a result of either solid conduction in dry rocks or partial melting since temperatures in excess of 700^{0}C are necessary at a few km depth. It seems likely that the enhanced conductivity in the upper and lower crust is due to a combination of factors, viz, presence of water (brine), ore mineralisation (e.g., carbon, sulphides and oxides), graphites, hydrated minerals and possibly rock alteration effects. The most dominant factor is very likely to be electrolytic conduction in the fluids contained in the rock pores and fissures and there may be in addition high temperature gradients. Brace (1971) has indicated that rocks below the water table are saturated with aqueous solutions to depths greater than 5 km. There is evidence from Hermance (1973b) that a large temperature gradient can reduce the resistivity of saturated upper crustal rocks by up to one order of magnitude. The presence of aqueous fluids is increasingly becoming the favoured factor responsible for the low electrical resistivity of crustal rocks (Connerney et al., 1980; Lee et al., 1983; Shankland and Ander, 1983; Jankowski et al., 1985; Haak and Hutton, 1985 among others).

Up to date no heat flow measurements have been made in SE Scotland and consequently the present thermal state

of the area is unknown; a knowledge of the latter will be an invaluable aid to assessing the subsurface composition of the area. All the available heat flow measurements in the United Kingdom (e.g., Richardson and Oxburgh, 1978; Oxburgh et al., 1980 and Lee et al., 1985) are concentrated mainly in England and a few in Northern Scotland and Wales. From their few measurements, Oxburgh et al. (1980) have presented a heat flow map of Britain defining broad belts of above average heat flow; they have also given an empirical linear correlation between heat flow (q_0) and surface heat production (A_0). Lee et al. (1985) using their new data have resolved some of the previous broad belts into separate components which reflect to some extent the geological structure and tectonic history of the U.K. They have also indicated that no single linear q_0-A_0 correlation is appropriate for the whole U.K. and that the existing data are insufficient to define the individual linear q_0-A_0 relationships. However, Ingham and Hutton (1982b) have used the q_0-A_0 relationship derived by Oxburgh et al. to estimate temperature-depth profiles for South Scotland. In the light of the evidence of Lee et al., the temperature-depth profile of Ingham and Hutton may require substantial revision.

Considering only resistivity, there are a number of possible candidates for the composition of the enhanced conductivity zone of the geoelectrical model, e.g., graphitic schist, basalts, gabbros, amphibolites, peridotites, etc. However, with other geophysical evidence to be satisfied as well, the number of possible candidates is narrowed down.

The gravity interpretation of the SUF profile has already been discussed above where it has been indicated that the proposed granite batholith from the gravity studies needs to be wet in order to satisfy the MT model and limited to crustal depths. Even then there are still some inherent problems. The present study as well as the previous longer period MT studies indicate that the conducting layer exists in both the Midland Valley and the Southern Uplands. This fact implies similar composition and hence it is a point not in favour of granite batholith underlying both the Midland Valley and the Southern Uplands. This is because the former is generally characterized by low lands and the latter by high elevation, while granite batholiths are usually associated with elevated ground (e.g., the Highlands) as has been demonstrated by Bott (1956), Bott and Masson-Smith (1957), for example.

Although there are no seismic studies directly along the present MT profile, but LISPB is to the west and there are also seismic refraction studies by Warner et al. (1982) along the SUF (i.e., along strike) and by Hall et al. (1983) across strike to the west of the MT profile. In contrast to LISPB, the new seismic studies indicate a modest lateral variation in the seismic velocity layering in the Southern Uplands typically indicating a P-wave velocity of 6 kms^{-1} at about 1 km depth increasing to 6.3 kms^{-1} at 2-5 km depth, 6.5 kms^{-1} at 10-15 km and higher than 6.5 kms^{-1} at depths greater than 20 km (Warner et al., 1982). Hall et al. (1983) have shown similar evidence. This new seismic evidence (> 6.3 kms^{-1}) militates against granite composition since the

velocities in granite are usually less than 6 kms^{-1}.

From both MT and gravity studies, there is evidence that the zone has a high conductivity and a low density. Its density value is 2650 kgm^{-3} (from Lagios and Hipkin, 1982) and hence a graphitic schist composition is inappropriate owing to its insignificant density contrast with the surrounding. Although the aeromagnetic anomalies (Fig. 8.5) are generally smooth and weak in the eastern Southern Uplands, but in the part of the Southern Uplands near the SUF and in the Midland Valley, the anomalies are stronger with the amplitude reaching 200 nT and even greater in some localities. Thus, the author concludes that the low density, enhanced conductivity zone exhibits some moderately strong aeromagnetic anomalies, with the latter implying at least moderate magnetisation. This evidence coupled with the new seismic evidence of Warner et al. (1982) and Hall et al. (1983) as well as the topographical characteristics of the Midland Valley and the Southern Uplands appear collectively to militate against granite composition.

It is thus provisionally proposed here that a partly serpentinized basaltic composition will satisfy the above geophysical evidence indicating the presence of a large volume of rock of high electrical conductivity, moderate magnetisation and low density. This proposed composition overcomes the shortcomings of the granite composition already referred to.

De Beer et al. (1982) have proposed that the crust of the Southern Cape Conductive Belt (SCCB) contains a mass of

partly serpentinized basalt (10-20% serpentine) accumulated there during Proterozoic subduction of oceanic crust from the south. They have based their hypothesis on the combined geophysical evidence which indicates the presence in the crust beneath the SCCB, of a large volume of rock of high conductivity, high magnetisation and a density of 2900 kgm^{-3}. Figure 8.7a shows schematically current concentrations within the SCCB. Figure 8.7b shows the conductive belt in relation to basement age provinces and the axis of the static magnetic anomaly, while a gravity model along a north-south section is shown in Fig. 8.7c. Apart from the high magnetisation and the higher density, the geophysical evidence is similar to that applicable in SE Scotland. Hence, a similar composition for both SE Scotland and the SCCB seems justifiable, but different percentage of serpentinization to account for the different magnetisation and density. De Beer et al. (1982) have discussed the process of formation of serpentinized rock and an extract from this is given here.

The reaction between basic silicates and water in the temperature range 200-500^{0}C leads to the formation of serpentine, $H_4Mg_3Si_2O_9$. Although there are several possible reactions for this formation, but it appears to proceed with minimal volume change in geological occurrences. Hence in view of the latter condition, Turner and Verhoogen (1960) prefer the reaction:

FIGURE 8.7

(a) The Southern Cape Conductive Belt (SCCB), South Africa with the current concentrations within it indicated by density of stippling.

(b) The conductive belt in relation to basement age provinces and the axis (line of crosses) of the static magnetic anomaly.
The dots show the magnetometer positions in the array (after De Beer and Gough, 1980).

(c) Observed Bouguer anomalies and calculated anomalies for the gravity model shown, along a north-south section near 22.5^{0}E. The densities are in kgm^{-3}.
The body C is in the conductive belt (after De Beer et al., 1982).

[a]

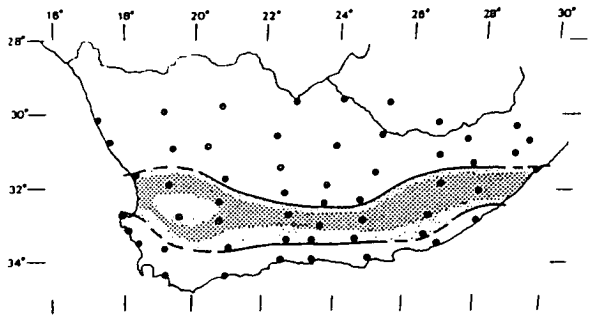
16°
18°
20°
22°
24°
26°
28°
30°
28°
30°
32°
34°

[b]

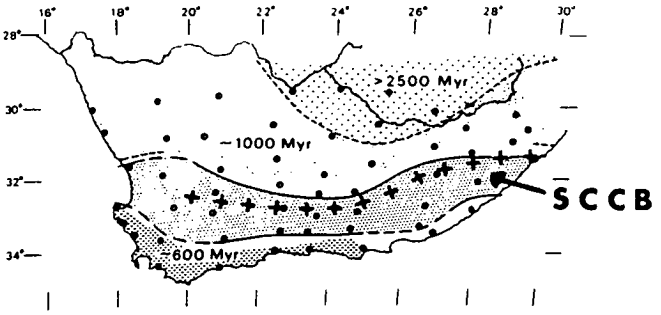
16°
18°
20°
22°
24°
26°
28°
30°
28°
30°
32°
34°
>2500 Myr
~1000 Myr
~600 Myr
SCCB

[c]

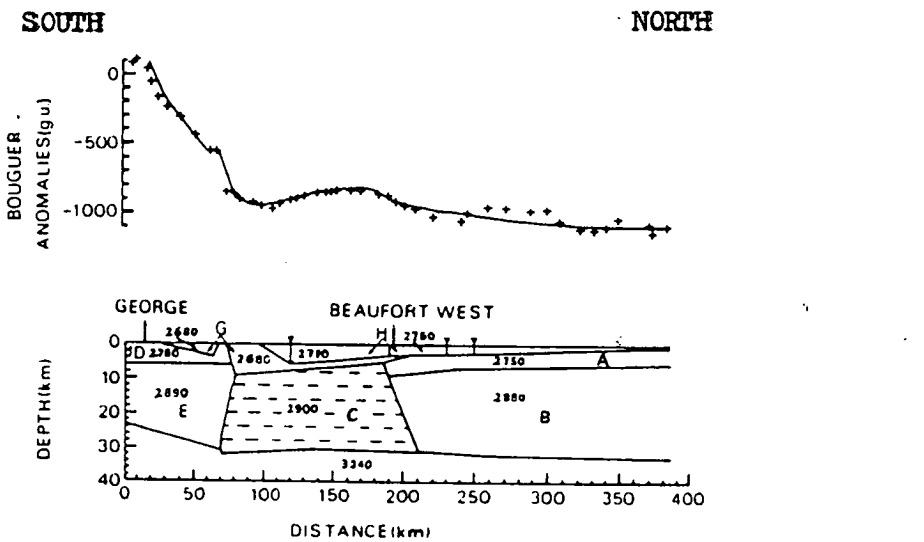
SOUTH
NORTH
BOUGUER ANOMALIES (gu)
0
-500
-1000
GEORGE
BEAUFORT WEST
DEPTH (km)
0
10
20
30
40
2680
G
H
2760
2760
2680
2710
2750
A
2890
E
2900
C
2880
B
3240
0
50
100
150
200
250
300
350
400
DISTANCE (km)

$$5Mg_2SiO_4 + 4H_2O \rightarrow 2H_4Mg_3Si_2O_9 + 4MgO + SiO_2 \qquad (8.2)$$

Olivine +water $\rightarrow$ serpentine + removed in solution

This reaction is dependent on the combined concentration of MgO and SiO_2 remaining low and hence large quantities of circulating water are essential. Fyfe et al. (1978) have indicated that convection of ocean water through porous newly formed basalts produces the requisite temperature conditions and the abundant water flow through the newly extruded basalt.

There are three crystalline forms of serpentine, viz, chrysotile, antigorite and lizardite and they are all porous. Most olivines and pyroxenes contain iron which is rejected from the serpentine and precipitated as magnetite. This precipitated magnetite is dominantly responsible for the electrical conductivity and the magnetic susceptibility of serpentinized rocks.

There are density data for serpentinites, e.g., Stesky and Brace (1973) have quoted 2250 kgm^{-3} with 14.5% porosity for a serpentinite (lizardite and chrysotile) from the Indian Ocean Ridge; 2500-3130 kgm^{-3} for serpentinized peridotite and 2570-2620 kgm^{-3} for serpentinized lherzolite. De Beer et al. (1982) have indicated that any density in the range from 2250 kgm^{-3} (100% serpentine) to about 3000 kgm^{-3} (unaltered basalt) can be provided by basaltic rock serpentinized in an appropriate fraction. Thus, the density of 2650 kgm^{-3} from the gravity model of Lagios and Hipkin (1982) will require slightly less than 47% serpentine; a higher density will imply a lower percentage of serpentine.

Mooney and Bleifuss (1953) have shown that the concentration of magnetite in fresh basalt is typically 1%. De Beer et al. (1982) have stated that the serpentinized fraction f required to give an overall magnetite percentage p' is given by

$$f = (p' - p_b)/(p_s - p_b) \qquad (8.3)$$

where p_b, p_s are the volume percentages of magnetite in the unaltered basalt and serpentinite respectively. From Mooney and Bleifuss (1953), p_b=1. Since the aeromagnetic anomalies in SE Scotland are only moderately strong, it may be justifiable to say that p' is perhaps not much larger than p_b and hence p_s is not large compared with p_b. Consequently, a large value of f is quite easily attainable. For instance if p'=1.12 and p_s=1.25, then with p_b=1, f=0.48, i.e., 48% serpentine which more than satisfies the density requirement earlier referred to. The parameters (p_s and p') can be varied to get the right mix of density, magnetisation and conductivity and consequently variations in the latter quantities, even locally, can be easily taken into account. Thus, a partly serpentinized basaltic composition is a simple and very versatile interpretation.

8.4 Tectonic implications of the 2D geoelectrical model

The present geoelectrical model indicates that the crustal/mantle conductor dips to the north and south of SAW and BUG respectively. It has been suggested in section

8.1.1 that this dipping may be associated with ancient subduction and hence related in some way to the Iapetus suture. Some of the several tectonic models which have been proposed for parts of the British Caledonides have been discussed in section 1.4.1. Figure 8.8 illustrates some of these tectonic models. It may be noted that no single model is entirely satisfactory so far; they indicate either northward or southward subduction or both. Thus, it can be said that the inferred subduction in the present study is in agreement with some of the tectonic models in this respect. It does appear that there may well have been a series of episodes of complex and possibly interrelated subduction in South Scotland. The latter has been demonstrated by Hutton et al. (1985) in their overview of the four separate MT studies which have now been undertaken in the Iapetus suture region. It may be noted that no definitive tectonic implications can be obtained from the geoelectrical model until additional extensive AMT/MT work is undertaken in South Scotland as a whole to delineate the exact lateral depth variation to the crustal/mantle conductor throughout the region. In addition, other geophysical as well as geological work need to be done in order that many critical facts, which are at present elusive, may be collected. Some suggestions in this connection are outlined in section 8.6 below.

FIGURE 8.8

Diagrams illustrating some of the models which have been proposed for parts of the British Caledonides (from Holland et al., 1979):

(i) after Dewey (1969); (ii) after Fitton and Hughes (1970); (iii) after Jeans (1973) and Gunn (1973); (iv) after Church and Gayer (1973); (v) after Lambert and McKerrow (1976); (vi) after Wright (1976) and (vii) after Phillips, Stillman and Murphy (1976).

The letters denote:- HBF, Highland Boundary Fault; SUF, Southern Uplands Fault; LD, Lake District; MT, Moine Thrust; TD, Tweedale; c, continental crust; o, oceanic crust and r, spreading ridge.

Dashed lines indicate early positions of subduction zones.

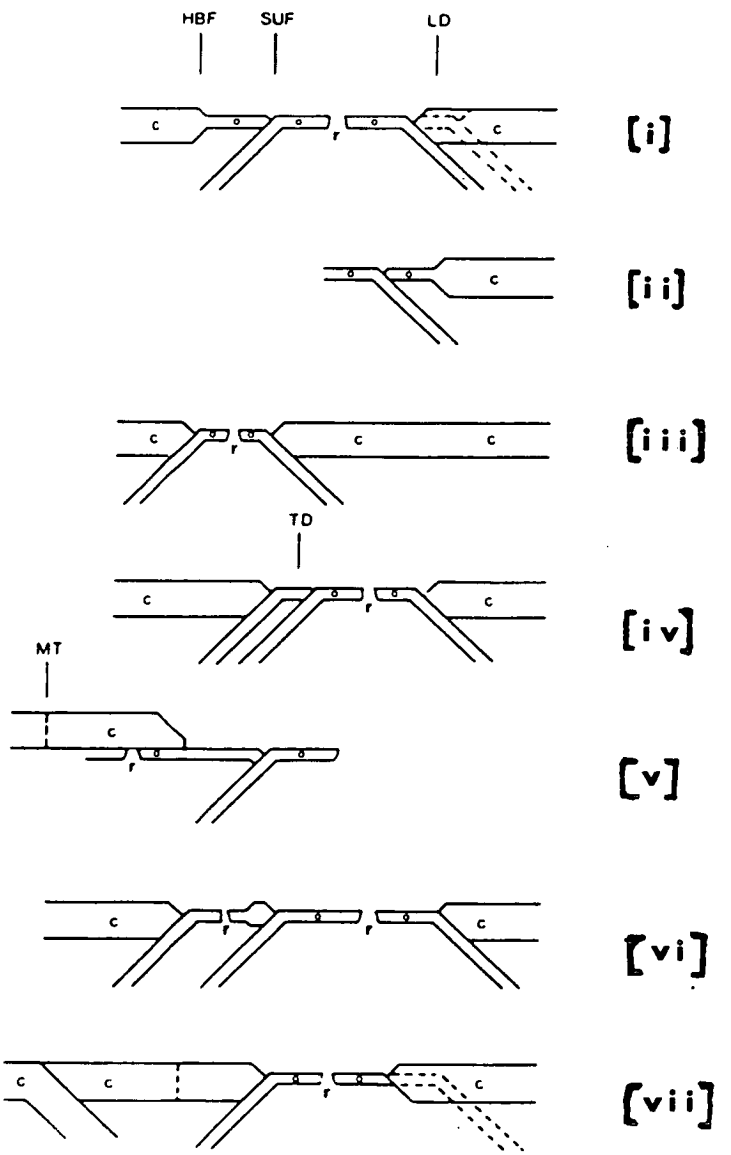
HBF
SUF
LD
c
r
[i]
[ii]
[iii]
TD
[iv]
MT
[v]
[vi]
[vii]

8.5 Overall summary and conclusions

8.5.1 Overall summary

Magnetotelluric (AMT/MT) soundings were made in 1982-84 at 22 sites in SE Scotland in the frequency range 0.01 to 1000 Hz using close station spacings. The natural temporal variations in the magnetic and electric components of the earth's field (3 magnetic and 2 electric components) were simultaneously recorded. These are the first detailed AMT measurements in this region. In addition to the AMT/MT measurements, VLF/R measurements were also made at 10 of the sites. Eight of the sites lie on a profile ($N40^{0}W$ geographic) approximately perpendicular to the Southern Uplands Fault (SUF) and these constitute the SUF profile study; 12 sites constituting the Duns study lie in a 2D array near Duns, where Habberjam deep resistivity methods have previously been used by the Leeds University group. The remaining two sites near Coldingham lie to the northeast of Duns area.

The data recordings were split into four overlapping bands and termed bands 1 to 4. Bands 1 to 3 constituted the audiofrequency magnetotelluric (AMT) and band 4 the MT. For the AMT data recordings, the Edinburgh Short Period Automatic Magnetotelluric system (Mk. 1) was used. This was a battery operated, digital 5 component data acquisition system which automatically selected and recorded data, analysed the data and plotted the results in real-time. A N.E.R.C. geologger was used to digitally record the MT data. This recorded all the field variations

without any infield data analysis capability.

The data have been analysed using classical tensorial analysis techniques. In order to elucidate the possible effects of data averaging on the earth's response functions, a comparison of averaging techniques is presented. From the comparison, it is concluded that it is more preferable to average impedance tensor elements lognormally than linear spectra averaging. Owing to the inevitable nearness to industrial works, there was considerable cultural noise problem at some of the SUF profile sites. A qualitative approach for processing noisy data was devised in order to extract some useful results from these. Further development of this approach will no doubt extend the application of the AMT/MT technique to very culturally noisy areas.

The AMT/MT data analysis results are presented at each site in terms of the apparent resistivity and phase plots, the corresponding Bostick transform resistivity-depth plots, average predicted coherences, number of estimates, skew and azimuth of major impedance plots.

In addition to the direct 1D inversion of the apparent resistivity and phase data using the Bostick transform, 1D layered modelling of the data has also been carried out using a Monte-Carlo algorithm. It is shown that it is preferable to model the invariant apparent resistivity and phase data (ϱ_{eff}, φ_{eff}) emanating from the determinant of the impedance tensor. The importance of modelling both the apparent resistivity and phase data cannot be overemphasized. A comparison of the Monte-Carlo layered

resistivity-depth models with the continuously varying resistivity-depth profiles resulting from the direct data inversion using the Bostick transform shows an excellent agreement. The computational time for the latter is less than 10% of that for the former. Hence, the Bostick transform is computationally efficient and is thus advantageous to incorporate it in real-time and routine MT analysis as a useful aid to interpretation.

A detailed comparison of the AMT/MT and Habberjam deep resistivity technique (HAB) is given and the 1D models for the Duns area obtained from the two techniques are compared. There is an excellent general agreement in the depth range of the subsurface (≈1.2 km) resolved by HAB. However, the AMT/MT technique provides more information at depth as well as a clear indication of the lateral variation in the electrical conductivity structure within the area. It is demonstrated very clearly that AMT/MT is a more useful low cost rapid coverage resistivity mapping technique and hence more suitable for reconnaissance survey than HAB. A detailed evaluation of both techniques from the exploration viewpoint reveals that AMT/MT is more cost- and exploration-effective with a much greater depth and lateral resolution.

For the purpose of the 2D modelling, the Duns sites have been projected on to the SUF profile to give a single traverse of 20 sites extending from N40^{0}W to S40^{0}E through a distance of 35.3 km. The remaining two sites to the northeast of Duns area are too far to be projected on to the profile and hence have been omitted. The data at the

20 sites have been rotated to a fixed azimuth of N50^{0}E geographic, with the E-polarisation direction parallel to the SUF and H-polarisation perpendicular to it. This corresponds to a fixed azimuth of N57^{0}E magnetic (used in the computer programme) having taken the magnetic declination as 7^{0}W of geographic north.

A collation of the individual site 1D models is presented in the form of a simplified 2D section and it demonstrates clearly the importance of close station spacings for a proper resolution of the subsurface structures.

Using the simplified 2D section as a basis for a starting model, 2D numerical modelling of the measured AMT/MT data has been done using a computer programme written by Brewitt-Taylor and Johns (1980) based on the modified finite difference method of Brewitt-Taylor and Weaver (1976). Model parameters (layer resistivities and depths) have been varied extensively in a trial and error fashion to obtain a satisfactory fit to the E- and H-polarisation apparent resistivity and phase data at all the sites. The resulting final 2D geoelectrical model and the fit of the model curves to the data at each of the sites are presented. The overall fit of the model curves to the measured data is generally very good.

The 2D geoelectrical model indicates a series of conductive layers (< 100 and 100-500 ohm-m) of varying thickness within the uppermost 2 km of the subsurface. The <100 ohm-m layer thins rapidly from north to south across the SUF. This series of layers is interpreted as a conductive sedimentary cover. This is thinnest under BER

and SCR (≈0.2 km) and thickens forming basin-like structures north and south of these sites respectively. The sedimentary cover is underlain by a resistive layer (> 1000 ohm-m). This layer is thinnest (<3 km) in the neighbourhood of SAW and BUG and it almost outcrops on the surface at BER and SCR. It is about 9 and 17 km thick respectively at the northwest and southeast ends of the profile.

Beneath the resistive layer is a good conductor (< 100 ohm-m) whose upper boundary is at depths varying from the upper crust to the lower crust. The base of the conductor lies within the upper mantle.

Beneath the conductor is a resistive layer (1000 ohm-m). This layer is not actually penetrated through by the longest period used in the present study and hence only the minimum depth to it is resolved. Its resistivity has been kept fixed at 1000 ohm-m.

The general causes of enhanced electrical conductivities are discussed. The possible causes which can give rise to the upper/lower crustal and upper mantle good conductor depicted by the 2D geoelectrical model are given. A simple versatile composition of the conductor as serpentinized basalt is postulated here based on a joint assessment of the aeromagnetic, gravity and MT results.

8.5.2 Conclusions

A detailed comparison of the 2D geoelectrical model obtained in the present study with previous results in

South Scotland and other regions indicates a good agreement. The present model provides a much better resolution of the subsurface structures than in the previous studies owing to close station spacing, broadband data and improved data quality. It can be clearly seen that the subsurface structural resolution is better in the Duns area than elsewhere on account of the very close station spacing (< 1 km). This thus underscores the importance of close station spacing for effective resolution of the subsurface structure, particularly the detection of its lateral variation.

The following main conclusions are drawn from the geoelectrical model:

(i) The 2D geoelectrical model indicates a significant lateral variation in the electrical conductivity structure in the region. A series of conductive sedimentary basin-like structures of varying thickness is in evidence within the uppermost 2 km.

(ii) The model exhibits more near-surface complexity in the Midland Valley than in the Southern Uplands in good agreement with the more complex geology in the former than in the latter.

(iii) The existence of a significant low resistivity layer in the lower crust and upper mantle, indicated by earlier studies, is confirmed by the present study which clearly delineates the hitherto poorly resolved upper boundary of the conductor. The conductor extends into the upper crust and the lateral depth variation to it is clearly delineated.

(iv) This conductor rises near to the earth's surface very noticeably (<4 km depth) in the neighbourhood of SAW and BUG and the axis of an elongated magnetic variation anomaly. It dips to the north and south of these sites. This conducting zone is suggested as being associated with ancient subduction and hence related to the Iapetus suture. It is also suggested that the conducting zone is responsible for the magnetic variation anomaly. This thus provides the hitherto unknown near-surface conductive zone coincident with the magnetic variation anomaly.

(v) A localized lateral variation in the depth to the crustal and upper mantle conductor is clearly in evidence in the Duns area in the neighbourhood of KET. This may probably be coincident with a fault zone.

(vi) The most probable cause of the upper mantle conductor is partial melting resulting from enhanced mantle temperatures. Partial melting may be partly responsible for the lower crustal conductor. The enhanced conductivity in the upper and lower crust may be due to a combination of factors - presence of fluid, ore mineralisation, graphites, hydrated minerals, rock alteration effects and there may be in addition high temperature gradients. The most dominant factor is probably electrolytic conduction in the fluids contained in the rock pores and fissures.

(vii) It is proposed here that a partly serpentinized basaltic composition is a simple and versatile means of satisfying the geophysical evidence indicating the presence in SE Scotland of a large volume of rock of high electrical conductivity, moderate magnetisation and low density. This

proposed composition overcomes the shortcomings of the granite composition proposed from previous gravity studies.

(viii) From 1D modelling investigations, it is clearly demonstrated that a very thin and very conductive upper/lower crustal layer is precluded by the AMT and MT data.

(ix) A comparison of the final 2D geoelectrical model with a 2D section derived from a collation of individual 1D models resulting from the invariant data, ϱ_{eff} and φ_{eff}, shows very close agreement. This clearly demonstrates that ϱ_{eff} and φ_{eff} do give correct averages for both 1D and 2D structures in this case. This is in agreement with the generalization of Ranganayaki (1984).

(x) The close agreement between the final 2D model and the 2D section of the individual site 1D models of ϱ_{eff} and φ_{eff}, especially with respect to any geophysical inferences which may be made, calls to question the justification for the additional effort and cost which 2D modelling entails. It is suggested that 1D modelling of the E- and H-polarisation responses may be used additionally to provide extreme bounds on the 2D section.

8.6 Suggestions for future work

In the present work some speculations have been put forward and hence warranting further studies to fully investigate them.

It is of considerable interest that to the southwest of the present AMT/MT profile, a number of profile studies be

undertaken across the Southern Uplands Fault and the South Scotland magnetic variation anomaly to investigate whether or not the conductivity structure of the present study is indeed continuous along the anomaly axis. For effective resolution of the subsurface structures, it is essential to use close station spacings (<1 km) and a wide frequency band spanning 16 kHz (VLF) to at least 1000 s.

Along the present profile, additional high frequency (16 kHz to 600 Hz) and long period (up to 1000 s) AMT/MT data need to be acquired at some of the present sites as well as the acquisition of the wide frequency band data at new sites so as to reduce the station spacings particularly along the SUF profile as well as extend the entire profile north and south. The interpretation of the combined new data set and the existing one will help resolve properly the subsurface structure and hence the exact depth variation to the high conductivity crustal/mantle layer can be mapped throughout the whole of South Scotland. This may enable the possible ancient subduction zones to be clearly identified and thus make possible the definitive assessment of the tectonic implications of a geoelectrical model for the region.

It is desirable that a concerted effort be made to measure high quality vertical magnetic field variations along the above profiles. The interpretation of these data will help immensely in ascertaining the structural strike direction as well as in better constraining the depth extent of the enhanced conductivity zone.

Detailed heat flow measurements in SE Scotland are highly desirable. These will shed light on the thermal state of the subsurface and hence give some idea of its possible composition. It may be noted that these measurements will be helpful in evaluating the geothermal prospects of the area.

A detailed static magnetic survey, geochemical and petrological studies in SE Scotland will be quite helpful in ascertaining whether or not the partly serpentinized basaltic composition proposed in the present study is plausible. It may be pointed out that at the end of the day, a direct way of knowing the exact subsurface composition is by means of very deep boreholes. However, the cost of the latter is quite high.

BIBLIOGRAPHY

Adam A., 1980

The change of electrical structure between an orogenic and an ancient tectonic area (Carpathians and Russian Platform), J. Geomagn. Geoelectr., 32, 1-46.

Agger H. E. and Carpenter E. W., 1964

A crustal study in the vicinity of the Eskdalemuir seismological array station, Geophys. J. R. astr. Soc., 9, 69-83.

Alperovitch I. M., Busnov V. P., Varlamov D. A., Konnov Yu. K., Konovalov Yu. F., Koschlakov G. V., Chernyaskii G. A., Sheinkman A. L. and Yakovlev I. A., 1982

Magnetotellurics in oil exploration in the U.S.S.R.: K. Vozoff (editor), SEG publication (Eng. trans.).

Archie G., 1942

The electrical resistivity log as an aid in determining some reservoir characteristics, Trans. Am. Inst. Min. Metall. Engrs., 146, 54-61.

Bailey R. C. and Edwards R. N., 1976

The effect of source field polarisation on geomagnetic anomalies in the British Isles, Geophys. J. R. astr. Soc., 45, 97-104.

Bailey R. C., Edwards R. N., Garland G. D., Kurtz R. and Pitcher D.H., 1974

Electrical conductivity studies over tectonically active area in Eastern Canada, J. Geomagn. Geoelectr., 26, 125-146.

Bamford D., Faber S., Jacob B., Kaminski W., Nunn K., Prodehl C., Fuchs K., King R. and Willmore P., 1976

A lithospheric seismic profile in Britain-I: preliminary results, Geophys. J. R. astr. Soc., 44, 145-160.

Bamford D., Nunn K., Prodehl C. and Jacob B., 1977

LISPB-III: Upper crustal structure of Northern Britain, J. Geol. Soc. London, 133, 481-488.

Bamford D., Nunn K., Prodehl C. and Jacob B., 1978

LISPB-IV: Crustal structure of Northern Britain, Geophys. J. R. astr. Soc., 54, 43-60.

Banks R. J., 1969

Geomagnetic variations and the electrical conductivity of the upper mantle, Geophys. J. R. astr. Soc., 17, 457-487.

Banks R. J., 1972
The overall conductivity distribution of the earth, J. Geomagn. Geoelectr., 24, 337-351.
Banks R. J., 1973
Data processing and interpretation in geomagnetic deep sounding, Phys. Earth Planet. Inter., 7, 339-348.
Banks R. J., Beamish D. and Geake M. J., 1983
Magnetic variation anomalies in northern England and southern Scotland, Nature, 303, 516-518.
Banks R. J. and Ottey P., 1974
Geomagnetic deep sounding in and around Kenya Rift Valley, Geophys. J. R. astr. Soc., 36, 321-335.
Baransky L., Golikov Yu., Feygin F., Harchenko I., Kangas J. and Pikkarainen T., 1981
Role of the plasmapause and ionosphere in the generation and propagation of pearl pulsations, J. Atm. Terr. Phys., 43, 875-881.
Beamish D., 1979
Source field effects on transfer functions at mid-latitudes, Geophys. J. R. astr. Soc., 58, 117-134.
Beblo M. and Bjornsson A., 1980
A model of electrical resistivity beneath N.E. Iceland, correlation with temperature, J. Geophys., 47, 184-190.
Bendat J. S. and Piersol A. G., 1971
Random data: Analysis and measurement procedures, Willey-Interscience, New York.
Bennett D. J. and Lilley F. E. M., 1972
Horizontal polarisation in array studies of anomalous geomagnetic variations, Nature Physical Sci., 237, 8-9.
Bentley C. R., 1973
Error estimation in two-dimensional magnetotelluric analyses, Phys. Earth Planet. Inter., 7, 423-430.
Berdichevsky M. N., 1960
Electrical prospecting by the telluric current method, Gostoptekhizdot, Moscow.
Berdichevsky M. N., Vanyan L. L., Feldman I. S. and Porstendorfer G., 1972
Conducting layers in the earth's crust and upper mantle, Gerlands. Beitr., Geophysik, 81, 187-196.
Berkman E., Orange A. and Smith R. D., 1984

Seismic and magnetotellurics combined: A case history of the South Clay Basin Prospect (abstr.), Geophysics, 49, 599 (paper presented at the 53rd annual international SEG Meeting in Las Vegas, 1983).

Blaxland A. B., Aftalion M. and Van Breeman O., 1979
Pb isotopic composition of feldspars from Scottish Caledonian granites and the nature of the underlying crust, Scott. J. Geol., 15, 139-151.

Bosinger T., Alanko K., Kangas J., Opgenoorth H. and Baumjohann W., 1981
Correlations between PiB type magnetic micropulsations, auroras and equivalent current structures during two isolated substorms, J. Atm. Terr. Phys., 43, 933-945.

Bostick F. X. (Jr.), 1976
A simple and almost exact method of magnetotelluric analysis (abstr.), Workshop on Electrical Methods in Geothermal Exploration, Snowbird, Utah.

Bostick F. X. (Jr.) and Smith H. W., 1962
Investigation of large-scale inhomogeneities in the earth by the magnetotelluric method, Proc. Inst. Radio Engrs., 50, 2339-2346.

Bott M. H. P., 1956
A geophysical study of the granite problem, Quart. J. Geol. Soc. London, 112, 45-67.

Bott M. H. P. and Masson-Smith D., 1957
The geological interpretation of a gravity survey of the Alston Block and the Durham Coalfield, Quart. J. Geol. Soc. London, 113, 93-117.

Brace W. F., 1971
Resistivity of saturated crustal rocks to 40 km based on laboratory measurements: in The structure and physical properties of the earth's crust (Heacock J. G., editor), Amer. Geophys. Un. monograph, 14, 243-255.

Brewer J. A., Matthews D. H., Warner M. R., Hall J., Smythe D. K. and Whittington R. J., 1983
BIRPS deep seismic reflection studies of the British Caledonides, Nature, 305, 206-210.

Brewer J. A. and Smythe D. K., 1984
MOIST and the continuity of crustal reflector geometry along the Caledonian-Appalachian orogen, J.

Geol. Soc. London, 141, 105-120.

Brewitt-Taylor C. R. and Johns P.B., 1980
Diakoptic solution of induction problems, J. geomagn. Geoelectr., Suppl. I, 32, 73-80.

Brewitt-Taylor C. R. and Weaver J. T., 1976
On the finite difference solution of two-dimensional induction problems, Geophys. J. R. astr. Soc., 47, 375-396.

Bullerwell W., 1968
Aeromagnetic map of part of Great Britain and Northern Ireland, sheet 11, Inst. Geol. Sci., London.

Cagniard L., 1953
Basic theory of the magnetotelluric method of geophysical prospecting, Geophysics, 18, 605-635.

Camfield P. A. and Gough D. I., 1977
A possible Proterozoic plate boundary in North America, Can. J. Earth Sci., 14, 1229-1238.

Camfield P. A., Gough D. I. and Porath H., 1971
Magnetometer array studies in the northwestern United States and southwestern Canada, Geophys. J. R. astr. Soc., 22, 201-221.

Campbell W. H., 1966
A review of the equatorial studies of rapid fluctuations in the earth's magnetic field, Ann. Geophys., 22, 492-501.

Campbell W. H., 1967
Geomagnetic pulsations, article in Physics of geomagnetic phenomena, Vol. 2 (edited by Matsushita S. and Campbell W. H.), Academic Press, New York.

Caner B., 1969
Electrical conductivity structure of the lower crust and upper mantle in Western Canada, Ph.D. thesis, Univ. of British Columbia, Canada.

Cantwell T., 1960
Detection and analysis of low frequency magnetotelluric signals, Ph.D. thesis, M.I.T., Cambridge, Mass., U.S.A.

Cerv V., Pek J. and Praus C., 1984
Models of induction anomalies in Czechoslavakia, J. Geophys., in press.

Chapman F. W. and Mathews W. D., 1953

Audiofrequency spectrum of atmospherics, Nature, 172, 455-456

Christie P. A. F., 1978

A report on the Cambridge North Sea experiment (Paper presented at 2nd UKGA, Liverpool), abstr., Geophys. J. R. astr. Soc., 53, 140.

Church W. R. and Gayer R. A., 1973

The Ballantrae ophiolite, Geol. Magazine, 110, 497-510.

Cochrane N. A. and Hyndman R. D., 1974

Magnetotelluric and magnetovariational studies in Atlantic Canada, Geophys. J. R. astr. Soc., 38, 385-406.

Cochrane N. A. and Wright J. A., 1977

Geomagnetic sounding near the northern termination of the Appalachian system, Can. J. Earth Sci., 14, 2858-2864.

Coggon J. H., 1971

Electromagnetic and electrical modelling by the finite element method, Geophysics, 36, 132-155.

Connerney J. E. P., Nekut A. and Kuckes A. F., 1980

Deep crustal conductivity in the Adirondacks, J. Geophys. Res., 85(B5), 2603-2614.

Cooley J. W. and Tukey J. W., 1965

An algorithm for the machine calculations of complex Fourier series, Mathematics of Computation, 19, 297-307.

Cull J. P., 1985

Magnetotelluric soundings over a Precambrian Contact in Australia, Geophys. J. R. astr. Soc., 80, 661-675.

Davies A., Wilson R. B. and Lovelock P. E. R., 1974

The Lower Carboniferous (Dinantian) sequence at Spilmersford, East Lothian, Scotland, Bull. Geol. Surv. Gt. Br., 45, 1-38.

Dawes G. J. K., 1980

Computer Programme Library, internal publication, Dept. of Geophysics, Univ. of Edinburgh, U.K.

Dawes G. J. K., 1981

An automatic wide-band magnetotelluric data acquisition system, Paper presented at the 4th IAGA Sci. Assem., Edinburgh.

Dawson T. W. and Weaver J. T., 1979

Three-dimensional induction in a non-uniform thin sheet at the surface of a uniformly conducting earth, Geophys. J. R. astr. Soc., 59, 445-462.

De Beer J. H. and Gough D. I., 1980
Conductive structures in southernmost Africa: a magnetometer array study, Geophys. J. R. astr. Soc., 63, 479-495.

De Beer J. H., Gough D. I. and Van Zijl J. S. V., 1975
An electrical conductivity anomaly and rifting in southern Africa, Nature, 255, 678-680.

De Beer J. H., Huyssen R. M. J., Joubert S. J. and Van Zijl J. S. V., 1982b
Magnetometer array studies and deep Schlumberger soundings in the Damara Orogenic Belt, South West Africa, Geophys. J. R. astr. Soc., 70, 11-29.

De Beer J. H., Van Zijl J. S. V. and Gough D. I., 1982
The Southern Cape Conductive Belt (South Africa): its composition, origin and tectonic significance, Tectonophysics, 83, 205-225.

De Beer J. H., Van Zijl J. S. V., Huyssen R. M. J., Hugo P. L. V., Joubert S. J. and Meyer R., 1976
A magnetometer array study in South West Africa, Botswana and Rhodesia, Geophys. J. R. astr. Soc., 45, 1-17.

Dekker D. L., 1983
A magnetotelluric survey of the Bowen Basin, Ph.D. thesis, Univ. of Queensland, Australia.

D'Erceville I. and Kunetz G., 1962
The effect of a fault on the Earth's natural electromagnetic field, Geophysics, 27, 651-665.

Dewey J. F., 1969
Evolution of the Appalachian/Caledonian Orogen, Nature, 222, 124-129.

Dewey J. F., 1971
A model for the Lower Palaeozoic evolution of the southern margin of the Early Caledonides of Scotland and Ireland, Scott. J. Geol., 7, 219-240.

Dewey J. F. and Pankhurst R. J., 1970
The evolution of the Scottish Caledonides in relation to their isotopic age pattern, Trans. Roy. Soc. Edin., 68, 361-389.

Dosso H. W., 1966
Analogue model measurements for electromagnetic variations near vertical faults and dykes, Can. J. Earth Sci., 3, 287-303.

Dosso H. W., 1973
A review of analogue model studies of the coast effect, Phys. Earth Planet. Inter., 7, 294-302.

Dosso H. W., Nienaber W. and Hutton V. R. S., 1980
An analogue model study of electromagnetic induction in the British Isles Region, Phys. Earth Planet. Inter., 22, 68-85.

Dragert H., Law L. K. and Sule P. O., 1980
Magnetotelluric soundings across the Pemberton Volcanic Belt, British Columbia, Can. J. Earth Sci., 17(2), 161-167.

Dvorak Z., 1975
Electrical conductivity models of the crust, Can. J. Earth Sci., 12, 962-970.

Eckhardt D. H., 1963
Geomagnetic induction in a concentrically stratified Earth, J. Geophys. Res., 68, 6273-6278.

Eckhardt D. H., 1968
Theory and interpretation of the electromagnetic impedance of the Earth, J. Geophys. Res., 73, 5317-5326.

Edwards R. N. and Greenhouse J. P., 1975
Geomagnetic variations in the eastern United States: evidence for a highly conducting lower crust? Science, 188(4819), 726-728.

Edwards R. N., Law L. K. and White A., 1971
Geomagnetic variations in the British Isles and their relation to electric currents in the ocean and shallow seas, Phil. Trans. Roy. Soc. London, 270, 289-323.

Everett J. E. and Hyndman R. D., 1967a
Magnetotelluric investigations in southwestern Australia, Phys. Earth Planet. Inter., 1, 49-54.

Everett J. E. and Hyndman R. D., 1967b
Geomagnetic variations and electrical conductivity structure in southwestern Australia, Phys. Earth Planet. Inter., 1, 24-34.

Fischer G., Schnegg P. A., Peguiron M. and Le Quang B. V.,

1981
An analytic one-dimensional magnetotelluric inversion scheme, Geophys. J. R. astr. Soc., 67, 257-278.

Fitton J. G. and Hughes D. J., 1970
Volcanism and plate tectonics in the British Ordovician, Earth Planet. Sci. Lett., 8, 223-228.

Fyfe W. S., Price N. J. and Thompson A. B., 1978
Fluids in the Earth's crust: in developments in geochemistry, 7, Elsevier, Amsterdam, 383pp.

Gamble T. D., Goubau W. M. and Clarke J., 1979a
Magnetotellurics with a remote reference, Geophysics, 44, 53-68.

Gamble T. D., Goubau W. M. and Clarke J., 1979b
Error analysis for remote reference magnetotellurics, Geophysics, 44, 959-968.

Garland G. D., 1975
Correlation between electrical conductivity and other geophysical parameters, Phys. Earth Planet. Inter., 10, 220-230.

Garson M. S. and Plant J., 1973
Alpine type ultramafic rocks and episodic mountain building in the Scottish Highlands, Nature Physical Sci., 242, 34-38.

George T. N., 1960
The stratigraphical evolution of the Midland Valley, Trans. Geol. Soc. Glasgow, 24, 32-107.

Goldberg S. and Rotstein Y., 1982
A simple form of presentation of magnetotelluric data using the Bostick transform, Geophys. Prosp., 30, 211-216.

Goubau W. M., Maxton P. M., Koch R. H. and Clarke J., 1984
Noise correlation lengths in remote reference magnetotellurics, Geophysics, 49, 433-438.

Gough D. I., 1973
The geophysical significance of geomagnetic variation anomalies, Phys. Earth Planet. Inter., 7, 379-388.

Gough D. I., De Beer J. H. and Van Zijl J. S. V., 1973
A magnetometer array study in southern Africa, Geophys. J. R. astr. Soc., 34, 421-433.

Gough D. I., McElhinney M. W. and Lilley F. E. M., 1974

A magnetometer array study in South Australia, Geophys. J. R. astr. Soc., 36, 345-362.

Grant F. S. and West G. F., 1965
Interpretation theory in applied geophysics, McGraw-Hill Book Co.

Green C. A., 1975
An induction study at micropulsation periods in the British Isles, Geophys. J. R. astr. Soc., 40, 225-240.

Green C. A., 1981
Continuous magnetic pulsations on the IGS array of magnetometers, J. Atm. Terr. Phys., 43(9), 883-898.

Gregori G. P. and Lanzerotti L. J., 1980
Geomagnetic depth sounding by induction arrow representation: a review, Rev. Geophys. Space Phys., 18, 203-210.

Greig D. C., 1971
The South of Scotland, British Regional Geology series, HMSO.

Gunn P. J., 1973
Location of the Proto-Atlantic suture in the British Isles, Nature, 242, 111-112.

Haak V. and Hutton V. R. S., 1985
Electrical resistivity in continental lower crust, J. Geol. Soc. London, in press.

Habberjam G. M., 1979
Apparent resistivity observations and the use of square array techniques, Geopublication Associates, Berlin.

Habberjam G. M. and Thanassoulas C., 1979
A deep resistivity sounding at Rookhope, Northern England, Trans. Roy. Soc. Edin., 70, 171-179.

Hall J., 1970
The correlation of seismic velocities with formations in the SW of Scotland, Geophys. Prosp., 18, 134-148.

Hall J., 1971
A preliminary seismic survey adjacent to the Rashiehill borehole, near Slamannan, Stirlingshire, Scott. J. Geol., 7, 170-174.

Hall J., 1974
A seismic reflection survey of the Clyde plateau lavas in North Ayrshire and Renfrewshire, Scott. J. Geol.,

9, 253-279.

Hall J., Powell D. W., Warner M. R., El-Isa Z. H. M., Adesanya O. and Bluck B. J., 1983
Seismological evidence for shallow crystalline basement in the Southern Uplands of Scotland, Nature, 305, 418-420.

Harris F. J., 1978
On the use of windows for harmonic analysis with the discrete Fourier Transform, Proc. IEEE, 66, 51-83.

Hermance J. F., 1973
Processing of magnetotelluric data, Phys. Earth Planet. Inter., 7, 349-364.

Hermance J. F., 1973b
An electrical conductivity model for the Sub-Icelandic crust, Geophysics, 38, 3-13.

Hermance J. F. and Garland G. D., 1968
Deep electrical structure under Iceland, J. Geophys. Res., 73, 3797-3800.

Hermance J. F. and Grillot L. R., 1974
Constraints on temperature below Iceland from magnetotelluric data, Phys. Earth Planet. Inter., 8, 1-12.

Hermance J. F. and Pedersen J., 1980
Deep structure of the Rio Grande Rift: a magnetotelluric interpretation, J. Geophys. Res., 85, 3899-3912.

Hessler V. P., Heacock R. R., Olesen J., Sucksdorff C. and Kangas J., 1972
Micropulsations associated with polar magnetic substorms, UAG R-220, Univ. of Alaska, College, 84-167.

Hipkin R. G., 1977a
A gravity survey over the Midlothian Coalfield, paper presented at the Southern Uplands workshop, Edinburgh.

Hipkin R. G., 1977b
A gravity survey of the South Midlothian Coalfield and the Southern Uplands Fault system, paper presented at the 1st UKGA, Edinburgh, abstr., Geophys. J. R. astr. Soc., 49, 289.

Hobbs B. A., 1975
Analytical solutions to global and local problems of

electromagnetic induction in the Earth, Phys. Earth Planet. Inter., 10, 250-261.

Hobbs B. A., 1982
Automatic model for finding one-dimensional magnetotelluric problem, Geophys. J. R. astr. Soc., 168, 253-266.

Holland C. H., Kelling G. and Walton S. E., 1979
O. T. Jones and after: A multitude of models, in The Caledonides of the British Isles reviewed, Geol. Soc. London special publication No. 8 (edited by Harris et al.), 469-481.

Hutton V. R. S., Harinarayana T., Novak M. and Sule P., 1985
Electromagnetic Induction Studies in the region of the Iapetus suture - an update, abstract, General Assembly of IAGA, Prague.

Hutton V. R. S., Ingham M. R. and Mbipom E. W., 1980
An electrical model of the crust and upper mantle in Scotland, Nature, 287, 30-33.

Hutton V. R. S. and Jones A. G., 1980
Magnetovariational and magnetotelluric investigations in South Scotland, J. Geomagn. Geoelectr., Suppl. I, 141-150.

Hutton V. R. S., Sik J. and Gough D. I., 1977
Electrical conductivity and tectonics of Scotland, Nature, 266, 617-620.

Hyndman R. D. and Cochrane N. A., 1971
Electrical conductivity structure by geomagnetic induction at the continental margin of Atlantic Canada, Geophys. J. R. astr. Soc., 125, 425-466.

Hyndman R. D. and Hyndman D. W., 1968
Water saturation and high electrical conductivity in lower continental crust, Earth Planet. Sci. Lett., 4, 427-431.

Ingham M. R., 1981
Lateral variation of the electrical conductivity structure across South Scotland, Ph.D. thesis, Univ. of Edinburgh, U.K.

Ingham M. R. and Hutton V. R. S., 1982a
Crustal and upper mantle electrical conductivity structure in Southern Scotland, Geophys. J. R. astr. Soc., 69, 579-594.

Ingham M. R. and Hutton V. R. S., 1982b
The interpretation and tectonic implications of the geoelectric structure of Southern Scotland, Geophys. J. R. astr. Soc., 69, 595-606.
Inoue Y., 1973
Wave polarisations of geomagnetic pulsations observed in high latitudes on the earth's surface, J. Geophys. Res., 78, 2959-2976.
Jacob A. W. B., 1969
Crustal phase velocities observed at the Eskdalemuir Seismic Array, Geophys. J. R. astr. Soc., 18, 189-197.
Jacobs J. A., 1970
Physics and chemistry in space, Vol. 1, Springer-Verlag Berlin.
Jacobs J. A., Kato Y., Matsushita S. and Troitskaya V. A., 1964.
Classification of geomagnetic pulsations, J. Geophys. Res., 69, 180-181.
Jacobs J. A. and Sinno K., 1960a
Occurrence frequency of geomagnetic micropulsations, Pc, J. Geophys. Res., 65, 107-133.
Jacobs J. A. and Sinno K., 1960b
World-wide characteristics of geomagnetic micropulsations, Geophys. J., 3, 333-353.
Jain S., 1964
Electrical resistivity of the crust and upper mantle at Eskdalemuir, South Scotland, Nature, 203, 631-632.
Jain S. and Wilson C. D. V., 1967
Magnetotelluric investigations in the Irish Sea and Southern Scotland, Geophys. J. astr. Soc., 12, 165-180.
Jankowski J., Tarlowski Z., Praus O., Pecova J. and Petr V., 1985
The results of deep geomagnetic soundings in the West Carpathians, Geophys, J. R. astr. Soc., 80, 561-574.
Jeans P. J. F., 1973
Plate tectonic reconstruction of the Southern Caledonides of Great Britain, Nature Physical Sci., 245, 120-122.
Jodicke H., Untiedt J., Oglemann W., Schulte L. and Wagenitz V., 1983

Electrical conductivity structure of the crust and upper mantle beneath the Rhenish Massif, Plateaus Uplift (edited by K. Fuchs et al.), Springer-Verlag Berlin, 288-302.

Jones A. G., 1977
Geomagnetic induction studies in Southern Scotland, Ph.D. thesis, Univ. of Edinburgh, U.K.

Jones A. G. and Hutton V. R. S., 1979a
A multi-station magnetotelluric study in Southern Scotland - 1. Fieldwork, data analysis and results, Geophys. J. R. astr. Soc., 56, 329-349.

Jones A. G. and Hutton V. R. S., 1979b
A multi-station magnetotelluric study in Southern Scotland - 2. Monte-Carlo inversion of the data and its geophysical and tectonic implications, Geophys. J. R. astr. Soc., 56, 351-368.

Jones D. S., 1964
The theory of electromagnetism, ch.6, Macmillan Co., New York.

Jones F. W., 1970
EM induction in a non-horizontally stratified two-layered conductor, Geophys. J. R. astr. Soc., 22, 17-28.

Jones F. W., 1973
Induction in laterally non-uniform conductors: theory and numerical models, Phys. Earth Planet. Inter., 7, 282-293.

Jones F. W. and Pascoe L. J., 1971
A general computer programme to determine the perturbation of alternating electric currents in a two-dimensional model of a region of uniform conductivity with an embedded inhomogeneity, Geophys. J. R. astr. Soc., 24, 3-30.

Jones F. W. and Pascoe L. J., 1972
The perturbation of alternating geomagnetic fields by three-dimensional conductivity inhomogeneities, Geophys. J. R. astr. Soc., 27, 479-485.

Jones F. W. and Price A. T., 1970
The perturbations of alternating geomagnetic fields by coductivity anomalies, Geophys. J. R. astr. Soc., 20, 317-334.

Jones F. W. and Price A. T., 1971
Geomagnetic effects of sloping and shelving discontinuities of earth conductivity, Geophysics, 36(1), 58-66.

Jones F. W. and Vozoff K., 1978
The calculation of magnetotelluric quantities for three-dimensional inhomogeneities, Geophysics, 43, 1167-1175.

Jupp D. L. B. and Vozoff K., 1976
Discussion on "The magnetotelluric method in the exploration of sedimentary basins" by Keeva Vozoff (1972), Geophysics, 41, 325-328.

Jupp D. L. B. and Vozoff K., 1977
Two-dimensional magnetotelluric inversion, Geophys. J. R. astr. Soc., 50, 333-352.

Kangas J., 1982
On the sources of short-period magnetic pulsations, in S. E. Hjelt (ed.): Geophysical and geodetic research in Finland and Hungary - Symposium papers, Department of Geophysics, University of Oulu, Finland, Report No. 5, 57-61.

Kato Y. and Kikuchi T., 1950
On the phase difference of earth currents induced by changes of the earth's magnetic field, Parts I and II, Sci. Reports of Tohoku Univ., Ser. 5, Geophys. J., 139-145.

Kaufman A. A. and Keller G. V., 1981
The magnetotelluric sounding method, ELsevier Scientific Publishing Company.

Keller G. V. and Frischknecht F. C., 1966
Electrical methods in geophysical prospecting, Pergamon Press, New York.

Keller G. V., Anderson L. A. and Pritchard J. F., 1966
Geological survey investigations of the electrical properties of the crust and upper mantle, Geophysics, 31, 1078-1087.

Kennedy W. Q., 1958
The tectonic evolution of the Midland Valley of Scotland, Trans. Geol. Soc. Glasgow, 23, 106-133.

Khitarov N. I., Slutskiy A. B. and Pugin V. A., 1970
Electrical conductivity of basalts at high T-P and

phase transitions under mantle conditions, Phys. Earth Planet. Inter., 3, 334-342.

Kunaratnam K., 1981
Spatial dependence of day-time vertical polarisation of Pc3-5 magnetic pulsations in Sri Lanka, J. Atm. Terr. Phys., 43, 1289-1294.

Kurtz R. D. and Garland G. D., 1976
Magnetotelluric measurements in eastern Canada, Geophys. J. R. astr. Soc., 45, 321-347.

Lagios E., 1979
Gravity and other geophysical studies relating to crustal structure of Southeast Scotland, Ph.D. thesis, Univ. of Edinburgh, U.K.

Lagios E., 1984
A geophysical study of the East Lothian volcanics, Southeast Scotland, Earth Planet. Sci. Lett., 67, 205-210.

Lagios E. and Hipkin R. G., 1979
The Tweeddale Granite - a newly discovered batholith in the Southern Uplands, Nature, 280, 672-675.

Lagios E. and Hipkin R. G., 1982
A geophysical approach to the granite batholith under the Eastern Southern Uplands, Pure Appl. Geophys., 120, 375-388.

Lambert R. St. J. and McKerrow W. S., 1976
The Grampian Orogeny, Scott. J. Geol., 12, 271-292.

Law L. K. and Riddihough R. P., 1971
A geographical relation between geomagnetic variation anomalies and tectonics, Can. J. Earth Sci., 8, 1094-1106.

Lee C. D., Vine F. J. and Ross R. G., 1983
Electrical conductivity models for continental crust based on laboratory measurements on high grade metamorphic rocks, Geophys. J. R. astr. Soc., 72, 353-372.

Lee M. K., Brown G. C., Wheildon J., Webb P. C. and Rollin K. E., 1985
Heat flow and heat production in Britain, abstr., 3rd Deep Geology Workshop, Univ. of Durham.

Leggett J. K., McKerrow W.S. and Eales M. H., 1979
The Southern Uplands of Scotland: A Lower Palaeozoic

accretionary prism, J. Geol. Soc. London, 136, 755-770.

Lienert B. R., 1980
The effect of source field polarisation on estimates of the magnetotelluric impedance tensor, Geophysics, 45, 1803-1812.

Lilley F. E. M., 1976
Diagrams for magnetotelluric data, Geophysics, 41, 766-770.

Lines L. R. and Jones F. W., 1973a
The perturbation of alternating geomagnetic fields by three-dimensional island structures, Geophys. J. R. astr. Soc., 32, 133-154.

Lines L. R. and Jones F. W., 1973b
The perturbation of alternating geomagnetic fields by an island near a coastline, Can. J. Earth Sci., 10, 510-518.

MacGregor M. and MacGregor A. G., 1948
The Midland Valley of Scotland, British Regional Geology series, HMSO.

Madden T. R., 1976
Random networks and mixing laws, Geophysics, 41, 1104-1125.

Madden T. R. and Nelson P., 1964
A defence of Cagniard's magnetotelluric method, Project NR-371-401, Geophys. Lab., M.I.T., Cambridge, Mass., U.S.A.

Madden T. R. and Swift C.M. (Jr.), 1969
Magnetotelluric studies of the electrical conductivity structure of the crust and upper mantle: in The Earth's crust and upper mantle (P. J. Hart, editor), Amer. Geophys. Un. Monograph, 469-479.

Mbipom E. W., 1980
Geoelectrical studies of the crust and upper mantle in Northern Scotland, Ph.D. thesis, Univ. of Edinburgh, U.K.

Mbipom E. W. and Hutton V. R. S., 1983
Geoelectromagnetic measurements across the Moine Thrust and the Great Glen in Northern Scotland, Geophys. J. R. astr. Soc., 74, 507-524.

McAdam A. D., 1974
The petrography of the igneous rocks in the Lower

Carboniferous (Dinantian) at Spilmersford, East Lothian, Scotland, Bull. Geol. Surv. Gt. Br., 45, 39-46.

McKerrow W. S. and Cocks L. R. M., 1977
The location of the Iapetus Ocean suture in Newfoundland, Can. J. Earth Sci., 14, 488-495.

McLean A. C. and Qureshi I. R., 1966
Regional gravity anomalies in the western Midland Valley of Scotland, Trans. Roy. Soc. Edin., 66, 267-283.

Mitchell A. H. G. and McKerrow W. S., 1975
Analogous evolution of the Burma Orogen and the Scottish Caledonides, Geol. Soc. Amer. Bull., 86, 305-315.

Molochnov G. V., 1968
Magnetotelluric sounding interpretation using the effective depth of penetration of electromagnetic field (in Russian), Izv. Akad. Nauk SSSR Fiz. Zemli, 9, 88-94 (ref. from Rokityansky, 1982).

Mooney H. M. and Bleifuss R., 1953
Magnetic susceptibility measurements in Minnesota, Part II: Analysis of field results, Geophysics, 18, 383-393.

Moseley F., 1977
Caledonian plate tectonics and the place of the English Lake District, Geol. Soc. Amer. Bull., 88, 764-768.

Nienaber W., Dosso H. W. and Hutton V. R. S., 1981
Electromagnetic induction in the British Isles Region: analogue model and field station results, Phys. Earth Planet. Inter., 27, 122-132.

Niblett E. R. and Honkura Y., 1980
Time-dependence of electromagnetic transfer functions and their association with tectonic activity, Geophys. Surv., 4, 97-114.

O'Brien D. P. and Morrison H. F., 1967
EM fields in an n-layer anisotropic half-space, Geophysics, 32, 668-677.

Orr D., 1973
Magnetic pulsations within the magnetosphere: A review, J. Atm. Terr. Phys., 35, 1-50.

Osemeikhian J. E. A. and Everett J. E., 1968

Anomalous magnetic variations in SW Scotland, Geophys. J. R. astr. Soc., 15, 361-366.

Oxburgh E. R., Richardson S. W., Wright S. M., Jones M. Q. W., Penney S. R., Watson S.A. and Bloomer J. R., 1980
Heat flow pattern of the United Kingdom, Second International Seminar on the results of E.E.C. Geothermal Energy Research, Strassbourg, 149-152.

Parkinson W. D., 1959
Directions of geomagnetic fluctuations, Geophys. J. R. astr. Soc., 2, 1-14.

Parkinson W. D., 1962
The influence of continents and oceans on geomagnetic variations, Geophys. J. R. astr. Soc., 6, 441-449.

Parkinson W. D., 1983
Introduction to geomagnetism, Scottish Academic Press, Edinburgh.

Parry J. R. and Ward S. H., 1971
Electromagnetic scattering from cylinders of arbitrary cross-section in a conductive half-space, Geophysics, 36, 67-100.

Pascoe L. J. and Jones F. W., 1972
Boundary conditions and calculation of surface values for the general two-dimensional electromagnetic induction problem, Geophys. J. R. astr. Soc., 27, 179-193.

Paterson N. R. and Ronka V., 1971
Five years of surveying with Very Low Frequency electromagnetic method, Geoexploration, 9, 7-26.

Patra H. P. and Mallick K., 1980
Geosounding Principles, 2: Time-varying Geoelectric Soundings, Elsevier Sci. Publishing Co.

Petiau G. and Dupis A., 1980
Noise, temperature coefficient and long time stability of electrodes for telluric observations, Geophys. Prosp., 28, 792-804.

Phillips W. E. A., Stillman C. J. and Murphy T., 1976
A Caledonian plate tectonic model, J. Geol. Soc. London, 132, 579-609.

Porstendorfer G., 1975
Principles of magnetotelluric prospecting, Geopublication Associates, Berlin.

Powell D. W., 1971
A model for the Lower Palaeozoic evolution of the southern margin of the early Caledonides of Scotland and Ireland, Scott. J. Geol., 7, 369-372.
Praus O., 1975
Numerical and analogue modelling of induction effects in laterally non-uniform conductors, Phys. Earth Planet. Inter., 10, 262-270.
Presnal D. C., Simmons C. L. and Porath H., 1972
Changes in electrical conductivity of a synthetic basalt during melting, J. Geophys. Res., 77, 5665-5672.
Price A. T., 1950
Electromagnetic induction in a semi-infinite conductor with a plane boundary, Quart. J. Mech. Appl. Math., 3, 385-410.
Price A. T., 1962
The theory of magnetotelluric methods when the source field is considered, J. Geophys. Res., 67, 1907-1918.
Price A. T., 1963
A note on the interpretation of the magnetic variations and magnetotelluric data, J. Geomagn. Geoelectr., Tokyo 15, 4, 241-248.
Pridmore D. F., Hohmann G. W., Ward S. H. and Sill W. R., 1981
Investigation of finite element modelling for electrical and electromagnetic data in three-dimensions, Geophysics, 46, 1009-1024.
Quon C., Vozoff K., Hoversten M., Morrison H. F. and Lee K. H., 1979
Localized source effects on magnetotelluric apparent resistivities, J. Geophys., 46, 291-299.
Raiche A. P., 1974
An integral equation approach to three-dimensional modelling, Geophys. J. R. astr. Soc., 36, 363-376.
Ranganayaki R. P., 1984
An interpretive analysis of magnetotelluric data, Geophysics, 49, 1730-1748.
Rankin D., 1962
The magnetotelluric effect of a dyke, Geophysics, 27,

666-676.

Rankin D., Garland G. D. and Vozoff K., 1965
An analogue model for the magnetotelluric effect, J. Geophys. Res., 70, 1939-1945.

Raspopov O. M., 1968
Possible excitation mechanism of type Pi2 geomagnetic field pulsations, Geomagn. Aeron., 8, 257-260.

Reddy I. K. and Rankin D., 1972
On the interpretation of magnetotelluric data in the plains of Alberta, Can. J. Earth Sci., 9, 514-527.

Reddy I. K. and Rankin D., 1973
Magnetotelluric response of a two-dimensional sloping contact by finite element method, Pure Appl. Geophys., 105, 847-857.

Richardson S. W. and Oxburgh E. R., 1978
Heat flow, radiogenic heat production and crustal temperatures in England and Wales, J. Geol. Soc. London, 135, 323-338.

Rikitake T., 1950
Electromagnetic induction within the earth and its relation to the electrical state of the earth's iterior, Bull. Earthq. Res. Inst. Tokyo, 28, 45-98.

Rikitake T., 1951
Changes in earth currents and the relation to the electrical state of the earth's crust, Bull. Earthq. Res. Inst. Tokyo, 29, 270-275.

Rikitake T., 1976
Earthquake prediction, vol. 9, Developments in Solid Earth Geophysics, Elsevier.

Rokityansky I. I., 1982
Geoelectromagnetic investigation of the Earth's crust and mantle, Springer-Verlag, Berlin.

Rooney D., 1976
Magnetotelluric measurements across the Kenyan Rift Valley, Ph.D. thesis, Univ. of Edinburgh, U.K.

Rooney D. and Hutton V. R. S., 1977
A magnetotelluric and magnetovariational study of the Gregory Rift Valley, Kenya, Geophys. J. R. astr. Soc., 51,. 91-119.

Roxis N., 1984
The development of deep sounding technique using

resistivity methods and an investigation of the associated interpretation problems, Ph.D. thesis, Univ. of Leeds, U.K.

Roy A., 1962
Ambiguity in geophysical interpretation, Geophysics, 27, 90-99.

Schelkunoff S. A., 1943
Electromagnetic waves, ch. 4, D. Van Nostrand Co., New York.

Schmucker U., 1964
Anomalies of geomagnetic variations in the southwestern United States, J. Geomagn. Geoelectr., 15, 193-221.

Schmucker U., 1970
Anomalies of geomagnetic variations in the southwestern United States, Bull. Scripps Inst. Oceanogr., La Jolla, Calif., 13, 1-165.

Schnegg P. A. and Fischer G., 1979
On-line determination of the apparent resistivities in audiofrequency magnetotelluric measurements, Paper presented at the 17th I.U.G.G. Gen. Assem., Canberra, (abstr.) IAGA Bulletin 43, 172.

Schwarz G., Haak V., Martinez E. and Bannister J., 1984
The electrical conductivity of the Andean crust in northern Chile and southern Bolivia as inferred from magnetotelluric measurements, J. Geophys., 55, 169-178.

Shankland T. J., 1975
Electrical conduction in rocks and minerals: parameters for interpretation, Phys. Earth Planet. Inter., 10, 209-219.

Shankland T. J. and Ander M. C., 1983
Electrical conductivity, temperatures and fluids in the lower crust, J. Geophys. Res., 88, 9475-9484.

Shankland T. J. and Waff H. S., 1977
Partial melting and electrical anomalies in the upper mantle, J. Geophys. Res., 82, 5409-5417.

Sims W. E. and Bostick F. X. (Jr.), 1969
Methods of magnetotelluric analysis, Technical Report No. 58, 1-86, Electrical Geophysics Research Lab., University of Texas, U.S.A.

Sims W. E., Bostick F. X. (Jr.) and Smith H. W., 1971
The estimation of magnetotelluric impedance tensor elements from measured data, Geophysics, 36, 938-942.

Smith B. D. and Ward S. H., 1974
On the computation of polarisation ellipse parameters, Geophysics, 39, 867-869.

Spies B. R., 1983
Recent developments in the use of surface electrical methods for oil and gas exploration in the Soviet Union, Geophysics, 48, 1102-1112.

Srivastava S. P., 1965
Theory of the magnetotelluric method for non-uniform conductors, J. Geomagn. Geoelectr., Tokyo 17, 3-4, 507-515.

Srivastava S. P., 1965b
Method of interpretation of magnetotelluric data when source field is considered, J. Geophys. Res., 70, 945-954.

Srivastava S. P., 1967
Magnetotelluric two- and three-layer master curves, Publ. Dominion Obs. Ottawa, vol. 35, No. 7.

Stanley W. D., 1984
Tectonic study of Cascade Range and Columbia Plateau in Washington State based upon magnetotelluric soundings, J. Geophys. Res., 89, 4447-4660.

Stanley W. D., Boehl J. E., Bostick F. X. (Jr.) and Smith H. W., 1977
Geothermal significance of magnetotelluric sounding in Eastern Snake River Plain-Yellowstone Region, J. Geophys. Res., 82, 2501-2514.

Stesky R. M. and Brace W. F., 1973
Electrical conductivity of serpentinized rocks to 6 kilobars, J. Geophys. Res., 78, 7614-7621.

Strangway D. W., Swift C. M. (Jr.) and Holmer R. C., 1973
The application of audiofrequency magnetotellurics (AMT) to mineral exploration, Geophysics, 38(6), 1159-1175.

Sule P. O. and Hutton V. R. S., 1984
A broadband magnetotelluric study in S.E. Scotland - Data acquisition, analysis and one-dimensional modelling, Paper presented at the 7th EM Induction

Workshop (Aug. 84), Univ. of Ife, Nigeria and submitted to Annales Geophysicae.

Summers D. W., 1976
The inversion of geomagnetic data, Ph.D. thesis, Univ. of Edinburgh, U.K.

Swift C. M. (Jr.), 1967
A magnetotelluric investigation of an electrical conductivity anomaly in the southwestern United States, Ph.D. thesis, Dept. of Geology and Geophysics, M.I.T., Mass., U.S.A.

Tikhonov A. N., 1950
Determination of the electrical characteristics of the deep strata of the earth's crust, Dokl. Akad. Nauk. SSSR, 73, No.2, 295-297.

Troitskaya V. A., 1967
Micropulsations and the state of the magnetosphere, article in Solar Terrestrial Physics (edited by J. W. King and W. S. Newman), Academic Press, London.

Tsokas G., 1980
A deep electrical sounding 10.5 km west of Duns in Scotland, M.Sc. thesis, Univ. of Leeds, U.K.

Turner F. J. and Verhoogen J., 1960
Igneous and metamorphic petrology, McGraw-Hill, New York, 694pp.

Uyeda S. and Rikitake T., 1970
Electrical conductivity anomaly and terrestrial heat flow, J. Geomagn. Geoelectr., 22, 75-90.

Valiant M. J., 1976
N.E.R.C. geologger technical handbook, IGS magnetic observatory, Hartland.

Van Zijl J. S. V., 1977
Electrical studies of the deep crust in various tectonic provinces of southern Africa, in The Earth's crust (edited by J. G. Heacock), Monogr. Amer. Geophys. Un., 20, 470-500.

Vero J., 1981
Changes of pulsation activity during two solar cycles, J. Atm. Terr. Phys., 43(9), 919-926.

Volker H., 1968
Observations of geomagnetic pulsations Pc3,4 and Pi2 at different latitudes, Ann. Geophys., 24, 245-252.

Vozoff K., 1972
The magnetotelluric method in the exploration of sedimentary basins, Geophysics, 37, 98-141.
Vozoff K., 1980
Electromagnetic methods in applied geophysics, Geophys. Surv., 4, 9-29.
Waff H. S., 1974
Theoretical considerations of electrical conductivity in a partially molten mantle and implications for geothermometry, J. Geophys. Res., 79(26), 4003-4010.
Wait J. R., 1954
On the relation between telluric currents and the earth's magnetic field, Geophysics, 19, 281-285.
Ward S. H., Peeples W. J. and Ryu J., 1973
Analysis of geomagnetic data, in Methods in computational physics (edited by B. A. Bolt), 13, 163-238, Academic Press, New York.
Warner M. R., Hipkin R. G. and Browitt C. W. A., 1982
Southern Uplands seismic refraction profile - preliminary results (abstract), Geophys. J. R. astr. Soc., 69, 279.
Weaver J. T., 1963
The electromagnetic field with a discontinuous conductor with reference to geomagnetic micropulsations near a coast line, Can. J. Phys., 41, 484-495.
Weaver J. T. and Brewitt-Taylor C. R., 1978
Improved boundary conditions for the numerical solution of E-polarisation problems in geomagnetic induction, Geophys. J. R. astr. Soc., 54, 309-317.
Weidelt P., 1972
The inverse problem of geomagnetic induction, J. Geophys., 38, 257-289.
Weidelt P., 1975
Electromagnetic induction in three-dimensional structures, J. Geophys., 41, 85-109.
White A. and Milligan P. R., 1984
A crustal conductor on Eyre Peninsular, South Australia, Nature, 310(5974), 219-222.
Williams A., 1969
Ordovician of the British Isles, in North Atlantic

geology and continental drift (Kay M., editor), Amer. Assoc. Petr. Geol. Mem. 12.

Williams A., 1975

Plate tectonics and biofacies evolution as factors in Ordovician correlation, in The Ordovician System (Bassett M. G., editor), Proceedings of a Palaeontological Association symposium, Cardiff Univ. Press and Nat. Mus. Wales, 18-53.

Williamson K., Hewlett C. and Tammemagi H. Y., 1974

Computer modelling of electrical conductivity structures, Geophys. J. R. astr. Soc., 37, 533-536.

Wilson J. T., 1966

Did the Atlantic close and then re-open? Nature, 211, 676-681.

Wright A. E., 1976

Alternating subduction directions and the evolution of the Atlantic Caledonides, Nature, 207, 270-272.

Young R. A. and Lucas J. E., 1984

Seismic exploration beneath volcanics: Snake River Plain, Idaho (abstract), Geophysics, 49, 600 (paper presented at 53rd annual international SEG meeting in Las Vegas, 1983).

Yungul S. H., 1961

Magnetotelluric sounding three-layer interpretation curves, Geophysics, 26, 465-473.

Zdhanov M. S., Golubev N. G., Varentsov Iv. M., Ambramova L. M., Schneer V. S., Berdichevsky M. N., Kulik S. N. and Bilinsky A. I., 1984

2D model fitting of geomagnetic anomaly in the Soviet Carpathians, Proc. of Baltic Shield Symposium, Department of Geophysics, University of Oulu, Rep. No. 8, 296-306.